Journal of Double Star Observations

VOLUME 20 NUMBER 2 April 1, 2024

Inside this issue:

Measurements of 95 Large Delta Magnitude Double Stars with HCDSF instrument, Part 1 2023.000-2023.499 Joerg Schlimmer	64
Measurements of 93 Large Delta Magnitude Double Stars with HCDSF instrument, Part 2 2023.500-2023.999 Joerg Schlimmer	68
Astrometric Measurements of 3 Binary Star Systems: WDS 00033+5332, WDS 05283+0358, and WDS 19557+3805 Joshua Lo, Aidan Lindhe-Johan, Aenea Briggs, Noah Smith, and Sabrina Stierwalt	75
Exploring Binary Stars—Fundamental Systems in Astronomy: Observation of HD 80460 Merliz M. Pérez Vázquez, Ian M. Pérez López, Victoria A. González Claudio, David R. Padilla Oyola, Carmen A. Pantoja Pantoja, Mayra E. Lebrón Santos, Lisa Storrie-Lombardi, Edward Gomez, Alice Hopkinson, Rachel Freed, and Sabrina Stierwalt	87
Some "Lost" Doubles in the WDS Roger C. Ceragioli	95
Desmos Analysis of the Binary Star CHR 259 (WDS 15496-0326): A Tutorial with HU 481 (WDS 16212+2259) Example Michael-James L. Ellis, Diana Holland, Halli Kinnick, and Russell M. Genet	114
A New Double Star Discovered During an Asteroid Occultation of UCAC4 339-186983 David Gault	122
Observations of 42 Double Stars Near Messier 35 Kaden Anderson, Hunter Castleton, Nisha Fletcher, Tristyn Montgomery, Preston Pack, Shaeden McCord, Elizabeth Eastep, Trinity Wilcox, Cash Lake, Kyler Ahlvers, Jillian Bath, Oliver Brumit, Adelaide Costello, Krosby Cox, Dante Hollowbreast, Viktoria Howard, Cecil Kunz, Boston McNutt, Brooklee McNutt, Catherine Murphree, Breanna Nielson, Cooper Reed, Ledger Ruesch, Sophie Sandoval, Layla Tate, Levi Walker, Heather Lambert, Kaelyn Porter, and Cameron Pace	125
Measurements of WDS 20310-2700 and WDS 20313-2707 Tyler D. Scott, Sarah Grace Bogle, and Kathryn M. Boeckers	141
WDS 18338+1744: Speckle Analysis of a Quadruple in Hercules John Major, Elias Faughn, Bradley Brungardt, and Paul McCudden	149
Observation and Measurements for the Double Star System HJ3203 Sofia A. Osorio Correa, Jeremy L. Curry Romero, Alondra S. Gonzalez Agosto, Fabian G. Rivera Rivera, Devon M. Rivera Moran, Carmen A. Pantoja Pantoja, Mayra E. Lebrón, Lisa Storrie-Lombardi, Edward Gomez, Alice Hopkinson, Sabrina Stierwalt, and Rachel Freed	157
Orbit Determination and Astrophysical Study of the Binary System HU 481 (= HD 147442) F. M. Rica	164

Inside this issue:

Observation of the Double Star System HD 21599 Gabriela R. Santiago Rodriguez, Alanys S. Pizarro Vélez, Carmen A. Pantoja Pantoja, Mayra E. Lebrón Santos, Edward Gomez, Lisa Storrie-Lombardi', Alice Hopkinson, Rachel Freed and Sabrina Stierwalt	171
Astrometric Measurements of Four Double Star Systems Corbin Breeden, Zoe Schurman, Michael Pylypovych, Atria Freeman and Kalée Tock	176
Astrometric Measurements and Physical Likelihood Assessments for HJ 4258, STF 1106, and VNI 1 Maiya Qiu, Nicholas Peh, Eden (Songxiao) Li and Kalée Tock	187
New Measurements of Some Double Stars in the Constellation Vulpecula Zsolt Szamosvari	197
A New Approach to Determine Orbits of Wide Binary Stars; Case: WDS 19377+3022 BU 144 Richard Nugent	209
Measurements of 40 Neglected Stars—Report of December 2023 Joseph L. Carro	222
Determining the Gravitationally Bound and Optical Components of Quadruple System WDS 18136-1536 Sierra Kasl-Godley, Dylana Wagorn, Joshua Curiel, Shannon Pangalos-Scott, Alexander Vasquez, Dag Harmsen, Bebe Simone Hart, Rachel Freed and Rebecca Chamberlain	228
Astrometric Measurements of WDS 18175-1638 HJ2829 AB, AC Joseph Leeber and Tristan May	235
Measurements of the Position Angle and Separation of Two Pairs in WDS 21406+5419 ES 35, an 11-Fold System Ian Gifford and Vaishak Pulkayath	242
Astrometric Measurements and Analysis of Four Star Systems Jules Miller, Pierce Arora, Kyler Gandrup, Joe Ross and Kalée Tock	250
Desmos Graphical Analysis of Binary Stars — A Tutorial with HU 481 (WDS 16212+2259) Example Russell Genet, Paul McCudden and Michael-James Ellis	264
Astrometric Measurements of Double Star System HEI 915, GRV 719, STI 2170, and RST 2351 Nathan Bowman, Kathikeya Vattem, Sophia Bhatti, Kavi Bidlack and Kalée Tock	275
Desmos Analysis of the Binary Star WDS 19471-1953 Michael-James L. Ellis and Russell M. Genet	285
Astrometric Measurements of Three Double Star Systems Near 5h of Right Ascension Leonid Vishnevskiy, Denis Levine, Nicholas Dunn, Khensa Musaddequr Rahman and Kalée Tock	293
Astrometry of Double Star WDS 18026-5234 Nora Furlong, Sofia Robinson, Beatrix Picotte, Ryan Fantasia, Romy Gaudet, Laurel Halfman and Mark H. Brooks Hedstrom	306
Observation and Investigation of 5 Physical Doubles in the Washington Double Star Catalog Liam Oscaris, Mel Neffe, Samuel Lafiaji, Dali Milo, Carter Zimmerman and Kayla Oltman	311

Measurements of 95 Large Delta Magnitude Double Stars with HCDSF instrument, Part 1 from 2023.000 - 2023.499

Joerg S. Schlimmer 64342 Seeheim-Jugenheim, Germany Email: js@epsilon-lyrae.de

Abstract

This report shows the results of 95 double star measurements made with the High Contrast Double Star Filter instrument (HCDSF).

1. Introduction

In a previous article a special filter for measurements of high contrast double stars was introduced and described in detail (Schlimmer, 2023). After two month of testing and optimization in January and February the HCDSF instrument was transitioned to standard operating mode. In this contribution the results of 95 measurements from 2023.000 to 2023.499 will be reported.

For the observations an extract of the WDS catalog was compiled first. The WDS catalog was downloaded and imported in an Excel file. To select the target stars some filter criteria were used:

Coordination : Declination > 0

• Separation : ≥ 6 "

• Secondary magnitude : ≤ 12

• Delta magnitude : ≥ 3

With these criteria a list of 2241 doubles stars were compiled for possible observations. Some of them were be picked up and marked in the Redshift Planetary software as target. The Redshift Planetary software will be used for mounting control.

2. Equipment and Methods

For observations a 12-inch Newtonian telescope was used. The focal length is 1500 mm. For the measurements of double stars with large magnitude differences, the HCDSF instrument was mounted on an ocular adapter. In the back focus of the HCDSF instrument a QHY 5-II color CMOS camera was mounted. Image scale is about 0.44 arc seconds per pixel.



Figure 1: High Contrast Double Star Filter (HCDSF) instrument mounted on ocular adapter on the 12-inch Newtonian telescope

The measurements were made in same way as other double stars observations without the HCDSF instrument. For each double star a video with 50 up to 200 frames was recorded. The number of the frames depended on the needed exposure time. In general, the longer the exposure time the fewer numbers of frames was recorded. Every frame of the video is like a single measurement. For data analyses REDUC software (Losse, 2016) was used. For each frame separation and position angle was automatically analyzed by the ELI interface. The standard deviation for measurements of the separation is usually smaller than \pm 0.15 arc seconds. The standard deviation for measurements of position angle depends on the separation of both components. For double stars with separation of about 5 arc seconds the standard deviation for position angle is usually \pm 1 degree.

3. Data

Table 1 shows the results of the 95 measurements with the HCDSF instrument from 2023.000 - 2023.499. The brightness was taken from WDS catalogue. Dm is the difference in magnitudes between the primary and secondary component. Average of dm is 6.24 magnitudes. N is the number of observations. Generally, every double star was observed only once. Date is given in Julian date (JD).

Table 1: Results of 95 double star measurements made with the High Contrast Double Star Filter (HCDSF) from 2023.000 - 2023.499

RA+DEC	Code	Magnitudes	m2-m1	PA	SEP	Date	N
03502+3449	ES 277AB	6.80,9.8	3,00	141.6	20.26	2023.049	1
03502+3449	WAL 25AD	6.80,10.30	3,50	11.0	71.53	2023.049	1
04018+1000	STT 70AB	5.81,11.21	5,40	229.6	11.86	2023.049	1
04018+1000	WAL 27AC	5.81,11.70	5,89	241.4	84.36	2023.049	1
04359+1631	BU 550AB	0.85,13.6	12,75	114.7	31.43	2023.049	1
04444+1109	BUP 68AB	5.41,11.23	5,82	96.7	67.96	2023.049	1
04444+1109	BUP 68BC	11.23,12.6	1,37	7.3	8.70	2023.049	1
04497+1554	HJ 3261AB	6.08,11.3	5,22	60.9	26.18	2023.049	1
04497+1554	BU 551BC	11.3,13.1	1,80	204.6	5.86	2023.049	1
05552+0724	H 6 39AB	0.77,14.5	13,73	113.0	37.52	2023.049	1
05552+0724	H 6 39AC	0.77,14.2	13,43	288.7	64.97	2023.049	1
05552+0724	H 6 39AD	0.77,13.5	12,73	345.7	71.79	2.023.049	1
05552+0724	H 6 39AE	0.77,11.0	10,23	154.9	176.48	2.023.049	1
05552+0724	SLE 831AF	0.77,12.1	11,33	266.3	169.05	2023.049	1
05552+0724	SLE 831AG	0.77,12.8	12,03	47.2	149.20	2.023.049	1
05552+0724	SLE 831AH	0.77,11.2	10,43	294.3	240.21	2023.049	1
05552+0724	SMR 29AJ	0.77,13.5	12,73	257.9	190.96	2023.049	1
00084+2905	H 5 32AB	2.22,11.11	8,89	285.6	92.79	2023.063	1
02383+3744	BU 305AC	6.16,11.37	5,21	205.7	20.64	2023.063	1
00365+5831	BU 1096AB,C	8.79,9.74	0,95	241.1	35.66	2023.079	1
00365+5831	SMR 24AB,E	8.79,12.	3,21	145.9	38.69	2023.079	1
00405+5632	H 5 18AD	2.35,8.98	6,63	282.8	70.89	2023.079	1
00447+4817	BU 231AB	4.54,11.2	6,66	303.0	34.36	2023.079	1
00491+5749	STF 60AB	3.52,7.36	3,84	327.6	13.54	2023.079	1
00491+5749	STF 60AE	3.52,10.15	6,63	126.2	65.95	2023.079	1
05552+0724	H 6 39AD	0.77,13.5	12,73	345.4	71.65	2023.095	2

04359+1631	STFB 2AC	0.85,11.3	10,45	31.5	136.34	2023.118	1
04230+1732	BUP 55AB	3.76,13.21	9,45	336.5	112.26	2023.140	1
04255+1756	H 6 101AC	4.26,11.12	6,86	234.8	76.26	2023.140	1
04498+0658	STT 560AB	3.22,11.31	8,09	173.8	72.70	2023.140	1
05133+0252	STF 654AB	4.62,8.50	3,88	63.7	6.90	2023.140	1
05133+0252	STF 654AC	4.62,11.43	6,81	157.6	182.15	2023.140	1
05145-0812	STF 668A,BC	0.3,6.8	6,50	203.7	9.35	2023.140	1
05320-0018	STFA 14AC	2.41,6.83	4,42	0.3	51.83	2023.140	1
05354-0555	STF 752AB	2.77,7.73	4,96	141.1	11.17	2023.140	1
05354-0555	STF 752AC	2.77,9.81	7,04	103.7	49.34	2023.140	1
05362-0112	BUP 81	1.69,11.34	9,65	58.0	179.52	2023.140	1
05407-0157	STF 774AC	1.88,9.55	7,67	9.7	57.59	2023.140	1
08404+1940	STF1254AB	6.44,10.37	3,93	54.7	20.68	2023.285	1
08404+1940	STF1254AC	6.52,7.61	1,09	342.9	63.24	2023.285	1
08404+1940	STF1254AD	6.52,9.20	2,68	44.3	82.74	2023.285	1
10084+1158	STFB 6AB	1.40,8.24	6,84	307.8	175.94	2023.285	1
11141+2031	STT 573AB	2.54,10.87	8,33	341.4	207.81	2023.285	1
11141+2031	BU 1282AC	2.54,12.69	10,15	28.5	98.24	2023.285	1
11475+2002	SHJ 130AB	7.52,9.94	2,42	30.6	71.54	2023.285	1
07346+3153	STF1110AB	1.93,2.97	1,04	51.2	5.37	2023.337	1
07346+3153	STF1110AC	1.93,9.83	7,90	164.4	69.59	2023.337	2
07346+3153	STF1110AD	1.93,10.07	8,14	221.8	178.30	2023.337	1
08404+1940	SMR 30AE	6.52,12.5	5,98	155.9	15.60	2023.337	1
09510+5902	STT 521	3.8,11.3	7,50	297.2	11.88	2023.375	1
10319+3223	HJ 482AB	5.90,11.8	5,90	249.0	58.93	2023.375	1
10332+4026	HJ 2534AB	4.75,11.6	6,85	4.8	16.87	2023.375	1
11416+3145	STT 575AB	5.79,9.75	3,96	313.0	42.80	2023.375	2
11007+4244	ES 2637	6.69,10.7	4,01	211.1	11.69	2023.397	1
11256+1627	HJ 4433AB	5.62,10.84	5,22	6.2	55.03	2023.397	1
11442+2513	STT 239	6.18,10.44	4,26	33.2	36.30	2023.397	1
11480+2013	STFB 7AB	4.59,9.03	4,44	355.9	74.44	2023.397	1
11509+1217	HJ 1201	6.42,11.65	5,23	189.8	14.66	2023.397	1
11512+3322	ARG 101	6.27,9.28	3,01	274.1	46.05	2023.397	1
12269+2816	SMR 58	4.4,12.	7,60	206.8	15.83	2023.417	1
12083+4354	ES 2641	8.17,11.18	3,01	259.1	15.83	2023.424	1
12225+2551	SHJ 143AB	4.86,11.8	6,94	58.6	37.00	2023.424	1
12225+2551	SHJ 143AC	4.86,8.90	4,04	168.3	64.94	2023.424	1
13100+1732	STF1728AB,C	4.43,11.45	7,02	352.5	82.85	2023.427	1
13119+2753	STT 578	4.30,12.1	7,80	178.3	134.97	2023.427	2
13221+4354	KZA 55AB	6.35,11.5	5,15	307.6	45.57	2023.430	1
13221+4354	KZA 55AC	6.37,11.96	5,59	59.4	68.24	2023.430	1
13253+0051	STT 265AB	7.37,11.03	3,66	293.9	25.52	2023.430	1
13253+0051	STT 265AC	7.37,12.19	4,82	75.9	70.79	2023.430	1
13375+3618	STF1768AC	4.98,11.55	6,57	322.0	212.10	2023.430	1
13396+1045	BU 612AB,C	5.62,11.0	5,38	274.5	118.3	2023.430	1
13547+1824	SHJ 169	2.72,9.99	7,27	84.8	114.29	2023.444	1

13567+0259	BU 461AB	7.08,11.9	4,82	235.2	33.11	2023.444	1
13567+0259	BU 461AC	7.08,11.2	4,12	220.3	42.27	2023.444	1
14016+0133	SHJ 171AB	4.25,9.41	5,16	290.8	82.27	2023.444	1
14016+0133	DRS 14AE	4.25,12.0	7,75	178.1	14.68	2023.444	1
14083+4927	H 6 112	5.45,11.05	5,60	270.3	76.05	2023.444	1
14193+1300	ENG 51	5.44,10.84	5,40	220.9	164.60	2023.444	1
14275+7542	HJ 2733AC	4.40,11.9	7,50	129.8	58.88	2023.444	1
14318+3022	HJ 2728	3.58,11.5	7,92	344.6	32.31	2023.444	1
14347+2945	STT 582AB	4.50,10.66	6,16	85.5	212.77	2023.444	1
14135+5147	STF1821AB	4.53,6.62	2,09	236.4	13.69	2023.457	1
14162+5122	STFA 26AB	4.76,7.39	2,63	33.0	38.81	2023.457	1
14252+5151	STT 580	4.10,11.46	7,36	182.2	69.37	2023.457	1
14321+3818	BU 616AB	3.04,12.7	9,66	122.8	53.04	2023.457	1
14407+1625	STF1864AB	4.88,5.79	0,91	114.3	5.44	2023.457	1
14407+1625	STF1864AC	4.88,10.63	5,75	165.1	127.81	2023.457	1
14411+1344	H 6 104AB,C	4.52,10.98	6,46	261.1	104.42	2023.457	1
14463+0939	STF1879AB,D	7.32,10.8	3,48	231.5	118.71	2023.457	1
14497+0759	A 1110AB,C	7.05,12.0	4,95	203.5	19.67	2023.457	1
14497+0759	A 1110AB,D	7.05,12.5	5,45	341.9	23.89	2023.457	1
14514+1906	STF1888AB	4.76,6.95	2,19	292.1	4.96	2023.457	1
15073+2452	ENG 52AB	4.97,11.53	6,56	39.5	103.33	2023.457	1
15155+3319	STFA 27AB	3.56,7.89	4,33	77.9	104.69	2023.457	1
15155+3319	SMR 31AC	3.56,14.30	10,74	3.9	92.70	2023.457	1

Acknowledgements:

This research has made use of the Washington Double Star Catalog maintained at the U.S. Naval Observatory.

This research has made use of the SIMBAD database, operated at CDS, Strasbourg, France

References:

Losse, Florent (2016), Reduc Software, http://www.astrosurf.com/hfosaf/uk/tdownload.htm#reduc# Schlimmer, S. Joerg (2023), A High Contrast Double Star Filter (HCDSF),

Measurements of 93 Large Delta Magnitude Double Stars with HCDSF instrument, Part 2 from 2023.500 - 2023.999

Joerg S. Schlimmer 64342 Seeheim-Jugenheim, Germany Email: js@epsilon-lyrae.de

Abstract

This report shows the results of 93 double star measurements made with the High Contrast Double Star Filter instrument (HCDSF). During the observations a few new optical components and one possible new double star were found.

1. Introduction

In a previous article a special filter for measurements of high contrast double stars (HCDSF) was introduced and described in detail (Schlimmer, 2023). For the observations an extract of the WDS catalog was compiled first. The WDS catalog was downloaded and imported in an Excel file. To select the target stars some filter criteria were used:

Coordination : Declination > 0

• Separation : ≥ 6 "

• Secondary magnitude : ≤ 12

• Delta magnitude : ≥ 3

With these criteria a list of 2241 doubles stars was compiled for possible observations. Some of these stars were be picked up and marked in the Redshift Planetary software as target. The Redshift Planetary software will be used for mounting control.

After two month of testing and optimization in January and February the HCDSF instrument was transitioned to standard operating mode. This contribution is part 2 of the measurements and covers the time from 2023.500 to 2023.999.

2. Equipment and Methods

For observations a 12-inch Newtonian telescope was used. Focal length is 1500 mm. For the measurement of double stars with large magnitude differences, the HCDSF instrument was mounted on an ocular adapter. In the back focus of the HCDSF instrument a QHY 5-II color CMOS camera was mounted. Image scale is about 0.44 arc seconds per pixel.



Figure 1: High Contrast Double Star Filter (HCDSF) instrument, ocular sleeve and filter unit in foreground, optical unit and CMOS camera in background. The filter unit consist of a polarization foil F1 and a polarization stripe F2.

The measurements were done in same way as other double stars observations without the HCDSF instrument. For each double star a video with 5 up to 200 frames was recorded. The number of frames depends on the needed exposure time. In general, the longer the exposure time the fewer numbers of frames are recorded. Every frame of the video is like a single measurement. For data analyses REDUC software (Losse, 2016) was used. For each frame, separation and position angle will be automatically analyzed by the ELI interface. The standard deviation for measurements of the separation is usually smaller than \pm 0.15 arc seconds. The standard deviation for measurements of the position angle depends on the separation of both components. For double stars with separation of about 5 arc seconds the standard deviation for position angle is usually \pm 1 degree.

3. Data

During the measurements new components of v1 CrB and β Lyr were found and will be discussed below. Also, a new double star in the neighborhood of 61 Cygni was found. Its nature is still uncertain.

3.1 New component of v1 CrB, WDS16224+3348, STFA 29, H N 81

In SIMBAD data base v CrB is listed as carbon star with C6 spectrum. In the WDS catalog it is listed as a red giant with a M2IIIab spectrum. The brightness of v CrB is 5.39 mag. At a separation of 355 arc seconds, an optical companion with 8.45 mag is known as STFA 29B (figure 2a). At a separation of 68 arc seconds component C could be found. This pair is already known as H N 81AC. Brightness of component C is 12.62 mag. A fourth component D is also known as STFA 29AD. Its brightness is 11.53 mag.

During my observations I found another component much closer to A at a separation of only 11.78 arc seconds (identified as "STFA 39A(1)" in Table 1). Its brightness is about 14 mag, so the contrast to A is 8.5 mag. Figure 2b shows only the neighborhood of the primary component A, which is covered by the filter F2 of the HCDSF instrument (Schlimmer, 2023). With the HCDSF instrument the brightness of A can be strongly reduced, so the new component outside the filter stripe F2 can be better observed.

Nevertheless, exposure time of each frame was 4 seconds. Finally the contrast of the image was reinforced. That's why a lot of noise caused by hot pixels can be seen.

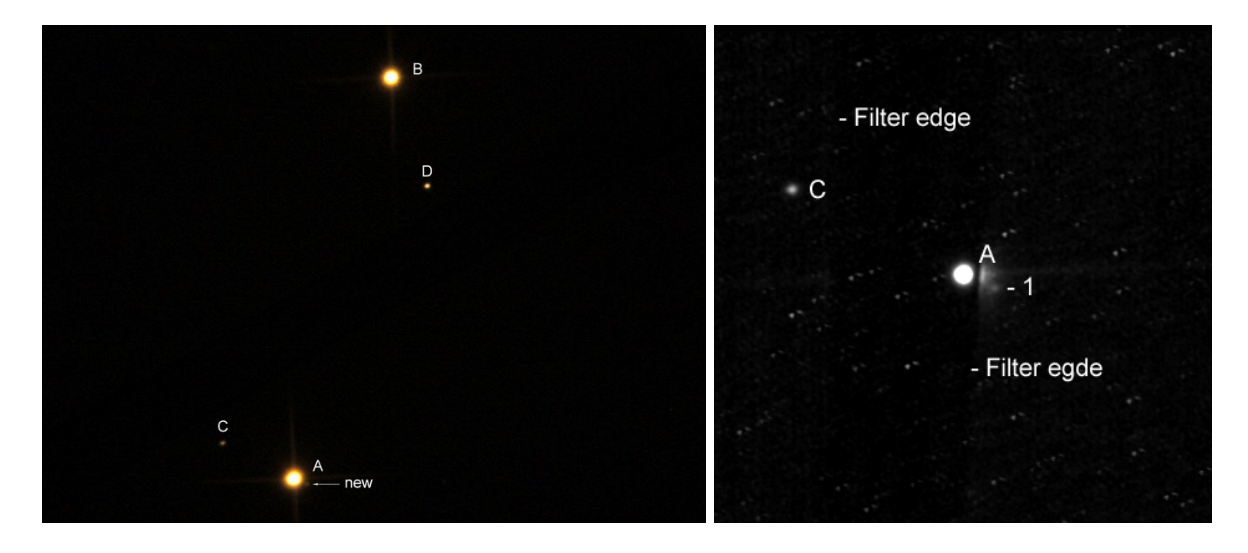


Figure 2a shows an 1280 x 960 pixel image of v CrB. Exposure time of each frame was 8s. The image is the result of 5 stacked images including dark frame correction. The image was made without HCDSF. Figure 2b shows the new component (1) next to A. Brightness of component A was strongly reduced by the HCDSF.

3.2 New component of β Lyr, WDS18501+3322, STFA 39AB

STFA 39AB is a wide pair with separation of about 45 arc seconds. The brightness of component A is 3.63 mag, brightness of component B is 6.69 mag. Due to similar parallax and proper motion of AB it could be accepted that STFA 39AB is a physical double star. On the other hand, all the other components are optical companions. Figure 3 shows an image of 26 stacked frames. Exposure time of each frame was 2 seconds. Components A, B and E are covered by filter F2 of the HCDSF instrument, so their brightness are reduced by 4 to 5 mag. Component C has a brightness of only 13.0 mag. In distance of 92.29 arc seconds at position angle of 175.4 degree a further optical component was found (identified as "BU 293A(1)" in Table 1). Its brightness is only 14.95 mag (GAIA3 DR3).

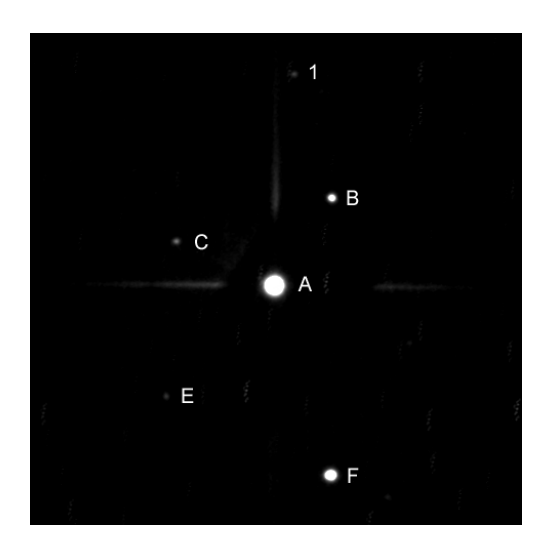


Figure 3 shows STFA 39 with new optical component (1). The image is a result of 26 stacked frames. Exposure time for each frame was 2s.

3.3 New double star next to 61 Cygni

61 Cygni is a well-known double star. Only both bright components AB are of physical nature. Stars in the neighborhood are only optical companions and aren't physically related to the AB components. At a separation of 184 arc seconds at position angle of 241 degree a new faint double star was found. The new double star is labeled as "New double" at the end of table 1. Its brightness can be estimated at 13.5 mag. The difference in brightness between the primary and the secondary component is 0.4 mag. Its separation is 2.24 arc seconds at position angle of 183.9 degree.

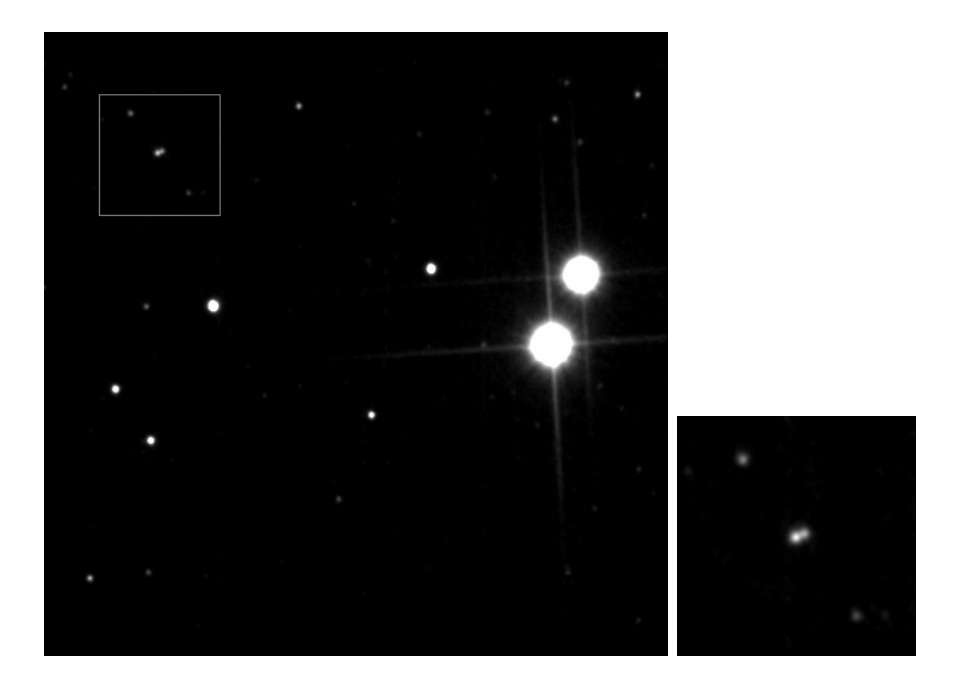


Figure 4a shows 61 Cygni with new double star in the neighborhood. Figure 4b shows a double magnification of the square in 4a. Exposure time was 1s.

3.4 Data

Table 1 shows the results of the 93 measurements with the HCDSF instrument from 2023.500 - 2023.999. The brightness was taken from WDS catalog. Dm is the difference in magnitudes between the primary and secondary component. Average of dm is 6.26 magnitudes. N is the number of observations. Usually, every double star will be observed only one time. Date is given in Julian date (JD).

Table 1 : Results of 93 double star measurements made with the High Contrast Double Star Filter (HCDSF) from 2023.500 - 2023.999

RA+DEC	Code	Magnitudes	dm	PA	SEP	Date	N	Notes
15127+48	35 ES 2648AB	7.28,11.25	3.97	340.7	26.35	2023.512	1	
15127+48	35 CTT 14AD	7.28,11.21	3.93	60.4	109.68	2023.512	1	
15193+01	46 STF1930AB	5.06,10.11	5.05	35.1	11.39	2023.512	1	
15232+30	17 STF1937AB,C	4.98,13.35	8.37	357.2	76.7	2023.512	1	
15249+58	58 BUP 162	3.42,8.87	5.45	48.8	252.56	2023.512	1	
15303+27	39 STF1951	7.89,11.88	3.99	293.7	17.58	2023.512	1	
15348+25	00 STT 297	8.3,12.0	3.7	332.6	13.89	2023.512	1	
15402+12	03 STT 300	6.32,10.07	3.75	260.9	14.98	2023.512	1	
15440+02	31 A 2230AC	5.95,9.23	3.28	207.8	191.92	2023.515	1	

45440.0004		5 05 40 05		205.0	472.04	2022 545		1
15440+0231	A 2230AD	5.95,10.95	5.00	285.0	172.84	2023.515	1	
15443+0626	HJ 1277AB	2.65,11.8	9.15	332.0	57.86	2023.515	1	
15462+1525	STF1970AB	3.66,9.96	6.3	263.7	30.30	2023.515	1	
16010+3318	S 676	5.47,10.51	5.04	44.5	147.80	2023.515	1	
16052+2211	BU 811AC	8.71,11.92	3.21	307.3	114.60	2023.515	1	
16105+4748	STT 307	7.67,10.71	3.04	201.3	17.48	2023.539	1	
16118+4222	STF2024	5.86,10.73	4.87	44.0	23.22	2023.539	1	
16143-0342	BUP 164AB	2.90,13.4	10.5	307.9	68.35	2023.515	1	
16219+1909	SHJ 227AB	3.76,10.05	6.29	226.5	43.27	2023.539	1	
16224+3348	H N 81AC	5.39,12.62	7.23	241.4	68.36	2023.611	2	
16224+3348	STFA 39A(1)	5.39,13	6.14	65.0	11.78	2023.611	2	v1 CrB
16224+3348	H 6 18BD	5.58,11.53	5.95	16.3	98.30	2023.539	1	
17016+1457	H 4 122	6.28,10.27	3.99	237.8	18.73	2023.682	1	
17146+1423	STF2140AB	3.48,5.40	1.92	103.4	4.72	2023.539	1	without F2
17150+2450	STF3127AB	3.12,8.3	5.18	292.7	13.97	2023.679	1	
17150+2450	STF3127AC	3.12,10.45	7.33	352.8	175.48	2023.679	1	
17150+2450	STF3127AD	3.12,10.59	7.47	89.4	191.62	2023.679	1	
17209+2430	S 687AB	5.12,9.33	4.21	55.5	223.26	2023.679	1	
17237+3709	STF2161AB	4.50,5.40	0.9	320.3	3.94	2023.682	1	
17328+4753	STF2189AB	7.83,11.24	3.41	97.4	20.89	2023.682	1	
17328+4753	STF2189AC	7.83,8.94	1.11	357.5	65.70	2023.682	1	
17346+0935	STFA 34AB	5.80,7.50	1.7	189.7	41.14	2023.679	1	
17395+4600	BU 1459AB	3.76,11.80	8.04	47.6	117.2	2023.682	1	
17479+3417	STT 336AD	6.58,10.64	4.06	162.7	41.17	2023.682	1	
17566+5129	BU 633AB	2.23,13.4	11.17	151.1	20.28	2023.682	1	
17566+5129	BU 633AD	2.23,12.9	10.67	9.8	58.71	2023.682	1	
17566+5129	BU 633AE	2.23,11.9	9.67	233.0	94.68	2023.682	1	
17566+5129	BU 633AF	2.38,11.67	9.29	112.4	124.65	2023.682	1	
17566+5129	BU 633AG	2.38,11.23	8.85	25.5	142.30	2023.682	1	
18011+4521	STF3129	7.59,10.64	3.05	166.7	30.38	2023.682	1	
18058+2127	STT 341AB,C	7.20,10.56	3.36	171.1	28.37	2023.693	1	
18058+2127	STT 341AB,D	7.20,10.48	3.28	100.8	39.44	2023.693	1	
18058+2127	STT 341AB,E	7.20,10.25	3.05	37.5	66.45	2023.693	1	
18058+2127	STT 341AB,G	7.20,7.64	0.44	238.1	132.48	2023.693	1	
18088+2049	AGC 8	4.36,11.8	7.44	136.7	23.07	2023.682	1	
18181+2318	BUP 181AB	6.68,11.5	4.82	222.4	37.45	2023.693	1	
18181+2318	BUP 181AC	6.68,10.04	3.36	124.9	152.98	2023.693	1	
18312+6526	KUI 86	6.64,10.47	3.83	41.9	22.26	2023.693	1	
18369+3846	H 5 39AB	0.09,9.5	9.41	184.8	84.87	2023.742	2	
18369+3846	STFB 9AC	0.09,11.0	10.91	252.1	79.40	2023.725	3	
18369+3846	STFB 9AE	0.09,9.5	9.41	39.0	83.36	2023.742	2	
18369+3846	SMR 33AP	0.09,12.	1.91	84.9	218.40	2023.685	2	
18369+3846	SMR 33AQ	0.09,12.	11.91	120.5	167.20	2023.683	1	
18369+3846	SMR 33AR	,	11.91	263.0	181.69	2023.685	2	
		0.09,12.		244.6				
18369+3846	SMR 33AT	0.09,12.	11.91		222.36	2023.685	1	
18426+5532	H 6 37AB	5.01,11.04	6.03	156.0	146.52	2023.693	1	
18443+3940	STFA 37AI	5.15,10.12	4.97	136.6	149.98	2023.693	1	CE not CD E !
18443+3940	SHJ 277CD,F	4.56,12.7	8.14	358.5	91.47	2023.682	1	CF not CD, F!
18443+3940	SHJ 277CD,G	4.56,14.2	9.64	289.8	74.68	2023.682	1	CG not CD,G!
18443+3940	SHJ 277CD,H	4.56,13.9	9.34	310.6	94.86	2023.682	1	CH not CD,H!
18443+3940	STF2383CE	5.25,12.3	7.05	332.2	61.84	2023.682	1	
18443+3940	STFA 37CI	5.25,10.12	4.87	36.2	120.28	2023.682	1	
18443+3940	SHJ 277EF	12.3,12.7	0.4	36.0	45.31	2023.682	1	

18499+3233	HO 440	5.25,12.7	7.45	174.6	18.29	2023.693	1	
18501+3322	STFA 39AB	3.63,6.69	3.06	147.6	45.54	2023.685	2	
18501+3322	BU 293AC	3.63,13.0	9.37	246.5	46.64	2023.682	1	
18501+3322	BU 293AE	3.63,10.14	6.51	316.6	67.06	2023.685	2	
18501+3322	BU 293AF	3.63,10.62	6.99	17.5	85.74	2023.685	2	
18501+3322	BU 293A(1)	3.63,14.95	11.32	175.4	92.29	2023.682	2	bet Lyr
18546+3656	ELS 7AB	13.6,13.8	0.2	338.2	8.47	2023.693	1	next to del Lyr
19307+2758	STFA 43AB	3.19,4.68	1.49	53.4	34.49	2023.693	1	bet Cyg
19307+2758	WAL 114AC	3.19,10.99	7.8	339.3	64.79	2023.693	1	bet cyg
19307+2758	CTT 17AD	3.19,12.24	9.05	31.6	107.05	2023.693	1	
	CTT 17AD	•	8.62	205.3	76.08		1	
19307+2758 19307+2758	SMR 34AG	3.19,11.81	9.31	43.9	161.2	2023.693	1	
		3.19,12.5						
19307+2758	SMR 34AH	3.19,12.5	9.31	118.2	53.88	2023.693	1	
19307+2758	SMR 34AI	3.19,12.5	9.31	131.6	37.38	2023.693	1	
19307+2758	SMR 34AJ	3.19,10.	6.81	209.0	139.09	2023.693	1	
19307+2758	SMR 34AK	3.19,11.5	8.31	276.4	142.0	2023.693	1	
19379+4917	HJ 1428AB	6.60,10.19	3.59	230.1	36.36	2023.805	1	
19379+4917	HJ 1428AC	6.60,10.97	4.37	242.8	64.95	2023.805	1	
19379+4917	HJ 1428BD	10.19,13.8	3.61	272.3	10.90	2023.805	1	
20136+4644	HJ 1495AB	3.93,13.4	9.47	327.4	36.23	2023.805	1	
20136+4644	STFA 50AC	3.93,6.97	3.04	173.0	106.66	2023.805	1	
20136+4644	BU 1483AF	3.93,13.9	9.97	168.0	43.43	2023.805	1	
20136+4644	BU 1483CG	6.97,14.2	7.23	94.7	37.52	2023.805	1	
20136+4644	ES 26DE	4.83,13.2	8.37	248.9	36.7	2023.682	1	
21069+3845	STF2758AB	5.20,6.05	0.85	153.8	32.02	2023.789	1	without HCDSF
21069+3845	STF2758AH	5.35,9.97	4.62	260.3	143.3	2023.805	1	
21069+3845	SMR 1AI	5.35,10.74	5.39	234.7	59.89	2023.805	1	
21069+3845	SMR 40AO	5.35,12.65	7.3	272.7	184.38	2023.805	1	
21069+3845	SMR 40AP	5.35,12.84	7.49	280.3	173.42	2023.805	1	
21069+3845	SMR 40AQ	5.35,13.19	7.84	288.2	81.40	2023.805	1	
21069+3845	New double	13.5,13.9	0.4	113.2	2.24	2023.805	1	d mag =0.4

4. Conclusion

As expected, the measurements have shown that the filter is accurate across a wide range of temperature changes. The temperature range during the observations was from 4°C in Winter to 20°C in Summer. No focus adjustments were needed. The stability was possible thanks to the carbon fiber reinforced plastic tubes.

Due to simultaneous reduction of brightness of close double stars, faint companions could be measured with greater accuracy. For example in epsilon Lyrae the components CF, CG and CH could be measured directly instead of measurements of CD-F, CD-G and CD-H.

Disadvantage of usage the HCDSF instrument is the longer exposure time. Especially in Sommer the S/N of the QHY 5-II color CMOS isn't good by exposure times more than 1s.

Acknowledgements:

This research has made use of the Washington Double Star Catalog maintained at the U.S. Naval Observatory.

This research has made use of the SIMBAD database, operated at CDS, Strasbourg, France

References:

Losse, Florent (2016), Reduc Software, http://www.astrosurf.com/hfosaf/uk/tdownload.htm#reduc#

Gaia Collaboration et al. (2016b): The Gaia mission (provides a description of the Gaia mission including spacecraft, instruments, survey and measurement principles, and operations); https://www.cosmos.esa.int/web/gaia/home

Gaia Collaboration et al. (2023j): Gaia DR3: Summary of the contents and survey properties. https://www.cosmos.esa.int/web/gaia/data-release-3

Schlimmer, S. Joerg (2023), A High Contrast Double Star Filter (HCDSF), Journal of Double Star Observations, Vol. 19 No 3 July 16, 2023 Page 284-294

Astrometric Measurements of 3 Binary Star Systems: WDS 00033+5332, WDS 05283+0358, and WDS 19557+3805

Joshua Lo, Aidan Lindhe-Johan, Aenea Briggs, Noah Smith, Sabrina Stierwalt Occidental College, Los Angeles, CA; contact: loj@oxy.edu

Abstract

We have taken astrometric measurements of three star systems: WDS 00033+5332 A 1500 AB,C, WDS 05283+0358 HJ 2266, and WDS 19557+3805 DAM 1 AB. We used the Las Cumbres Observatory telescopes to take images of these star systems, and we then analyzed them using Afterglow Workbench. For WDS 00033+5332, we found the position angle to be $81.62^{\circ} \pm 0.45^{\circ}$ and an angular separation of $9.01^{\circ} \pm 0.04^{\circ}$. Based on our analysis, we were not able to determine whether the WDS 00033+5332 double is physical. For WDS 05283+0358, we found the position angle to be $37.58^{\circ} \pm 0.15^{\circ}$ and an angular separation of $7.29^{\circ} \pm 0.04^{\circ}$. It is already known that WDS 05283+0358 is a physical double, and our new data supports this claim. For WDS 19557+3805, we found the position angle to be $234.64^{\circ} \pm 0.63^{\circ}$ and an angular separation of $6.89^{\circ} \pm 0.10^{\circ}$. Our new data points suggest this system is gravitationally bound

1. Introduction

In this paper we found astrometric measurements of three binary star systems: WDS 00033+5332 A 1500 AB,C, WDS 05283+0358 HJ 2266, and WDS 19557+3805 DAM 1 AB. Our goal was to provide more current measurements on these star systems so we can better understand their orbits. None of these systems have been measured in the last seven years, so this new information will give us a better understanding of these star systems.

We utilized the Stelle Doppie database¹ to search the Washington Double Star (WDS) catalog (Mason et al. 2001) for star systems in which there was a significant change in the position angle and separation from the first measurement to the most recent. We also wanted to find a system that hadn't been measured since 2015 or earlier, so that we could provide information on a star that hadn't been studied in a while.

Since the discovery of WDS 00033+5332 A 1500 AB,C in 1917 (Aitken 1932), there have been a total of seven measurements. The primary star has a spectral class of A3. This star system is composed of three stars, however, since stars A and B are so close in space, they cannot be resolved by our observations. Thus, we treat the combination of these as a primary star of magnitude 9.29, and star C as the secondary star of magnitude 13.10. In 1917, the first recorded angular separation was 8.60 arcseconds and the position angle was 78.6°. The most recent measurements were in 2014, and the angular separation was 9.394 arcseconds and the position angle was 82.05° (Zacharias et al. 2015). The physical nature of this binary is not known.

WDS 05283+0358 HJ 2266 was discovered nearly 200 years ago in 1830 (Herschel 1833). Since then, 8 other measurements have been taken bringing the total number of measurements to 9. Using these measurements, it has been determined that this is a physical binary system based on the Common Proper Motion of the binary. The data in this collection is meant to provide data to support a more complete picture of the movement of the system.

¹ https://www.stelledoppie.it/

The binary system WDS 19557+3805 DAM 1 AB was first discovered in 1998 (Skrutskie et al. 2006). Since its discovery there have been 7 other measurements that have been made. This double is a part of a quintuple system, however the nature of this double is uncertain. The first recorded separation and position angle were 7.22 arcseconds and 232.7° respectively. The current measurements are 6.641 arcseconds and 236.62° (Zacharias et al. 2015).

2. Equipment and Methods

In order to get the images of our star systems, we used the Las Cumbres Observatory (LCO), which is a network of 25 telescopes at multiple sites around the world. These can be controlled remotely, and because of this, our images were taken at different locations. However, the images were all taken using the same instrument, a 0.4-m telescope, with an SBIG STL6303 camera to capture the images. The images for WDS 00033+5332 and WDS 19557+3805 were taken by a telescope at LCO's Haleakala site in Hawaii. The images for WDS 05283+0358 were taken in Cerro Tololo, an observatory in Chile. For all our images, we used a Bessel V filter.

To ensure that we used an optimal exposure length for our systems, we used test images so that if they were either undersaturated or oversaturated, we could adjust our exposure length to get better results. Some of the star systems had primary and secondary stars with similar magnitudes, so it was easier to choose an exposure. However, for the star systems with larger changes in magnitude between the stars, we had to be careful to choose an exposure that allowed us to accurately see the secondary star without oversaturating the primary star. For WDS 19557+3805, we used an exposure time of 3s, for WDS 00033+5332 we used a 2s exposure, and for WDS 05283+0358 we used an exposure of 4s. After submitting our test images and determining a good exposure to use, we requested 10 images of each star.

After, retrieving our calibrated images from the LCO database, we used Afterglow Workbench² to analyze our images. Specifically, we used Afterglow to measure the angular separation between our primary and secondary stars and the position angle of the stars. After recording the data, we calculated the mean, standard deviation, and standard error of the mean for each star system. We were also able to obtain historical data about the star systems by requesting data through Dr. Rachel Matson from the Washington Double Star Catalog (Mason et al. 2001).

3. Data

Data for each star was collected by the LCOGT 0.4 m telescopes SBIG 6303 CCD camera with a Bessell-V filter. The FITS were reduced by LCOGT using the BANZAI pipeline to calibrate the images. During processing many tasks were performed including bad-pixel masking, bias subtraction, dark subtraction, and flat field division. The data was then analyzed in Afterglow Workbench to find the separation and position angle data for each of the binary systems. An example of these measurements is given in Fig 1.

² https://afterglow.skynetjuniorscholars.org

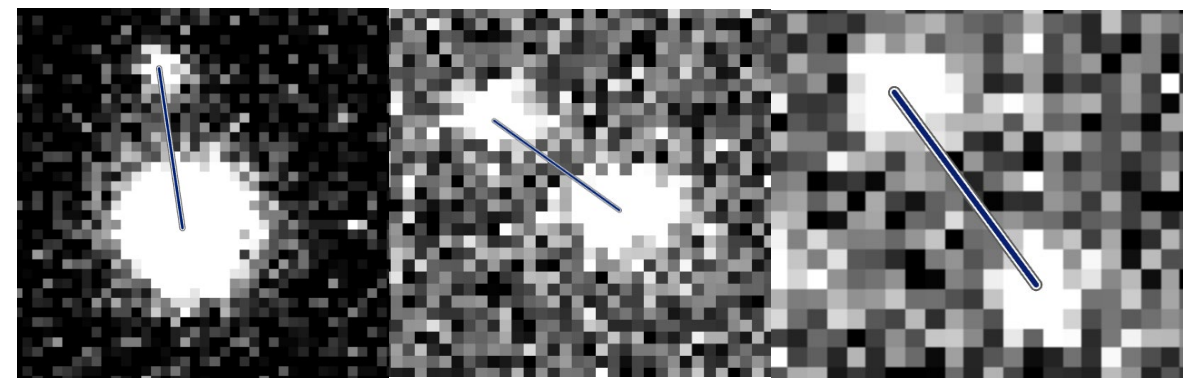


Figure 1. Example of a measurement image for WDS 00033+5332 A 1500 AB,C on the left, WDS 05283+0358 HJ 2266 in the middle and WDS 19557+3805 DAM 1 AB on the right.

Table 1. New Measurements for 3 Binary Star Systems							
Binary System (WDS)	Observatory	Date of Observations	# of Images	Mean of PA(°)	Standard Deviation of PA	Standard Error of the Mean	
00033+5332	Haleakala	2023.11.17	9	81.62	1.35	0.45	
05283+0358	Cerra Tololo	2023.11.22	10	37.58	0.47	0.15	
19557+3805	Haleakala	2023.11.22	10	234.64	1.14	0.63	

Table 2. Separation for 3 Binary Star Systems							
Binary System (WDS)	# of Images	Mean of Separation (arcsec)	Standard Deviation of Separation	Standard Error of the Mean			
00033+5332	9	9.01	0.12	0.039			
05283+0358	10	7.29	0.14	0.04			
19557+3805	10	6.89	0.17	0.096			

4. Discussion

The historical data for Table 2, WDS 00033+5332 A 1500 AB,C, Table 3, WDS 05283+0358 HJ 2266, and for Table 4, WDS 19557+3805 DAM 1 AB, was requested from the U.S. Naval Observatory and provided from the Washington Double Star Catalog (Mason et al. 2001). The historical data for Table 2 consists of 7 data points starting in 1917.68 and ending in 2014.752. The historical data for Table 3 consists of 9 data points starting in 1831.09 and ending in 2015.0. The historical data for Table 4 consists of 6 data points starting in 1998.39 and ending in 2015.41. Each table shows the position angle (PA) in degrees, the separation (Sep) in arcseconds and the measurement method used for each binary star system.

The historical data for position angle and separation in Table 2, Table 3, and Table 4 were converted into x-y coordinates so that the data could be plotted using the following equations:

$$x(RA) = \rho cos\theta$$

 $y(DEC) = \rho sin\theta$

Where x is the right ascension and y is the declination, ρ is the angular separation and θ is the position angle. The date for each measurement is shown.

Table 3. Historical and Current Measurements of WDS 00033+5332 A 1500 AB,C								
Date	PA (deg)	Sep (arcsec)	x (RA, arcsec)	y (DEC, arcsec)	Source			
1917.68	78.6	8.60	1.70	8.43	Ma: Micrometer with refractor			
1928.77	79.2	8.90	1.67	8.74	Ma: Micrometer with refractor			
1998.85	81.4	9.34	1.26	8.34	E2: Two Micron All-Sky Survey			
2003.591	81.6	9.250	1.351	9.151	Eu P: UCAC3			
2012.797	82.16	9.307	1.281	9.303	Er: USNO URAT			
2013.74	81.90	9.330	1.325	9.311	Er: USNO URAT			
2014.752	82.05	9.351	1.300	9.303	Er: USNO URAT			
2023.879	81.61	9.013	1.313	8.915	P: Photographic Technique			

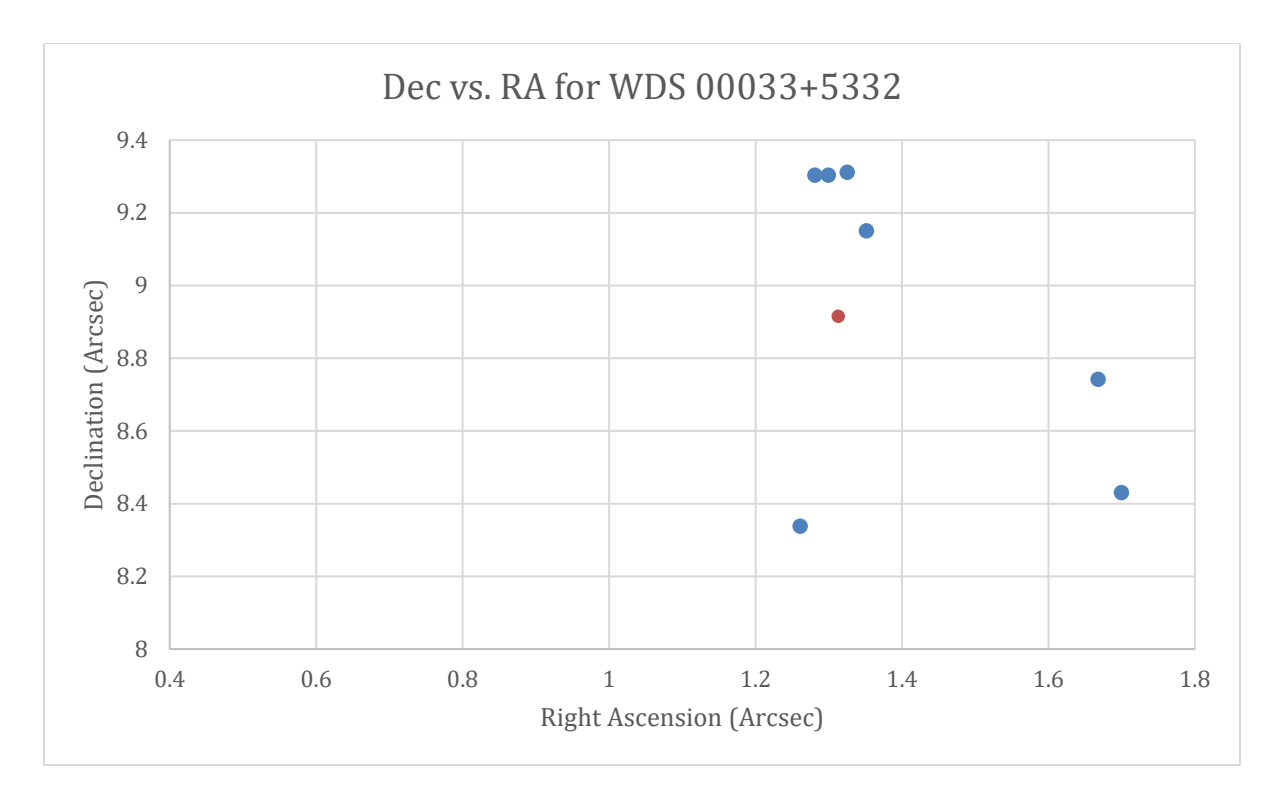


Figure 2. x(Right Ascension), and y(Declination) of the historical data (blue) and current data (orange)

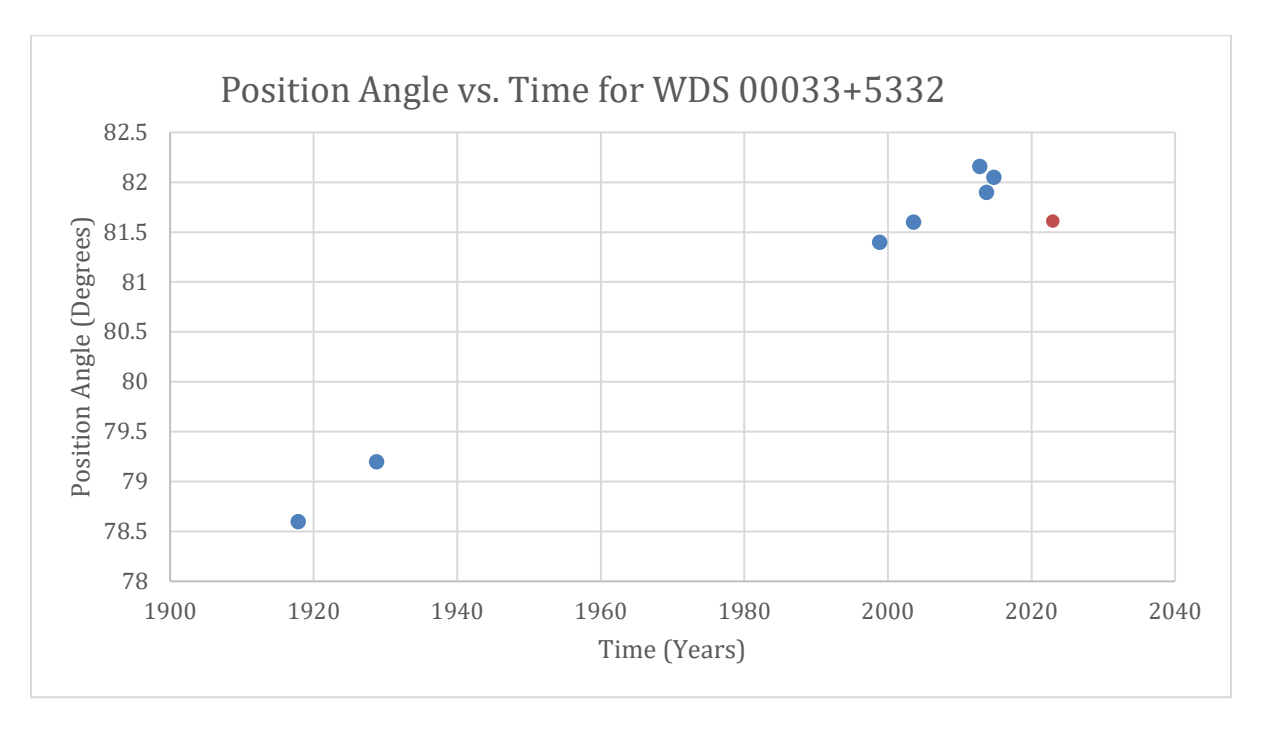


Figure 3. Position Angle vs. Time of the historical data (blue) and current data (orange)

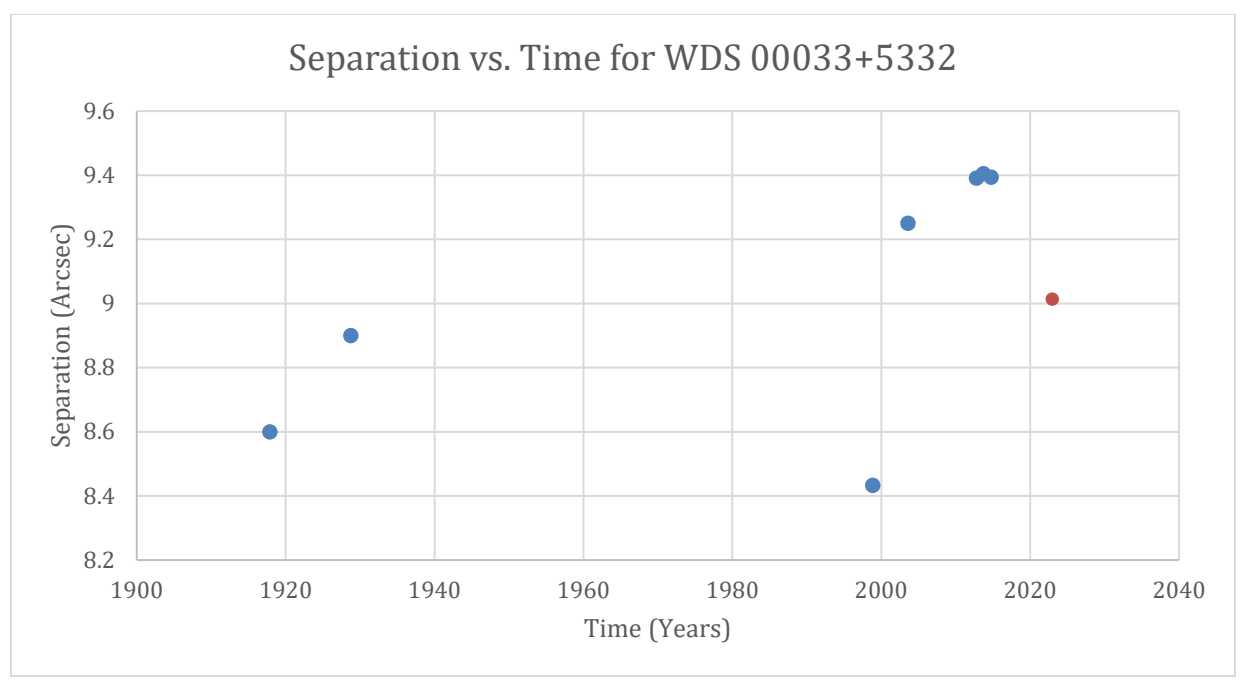


Figure 4. Separation vs. Time of the historical data (blue) and current data (orange)

For WDS 00033+5332, the position angle data (Figure 3) shows that the position angle has decreased from the 2015 measurement, after a steady increase from the first measurement in 1917. The separation data (Figure 4) shows that the separation seems to be increasing and decreasing with time. This cyclic variation could occur if the system was rotating in an ellipse, but such rotation is not consistent with the mostly steadily increasing position angle. If we decide the recent data points are more reliable than the pre-1930 data points, then the position angle traces out a clear arc with our new data point being the first along the return portion of the orbit. Similarly, if the 2MASS data point from 1998 is not considered due to its outlier status, the position angle would again trace out an orbit highly consistent with a physically bound pair. However, if we take all of the data equally, the decrease in both separation and position angle indicated by our new data point suggests the binary pair may be unphysical. Although this pair is likely unphysical, more observations on a longer timeline are needed to know for sure.

Table 4. Hi	Table 4. Historical and Current Measurements of WDS 05283+0358 HJ 2266								
Date	PA (deg)	Sep (arcsec)	x (RA, arcsec)	y (DEC, arcsec)	Source				
1831.09	43.8	4.0	2.77	-2.89	Mb: micrometer with reflector				
1910.14	41.8	7.987	5.32	-5.95	Pa: photographic, with astrograph				
2000.06	38.5	7.49	4.66	-5.86	E2: Two Micron All-Sky Survey				
2000.102	38.1	7.504	4.63	-5.91	Eu: UCAC				
2001.05	37.6	7.59	4.63	-6.01	C: CCD or other two-dimensional electron imaging				

2013.001	37.63	7.473	4.56	-5.92	Er: USNO URAT
2013.97	37.44	7.473	4.54	-5.93	Er: USNO URAT
2014.961	37.44	7.458	4.53	-5.92	Er: USNO URAT
2015.0	37.40	7.412	4.50	-5.89	Hg: Gaia
2023.89	37.58	7.2884	4.45	-5.77	P: Photographic Technique

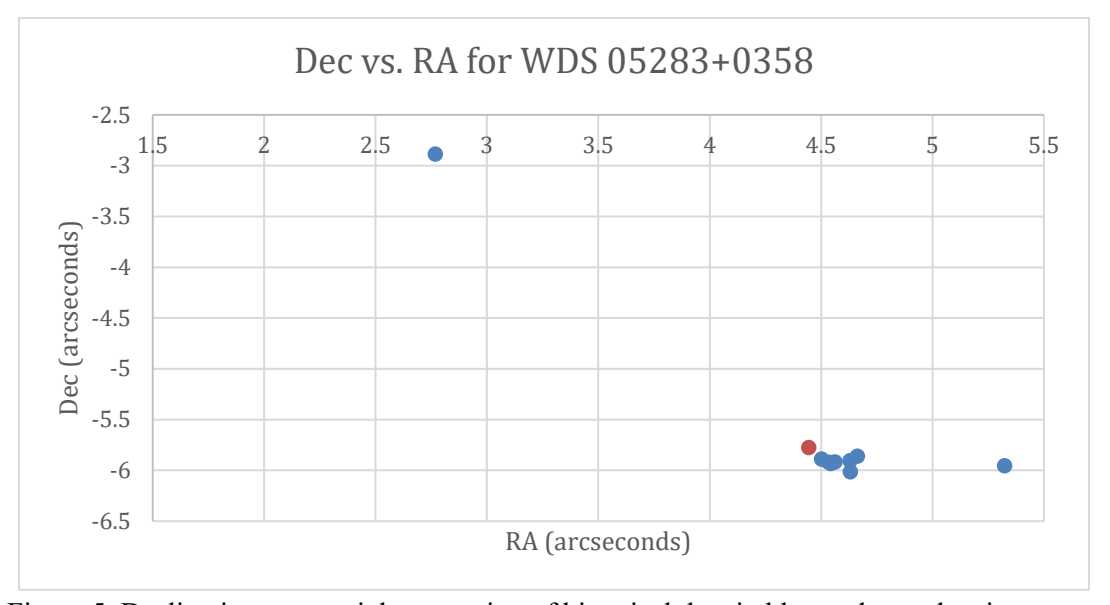


Figure 5. Declination versus right ascension of historical data in blue and new data in orange.

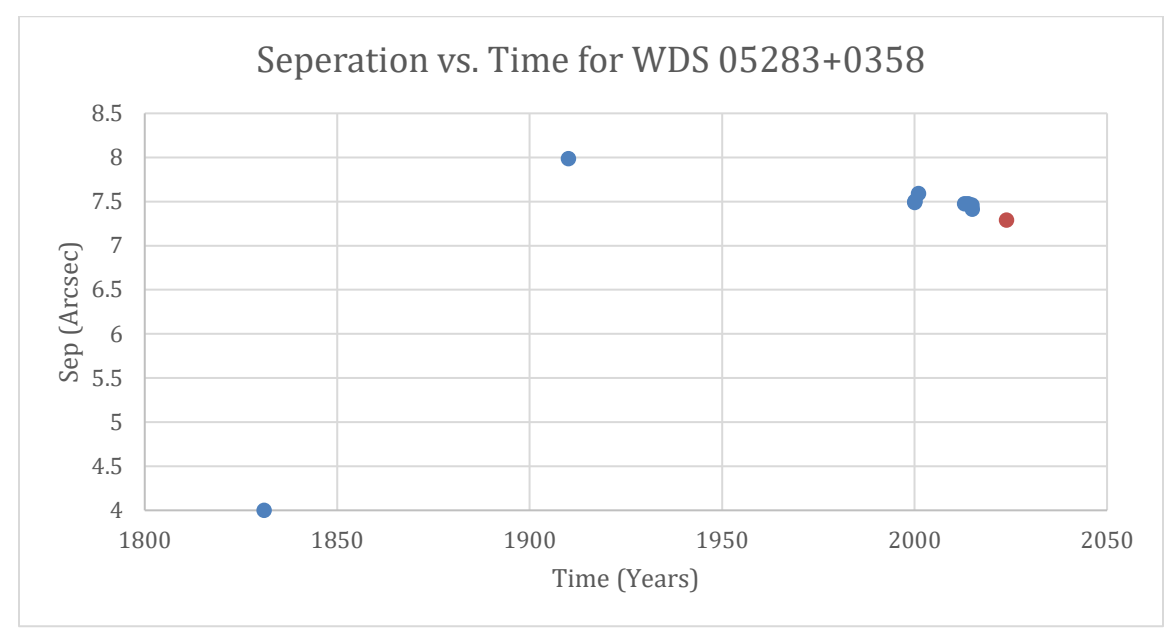


Figure 6. Separation vs. Time of the historical data (blue) and current data (orange).

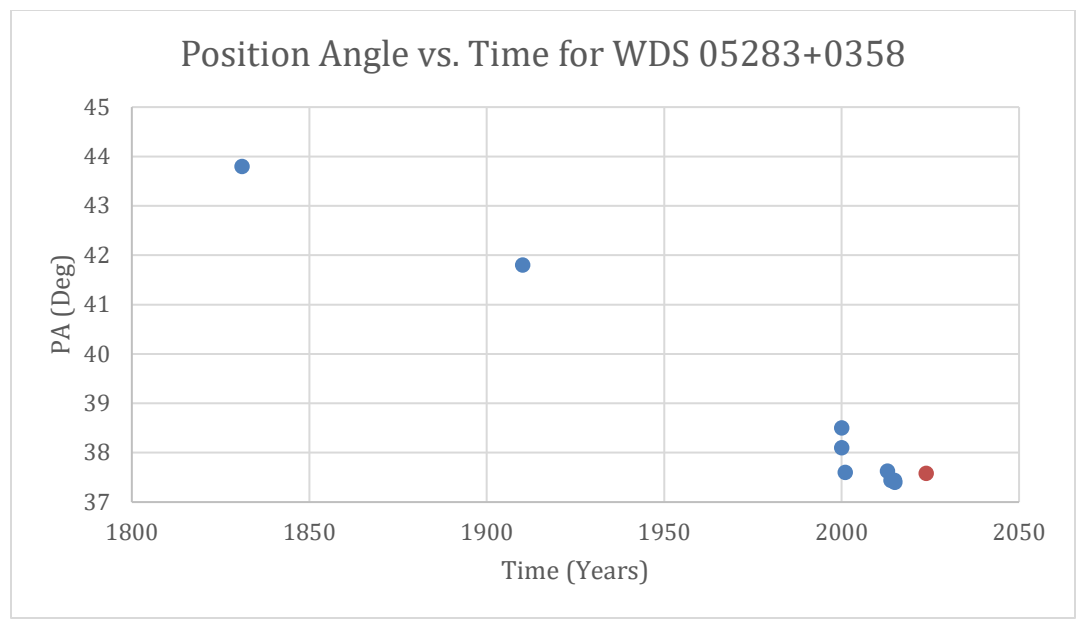


Figure 7. Position Angle vs. Time of the historical data (blue) and current data (orange).

WDS 05283+0358 is known as a physical binary thanks to the backlog of convincing historical data. The observations taken here agree with prior trends for the binary system indicating that the system is acting as expected of a physical double. The position data (Figure 5) indicates that the orbital pattern observed by the previous data points, especially those since 2000, has continued in a consistent manner. When examining the separation over time measurements (Figure 6) it appears that separation has increased since the early 1830s when the first measurement was taken but has come down since the early 1910s measurement. The new data point follows this downward trend which indicates that the binary is moving in an elliptical manner when viewed from Earth. The PA data (Figure 7) falls into the group of data points taken since 2000 that indicate a nearly linear relationship for the rotation of the star over time. None of these data points disagree with the expectation of a physical binary system and thus further support this classification. These new data points help further classify the orbital motion of the star for future study. They also prove the validity of our observation and analysis methods.

Table 5. Historical and Current Measurements of WDS 19557+3805 DAM 1 AB									
Date	ate PA (deg) Sep (arcse		x (RA, arcsec)	y (DEC, arcsec)	Source				
1998.39	232.7	7.22	-4.38	-5.743	E2: Two Micron All-Sky Survey				
2012.552	234.46	6.900	-4.011	-5.615	Er: USNO URAT				
2013.519	234.54	6.886	-3.995	-5.609	Er: USNO URAT				
2014.509	234.70	6.860	-3.964	-5.599	Er: USNO URAT				
2015.0	234.765	6.860	-3.958	-5.603	Hg: Gaia				

2015.410	234.70	6.881	-3.976	-5.616	Er: USNO URAT
2023.89	236.62	6.641	-3.654	-5.546	P: Photographic Technique

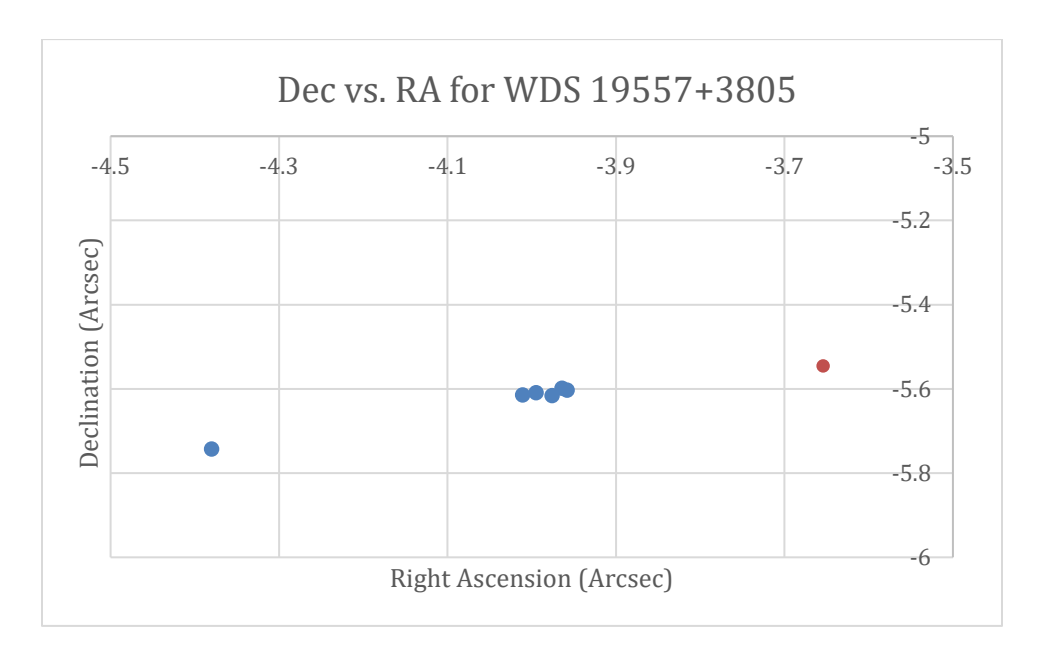


Figure 8. x(Right Ascension), and y(Declination) of the historical data (blue) and current data (orange)

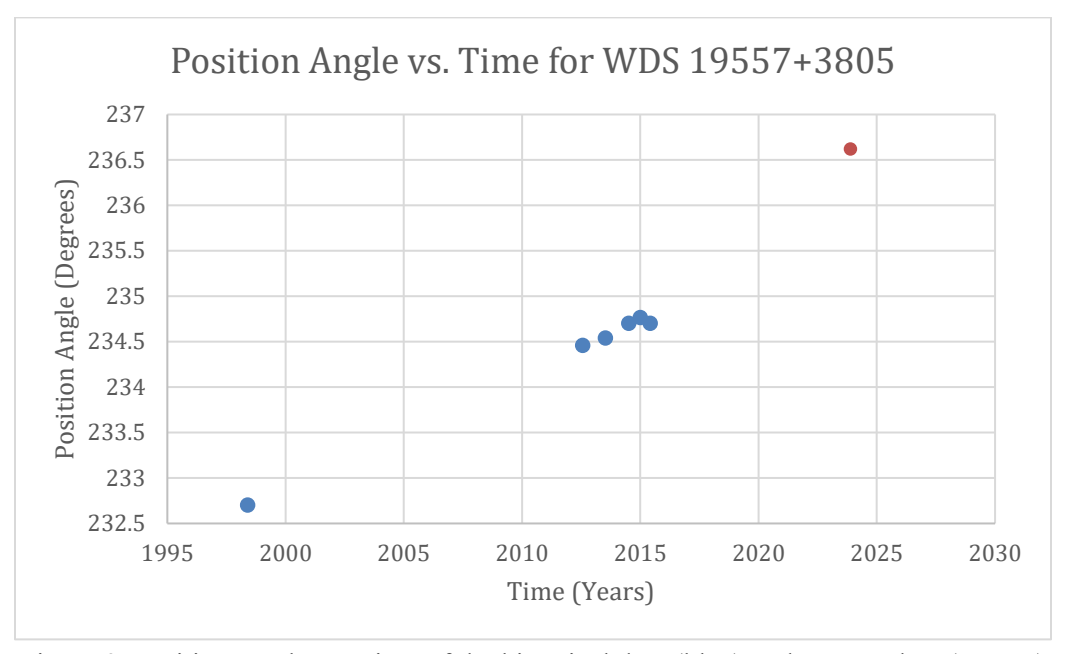


Figure 9. Position Angle vs. Time of the historical data (blue) and current data (orange)

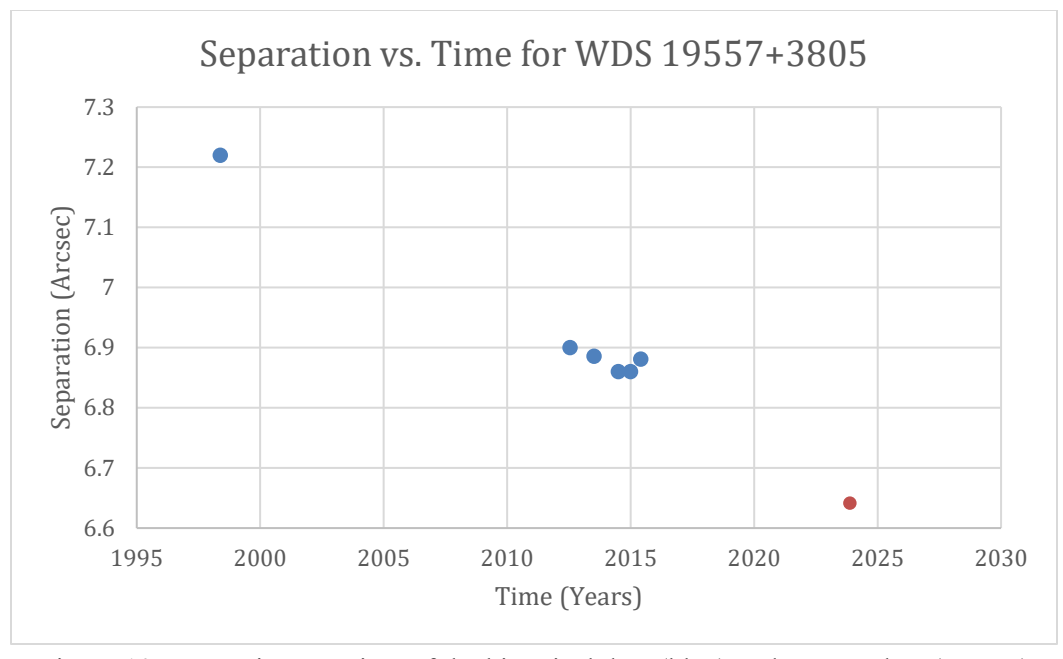


Figure 10. Separation vs. Time of the historical data (blue) and current data (orange)

WDS 19557+3805 appears to have a clear linear relationship when looking at both the position angle vs. time graph (Figure 9) and the separation vs. time graph (Figure 10). The position angle has been increasing steadily since the first measurement in 1998, and the data that we found continues this trend. The separation has been steadily decreasing since the first measurement when looking at the historical data, and the data point we found is consistent with this trend. Although it is currently uncertain if the system is gravitationally bound, our new observations strongly suggest that the system is physical because it seems as if these stars are indeed in an orbit.

Table 6. Parame	Table 6. Parameters from Gaia Data Release 3										
Binary System (WDS)	Star	Parallax (mas)	Distance (pc)	Proper Motion in RA (mas/year)	Proper Motion in Dec (mas/year)						
00033+5332	Primary	-1.7318 ± 0.8620		-8.1322 ± 0.6100	5.3859 ± 0.6702						
	Secondary	0.9505 ± 0.0112		5.8170 ± 0.0093	-4.5214 ± 0.0095						
05283+0358	Primary	0.5861 ± 0.0192	1700	6.9393 ± 0.0209	-5.0661± 0.0147						
19557+3805	Primary	0.1962 ± 0.0111		-2.9698 ± 0.0118	-4.6484 ± 0.0132						
	Secondary	1.5471 ± 0.0136	633	3.7568 ± 0.0135	20.7847 ± 0.0164						

In Table 6, we report the parallax and derived distance estimates for as many of our stars as are available in the Gaia Data Release 3 (Gaia Collaboration 2016b; 2023j). Parallax measurements can be used to rule out a physical double if the separation in distance is too large. However, incomplete Gaia data does not allow for this check for our three binary star systems. For WDS 00033+5332, Gaia gives a negative parallax for the primary star. Although negative parallaxes can be used statistically, they are not physical and thus cannot be easily interpreted for individual stars (Luri et al. 2018). A positive parallax is given for the secondary star, however, a distance isn't given for either star. Even with the parallax values for both stars, the distance can't be estimated due to incomplete photometry for the stars. As described by Luri et al. (2018), the determination of reliable distances requires more than simply inverting the parallax. For WDS05283+0358, parallax and distance estimates are only available for the primary star. For WDS 19557+3805, although parallax values are given for both stars, a distance is only estimated for the secondary due to incomplete photometry for the primary.

5. Conclusions

In this study, we were able to provide data points on the positions of three star systems: WDS 00033+5332 A 1500 AB,C, WDS 05283+0358 HJ 2266, and WDS 19557+3805 DAM 1 AB. By using the separation and position angle of each of these star systems and comparing them to historical data points, we were able to determine whether these systems are physical and gravitationally bound. We were not able to conclude whether WDS 00033+5332 is physical, so it will remain uncertain. WDS 05283+0358 is already known to be a physical double, and our new data point supports the idea that these stars are gravitationally bound. Our new data point strongly suggests that WDS 19557+3805 is physical.

Acknowledgements

This research has made use of the Washington Double Star Catalog maintained at the U.S. Naval Observatory.

This work has made use of data from the European Space Agency (ESA) mission Gaia (https://www.cosmos.esa.int/gaia), processed by the Gaia Data Processing and Analysis Consortium (DPAC, https://www.cosmos.esa.int/web/gaia/dpac/consortium). Funding for the DPAC has been provided by national institutions, in particular the institutions participating in the Gaia Multilateral Agreement.

This research has also made use of data provided by Stelle Doppie: https://www.stelledoppie.it

The authors would like to thank the Las Cumbres Observatory for the use of their observatories in gathering our data.

The authors would like to thank Dr. Rachel Freed for her help in gaining a better understanding of star doubles and for helping us gain access to the Las Cumbres Observatory

References

Aitken, R.G. (1932). Aitken Double Star Catalog. (1932QB821.A43)

Gaia Collaboration et al. (2016b). The Gaia mission. Astronomy & Astrophysics, 595, A1.

Gaia Collaboration et al. (2023j). Gaia DR3: Summary of the contents and survey properties. Astronomy & Astrophysics, 674, A1.

Herschel, J.F.W. (1833). Fifth Catalogue of Double Stars observed at Slough in the years 1830 and 1831 with the 20-feet Reflector, Memoirs of the Royal Astronomical Society, 6, 1.

Luri, X. et al. (2018). Gaia Data Release 2: Using Gaia parallaxes, Astronomy & Astrophysics, 616, A9. Mason, B.D. et al. (2001). The 2001 US Naval Observatory Double Star CD-ROM. I. The Washington Double Star Catalog. Astronomical Journal, 122, 3466. https://crf.usno.navy.mil/wds/

Skrutskie, M.F. et al. (2006). The Two Micron All Sky Survey (2MASS), Astronomical Journal, 131, 1163. Zacharias, N. et al. (2015). The First US Naval Observatory Robotic Astrometric Telescope Catalog. Astronomical Journal, 150, 101.

Biography

Joshua Lo, Aidan Lindhe-Johan, Aenea Briggs, and Noah Smith are physics students at Occidental College. Sabrina Stierwalt is a physics professor at Occidental College.

Exploring Binary Stars – Fundamental Systems in Astronomy: Observation of HD 80460

Merliz M. Pérez Vázquez¹, Ian M. Pérez López¹, Victoria A. González Claudio¹, David R. Padilla Oyola¹, Carmen A. Pantoja Pantoja¹, Mayra E. Lebrón Santos¹, Lisa Storrie-Lombardi², Edward Gomez², Alice Hopkinson², Rachel Freed³, Sabrina Stierwalt⁴

¹University of Puerto Rico-Río Piedras, San Juan, Puerto Rico; merliz.perez@upr.edu

²Las Cumbres Observatory; Goleta, California

³ InStAR; Arizona

⁴ Occidental College, Los Angeles, California

Abstract

We report the measurement of the position angle and separation for the double star system HD 80460. We made use of a 0.4m telescope from Las Cumbres Observatory (LCOGT) and a DeltaRho 350 + QHY600 camera. An analysis was made with the historical data from the Washington Double Star (WDS) catalog. A search was made with SIMBAD for spectral type, parallax, and proper motion for the double star.

1. Introduction

Double star systems have captured the attention of astronomers, scientists, and amateurs due to their peculiar formation and relative brightness and colors (e.g. Palencia et al. 2017). These double stars are fundamental to our understanding of the universe as they allow a way to determine the mass of the stars. The Stellarium planetarium allowed us to locate the constellations visible from our location and finally choose the double star to study. We used Stelle Doppie platform, to select the double star for our study. This program facilitates the selection of a double stars from the Washington Double Star (WDS) catalog.

To select the double star, we considered an apparent magnitude between 9 < m < 11 and $\Delta m < 3$. We selected HD 80460 which is in the majestic constellation of Ursa Major (basic properties are shown in Table 1). Figure 1 shows an image of the system from the Digitized Sky Survey taken from Stelle Doppie.

Table 1. HD 80460 coordinate and apparent magnitudes of the stars.

Double star name	RA (2000.0)	DEC (2000.0)	m_1	m_2
HD80460	09 ^h 22 ^m 35.60 ^s	+62° 50' 35.5"	10.04	10.30

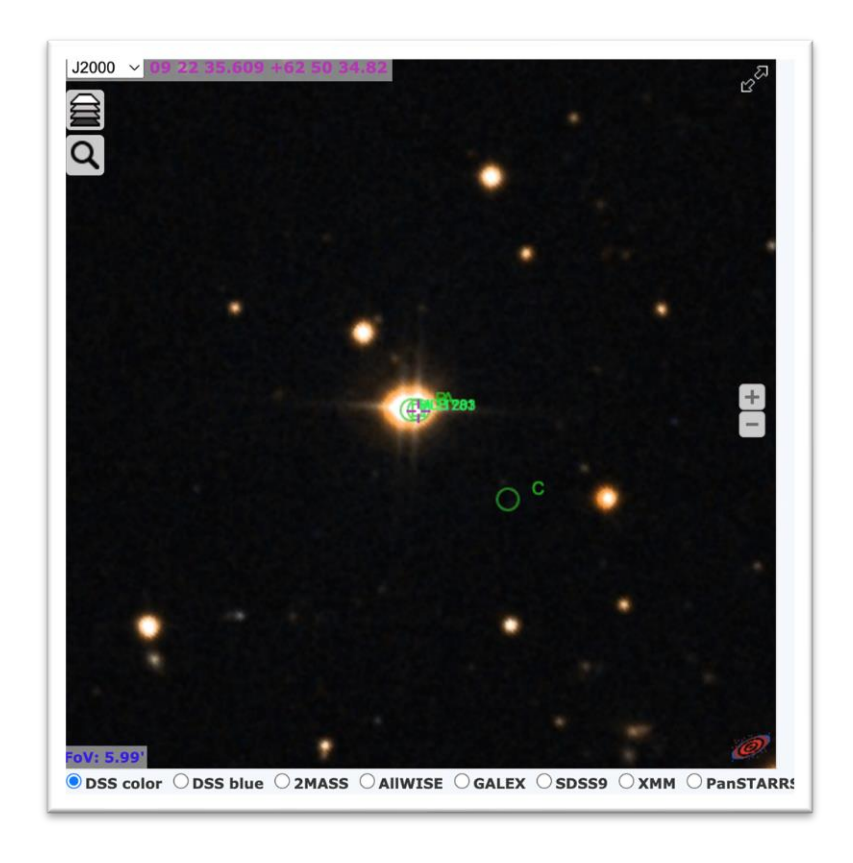


Figure 1: Image of HD 80460 from the Digitized Sky Survey (DSS)

2. Equipment and Methods

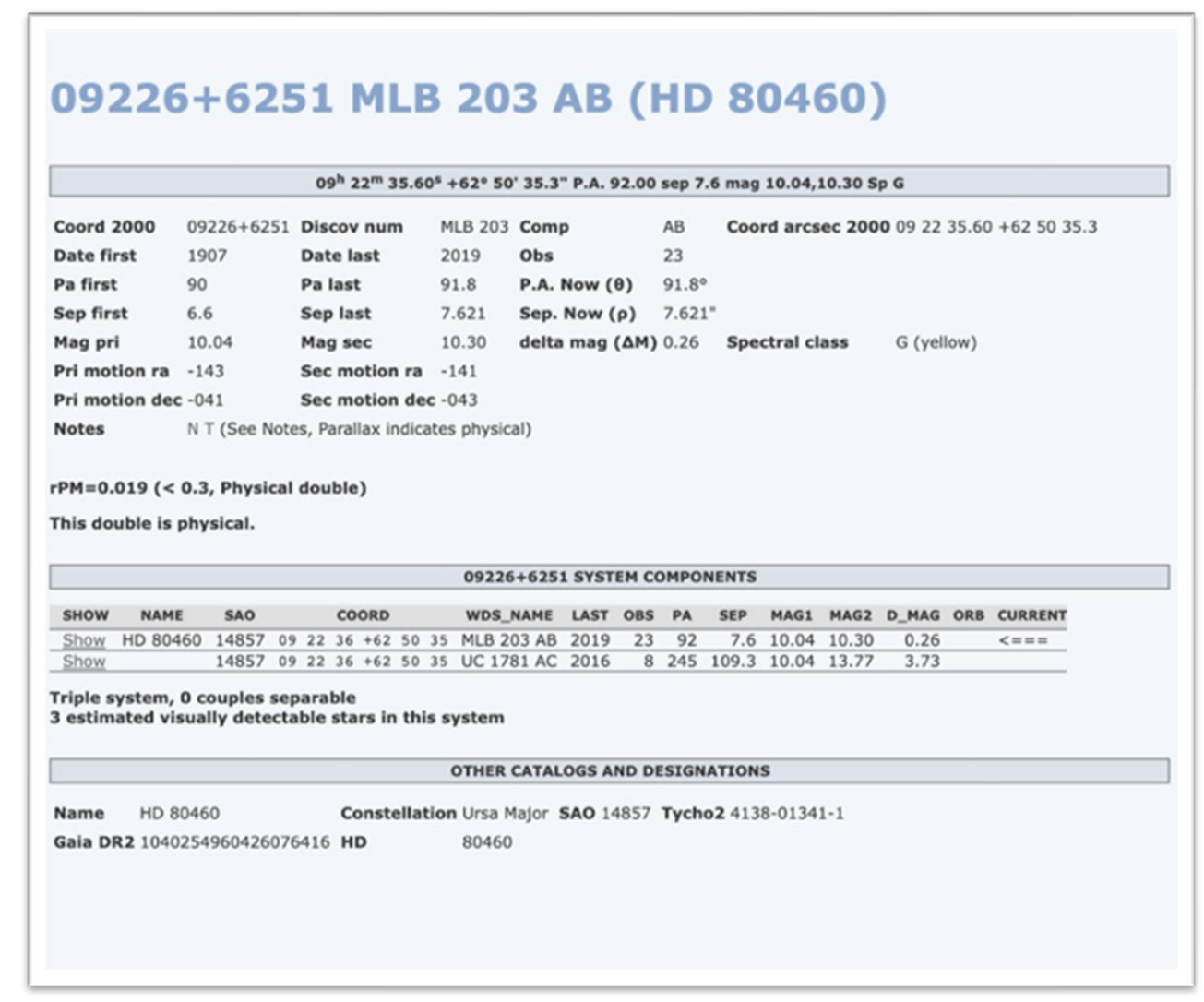
We used the following software for our research:

Stellarium:

Stellarium is a planetarium simulation program that offers an immersive experience for desktop computer users. With its advanced calculations, it can accurately determine the positions of celestial bodies such as the Sun, Moon, planets, constellations, and stars. Thanks to the Stellarium platform, we were able to locate the constellations visible from our location and ultimately choose our HD 80460 double star (Zotti, G., Wolf, A. 2022).

Stelle Doppie:

Stelle Doppie is a database with information from the renowned Washington Double Star Catalog and seamlessly integrates it with data from other credible astronomical sources. The platform's unique integration of data from multiple sources makes it a comprehensive and dependable resource for studying double stars. For our research we selected WDS 09226+6251 MLB 203 AB (HD 80460). Figure 2 shows a screenshot of data from Stelle Doppie.



The Journal of Double Star Observations

Figure 2: Screenshot of the Stelle Doppie system with the information of the binary star system chosen

LCOGT

LCOGT is a global network of robotic telescopes that enables researchers to access celestial objects from different locations on Earth. We used the observing portal to submit or observation requirements. We selected the 0.4m telescope with the DeltaRho 350 + QHY600 camera (Bessell-V filter and exposure time).

AstroImageJ:

AstroImageJ is a platform that offers a specialized display environment and tools tailored for the display of astronomy specific images, as well as for the calibration and reduction of astronomy specific image data. The AstroImageJ platform was used to measure the Position Angle (PA) and Separation (SEP) of HD 80460. Figure 4 shows an example of measurements with AstroImageJ.

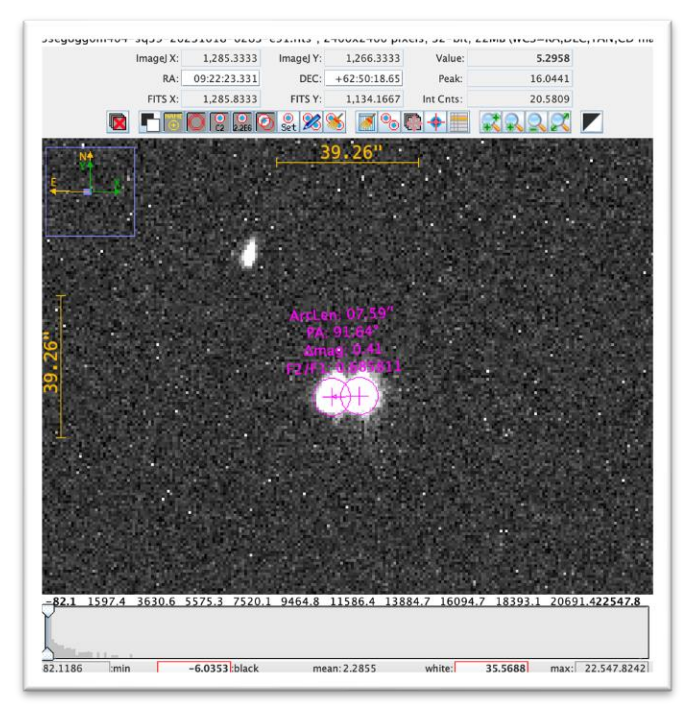


Figure 4: Example of AstroImageJ measurement of HD 80460 Double star Sep=07.59", PA=91.64°

SIMBAD:

SIMBAD is an astronomical database that provides information on astronomical objects beyond our solar system. It is maintained by the Centre de Données astronomiques de Strasbourg (CDS) in France. In a search in SIMBAD, the names of the two stars of HD 80460 were found. The primary star is called HD80460A, and the secondary star is called HD80460B. According to this Platform, the primary star is a High Proper Motion Star, has a parallax of 12.3238 [0.013] mas and its spectral type was not found. Regarding the second star, it was found that its parallax is 12.3432 [0.0136] mas and its spectral type is K0 but classified D quality.

Gaia:

The Gaia archive encompasses derived data such as positions, parallaxes, proper motions, radial velocities, and luminosity measurements (Gaia Collaboration et al. 2016). We used the Gaia platform to identify the names of our double star, in addition to the parallax, spectral type, RA and DEC.

3. Data

Table 2 shows the date, exposure time (s), PA (degrees) and SEP (arcmin). These images were taken with a 0.4m telescope from LCOGT (Fall 2023, Bessell-V filter).

Table 2: Data of double star HD 80460 observed with LCOGT.

Date	Exp time	PA (deg)	SEP (arcmin)
	(8)		
oct.19.2023			
001.17.2023	5	91.90	0.04
		71.70	0.01
oct.19.2023			
	1	91.94	0.13
oct.19.2023			
001.17.2023	0.5	92.10	0.13

oct.19.2023	1	92.10	0.13
oct.19.2023	5	91.64	0.13
oct.19.2023	5	91.15	0.12
oct.19.2023	2	91.72	0.39
oct.19.2023	1	91.81	0.11
oct.19.2023	1	90.23	0.12
oct.19.2023	1	92.98	0.13
Av	verage:	91.8	0.14
Standar	d deviation:	0.7	0.09

4. Discussion

The stars are close to each other. Of the ten observations that were made, the average PA is 91.8° with a standard deviation is 0.7°. The average SEP is 0.14 arcmin and its standard deviation is 0.09 arcmin. The historical data is presented in Table 3. Observations were found from the year 1907 to 2019. The first column presents the date on which the observation was made, the second column shows the PA, the third column shows the SEP, the fourth column shows the telescope aperture (m), the fifth column shows the number of nights of the observation, the sixth column shows the RA in arcsec, and the last column shows the DEC in arcsec. This table was used to plot the orbit in a Cartesian graph. For the x axis we calculated: Sep \times sin (PA) and for the y axis we calculated: -Sep \times cos (PA). We searched SIMBAD and found HD 80460A doesn't have a spectral type. The name of the secondary star is HD 80460B and have a K0 spectral type. The parallax of the principal star HD 80460A is 12.3238 [0.013] mas, and for HD80460B is 12.3432 [0.0136] mas. In Table 4, we presented the data retrieved from Gaia DR3 for both stars, HD80460A and HD80460B. The first column lists the name of each star, the second column shows its parallax along with the corresponding error, the third column displays the right ascension, and the fourth column indicates the declination. Moving forward, the fifth column represents the proper motion in the right ascension with its error, the sixth column conveys the proper motion in declination with its error, and the final column outlines the distance in parsecs in arcseconds.

Table 3: Historical Data for HD 80460 from the WDS Database

Date	PA (degrees)	Sep (arcsec)	Telescope aperture (m)	Number of nights	RA (arcsec)	DEC (arcsec)
1907.22	90.4	6.558	0.3	1	6.56	0.05
1907.72	88.8	7.0	0.3	2	6.10	-0.15
1908.22	89.3	8.633	0.3	1	8.63	-0.11
1921.22	88.5	7.23	0.6	2	7.23	-0.19
1930.15	96.8	7.046	0.2	1	6.10	0.83
1957.18	92.4	7.143	0.2	1	7.14	0.30
1974.274	90.717	7.522	0.7	5	7.52	0.09
1981.309	91.045	7.521	0.7	1	7.52	0.14
1984.231	90.880	7.501	0.7	1	7.50	0.12
1985.00	90.5	7.20	0.5	2	7.20	0.06
1986.193	90.966	7.522	0.7	6	7.52	0.13
1986.981	91.146	7.513	0.7	1	7.51	0.15
1989.233	91.157	7.572	0.7	2	7.57	0.15

1991.62	91	7.574	0.3	1	7.57	0.13
1999.05	91	7.56	1.3	1	7.56	0.13
2003.274	91.4	7.582	0.2	7	7.58	0.19
2012.256	91.7	7.61	0.7	2	7.61	0.23
2013.067	91.71	7.561	0.2	5	7.56	0.23
2014.097	91.59	7.597	0.2	10	7.59	0.21
2015.0	91.60	7.726	1	1	7.72	0.22
2015.101	91.64	7.597	0.2	10	7.59	0.22
2015.5	91.64	7.6147	1	1	7.61	0.22
2016.0	91.3	7.58	1	1	7.58	0.17
2019.120	91.8	7.621	0.7	1	7.62	0.24

In Figure 5 we show the historical data plotted in a Cartesian coordinate system with RA (arcseconds) in the x axis and Dec (arcseconds) in the y axis. The blue line is a second order polynomial fit (R^2 = 0.04). The blue dots are the historical data, and the red dot is our new measurement for HD 80460.

Historical Data Plot

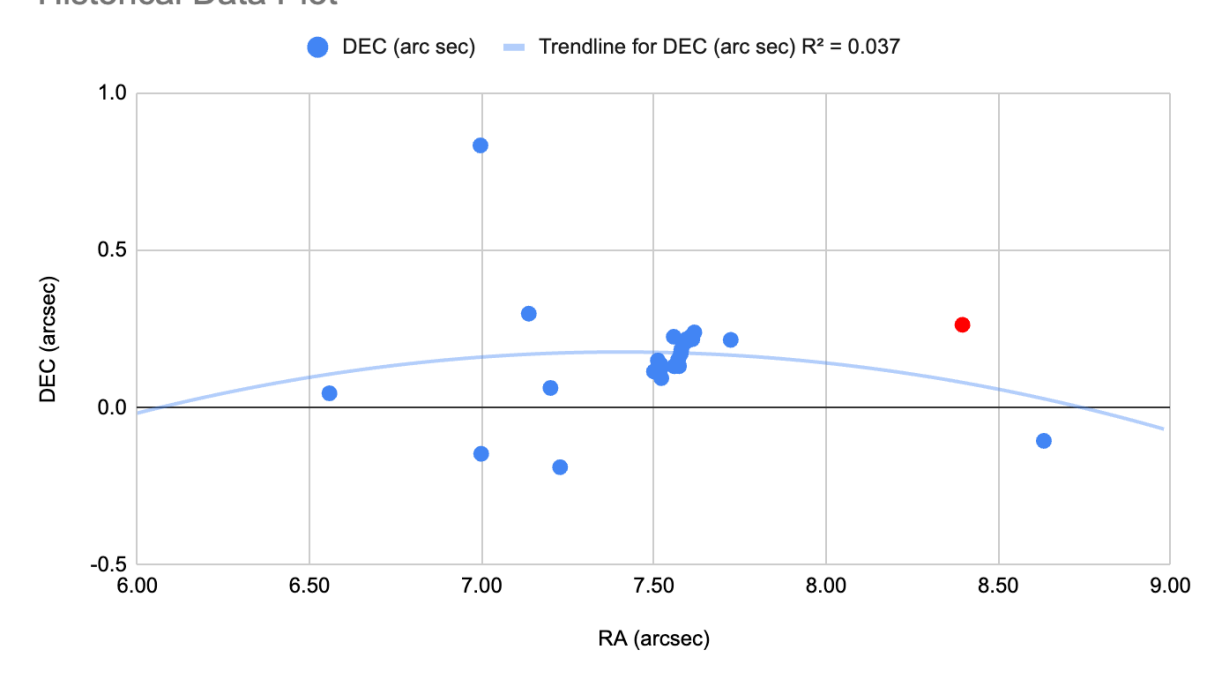


Figure 5: Shows the historical data plotted in a Cartesian coordinate system with RA (arcseconds) in the x axis and Dec (arcseconds) in the y axis. The blue line is a second order polynomial fit. The blue dots are the historical data, and the red dot is our new measurement for HD 80460

Table 4: Gaia DR3 measurements of the System HD80460A and HD80460B.

Double star name	Parallax	RA (2000.0)	DEC (2000.0)	pmRA[error]	pmDE [error]	Dist	Dist
	[error] mas					(parsec)	(lightyears)

HD80460A	12.32 [0.013]	09 ^h 22 ^m 35.60 ^s	+62° 50' 35.34"	-142.92 [0.011]	-40.92[0.012]	80.84	263.53
HD80460B	12.34 [0.014]	09 ^h 22 ^m 36.70 ^s	+62° 50' 35.17"	-140.84[0.011]	-43.53[0.013]	80.72	263.21

5. Conclusions

Binary star systems, where two stars orbit a common center of mass, offer insights into various aspects of astrophysics. Observations of double stars at various stages provide important data to validate and improve theoretical models, improving our understanding of the birth, life, and fate of stars. The motion of binaries within galaxies can provide information about mass distribution, contributing to our understanding of dark matter and the overall structure of galaxies.

In conclusion, with our observations and the historical data, we were able to observe that the values we made were similar to the values of the historical data. We used Stelle Doppie, which informed us that this system was physical. This is why the Gaia DR3 platform was used to observe the relationship that both stars showed, since, according to our graph, the value was too low to identify them as a physical pair. The data obtained from Gaia DR3 is consistent with the system being a physical system. The proper motions of the stars are similar indicating that the stars are moving together in space. In addition, the distance values of each star are very similar (< 1 ly difference). This is an interesting system that would benefit from more observations that would help establish its orbit and clarify its true nature.

Acknowledgements

This research has made use of the Stellarium planetarium. We want to acknowledge Gianluca Sordiglioni, the creator of www.stelledoppie.it platform. This research has made use of the Washington Double Star Catalog maintained at the U. S. Naval Observatory. We further thank Dr. Brian Mason for the historical data provided. This work makes use of observations from the Las Cumbres Observatory global telescope network. This research has also used the SIMBAD database, operated at CDS, Strasbourg, France. This work has made use of data from the European Space Agency (ESA) mission Gaia (https://www.cosmos.esa.int/gaia), processed by the Gaia Data Processing and Analysis Consortium (DPAC, https://www.cosmos.esa.int/web/gaia/dpac/consortium). Funding for the DPAC has been provided by national institutions, particularly the institutions participating in the Gaia Multilateral Agreement. In addition, this work was assisted by Alejandra Negrón (UPRRP student).

References:

Collins, K. A., Kielkopf, J. F., Stassun, K. G., & Hessman, F. V. (2017). AstroImageJ: image processing and photometric extraction for ultra-precise astronomical light curves. *The Astronomical Journal*, 153(2), 77.

"Las Cumbres Observatory Global Telescope Network", Brown, T. M. et al., Publications of the Astronomical Society of the Pacific, 2013, Volume 125, issue 931, pp.1031-1055

Gaia Collaboration et al. (2016): Description of the Gaia mission (spacecraft, instruments, survey and measurement principles, and operations).

Gaia Collaboration et al. (2018b): Summary of the contents and survey properties.

Palencia, R. B., (2017). Observación de Estrellas Dobles. Marcombo.

Shore, S. N. (n.d.). *Binary star*. Binary Star - an overview | ScienceDirect Topics. https://www.sciencedirect.com/topics/earth-and-planetary-sciences/binary-

star#:~:text=Binary%20Stars&text=They%20present%20theaters%20in%20which,the%20ev olution%20of%20single%20stars.

The Journal of Double Star Observations

 $Stelle\ doppie\ -\ double\ star\ database.\ (n.d.).\ \ https://www.stelledoppie.it/index2.php?section=1$

The Washington Double Star Catalog. Washington Double Star Catalog - Current Version. (n.d.). http://www.astro.gsu.edu/wds/

Viii, Russell Genet, et al. Small Telescope Astronomical Research Handbook: Preliminary Edition.

https://vizier.cds.unistra.fr/viz-bin/VizieR-S?Gaia%20DR3%201040254960426076416

https://vizier.cds.unistra.fr/viz-bin/VizieR-S?Gaia%20DR3%201040254964721358592

Zotti, G., Wolf, A. (2022). Stellarium: Finally at Version 1.0! And beyond. Journal of Skyscape Archaeology, 8(2), 332–334. https://doi.org/10.1558/jsa.25608

Some "Lost" Doubles in the WDS

Roger C. Ceragioli University of Arizona, Tucson, AZ; <u>lensbender@msn.com</u>

Abstract

The present paper discusses six double stars that appear to be misidentified in the WDS. After obtaining the relevant data files, and consulting the publications underlying them, the author has employed Aladin Lite (along with superimposed Gaia DR3 data), together with (in some cases) his own observations, to argue for corrected identities. The doubles in question are the following: HO 638AE (= SMR 7); POP 137; OL 222; DJU 8 (= MLR 85); GCB 63 (= J 1224BC); and HU 2AB.

Introduction

The Washington Double Star Catalog (WDS) contains thousands of pairs of stars for which there is no measurement more recent than about 40 years ago. Why this is so varies from star to star. Some may be intrinsically difficult to observe because of a large differences in magnitude or faintness of both components, or simply because they lie in the southern hemisphere of the sky, while most double-star observers are still in the northern hemisphere. In still other cases, however, a confusion of identity has arisen, occasioned by mistakes in published papers, their limited accuracy in the determination of stellar coordinates, or from errors in progenitor catalogs that fed into the WDS. Six of these "lost" doubles are discussed in the present paper. Four have clear solutions. For the remaining two, possibilities are suggested.

HO 638

The first (and most complex) case concerns the 638th double in a list of discoveries made by George Washington Hough (1836-1909), Director of the Dearborn Observatory at Northwestern University. Located near 13 Sagittae, this double was first measured by Hough in 1899.08, according to the catalog of Hough's doubles published in 1907 by Eric Doolittle (1869-1920), Director of the Flower Observatory at the University of Pennsylvania:

^{1.} Doolittle (1907), 113. The WDS gives 1889.08 as the date of first measurement, apparently following a mistake in Aitken (1932),

^{2, 1157 (#13225).} See Fig. 4 below.

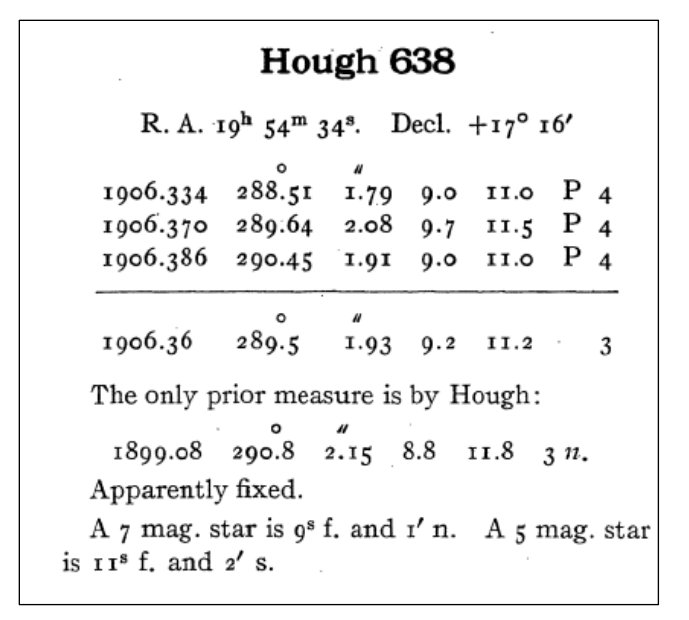


Figure 1. Measures of Hough 638 as published by Doolittle

Further measures followed in 1906 (by Doolittle himself), 1912 (by R. Jonckhèere), and finally in 1928 (by P. Fox). Then nothing up to the present. In the meantime, a nearby, easily-seen double star (WDS 20000+1736 SMR 7) was apparently first found in 2009 by J.S. Schlimmer.² Although thought to be a new discovery, the present author contends that SMR 7 is, in fact, Hough's star 638, which in the interval between 1928 and 2009 had been misidentified as a different, brighter star, lying near HO 638.

First Case of Mistaken Identity

The coordinates of HO 638 as given by Doolittle (Fig. 1, for epoch 1880) are: RA 19h 54m 34s; DEC +17° 16′. Precessed to J2000, these yield: 19h 59m 59s; +17° 36′. The J2000 coordinates for SMR 7, as given on the WDS website (rounded identically to Doolittle's) are: 19h 59m 59s; +17° 36′ – in other words, the same. Meanwhile, the J2000 coordinates for the star listed in the WDS as "HO 638AE" are: 20h 00m 08s; +17d 37m. These differ from Doolittle's precessed coordinates by 9s of RA and 1′ of DEC.

At this point, an image of the field may be of assistance. Recently, the author took the following image, using the 30-cm refractor he described in an Oct. 2023 article, published in the *Journal of Double Star Observations (JDSO)*:⁵

^{2.} Schlimmer (2010).

^{3.} The epoch is stated in Doolittle (1907), 9.

^{4.} All precessed coordinates in this paper were calculated using the online tool supplied by the Chandra X-Ray Center. *Cf.* https://cxc.harvard.edu/toolkit/precess.jsp.

^{5.} Ceragioli (2023), 365.

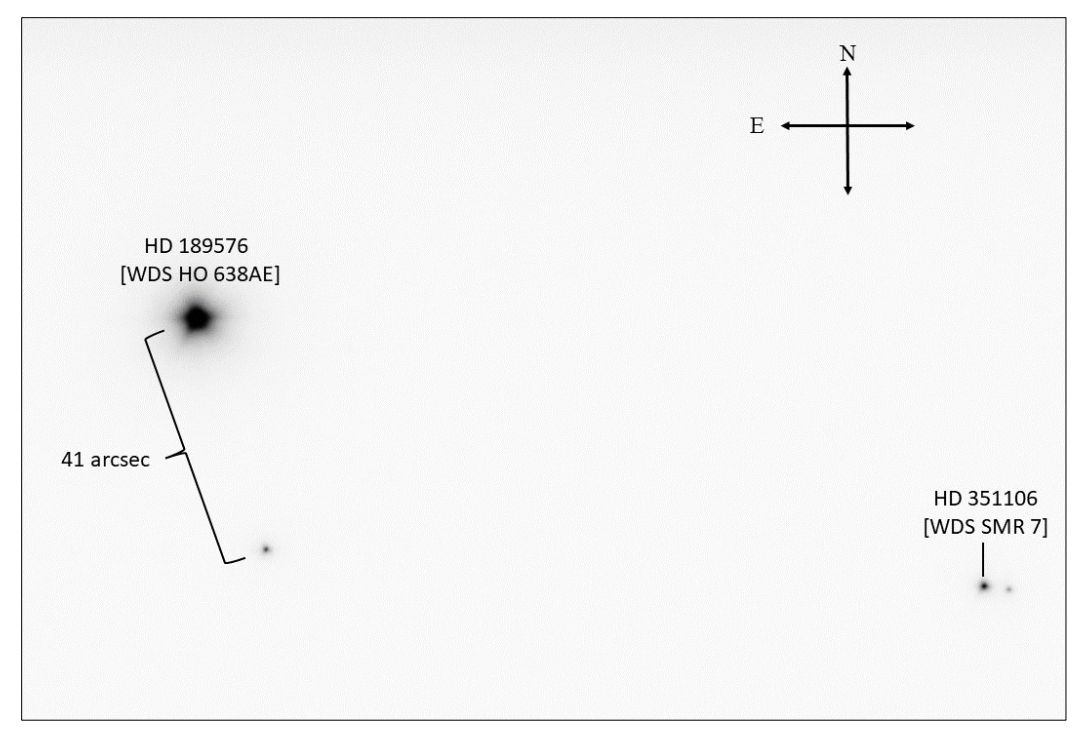


Figure 2. Field of WDS HO 638AE and SMR 7

Four stars are visible in the image: 1) HD 189576, a star of Vmag = 6.98 (but variable) according to the SIMBAD database; 2) HD 351106, a star of Vmag = 10.04 also according to SIMBAD, together with a fainter companion at θ = 263.5°, and ρ = 4.29" according to the author's measurements made at J2023.70; and a star 41 arcsec SW of HD 189576 (listed in Gaia DR3 as source 1820488786830292096). Notice that in the image, there is no companion to HD 189576, the putative WDS HO 638A, but there is a companion of HD 351106. This latter happens to lie in the general direction that Hough and Doolittle assigned to the secondary star of HO 638, although at double their distance. After the lapse of a century, a change in position angle and separation would not be a surprise.

The next person to measure HO 638 was the famous French double-star observer, Robert Jonckhèere (1888-1974), in 1912. His numbers for position angle (PA) and separation (Sep.) showed no clear change from what preceded.⁶ By 1928, however – nearly 30 years after Hough's original measurement – the situation was different. Philip Fox (1878-1944), successor to Hough at Dearborn, measured a change. His administrative duties at Northwestern, however, as well as at the Adler Planetarium (being its first director), and his extensive service in the US Army until the end of his life seem to have prevented him from publishing many of his later double star measurements. These were edited and printed in 1946 by George Van Biesbroeck (1880-1974), the famous Belgian-American double-star specialist at the Yerkes Observatory, in the *Annals of the Dearborn Observatory*:⁷

^{6.} Jonckhèere (1912), 8. Special thanks to B. Mason for supplying a scan of this difficult-to-find article. Jonckhèere's means are reproduced in Aitken (1932), 2, 1157 (#13225). Cf. Fig. 4 below.

^{7.} Van Biesbroeck (1946), 36. On Fox, see: Lee, O.J. (1944).

13225 Ho 638	BD.+-17 ⁰ 4180	
R.A. 19 ^h 57 ^m 5	Decl. + 17 ⁰ 29	•
1927.586 28.445 28.456	282°9 282°0 282°8	2 : 37 2.88 2.82
1928.162	282.6	2.69
The identification is	by Van Biesbroed	k

Figure 3. Philip Fox's Measurements of HO 638 in 1927-8

Fox's mean position angle has decreased from earlier measures by about 7-8°, and his separation has increased by about 0.6-0.7".

But one should notice the curious postscript: "The identification is by Van Biesbroeck." Perhaps Fox's observational notes left some doubt as to which star he had measured? No magnitude estimates are given, contrary to Hough, Doolittle, and Jonckhèere, who had estimated the components as being roughly of 9th and 11th mag (*cf.* Fig. 1 above). Van Biesbroeck gave the position as RA 19h 57.5m; DEC +17d 29m. The epoch here is 1950. Precessed to J2000, we obtain: 19h 59m 45s; +17d 37m. This is clearly not HD 351106 (WDS SMR 7), nor is it HD 189576 (WDS HO 638AE), as a comparison with the coordinates given previously will show. Instead, the star closest to Van Biesbroeck's coordinates is HD 351109, a single star of Vmag = 9.02 according to SIMBAD, with B1950 RA of 19h 57.5m, and DEC of +17d 29m. This is clearly correct, since Van Biesbroeck explicitly names the star as BD +17° 4180, which is equivalent to HD 351109. It is not listed as a double in the WDS. And Gaia DR3 data show it to be a single star. Hence, Van Biesbroeck's identification of Fox's double is in error.

A further reference to HO 638 occurs in R.G. Aitken's 1932, New General Catalogue of Double Stars Within 120° of the North Pole (one of the feed catalogs for the WDS):

13225	3120			Но 638	
		19h	57 7	+17° 28′	
			55.5	20	
	1889.08	290°8	2″15	8.811.8	3n Ho
	1906.36	289.5	1.93		3 Doo
	1912.70	289 . 9	2.34		2 J

Figure 4. Hough 638 in Aitken's New General Catalogue of Double Stars

Here we see, in the first place, the erroneous date of 1889.08 for Hough's original observation (later propagated into the WDS data), instead of 1899.08 (*cf.* Fig. 1). This is apparently a typo. Secondly, we find two positions given for the double, referenced to Epochs 1950.0 and 1900.0. These when precessed to J2000 both give the same result to within the implied uncertainties, namely RA 20h 00.0m; DEC +17d 36m. The J2000 coordinates of HD 351106 are: RA 20h 00.0m; DEC +17d 36m. Hence, Aitken's coordinates would seem to point to this star as HO 638, and not to HD 351109 or 189576.

^{8.} Van Biesbroeck (1946), 7.

In other words, both Doolittle and Aitken appear to identify HO 638 with the acknowledged double HD 351106, now called SMR 7 in the WDS. Van Biesbroeck introduced some confusion by identifying HO 638 with HD 351109.

Notice further that in Doolittle's description (*cf.* Fig. 1), a 7th mag. star is said to lie 9s following (*i.e.*, east) and 1' north of HO 638. This too is nearly correct for HD 189576 with respect to HD 351106, the coordinate differences being RA +09.5s; DEC +43". Thus, Doolittle's HO 638 cannot have been HD 189576 (as currently indicated in the WDS), but must have been HD 351106 (currently called SMR7). The magnitudes, coordinates, and verbal description all point in this direction.

Doolittle also noted that a 5th mag. star lay a little to the southeast of HO 638. This must refer to 13 Sagittae itself, the only 5th mag. star in the vicinity. In J2000 coordinates, it lies 4s to the east and 5' to the south, rather than the stated 11s and 2'. It is possible that Doolittle misread his own notes, or measured wrongly. Nevertheless, there is a 5th mag. star in the general direction he indicated.

Hence, the present author would propose retiring the current designations WDS 20001+1737 HO 638AE and WDS 20000+1736 SMR 7, combining all the measures and introducing a new designation: WDS 20000+1736 HO 638. The first measure was made in 1899.08 at $\theta = 290.8^{\circ}$; $\rho = 2.15''$. The last currently published is 2020.725 at $\theta = 263.9^{\circ}$; $\rho = 4.04''$. The author's more recent measure (not yet published) at 2023.70, is $\theta = 263.5^{\circ}$; $\rho = 4.29''$.

A table of numbers may help to elucidate this discussion:

Observer/Cataloger	Star (Catalog)	Cited Coordinates (Epoch)	J2000 Coordinates
Hough/Doolittle	HO 638	19h 54m 34s +17d 16m (1880)	19h 59m 59s +17° 36′
			$(= 20h\ 00.0m\ +17^{\circ}\ 36')$
Fox/Van Biesbroeck	HO 638	19h 57.5m +17d 29m (1950)	19h 59.8m +17° 37′
Aitken	HO 638 (ADS 13225)	19h 57.7m +17d 28m (1950)	20h 00.0m +17° 36′
Schlimmer, et al.	SMR 7 (WDS)	N/A	19h 59m 59s +17° 35′ 56″
			(= 20h 00.0m +17° 36′)
N/A	HO 638AE (WDS)	N/A	20h 00m 08s +17° 36′ 39″
			$(= 20h\ 00.1m\ +17^{\circ}\ 37')$

Table 1. Stars and Coordinates

But if WDS HO 638AE is the same pair of stars as WDS SMR 7, then can they be connected using proper or orbital motion? Here we may avail ourselves of the most recent Gaia data release (DR3) for SMR 7. Doing so via the SIMBAD website and its application VizieR, we find that this is an optical double: the primary star has a parallax of 4.42 mas/yr, giving a distance of 226 pc, while the secondary has a parallax of 0.90 mas/yr, giving a distance of 1116 pc. Hence, these stars lie about 2900 light years apart from one another. Their proper motions are quite different as well. The "primary" shows a motion of Δ RA = +14.8 mas/yr, and Δ DEC = +18.6 mas/yr, while the "secondary" shows Δ RA = +0.3 mas/yr, and Δ DEC = +6.9 mas/yr. So, indeed, not only is the apparently brighter star much less intrinsically luminous than the apparently fainter star, it is drifting (to the northeast) much faster as well.

If we transform the PA and Sep. of the pair into a differential RA and DEC (using numbers given in the WDS data file for 2020), retroject backwards to 1900 (using the Gaia proper motions), and then convert back to PA and Sep., we obtain: 293.2° and 2.48". This compares with Hough's and Doolittle's numbers of

about 290°, and 2" (cf. Fig. 1). Although the retrojected numbers are not extremely close to the measured, they are not wildly different, and the uncertainties in the underlying data may account for the differences.

Another way to proceed is to graph the data in a plotting program, such as R. Harshaw's Excel-based spreadsheet, Plot Tool 3.19. First, however, we present a table of the combined data for HO 638AE and SMR 7, derived from WDS data files:

НО 638	1899	1928 20	291	264	2.2 4.3									195	958.80 +1	735	55.6
	1899.08	290.8			2.15		8.8		11.8	•			0.5	3	Ho_1907	Ma	5
	1906.36	289.5			1.93		9.2		11.2				0.5	3	Doo1907	Ma	
	1912.70	289.9			2.35		9.1		10.5				0.4	2	J_1912h	Ma	3
	1928.16	282.6			2.69								0.5	3	Fox1946	Ma	N 0
	1997.66	266.7			3.56		9.098	0.041	9.601	0.024	1256	245	1.3	1	TMA2003	E2	7
	2001.563	266.6	0.1		3.904	0.033	9.98	0.02	11.37	0.07	609	70f	0.2	4	UC_2013b	Eu	P 7
	2009.633	260.8			3.63		*		3.4				0.2	1	Smr2010	C	7
	2009.8021	265.1			4.00				3343	5140			0.7	2	WSI2013b	Su	7
	2010.474	265.0		:	4.06				0.00		550		0.7	2	WSI2011b	Cu	P 7
	2010.672	262.4			3.86				10.00	5.00			0.2	1	Smr2011b	C	7
	2011.581	261.9			4.06								0.2	1	Smr2012	C	7
	2012.711	264.3			4.17				S#0.	0,000			0.3	2	Smr2013	C	7
	2013.704	265.3			4.15								0.3	2	Smr2014b	C	7
	2014.751	264.9			4.1								0.3	1	Smr2015b	C	7
	2015.0	264.702			4.120		9.930		11.235	3. - 0	673	440	1.0	1	Kpp2018m	Hg	7
	2015.745	264.0			4.08								0.3	1	Smr2016	C	7
	2016.683	263.5			4.09								0.3	1	Smr2018	C	7
	2018.789	264.6			3.60								0.3	1	Smr2019	C	7
	2020.725	263.9			4.04								0.3	1	Smr2021c	C	7
	2023.700	263.5			4.29								0.3	1	Cg12023	C	7

Table 2. Combined Data for HO 638AE and SMR7

Note that the author has corrected the date of Hough's observation from the erroneous 1889.08 to 1899.08, and has appended his own unpublished 2023.70 measurement. If these data are graphed in Plot Tool 3.19, we obtain the following:

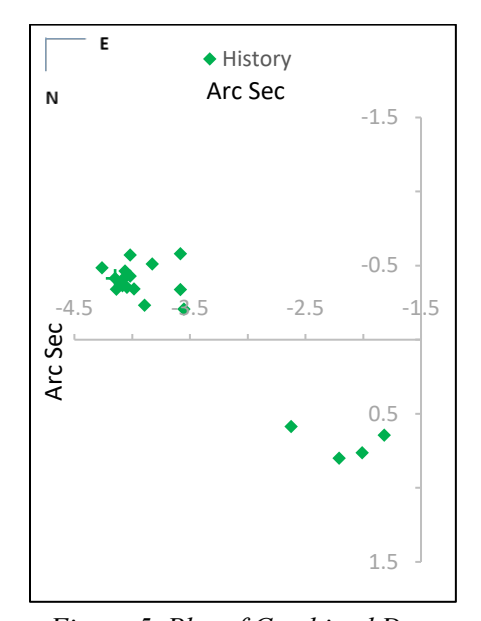


Figure 5. Plot of Combined Data

In this graph, we have the measured PAs and Seps transformed from polar to rectangular coordinates (*i.e.* relative RAs and DECs in arcsec), where the brighter star is located at (0, 0), outside the graph's limits.

Notice, also, that the cardinal directions on the sky are reversed N-S and E-W with respect to Fig. 2 above, now following standard double-star conventions with N at bottom and E to the right.

There are two clumps of data points, but no crystal-clear trend. This is because of a some outliers in the data (especially since 1997). If one examines the run of the Seps in Table 2 above, these can easily be spotted, namely the measurements at 1906.36, 2009.633, 2010.672, and 2018.789. In addition, the run of the PAs reveals an outlier at 2011.581. If one eliminates these data points and re-graphs, one obtains:

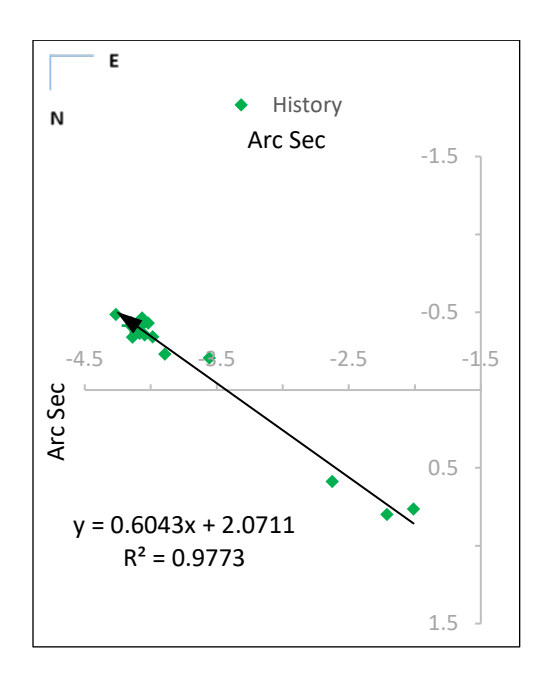


Figure 6. Data Re-graphed with Outliers Eliminated

Now a trend is clear. A trend line has been added, as well as its linear equation. The R² (goodness-of-fit) value is high (0.9773), indicating that the remaining data points conform well to the trend line. This suggests that, in fact, one and the same pair of stars has been measured from Hough down to the present day, as the documentary evidence already discussed indicates.

Second Case of Mistaken Identity: POP 137

The double star WDS 21313+4455 POP 137 has not been measured since 1986. The precise coordinates given for this pair in the WDS, namely 21h 31m 20.20s +44° 54′ 23.5″, point to the star BD +44 3848 (Vmag = 10.29, according to SIMBAD) as POP 137. Yet according to Gaia DR3, that is a single source.

Consulting the original publications about POP 137, stemming from its discoverer, G.M. Popović, and his collaborator, D.J. Zulević, at Belgrade Observatory in what was then Yugoslavia, we find that their double was not BD +44 3848, but rather a fainter star 1 arcmin to the north:

POP 137	21275N4429 21296N4442 21313N4455	+44.3848(9.4) 0 s +1 arc min.	86.709 86.862 86.786	106.9 104.0 105.4	1.90 2.10 2.00	11.5-11.5 0.3 0.2	112	POP
			86.709 86.862 86.786	102.3 102.8 102.6	1.60 1.68 1.64	0.1 0.1 0.1	1 1 2 1 1 2 2n	ZUL

Figure 7. Popović and Zulević's identification of POP 137

They indicate their star by differentiation from BD +44 3848, saying its RA is the same, but its DEC is increased by 1 arcmin. It has a PA of about 104.0° and Sep. of about 1.8". The magnitude of both stars (they say) is about 11.5, and not 10.5 as the WDS has it. Clearly, they are pointing to a fainter, close double lying to the north of BD +44 3848. And there is such a double.

The author recently took the following image:

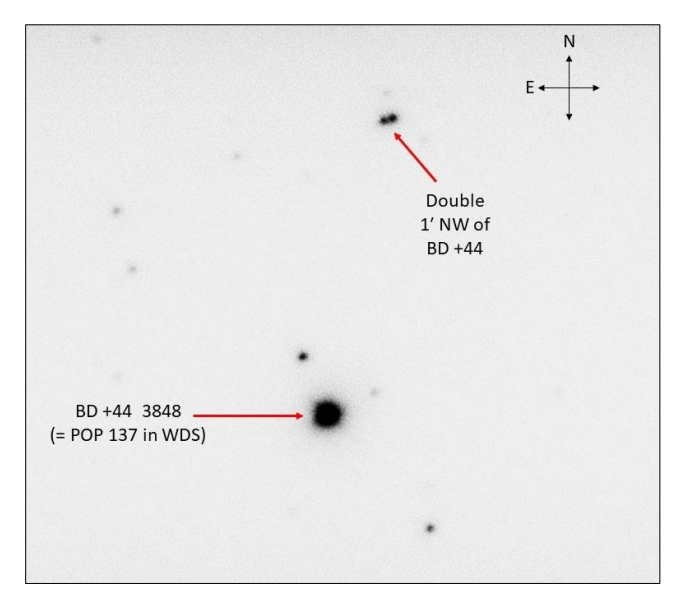


Figure 8. BD +44 3848 and Double Star to NW

Here we see, clearly marked, BD +44 3848 (below center), and above to the right at Δ RA = -1.5s; Δ DEC = +1′ 05″, an equal double as indicated by Popović and Zulević. Its PA and Sep. are 105.6° and 2.04″, as measured recently at J2023.90 by the author, closely matching their numbers. Thus, we have likely found the true POP 137.

The Gaia DR3 Gmags for this pair are 13.0 and 13.3, significantly fainter than BD +44 3848, and fainter than Popović and Zulević's visual estimate of 11.5. Both stars lie at nearly the same distance (450 pc), according to Gaia DR3 data, and have very similar proper motions to one another, pointing to their forming a true binary. Hence, the WDS should probably be changed to reflect all this.

Third Case of Mistaken Identity: OL 222

This double was measured twice by its discoverer, Charles P. Olivier, in the years 1939-1947 at the University of Pennsylvania. His position (in 1950 coordinates) is given as: RA = 22h 11m; $DEC = +13^{\circ} 31'$. Precessed to J2000, we have 22h 13.5m; +13° 46':

01 194	9.6 10	.1
22 ^h 11 ^m	+13°	31'
39.705 39.790	244.3 243.0	2.98 3.10
39.748	243.6	3.04
42.876 43.805 46.758	241.5 244.0 238.3	3.42 3.84 3.+
47.876	237.2	3.65

Figure 9. Olivier's Measures of OL 222

Olivier gives estimated magnitudes of 9.6 and 10.1. The mean PA and Sep. would be 241.9° and 3.35" respectively for the mean date of 1942.5.

Consulting Aladin Lite for the precessed position, we find the following field (with Gaia DR3 sources superimposed as small blue squares):

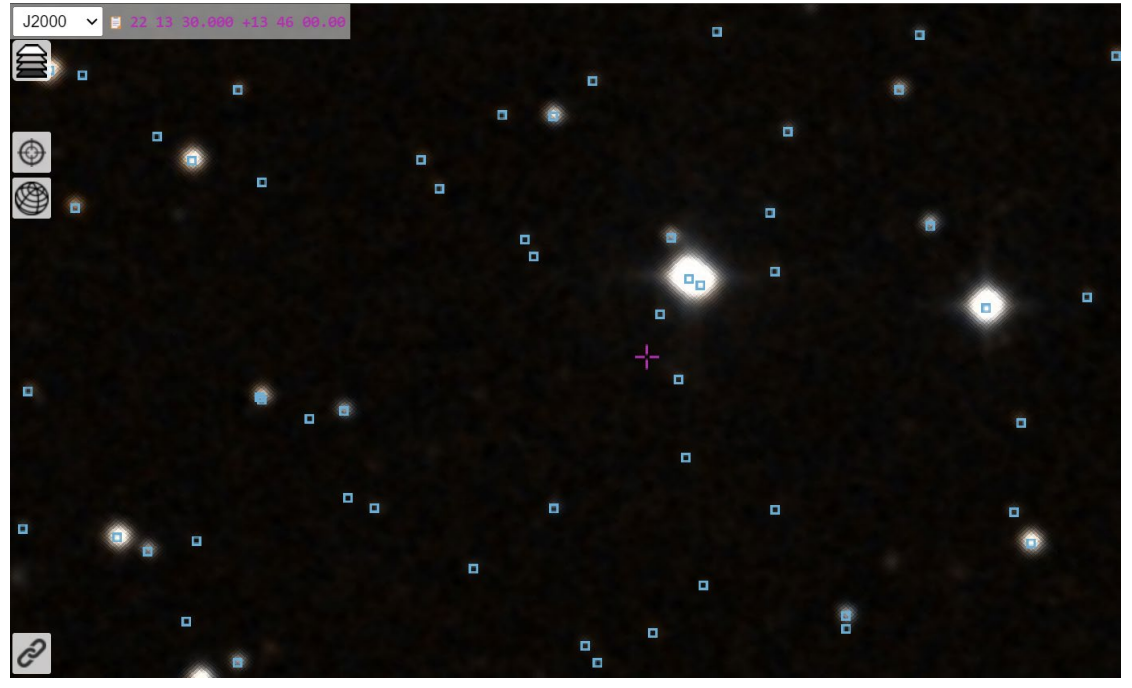


Figure 10. The Aladin Lite Field Centered on J2000 RA 22h 13.5m; DEC +13° 46'

^{9.} Cf. Barton et al., (1949), 43, where the double is termed "Ol 194."

Here north is up and east is to the left as usual in this photographic star atlas. Just a little way from the purple cross, which marks the queried position, we see what is clearly an elongated star (Gaia DR3 source 2734841625686892416) with Gmag of 11.8. Accompanying it at a short distance is another star of Gmag 12.2, according to Gaia data. Working from the precise Gaia DR3 coordinates, we find a PA of 243.7°, and a Sep. of 3.66″, which are very similar to Olivier's numbers.

Consulting the WDS catalog, we find that precise coordinates for OL 222 are lacking altogether there. Instead, we have the approximate position, RA = 22h 10.0m; DEC = $+13^{\circ}$ 46′. This leads to a location 3.5 minutes of RA to the west, where there is no nearby double matching Olivier's description. The closest significant double is STT 463, whose separation is close to Olivier's number, but whose position angle is different by nearly 120°. Olivier had estimated a magnitude difference of about 0.5 for the components in his double. But the Δ Mag for STT 463 is 3.3. All this suggests that Gaia DR3 source 2734841625686892416 is probably Olivier's "lost" double.

The author recently imaged this star along with the star TYC 1149-1573-1, lying to the west:



Figure 11. The Probable Double OL 222 (Left) and the Single Star TYC 1149-1573-1 (Right)

The image should be compared to the Aladin Lite view, shown above in Fig. 10. The author's J2023.90 measurement of the putative OL 222 gives PA = 242.6°; and Sep. = 3.60". Clearly, there has been almost no relative movement since Olivier's measurement 80 years ago. This makes sense, when we consult the Gaia DR3 data for the components. Their parallaxes and proper motions differ but little from one another, and their relative proper motions over 80 years would lead to a Δ RA of about 0.04° and Δ DEC of 0.03°, which would not be clearly measurable except by satellite or speckle techniques on large ground-based telescopes, neither of which existed in Olivier's day. Hence, the present author proposes Gaia DR3 source 2734841625686892416 as OL 222.

Fourth Case: DJU 8

Unfortunately, the next case does not lend itself to results as neat as the preceding. In 1956, P.M. Djurković and Lj.M. Dačić at the Belgrade Observatory, published a measurement of a new double. ¹⁰ This, they said, consisted of two 10th mag. stars having PA = 35.1°, and Sep. = 0.58″. The double's location on the sky (in

^{10.} Djurković et al. (1956), 10.

1950.0 coordinates) was: RA = 22h 44.8m; DEC = $+65^{\circ}$ 56'. They designated the star Bd [presumably "Belgrade"] 9. In the WDS, it is called DJU 8:

```
MESURES MICROMÉTRIQUES D'ÉTOILES DOUBLES

Faites au réfracteur de 0.65 m d'ouverture

par P. M. DJURKOVIĆ (Dj) et LJ. M. DAČIĆ (Dc)

ADS № et Époque Θ ρ
désignation 1956 + ° " Grandeurs Dj Dc

Bd 9<sup>5</sup> 800 35.1 0.58 10.5 —10.9 2 1

1950.0

5 α = 22 44.8, δ = +65 56
```

Figure 12. Djurković and Dačić's Mean Measures, Magnitudes, and 1950.0 Position for WDS DJU 8

If we precess the coordinates to J2000, we obtain: 22h 46.6m; +66° 12′. This is a position lying about 3 minutes of RA west of iota Cephei. On consulting Aladin Lite with superimposed Gaia DR3 data, we find no obvious nearby candidate star for DJU 8. The WDS gives no precise coordinates or observations more recent than those made in 1963-1967 by Charles E. Worley (1935-1997), the famous double-star observer at the United States Naval Observatory (the USNO, home of the WDS), indicating a known problem with DJU 8. Worley gave its coordinates as 22h 43.1m; +66° 12′, noting that the position can be "interpreted as the right ascension and declination of the pair for 1900." This is (he indicated) the identifier used in the *Index Catalogue of Visual Double Stars* (IDS), the all-sky successor to Aitken's earlier catalog, and predecessor of the WDS. ¹² Indeed, consulting the IDS shows exactly these numbers for epoch 1900.

As one can immediately see, however, while the declination matches Djurković and Dačić's when precessed to J2000, if we precess backwards to J1900, we obtain: 22h 43.0m; +65° 40′. Hence, it would appear that by mistake, the IDS's RA is for J1900, whereas its DEC is for J2000. ¹³ Meanwhile, the WDS identifier calls the star 22466+6644 DJU 8, suggesting a position of 22h 46.6m; +66° 44′. This would appear to be IDS's coordinates (assumed to be uniformly for J1900) precessed to J2000.

Laying aside these positional problems, if we consider Worley's measured PAs and Seps, we have the following:

D	IU			22 43.1	+66 12
63.690 65.721 67.830	38.4 37.8 41.1	0.58 0.91 0.79	1	5 0.0 2 5 -0.1 2 5 +0.1 2	0.8 26
65.747	39.1	0.76	3N	0.5	26-INCH

Figure 13. Charles Worley's Measures of DJU 8

^{11.} Cf. Worley (1971), 129. For the quotation, cf. p. 10.

^{12.} Cf. Jeffers et al. (1963), 2, 768.

^{13.} The discrepancy in RA (43.1m *versus* 43.0m) may be due to differences in rounding. Even the IDS's editors publicly lamented the great number of errors they themselves had found in their catalog, and appealed for observers to help in correcting these. *Cf.* Jeffers *et al.* (1963), 1, xiv.

Worley was a very experienced observer and professional astronomer, using a 66-cm refracting telescope and a filar micrometer. We can easily see that for this close pair, the PAs of his three individual observations (the last line in Worley's table gives his means) from 1963, '65, and '67 varied between 37.8° and 41.1°, while his Seps varied between 0.58" and 0.91". This is helpful in that it shows how much even an expert visual observer can vary when using a micrometer on a close double star. We have no equivalent information from Djurković and Dačić, but only their means. Still, it is enough to show us that we should not be too surprised if when using modern measurement techniques (direct CCD imaging or speckle interferometry), we find the numbers obtained to be somewhat different, although (hopefully) more consistent.

For reasons that are probably self-evident, no one has measured DJU 8 since Worley's time. One cannot, in fact, be sure which star these men had been looking at. Still, if we attend once again to Aladin Lite, superimposing the Gaia DR3 data sources on it, a possibility emerges. Closer to iota Cephei there is a known 10th mag. double (matching Djurković and Dačić's estimates), namely MLR 85, discovered by Paul Muller (1910-2000), the famous French double-star observer. According to the WDS's data sheet, Muller first observed his star in 1970. Perhaps in reality it was this star that Djurković, Dačić, and Worley had earlier observed and measured, prior to Muller's "discovery?" The J2000 coordinates of MLR 85 are: RA = 22h 47.8m; DEC = +66° 14′. This is relatively close to the J2000 precessed coordinates of Djurković and Dačić, namely: 22h 46.6m; +66° 12′. Principally, we have an error in RA of a little over 1 minute:

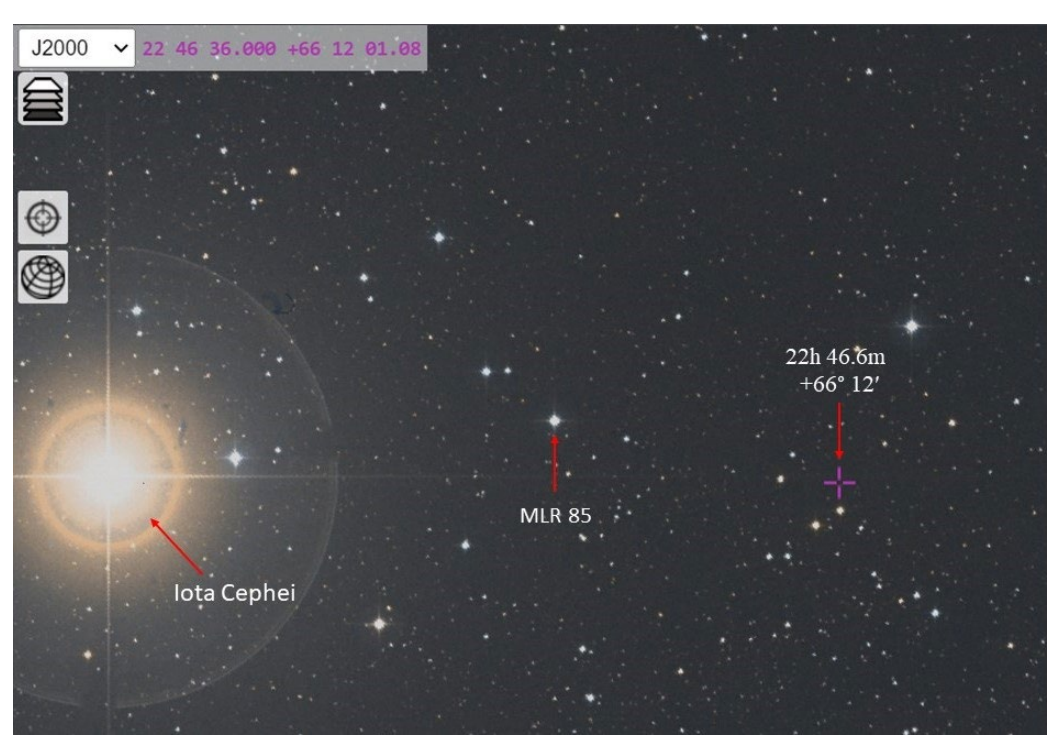


Figure 14. Aladin Lite Image of the Sky Between Iota Cep and Djurković/Dačić's Stated Position of Their Double (Precessed to J2000), Containing MLR 85

Although several other 10th-mag doubles lie in the vicinity (for example, HU 984 and MLB 274), none has a PA and Sep. close to that recorded for DJU 8. Only MLR 85 is close, and indeed very close:

MLR	85 1970	2017 12	35	37	1.0	1.0 10.72	10.86 G	5	+056+6	300 +	056+000	+65	1807 N	224748.2	8+66133	33.8
	1970.59	35.			1.0		10.1		10.3				0.7	1 Mlr1973a	Ma 2	2
	1973.58	38.9			0.80				•				0.5	2 Mlr1978b	Ma 2	2
	1981.64	35.4			0.73				•				0.5	3 Mlr1984	Ma 4	4
	1981.65	33.2			0.81								0.6	2 Hei1983a	Ma 2	2
	1989.60	37.5			0.79	•							0.5	3 Mlr1990	Ma 4	4
	1991.71	30.5			0.839		10.721	0.050	10.858	0.05	7 530	100	0.3	1 TYC2000a	Ht 9	5
	1991.71						11.644	0.067	11.657	0.06	8 430	90	0.3	1 TYC2000a	Ht 7	7
	2001.9279	35.1		:	0.84						560	45	0.7	1 WSI2002	Su P 6	6
	2004.715	35.7			0.91				0.2				0.5	2 Drd2009	C 7	7
	2008.655	34.6			0.941						530	340	0.7	1 Gii2012	S 7	7
	2015.0	37.005			0.947		10.158		10.498		673	440	1.0	1 Kpp2018m	Hg 7	7
	2016.0	36.45	0.00		0.98923	0.00003	10.375		10.686		584	436	1.0	1 ElB2021	Hg 7	7
	2016.0						10.231		10.185		502	228	1.0	1 ElB2021	Hg 7	7
	2016.0						9.274		9.286		759	294	1.0	1 ElB2021	Hg 7	7
	2017.7719	37.34	2.62		0.952	0.052							0.3	1 Bvd2018a	C1 7	7

Figure 15. WDS Data for MLR 85

We see for the micrometric measurements made in the 1970s and '80s by Muller and Wulff Dieter Heintz (1930-2006), the famous German double-star observer, PAs and Seps identical in range to Worley's from the 1960s. Only with the advent of CCD arrays and the Gaia satellite has the Sep. stabilized at about 1 arcsec. The author's own recent measurement at J2023.90 is PA = 34.2°; Sep. = 0.97". Djurković and Dačić had given estimated magnitudes of 10.5 and 10.9 for their components, close to the Gaia DR3 Gmags of 10.4 and 10.7 for MLR 85. Thus, the balance of evidence would seem to favor the notion that DJU 8 must in fact be MLR 85. This is why no one has found or measured the former since 1967 – because it is the latter, whose position has been clearly known since 1970. Many measurements have been made since then.

Fifth Case: GCB 63

The 63rd star in a list of measures published in 1932 by the French comet hunter and double-star observer, Michel Giacobini (1873-1938), who worked for decades at the Paris Observatory, also presents grave difficulties of identification. GCB 63 has not been measured since 1970, and with good reason. If we take Giacobini's coordinates (for epoch 1930.0) – namely, RA = 22h 00m 50s; DEC = $+23^{\circ}$ 48′ – and precess them to J2000, we obtain: 22h 04.1m; $+24^{\circ} 08'$. Aladin Lite, when queried for this position, shows nothing and, moreover, no plausible double star close by. Giacobini had estimated his pair as of mag. 10.5 and 11, with PA = 358.8° and Sep. = 1.43'' for the mean date of 1930.5. This should easily be seen in the Gaia DR3 data. But there is nothing near the stated position.

Forty years later, Richard L. Walker (1938-2005), an astronomer of the USNO, used the observatory's 1-meter reflector stationed near Flagstaff, Arizona to observe GCB 63. Walker's measurement in 1970 gave a result close to Giacobini's, namely PA = 1.9°; Sep. = 1.57", suggesting that he had observed the same star. Walker's stated position (likely taken from the IDS), when precessed to J2000, is RA = 22h 04.0m; DEC = $+24^{\circ}$ 09'. He does not give estimated magnitudes for the pair, but a Δ Mag of 0.3, not dissimilar to Giacobini's 0.5:

^{14.} Giacobini (1932), 31.

^{15.} Walker (1972), 58.

^{16.} Walker's stated coordinates are identical to IDS's coordinaters for Epoch 1900. Cf. Jeffers et al. (1963), 2, 742.

GC	63			21 59.4	+23	40	
70.773	1.9	1.57	2	2 +0.6	0.3	40	
70.773	1.9	1.57	1N	0.3	40-IN	СН	

Figure 16. R.L. Walker's Measurement of GCB 63 in 1970

After Walker, there is no further observation up to the present, since the exact location of this double star is uncertain. The current WDS position is simply Walker's, precessed to J2000. Casting further afield, we find WDS J 1224BC lies 10' south and somewhat east of Giacobini's nominal location, at J2000 RA = 22h 04.3m; DEC = +23° 58'. This star has been observed a number of times, having seven recorded PAs and Seps in its WDS data sheet, since R. Jonckhèere first recorded it in 1916:

J	1224BC	1916	2016	7 357	0	0.5	1.6 12.39	13.2	+004-0	07				220419.24	1+2 35	805.8
	1916.	83	356.6			0.48		11.0	11.0			0.7	1	J1917a	Ma	3
	1946.	33	1.2			1.73	•					2.1	3	VBs1954	Mb	0
	1949.	62	355.7			1.22		10.6	11.8			0.4	2	J1949b	Ma	0
	1953.	85	5.2			1.23		10.6	11.3			0.4	3	Cou1953e	Mc	0
	2009.	830	28.30			1.48						0.4	1	Bko2010b	С	7
	2013.	818	0.2	0.4		1.556	0.012					0.8	1	Gii2022	S	7
	2016.	0	359.75	0.00		1.57259	0.00002	12.797	13.193		584 436	1.0	1	E1B2021	He	7

Figure 17. WDS Data for J 1224BC

Examining these data, we see that Jonckhèere's first measurement contains an anomalous separation for 1916.83, which is a whole second of arc smaller than what follows. Perhaps a typo is involved in the original printing. The Gaia DR3 data for this pair do not support the notion of a large relative proper motion. Nor do the succeeding measurements down to 2016.0 suggest a large orbital motion. Any actual motion over 100 years would be impossible to verify with ground-based equipment. The rest of the measured Seps from 1946 onward cluster in the range of 1.2-1.7" with a mean of 1.46". The Gaia datum from 2016.0 is 1.57", which happens to be the same number as Walker's mean from 1970 for GCB 63.

The PAs for J 1224BC likewise fluctuate, and except for Berkó's anomalous measurement of 2009.83, the rest of the measures cluster in the range of 355.7° to 5.2°, the mean being 359.78° which is virtually the same as the Gaia 2016.0 datum of 359.75°. Walker's and Giacobini's PAs for GCB 63 are insignificantly different, falling within the same range. And finally, let us note that Jonckhèere and Couteau's visual magnitude estimates for J 1224 BC average to 10.7 and 11.4, which are close to Giacobini's original 1932 estimate for GCB 63 of 10.5 and 11.

Thus, it seems reasonably certain that GCB 63 must, in fact, be the same as J 1224BC. If so, Giacobini's 1930.0 coordinates, instead of saying: $RA = 22h\ 00m\ 50s$; $DEC = +23^{\circ}\ 48'$, ought to have read: $RA = 22h\ 01m\ 04s$; $DEC = +23^{\circ}\ 38'$. If we take the J2000 coordinates for many of his pairs and precess them to J1930, then comparing the latter to the numbers in his 1932 article, we find that errors of up to 30 or 40s in RA are frequent. Hence an error of 14s with GCB 63 would not be unusual. Errors of greater than 1' or 2' in declination, on the other hand, are not easily found in his list.

^{17.} Cf. Jonckhèere (1917), 163.

Hence it may be that we are dealing with a typo in Giacobini's list. But even an error of 10 arcmin is only about 1/3 the apparent diameter of the Moon. If on pointing a telescope at the nominal sky location and examining the field visually, an observer did not find GCB 63 at image center, a scan around the field would likely reveal it. In this way, R.L. Walker might have found J 1224BC while looking for GCB 63, and not have recognized that he had found a "different" double.

Finally, it should be noted that E. Berkó already suggested the possible equivalence of GCB 63 with J 1224BC in 2010.¹⁸

Sixth Case: HU 6AB

The last case of mistaken identity has a more definitive conclusion. WDS 01220-0927 HU 6AB has not been measured since 1953. Its precise J2000 coordinates, as given in the WDS are RA 01h 21m 59.14s; DEC -09 27' 27.8".

Querying Aladin Lite for this position produces the following result:



Figure 18. Aladin Lite Field Centered on WDS 01220-0927 HU 6

The bright star (centered under purple cross) is the supposed double. Yet the superimposed Gaia DR3 sources show only a single small blue box, meaning that to the limit of Gaia's resolution (approximately 0.4 arcsec) there is no companion. Earlier measures from 1899 (by W.J. Hussey) and 1953 (by P. Couteau) indicated Seps of between 0.52 and 0.72 arcsec, which ought to be resolved in Gaia DR3, especially since the Δ Mag between the components is only 0.2 according to the WDS data.

^{18.} Berkó (2010), 39, note 350.

But note the slightly less bright star to the southwest. This is the "C" star of the system. As currently catalogued, the two bright stars in Fig. 18 (with PA and Sep. of about 245° and 51.7") form the double HJ 2039AB,C – an object first catalogued by John Herschel in 1830. Hussey in 1899 found the much closer star, currently catalogued in the WDS as HU 6B, a companion of A. In other words, the brighter star ought to be double. Yet Gaia DR3 finds it single. Rather, it is the "C" star that has a tiny pair of blue boxes, which are more easily seen in the next illustration, giving an expanded view:



Figure 19. Expanded View of the "C" Star in Aldin Lite

Of this double, the brighter component has a Gmag of 10.9, and the fainter a Gmag of 11.1, according to Gaia. The PA and Sep., derived from DR3 precision coordinates, are 234.0° and 0.52". These values are not far from the data given in the WDS data file for "HU 6AB":

HU	6AB 189	9 1953	6 240 246	0.6	0.7 9.8	10.0 F	0	+024-	023	-10 295	012159.14-092	727.8
	1899.87	240.3		0.61		9.1		9.3		0.9	3 Hu_1900a Ma	3
	1920.897	227.0		0.63		10.5		10.8		1.0	3 VBs1927a Ma	3
	1929.60	238.4		0.66		10.5		10.8		0.6	3 Vou1932 Ma	0
	1942.62	232.0		0.52						0.4	3 Vou1955 Ma	0
	1948.95	233.7		0.68						2.1	3 VBs1954 Mb	0
	1953.89	240.3		0.72		10.1		10.1		0.4	2 Cou1953e Mc	0

Figure 20. WDS Data File for "HU 6AB," Last Measured in 1953

William J. Hussey (1862-1926) was a well-known American double-star astronomer, who worked at the Lick Observatory and the University of Michigan. In 1900, he published a paper listing 100 new doubles he had found at Lick. It is the sixth star in his list that is of interest to us:

	6. DM. $-10^{\circ}294$.										
$\alpha = 1^{\text{h}} 16^{\text{m}} 57^{\text{s}}$; $\delta = -9^{\circ} 59'.2$											
1899.756	239.0	0.59	9.2	9.2							
.917	240.8	0.60	9.2	9.2							
.933	241.2	0.64	9.0	9.5							
1899.87	240.3	0.61	9.1	9.3							
This is the	e companie	on of 1/20	39.								

Figure 21. Hussey's Measures from 1899

Hussey identifies his star as "DM. -10°294." This is equivalent to the modern designation "BD -10 294," which is the "C" star, shown above in Figs 18 and 19, and not the "A" star. The latter is BD -10 295. As

we shall soon see, later catalogs confused these designations. Notice also that Hussey explicitly says: "This is the companion of h 2039," meaning the secondary star ("companion") in John Herschel's pair, called HJ 2039 in the WDS. So Hussey explicitly notes that it is the fainter star of HJ 2039, namely BD -10 294, that is his double.

George Van Biesbroeck also understood the matter this way in 1927, when he published a list of double-star measurements made at the Yerkes Observatory:

719	H	Hu $6=B.D10^{\circ}294$						
	$1^{\rm h}19^{\rm m}27^{\rm s}$	-9°43	10 ^M 5	510 ^M 8				
	1920.697	222°4	0″70	0 _{M} 3				
	20.968	231.5	.65	.3				
	21.025	227.0	0.55	0.3				
	1920.897	227.0	0.63	0.3	$\overline{3n}$			
	1899.87	240.3	0.61	Hu(1)	3			
	With B.D10	0°295 this	star mal	kes Herse	chel	2039.		

Figure 22. Van Biesbroeck's Measures of HU 6 from 1920.

Here we could ask for nothing clearer. Van Biesbroeck explicitly equates HU 6 with BD -10 294, and says that in conjunction with BD -10 295, the pair make the double HJ 2039.

Unfortunately, the matter became confused in Aitken's 1932 compilation, *New General Catalog of Double Stars*, known as the ADS. Here, the brighter star (BD -10 295) is named HU 6. This is probably the origin of the error we presently find in the WDS:

1101	719		Hu 6 —10				
		14	19 74 17.0	—9° 43′ 59	9.1 F0		
	1899.87	240°3	0.61	9.1-9.3	3n Hu		
	1920.90	227.0	0.63		3 VBs		
			A	B-C=h 2039			
	1830+	237:1	35±	9	1n h		
	1904.43	24 0.2	46757		2 Gallo		

Figure 23. Aitken's Catalog Listing for HU 6 in 1932.

HU 6AB is here equated with BD -10 295, leaving BD -10 294 implicitly as HU 6C. The pairing HU 6AB,C is identified as HJ 2039. All this is just as in the modern WDS catalog.

By now, however, it should be clear that this identification is erroneous. Both Hussey and Van Biesbroeck identified HU 6 as the fainter component of HJ 2039, namely the star BD -10 294, which is what Gaia DR3 shows to be double. Hence, the confusion in the WDS ought to be cleared away. The author recently measured this double, and found its J2023.94 PA and Sep. to be 237.2°, and 0.43". The PA is not significantly changed from earlier measures; the Sep. may be a little smaller. An image of the pair (as part of HJ 2039) is shown below:



Figure 24. Author's Recent Image of HJ 2039, Where HU 6 is the Fainter Component (Lower Left)

Conclusions

From the six cases just discussed, it is clear that by delving into original publications, as well as making judicious use of the SIMBAD database (along with Gaia DR3 data) and selected new observations, we can in many cases clear away old errors and improve the WDS. The total number of additional misidentifications is not known or easily ascertained, since not all doubles lacking a recent measurement are subject to such errors. There are many Rossiter and van den Bos pairs, for example, which because of their southerly location and small Seps have not been observed for decades. Nevertheless, they are real pairs. Many can be found in Aladin with superimposed Gaia DR3 sources. The present author continues to image those pairs that lie north of -30° declination (with Seps > 0.4"), using lucky imaging and stacking via the REDUC software of Florent Losse. It is as part of this measurement program that the author became aware of WDS "lost" doubles. More are yet to be found and researched, and the author plans to continue doing so in future.

Acknowledgments

This research has made use of the Washington Double Star Catalog maintained at the U.S. Naval Observatory. The author wishes to thank the USNO, and Dr. Brian Mason for his prompt, kind, and extensive assistance. Also, F. Losse for the use of *REDUC*; T. Edelmann for *FireCapture*; and G. Sordiglioni for *Stelle Doppie*. The author also acknowledges and thanks *Stellarium*, and the CDS for the SIMBAD database, Richard Harshaw for the development and use of Plot Tool 3.19. Harshaw, Mason, and Mark Copper kindly read and commented on earlier versions of this paper. The author profited greatly thereby and renders his sincere thanks.

References

Aitken, R.G. (1932). New General Catalogue of Double Stars Within 120° of the North Pole, (Carnegie Institution), vols 1-2.

Barton, S.G. & C.P. Olivier. (1949). "1162 Measures of 1125 Double and Multiple Stars, Made with the Eighteen-Inch Refractor of the Flower Astronomical Obervatory." *Publications of the University of Pennsylvania, Astronomical Series*, 7(1), 1-44.

Berkó, E., (2010), "Measures of Double Stars with a DSLR Camera and 35.5-cm Reflector from 2009.200 to 2009.835," Webb Society Double-Star Section Circular, 18, 23-39.

Ceragioli, R. (2023). "Measurements of 50 Double Stars with 25 and 30-cm Refractors." JDSO, 14(4), 364-381.

Djurković, P.M. & Lj.M. Dačić. (1956). "Mesures micrométriques d'étoiles doubles, faites au réfracteur de 0.65-m d'ouverture." Bulletin de l'Observatoire Astronomique de Beograd, 21(3-4), 10.

Doolittle, E. (1907). "Catalogue and Remeasurement of the 648 Double Stars Discovered by Professor G.W. Hough." *Publications of the University of Pennsylvania, Astronomical Series*, 3(3), 1-176.

Giacobini, M., (1932), "Liste de 64 étoiles doubles nouvelles découvertes à l'Observatoire de Paris," *Journal des observateurs*, 15(3), 29-32.

Jeffers, H.M, W.H. van den Bos & F.M. Greeby (eds). (1963). *Index Catalogue Of Visual Double Stars*, 1961.0, vols 1-2.

Jonckhèere, R. (1912). Journal astronomique, 2(26), 5-8.

Jonckhèere, R.. (1917). "Catalog and Measures of Double Stars Discovered Visually from 1905 to 1916 within 105° of the North Pole and Under 5" Separation." *Memoirs of the Royal Astronomical Society*, 61, 1-205.

Lee, O.J. (1944). "Philip Fox, 1878-1944." Popular Astronomy, 52(8), 365-370.

Mason, B.D. et al., "Washington Double Star Catalog." Retrieved from http://www.astro.gsu.edu/wds/

Schlimmer, J.S. (2010). "Discovery of a New Double Star in Sagitta (HD311506)." *Journal of Double Star Observations*, 6(2), 154-155.

Van Biesbroeck, G. (edit.). (1946). "Measures of Double Stars by Philip Fox." *Annals of the Dearborn Observatory of Northwestern University*, 6, 1-42.

Walker, R.L., (1972), "Micrometer Measures of 618 Double Stars," *Publications of the United States Naval Observatory*, 2nd Series, 22(5), 1-66.

Worley, C.E. (1971). "Micrometer Measures of 1,343 Double Stars," *Publications of the United States Naval Observatory*, 2nd Series, 22(2), 1-136.

.....

About the author: Roger Ceragioli works at the Richard F. Caris Mirror Lab, University of Arizona, Tucson, USA. His expertise is in optical fabrication and design; he is co-manager in the optical production of the Giant Magellan Telescope's primary mirrors. He has written extensively on the history of telescopes, and co-authored a book analyzing modern astronomical optics for amateur astronomers. He holds a Ph.D. in Classical Philology from Harvard University.

Desmos Analysis of the Binary Star CHR 259 (WDS 15496-0326)

Michael-James L. Ellis^{1,2}, Diana Holland², Halli Kinnick², and Russell M. Genet¹

- 1. Eastern Arizona College, Payson, Arizona
 - 2. Payson High School, Payson, Arizona

Abstract Desmos, an online graphing calculator was used to analyze observations of the Binary Star WDS 15496-0326 (CHR 259), including a speckle interferometry observation first reported in this paper obtained with the 1.5-meter telescope at Mt. Wilson Observatory on 2023.4889 that measured a position angle of 309.01° and a separation of 0.470". Since this observation and one other recent observation closely aligned with Tokovinin's 2018 published orbit, there is no need to recalculate the orbit at this time.

Introduction

New speckle interferometry observations of the binary star WDS 15496-0326 (CHR 259) were made by students, instructors, and astronomers at Mt. Wilson Observatory in June of 2023. The Desmos online graphing calculator was used to analyze the published observations of CHR 259 and the new observation from Mt. Wilson. These observations were compared with the apparent orbital plot from the USNO Sixth Catalog of Orbits of Visual Binary Stars (hereafter the 6th Orbit Catalog) to determine if it would be worthwhile to calculate a new orbit (Matson et al. 2023).

The Desmos analysis in this paper is located at https://www.desmos.com/calculator/ofmie1xfh3. Desmos accounts are free. Anyone can start an account and download this analysis to their account.

Discovery of HU 256 as a Double Star

Astrometry "is a branch of astronomy that involves precise measurements of the positions and movements of stars and other celestial bodies" (Wikipedia 2024). Obtaining highly accurate positions for stars with telescopes located on Earth is hampered by atmospheric distortions (seeing). To overcome this difficulty, the European Space Agency launched the Hipparcos astrometric telescope in 1989 (Peryman 2010).

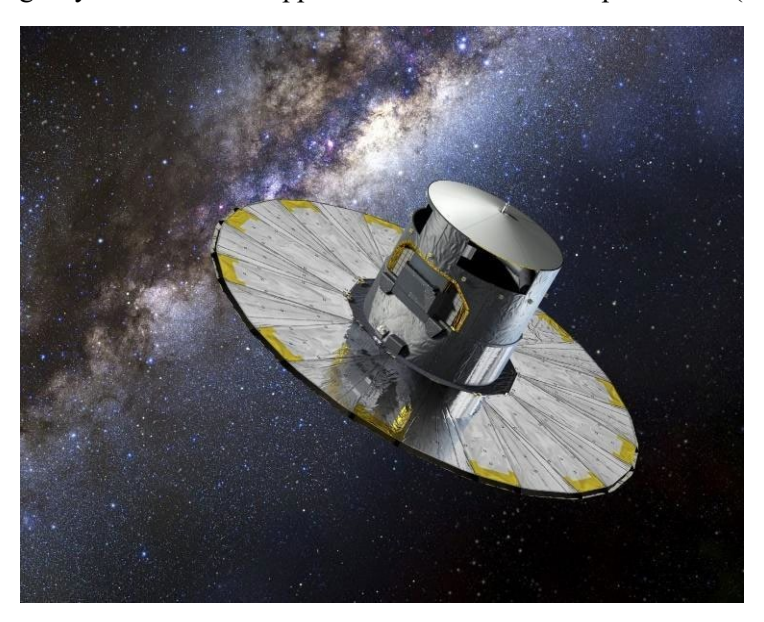


Figure 1: The European Space Agency's Hipparcos astrometric space telescope operated between 1989 and 1993, gathering precise data on the positions and radial velocities of over 100,000 stars.

Hipparcos is an acronym for High Precision Parallax Collecting Satellite, and also a reference to the Greek astronomer Hipparchus (190-120 BC) who discovered the precession of the equinoxes. Hipparcos operated from 1989-1993, scanning the sky multiple times with its two telescopes. It obtained the accurate positions and radial velocities of $\sim 118,200$ nearby stars in our galaxy.

Each star was observed multiple times to increase precision by averaging out small measurement errors. There were, however, several stars with changes in position over the three years that were larger than just measurement errors. It seemed likely that at least some of these "problem stars" might not be single stars but were binary stars with the apparent separations between the two stars so small that Hipparcos could not resolve them as two separate stars. Perhaps their photocenters (apparent locations of the unresolved stars) were in motion. WDS 15496-0326 (CHR 259) was one of these problem stars.

Hipparcos, with an aperture of only 0.3 meters, didn't have sufficient resolution to determine if these problem stars were two stars, let alone make the many observations over a number of years it would take to determine if these were gravitationally bound binary stars rotating around a common center of gravity. However, much larger Earth-based telescopes might be able to resolve many of these stars if they overcome the effects of atmospheric turbulence via speckle interferometry. Speckle interferometry overcomes atmospheric distortion by taking many hundreds of exposures so short (typically tens of milliseconds) such that atmospheric jitter is essentially frozen out (Genet 2015). A complex, computerized mathematical technique, bispectrum analysis, is then used to synthesize an image much like one would see from space via a deconvolution process that uses similar observations of a nearby single star to remove optical distortions.

The three years of the Hipparcos astrometric space telescope observations were completed in 1993 and were used to calculate stellar positions and radial velocities with a central (as of) date of 1991.25. Although the analysis was not completed and published as a catalog until 1997 (Fabricius & Makarov 2000) Hipparcos 1997), lists of some of the problem stars that included CHR 259 began circulating by 1993. Astronomers with access to large-aperture telescopes instrumented for speckle interferometry lost no time in observing these problem stars to determine if they were double stars. In early 1995, Brian Mason et al. (1999) were the first to obtain a speckle interferometry observation of CHR 259, using the historic 2.5-meter Hooker telescope at Mt. Wilson Observatory. They discovered that it was indeed a double star.

Establishing HU 256 as a Gravitationally Bound Binary

While a single speckle interferometry observation can discover that a star, previously thought to be a single star is; in fact, a double star, determining whether or not it is a gravitationally bound binary star takes many observations over years, decades, or even centuries, depending on the length of the binary's period. Besides their discovery observation, the Mason et al. (1999) team obtained three more speckle observations of HU 256 between 1995 and 1997. Mason et al. (2001) then observed CHR 259 with the 2.1-meter telescope at McDonald Observatory in 1999, while Lewis Roberts and Mason (2018) used adaptive optics on the 3.6-meter telescope on the summit of Haleakalā on Maui for a 2003 observation. Back on the 2.5-meter telescope at Mt. Wilson Observatory in 2006, William Hartkopf and Mason (2009), obtained another speckle interferometry measurement. Andre Tokovinin et al. (2010) made two measurements of CHR 259 on the SOAR (Southern Astrophysical Research) 4.1-meter telescope in Chile in 2009. Jack Drummond (2014) obtained three observations in 2011 using the 3.5-meter telescope equipped with adaptive optics at the Starfire Optical Range at Kirtland Air Force Base near Albuquerque, New Mexico. Andre Tokovinin et al. (2015, 2018) contributed two more SOAR observations in 2014 and 2016. At this point, Tokovinin (2018) concluded that there were sufficient observations to calculate and publish an orbit, officially establishing HU 256 as a binary.

Tokovinin et al. (2019, and 2022) contributed two more speckle interferometry observations in 2018 and 2021 that were not included in the orbit published in the 6th Orbit Catalog but were included as published observations in the Washington Double Star Catalog (2023). These two observations rounded out the

currently published observations. These published observations are shown in Table 1. Label is the observer (first author) and year of observation, Date is the year and fractional year, PA is the position angle (°), Sep is the separation ("), Ap is the aperture of the telescope in meters, Ref is the published reference code, and Tq is the technique used for the observation (Hh is Hipparcos, Sc, Su, S, and St are all various types of speckle interferometry, while A is adaptive optics.

Label	Date	PA	Sep	Ар	N	Ref	Tq
Hip1991	1991.2500	106	0.2000	0.3	1	Fab2000b	Hh
Hrt1995	1995.1432	91.2	0.2770	2.5	1	Hrt1999d	Sc
Hrt1996	1996.4319	86.3	0.2620	2.5	1	Hrt1999d	Sc
Hrt1996	1996.6998	86.3	0.2540	2.5	1	Hrt1999d	Sc
Hrt1997	1997.4585	80.8	0.2540	2.5	1	Hrt1999d	Sc
Msn1999	1999.1667	71.5	0.2290	2.1	2	Msn2001b	Su
Rbr2003	2003.5069	65.1	0.1000	3.6	1	Rbr2018	Α
Hrt2006	2006.5595	14.6	0.1590	2.5	1	Hrt2009	Su
Tok2009	2009.2643	353.5	0.2059	4.1	1	Tok2010	S
Tok2009	2009.2643	353.6	0.2051	4.1	1	Tok2010	S
Rbr2009	2009.2648	356.7	0.1934	5.1	1	Rbr2013a	Ac
Dru2011	2011.2180	342.9	0.2330	3.5	2	Dru2014	Α
Dru2011	2011.3197	340.9	0.2360	3.5	1	Dru2014	Α
Dru2011	2011.4730	341.4	0.2410	3.5	1	Dru2014	Α
Tok2014	2014.1844	329.3	0.2897	4.1	2	Tok2015c	St
Tok2016	2016.1376	323.3	0.3285	4.1	2	Tok2018c	St
Tok2018	2018.1798	318.5	0.3685	4.1	2	Tok2019c	St
Tok2021	2021.3188	312.9	0.4261	4.1	2	Tok2022f	St

Table 1: Published observations of WDS 15496-0326 (CHR 259).

Recent Observation of CHR 259

As part of the Known Binaries Program (Hardy et al. 2023), speckle interferometry observations were obtained for 50 close binaries on the 1.5-meter telescope at Mt. Wilson Observatory in June 2023 by a group of students, instructors, and amateur and professional astronomers (Faughn et al. 2023). Included was an observation of WDS 15496-0326 (CHR 259). The Speckle Toolbox (Rowe and Genet 2015, Harshaw et al. 2017) was used to reduce the observations of CHR 259 and a nearby single reference star, resulting in a Position Angle of 309.01° and a Separation of 0.470" on 2023.4889. The bispectrum reconstructed image of the binary obtained at Mt. Wilson Observatory is shown in Figure 2.

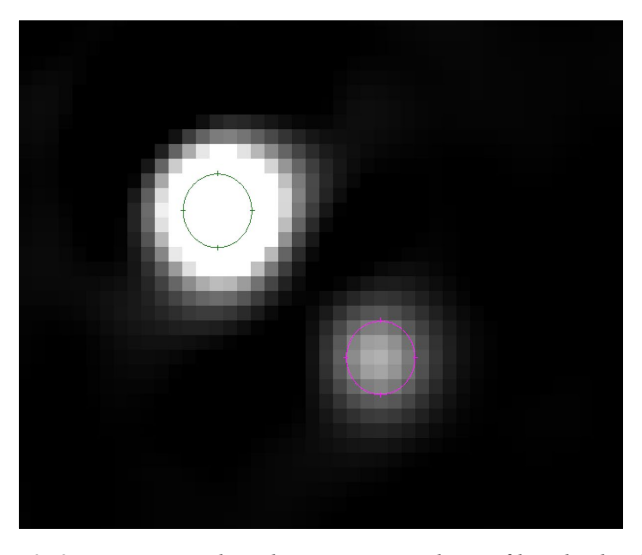


Figure 2: Image of CHR 259 reconstructed via bispectrum analysis of hundreds of short exposures of the

binary and a nearby single reference star used for deconvolution. Each pixel is only 0.03" in width.

Desmos Analysis

The starting point for the Desmos analysis of CHR 259 was the orbital plot of CHR 259 downloaded from the Sixth Catalog of Orbits of Visual Binary Stars (Matson et al. 2023, hereafter the 6th Orbit Catalog). This plot is shown in Figure 3.

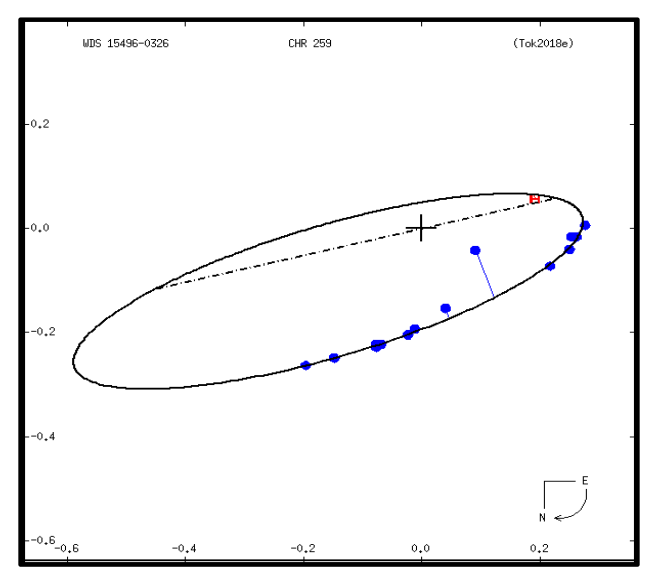


Figure 3: Orbital plot of CHR 259 from the 6th Orbits Catalog.

The 6^{th} Orbit plot was inserted as a background image in Desmos. Following the procedure outlined by Genet et al. (2024), the image was rotated 90° counterclockwise to place celestial north along the positive x-axis. The background image scale (width and height), which in Desmos is a default of 10.0 units, was rescaled to 1.027 units to match the scale of the 6^{th} Orbit plot, and the primary star location (the + on the 6^{th} Orbit plot was translated to 0.122 units in x and -0.154 in y to be coincident with the Desmos (0,0) Cartesian origin. The final rotated, scaled, and translated 6^{th} Orbit background plot is shown in Figure 4.

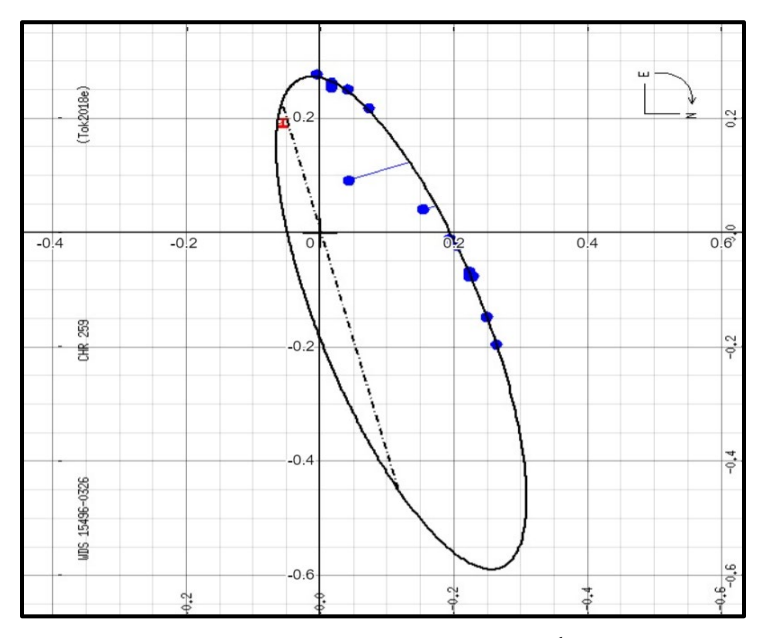


Figure 4: Appropriately rotated, scaled, and translated 6th Orbital plot of HU 259.

All the past observations shown in Table 1, as well as the recent observation at Mt. Wilson Observatory, were labeled, again following the procedures in Genet et al. (2024). These added labels are shown in Figure 5 (left), while a highly magnified view is shown on the right where it can be seen how each Desmos plotted point (red x) is in the center of the 6th Orbit plot's round blue points, demonstrating that the 6th Orbit background plot is properly registered with Desmos Cartesian coordinate system.

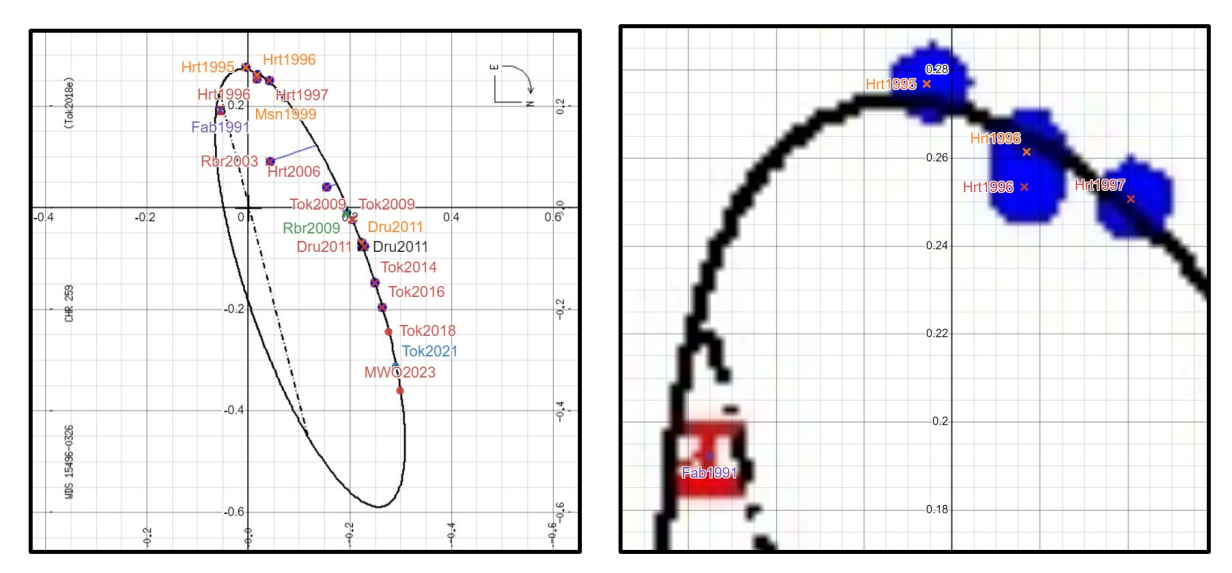


Figure 5: Orbital plot with added labels (left) and magnified image showing registration of Desmos points with the background.

For an ellipse not centered on the origin and not coincident with the x-axis, as is the binary star case, one can use the general parametric equations for an ellipse in the Cartesian plane:

 $x = (h + a \cos t)(\cos q) + (k + b \sin t)(-\sin q)$

 $y = (h + a \cos t)(\sin q) + (k + b \sin t)(\cos q)$

where:

a is the semi-major axis

b is the semi-minor axis

q is the angle from the x-axis to the ellipse major axis

h is the offset of the center of the ellipse from the primary star (the "+") along the ellipse's primary axis *after* the ellipse has been rotated

k is the y offset of the center of the ellipse from the primary star (the "+") perpendicular to the ellipse's primary axis *after* the ellipse has been rotated

(t is just the parametric variable that traces out the ellipse from 0 to 360°)

These two equations, which form the (x,y) points for an ellipse, were entered into Desmos. The first part of this equation can be seen upper left in Figure 6. The five parameters are displayed by Desmos on the left so that values can be entered directly if known, or sliders adjusted as desired. The sliders were iteratively adjusted to fit the 6^{th} Orbit background ellipse. The Desmos ellipse (orange dots) overlays the black background 6^{th} Orbit ellipse.

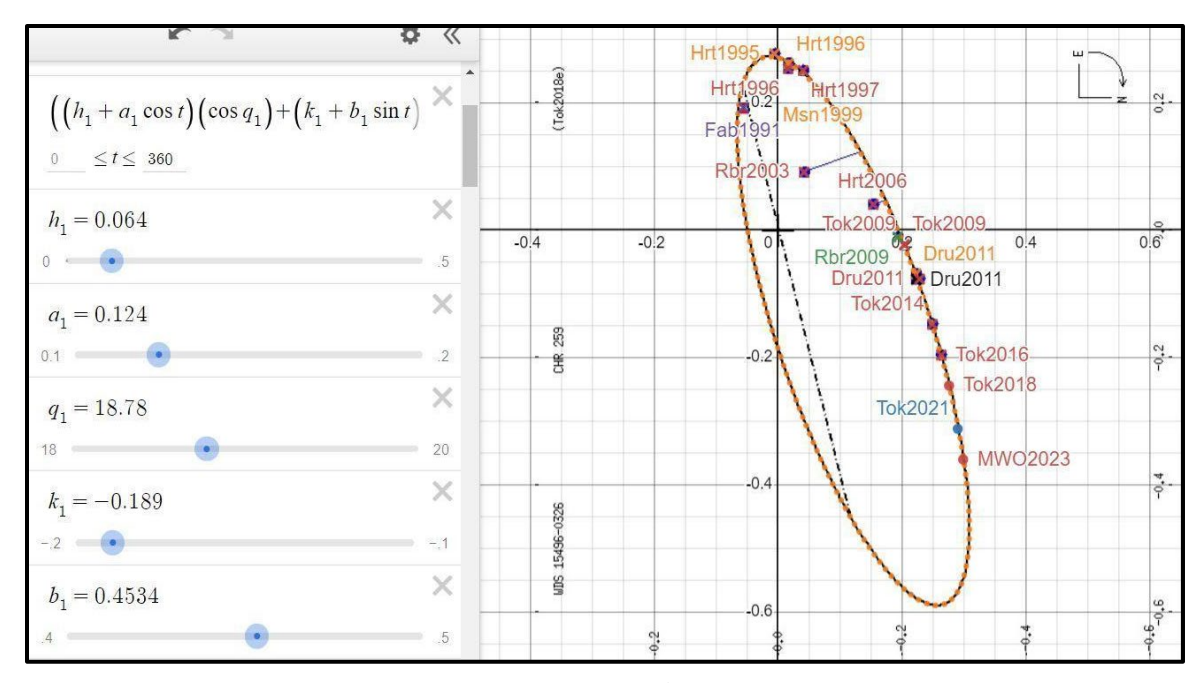


Figure 6: Orbital plot of WDS 15496-0326 from the 6th Orbit Catalog with matching Desmos plot and observation points including three unpublished observations.

Finally, while the recent observations seemed to follow the Tokovinin orbit published in 2018, a new orbit (green line in Figure 7 left) was created in an attempt to obtain an even better fit. An enlarged view (Figure 7 right) suggests that Tokovinin's 2018 orbit is a good fit to the speckle observations over the past decade, including three new ones made since the orbit was published. It is possible that future observations might follow the new green-line orbit. If they do, the orbital period would be somewhat shorter, and hence the combined mass of the two stars somewhat greater than currently estimated. Continued observations over the next decade should settle this question.

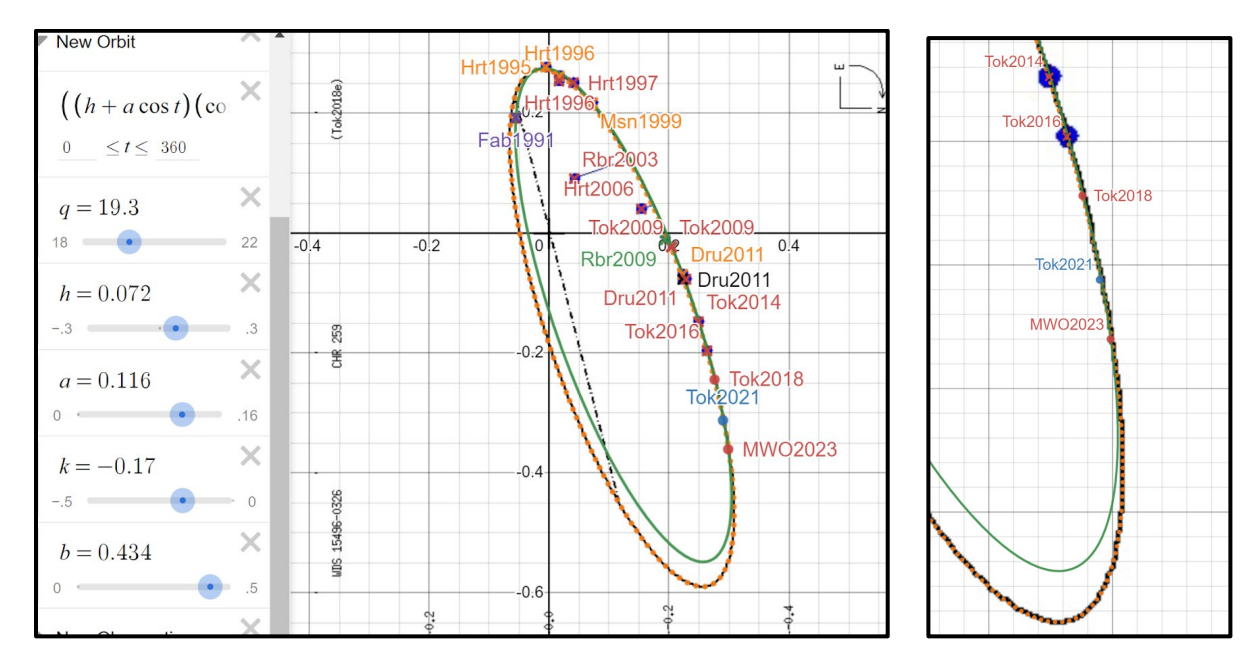


Figure 7: New orbital plot (green line, left), and magnified view (right).

Conclusions

WDS 15496-0326 (CHR 259), previously thought to be an unremarkable single star, was identified in 1994 as a "problem star" by the Hipparcos astrometric space telescope, and discovered, via speckle interferometry observations on the historic 2.5-meter telescope at Mt. Wilson Observatory, to be a double star. After 21 years of speckle interferometry observations on six different large-aperture mountaintops telescopes, Andre Tokovinin's published orbit in 2018 officially confirmed CHR 259 as a gravitationally bound binary pair.

Since then, Tokovinin obtained two more speckle observations, and one of us (Genet), along with others, obtained a recent speckle observation of this binary on the historic 1.5-meter telescope also on Mt. Wilson Observatory, just yards away from the discovery 2.5-meter telescope. Reduction of this observation (this paper) yielded a position angle of 301.01° and separation of 0.470" on 2023.4889.

Desmos analysis of all 18 previously published observations and the one observation described in this paper conform to Tokovinin's 2018 published orbit, hence no new orbit needs to be calculated at this time.

Acknowledgments

The United States Naval Observatory supplied past observations of WDS 16212+2259 from their Washington Double Star Catalog. The background plot was from the Sixth Catalog of Orbits of Visual Binary Stars. We utilized Dave Rowe's Speckle Tool Box and the Desmos graphing calculator for reduction and analysis. The Institute for Student Astronomical Research (InStAR) purchased time on the 1.5-meter telescope at Mt. Wilson Observatory where the new speckle interferometry of WDS 16212+2259 was made. Gravic Inc. provided travel funds for students to attend the run. Rachel Freed, Reed and Chris Estrada, Nick Hardy, Leon Bewersdorff, Joseph Burch, Paul McCudden, Tom Smith, and others helped organize the run and manage the observations. Thomas Meneghini, the Director of the Mt. Wilson Observatory, and his staff provided support during the run. We thank Payson High School and Eastern Arizona College for their support of this analysis. Finally, we thank several external reviewers for their helpful comments.

References

- Drummond, J. 2014. Binary Stars Observed with Adaptive Optics at the Starfire Optical Range. *The Astronomical Journal*, 147, 65.
- Fabricius, C., and V. Makarov. 2000. Hipparcos astrometry for 257 stars using Tycho-2 data. *Astronomy & Astrophysics Supplement Series*, 144, 45.
- Genet, R. 2015. Speckle Interferometry of close Visual Binaries. *Journal of Double Star Observations*, 11, 183.
- Genet, R., P. McCudden, & M. Ellis. 2024. Desmos Analysis of Known Binaries: WDS 16212+2259 (HU 481) Example. *Journal of Double Star Observations*, in press.
- Faughn, E., J. Major, & P. McCudden. 2023. Speckle Astrometry of WDS 18181-0120. *Journal of Double Star Observations*, 19, 421.
- Hardy, N., L. Bewersdorff, D. Rowe, R. Genet, R. Wasson, J. Armstrong, S. Dixon, M. Harris, T. Smith,
 R. Freed, P. McCudden, S. Rajkumar, M. Davis, C Giavarini, R. Snyder, R. Wolly, M. Calvin, S.
 Cotton, & M Rabin. 2023. Automated Speckle Interferometry of Known Binaries: With WDS 12274-2843 B228 as an Example. *Journal of Double Star Observations*, 19, 106.
- Harshaw, R., D. Rowe, & R. Genet. 2017. The Speckle Toolbox: A Powerful Data Reduction Tool for CCD Astrometry. *Journal of Double Star Observations*, 13, 52.
- Hartkopf, W. & B. Mason. 2009. Speckle Interferometry at Mount Wilson Observatory: Observations Obtained in 2006-2007 and 35 New Orbits. *The Astronomical Journal*, 138, 813.
- Hipparcos. 1997. Hipparcos and Tycho catalogues. Astrometric and photometric star catalogues derived from the ESA Hipparcos Space Astrometry Mission, Publisher: Noordwijk, Netherlands: ESA Publications Division, Series: ESA SP Series vol no: 1200, ISBN: 9290923997.

- Matson, R., S. Williams, W. Hartkopf, & B. Mason. 2023. *Sixth Catalog of Orbits of Visual Binary Stars*, U.S. Naval Observatory, Washington, DC. http://www.astro.gsu.edu/wds/orb6.html
- Mason, B., C. Martin, W. Hartkopf, D. Barry, M. Germain, G. Douglas, C. Worley, G. Wycoff, T. Ten Brummelaar, & O. Franz. 1999. Speckle Interferometry of New and Problem Hipparcos Binaries. *The Astronomical Journal*, 117, 1890.
- Mason, B., W. Hartkopf, E. Holdenried, & T. Rafferty. 2001. Speckle Interferometry of New and Problem Hipparcos Binaries II. Observations Obtained in 1998-1999 from McDonald Observatory. *The Astronomical Journal*, 121, 3224.
- Peryman, M. 2010. The Making of History's Greatest Star Map. Springer.
- Roberts, L., R. & B. Mason. 2018. Astrometric and Photometric Measurements of Binary Stars with Adaptive Optics: Observations from 2001 to 2006. *Monthly Notices of the Royal Astronomical Society*, 473, 4497.
- Rowe, D., and R. Genet. 2015. User's Guide to PS3 Speckle Interferometry Reduction Process. *Journal of Double Star Observations*, 11 (1s), 266.
- Tokovinin, A., B. Mason, & W. Hartkopf. 2010. Speckle Interferometry at the Blanco and SOAR Telescopes in 2008 and 2009. *The Astronomical Journal*, 139, 743.
- Tokovinin, A., B. Mason, W. Hartkopf, R. Mendez, & E. Horch. 2015. Speckle Interferometry at SOAR in 2014. *The Astronomical Journal*, 150, 50.
- Tokovinin, A. 2018. Orbital Elements published in the IAUDS #125.
- Tokovinin, A., B. Mason, R. Mendez, E. Horch, & C. Bricefio. 2019. Speckle Interferometry at SOAR in 2018. *The Astronomical Journal*, 158, 48.
- Tokovinin, A., B. Mason, W. Hartkopf, R. Mendez, & E. Horch. 2018. Speckle Interferometry at SOAR in 2016 and 2017. *The Astronomical Journal*, 155, 235.
- Tokovinin, A., B. Mason, R. Mendez, & E. Costa. 2022. Speckle Interferometry at SOAR in 2021. *The Astronomical Journal*, 164, 58.
- Washington Double Star Catalog. 2023. United States Naval Observatory, https://www.astro.gsu.edu/wds/ Wikipedia 2023a, Definition of astrometry, https://en.wikipedia.org/wiki/Astrometry

A New Double Star Discovered During an Asteroid Occultation of UCAC4 339-186983

David Gault

Trans-Tasman Occultation Alliance <u>dave4gee@yahoo.com.au</u> International Occultation Timing Association (IOTA), Fountain Hills, AZ

Abstract

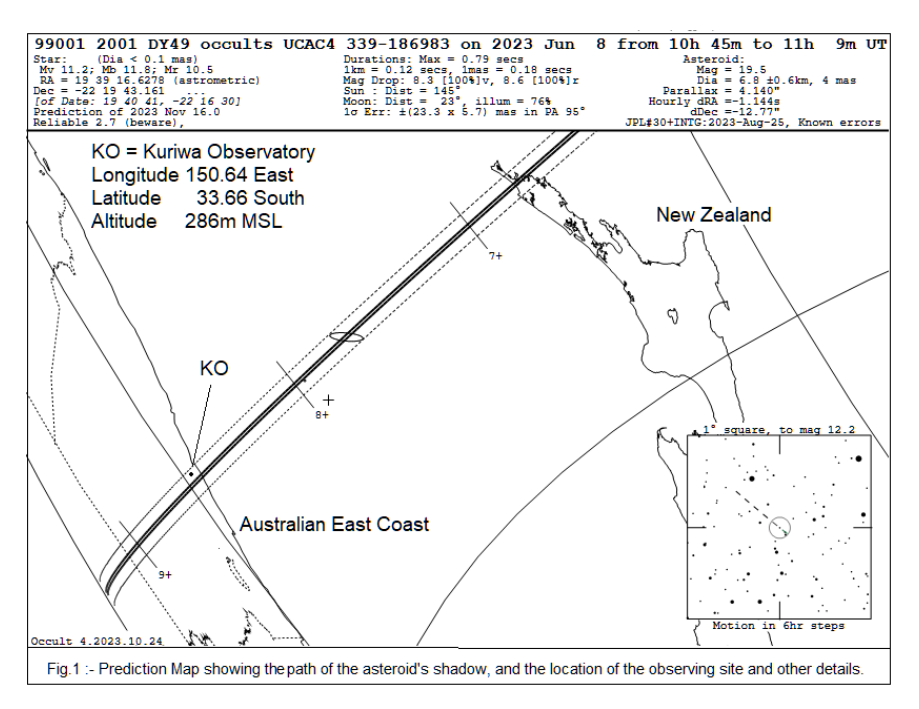
On June 8, 2023, (22001) 2001 DY49 occulted UCAC4 339-186983 as observed from Kuriwa Observatory (KO), cited in the Blue Mountains, west of Sydney, Australia. Two separate extinctions of the star were observed consistent with the star being a double star of magnitudes 11.7 and 12.3, separated by 51.1 mas at PA 50.6 deg. The star is a hitherto unknown double star.

1. Introduction

The observation of asteroid occultations can yield information about the asteroid; size and shape as well as astrometry that ties the asteroid's orbit to the star at event epoch. The observation can also yield information about the star – in this case it's double star nature that has not been observed before.

2. Circumstances

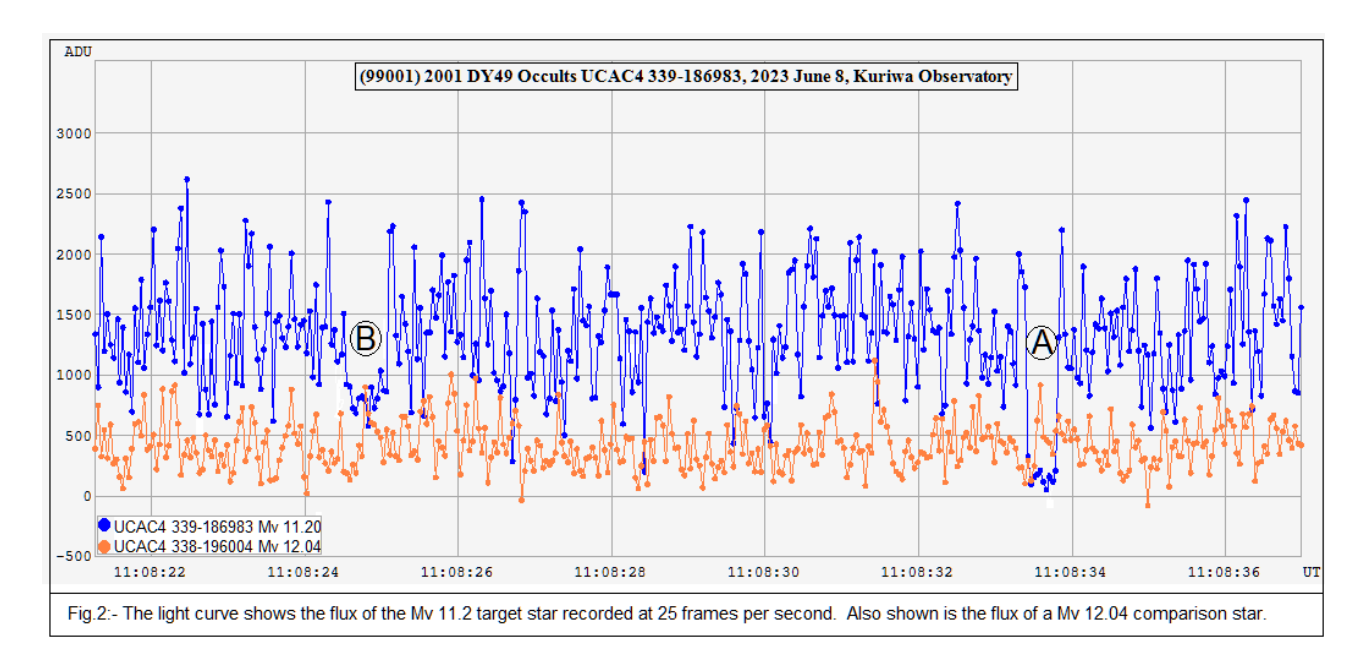
Fig. 1 shows the circumstances of the observation. The prediction is a computation based on the orbit, supplied by JPL Horizons and Gaia DR3 star coordinates. The path of the asteroid's shadow passed across the South Pacific Ocean, the northern tip of New Zealand, across the Tasman Sea, and across Australia. The star and asteroid were observed to be at 19 degrees altitude and 104 degrees azimuth from the observing site.



3. The Observation

A 30cm Schmidt Cassegrain

telescope equipped with a video camera operating at 25 frames per second, with GPS time inserted on every frame was used to record the observation. Fig, 2 shows the light curve recorded for the target star + asteroid, as well as a comparison star.



The fainter B star was occulted first for a duration of 0.70 seconds. The extinction of light was shallower than expected because the brighter A star remained in view. 8.3 seconds later the brighter A component was occulted for a duration of 0.38 seconds. The extinction of light was shallower than expected because the fainter B star remained in view. The event times are listed in Table 1.

Table 1. Event times

Event	Time – UTC	± (sec)
d1	11:08:24.3	0.1
r1	11:08:25.1	0.1
D2	11:08:33.39	0.04
R2	11:08:33.77	0.04

4. Reduction of Observation

The circumstances and observed times were reduced and plotted on the fundamental plane using Occult4 software as shown on Fig.3.

5. Double Star Characteristics

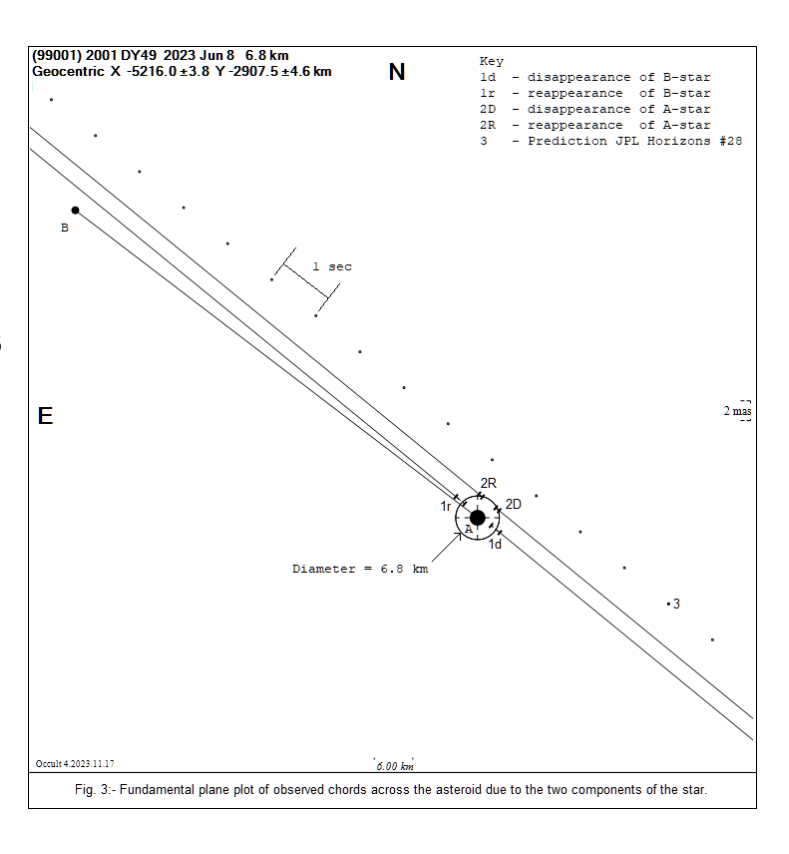
Star	UCAC4 339-186983
Coordinates (J2000)	19h 39m 16.6278s,
	-22° 19m 43.161s
Mag. A	11.8 +/- 0.1 (V)
Mag. B	12.1 +/- 0.1 (V)
Separation	5.1 +/- 0.1 mas
Position Angle	50.6° +/- 2.8°

2023.4356

Acknowledgements

Observation Epoch

The author wishes to acknowledge;



- The Washington Double Star Catalog maintained at the U.S. Naval Observatory.
- This work has made use of data from the European Space Agency (ESA) mission Gaia (https://www.cosmos.esa.int/gaia), processed by the Gaia Data Processing and Analysis Consortium (DPAC, https://www.cosmos.esa.int/web/gaia/dpac/consortium). Funding for the DPAC has been provided by national institutions, in particular the institutions participating in the Gaia Multilateral Agreement.
- The asteroid's orbit was supplied by JPL Horizons Solar System Dynamics Small Body Orbit database. https://ssd.jpl.nasa.gov
- David Herald for is help and guidance.

Observations of 42 Double Stars Near Messier 35

Kaden Anderson¹, Hunter Castleton¹, Nisha Fletcher¹, Tristyn Montgomery^{2,3}, Preston Pack¹, Shaeden McCord³, Elizabeth Eastep³, Trinity Wilcox³, Cash Lake³, Kyler Ahlvers⁴, Jillian Bath⁴, Oliver Brumit⁴, Adelaide Costello⁴, Krosby Cox⁴, Dante Hollowbreast⁴, Viktoria Howard⁴, Cecil Kunz⁴, Boston McNutt⁴, Brooklee McNutt⁴, Catherine Murphree⁴, Breanna Nielson⁴, Cooper Reed⁴, Ledger Ruesch⁴, Sophie Sandoval⁴, Layla Tate⁴, Levi Walker⁴, Heather Lambert³, Kaelyn Porter⁴, Cameron Pace¹

- 1. Southern Utah University, Cedar City, Utah
 - 2. SUCCESS Academy, Cedar City, Utah
 - 3. Launch High School, Cedar City, Utah
 - 4. White Pine Middle School, Ely, Nevada

Abstract

For this work we observed 42 stars near M35. Of these, 30 were first observed in 1926 and the remainder largely have a first observation in 1998. In most cases, plots of historical measurements are consistent with linear motion, although less than 1" of motion has been observed over this time, which makes interpreting these plots difficult. We used Gaia DR3 data to better understand the nature of these stars. Most of them are not physically associated with each other, however 26 are cluster members. We found that WDS06085+2414 is a cluster member and likely a true binary, while WDS06079+2435 is probably a binary, although it is not a cluster member.

Introduction

In this paper, we investigate 42 double stars located within and near the open cluster Messier 35 (Dias et al. 2021). This region was selected because of the abundance of double stars available within a single frame. The open cluster NGC 2158 (Poggio et al. 2021) is also nearby, although it is out of the field of view of our images, and none of the stars we observed appear to be members of this cluster. Our analysis involves the measurement of the stars' astrometry (separation and position angle) and comparison of our measurements with historical data. Gaia DR3 (Gaia collaboration et al. 2016b, 2023j) parallax and proper motion measurements were also used to assess the physical nature of our observed systems. The Gaia data was also helpful in determining whether any of the systems are members of M35.

For 40 of the stars in our study, the most recent observation dates to 2015, while one is from 2016 and another dates to 2013. As for the first observation, 30 of the systems have an original observation date to 1926, with a single star having been first observed in 1894. The remaining 11 stars were first observed in 1998. Thus, we have a baseline of nearly a century for about three-fourths of the stars, while the remainder have an observational baseline of about 25 years.

Methods

We observed these systems using the Great Basin Observatory located in Great Basin National Park, Nevada. Technical specifications of the observatory and its instruments are provided in Anselmo et al 2018. This observatory is managed and maintained by a consortium consisting of Great Basin National Park and the Park's Foundation, Southern Utah University, and the University of Nevada-Reno. Twelve images of the selected region were taken on February 13th, 2023. The images were taken in the V filter and had an exposure time of 300 seconds to maximize the signal to noise of the star systems in the field of view, which is shown in Figure 1. The systems studied in this paper are indicated, with those systems having at least one star belonging to M35 shown as blue ovals, while systems whose Gaia DR3 parallax and proper motion are inconsistent with cluster membership are shown in red. The radius in which half of the cluster members are found (the r₅₀) is also shown (Cantat-Gaudin, Anders 2020).

AstroImageJ (Collins et al. 2017) was used to verify that the components of the systems were not overexposed. Several systems (06071+2429, 06087+2416, 06087+2412, 06088+2417) were found to be saturated and therefore unmeasurable,which left 42 systems for study. AstroImageJ was also used to reduce the images, which were dark, bias, and flat corrected. The images were then plate solved with http://nova.asrometry.net/ (Lang 2010). Finally, AstroImageJ was used to measure the separation (ρ) and position angle (θ) of the stars.

We have found that the aperture size affects the standard deviation of the measurements of a given system across several images. The effect is quite small (usually less than 0.1 arcsec), especially for well-resolved systems. However, it becomes more of an issue with more closely-spaced stars. This effect seems to be related to how AstroImageJ calculates the centroid within the selected aperture size. Generally, the suggested aperture size provided in the seeing profile will yield measurements with the smallest standard deviation. As we measured our stars, we varied the aperture size and noted how the different diameters affected the standard deviation for that system. We then recorded the separation and position angle that yielded the smallest standard deviations, and we report those values in Table 1.

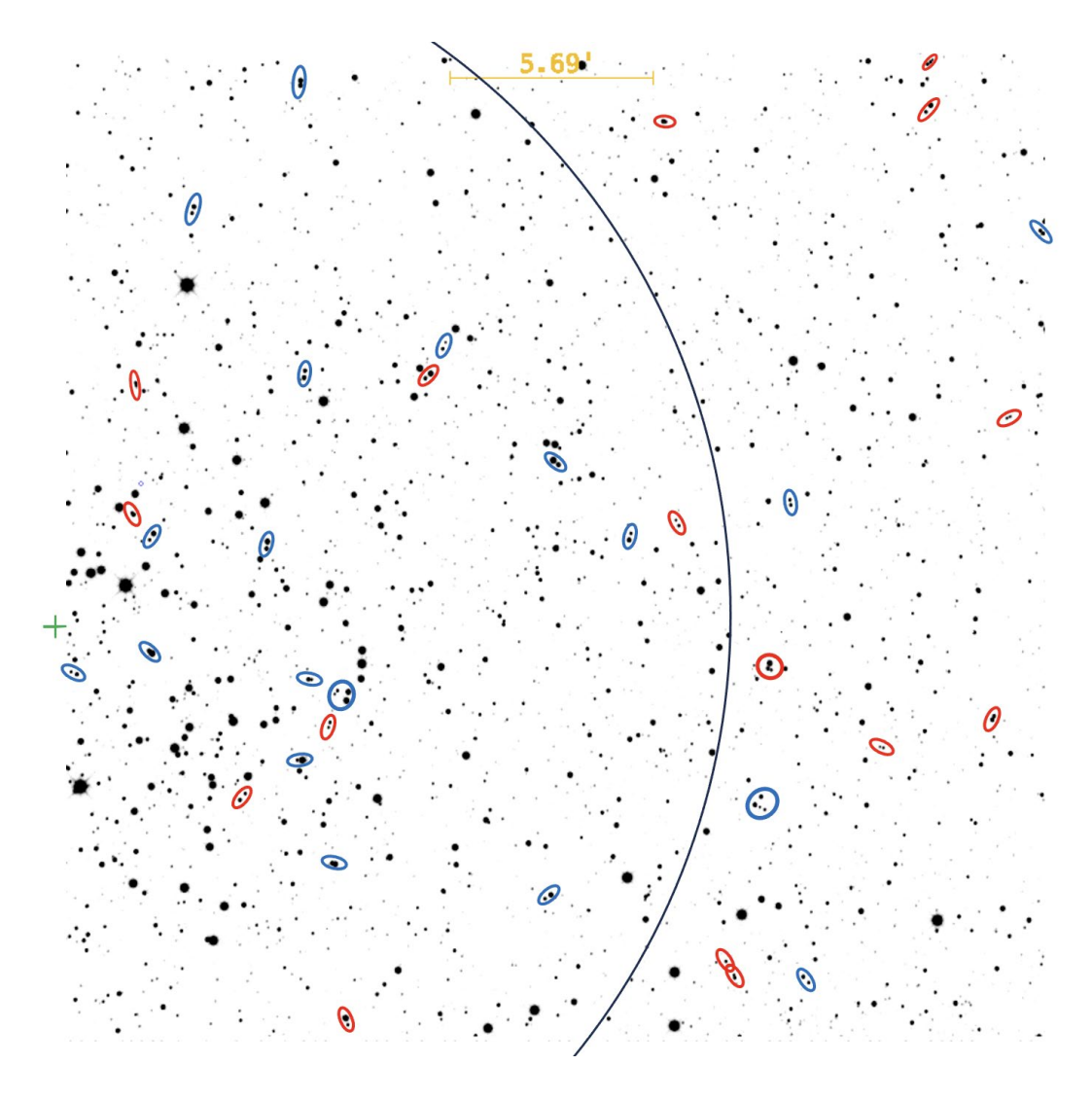


Figure 1 Finder chart of the stars we imaged. The green cross indicates the center of M35, while the curved line shows the r_{50} (the radius which encloses half the cluster members) of the cluster. Blue marks denote systems whose Gaia observations indicate that at least one system member is also a cluster member, while red marks indicate systems whose Gaia measurements are inconsistent with cluster membership. Most of those systems within the angular extent of M35 have at least one cluster member, while those whose distance is greater than this are typically not members.

Results

Our measurements of rho and theta for the 42 stars in this study are presented in Table 1. Additionally, we assessed cluster membership via proper motion and parallax information extracted from the Gaia DR3 database. Column 4 indicates those stars that are likely cluster members, and further details of the cluster membership criteria are provided in the Discussion.

WDS Identifier	Rho (Error)	Theta (Error)	Cluster, Binary
06071+2419	6.92 (0.04)	157.2 (0.21)	
06071+2427	5.88 (0.17)	296.2 (0.39)	
06071+2432	6.69 (0.02)	47.1 (0.18)	В
06073+2418	6.07 (0.06)	77.6 (0.29)	
06073+2435	13.69 (0.02)	146.6 (0.04)	
06073+2437	6.31 (0.05)	128.9 (0.28)	
06075+2411	13.34 (0.02)	224.1 (0.08)	В
06076+2411	8.72 (0.04)	37.00 (0.23)	
06076+2416AB	17.1 (0.04)	324.9 (0.08)	А
06076+2416AC	9.30 (0.03)	247.8 (0.12)	А
06076+2416CD	9.26 (0.06)	244.8 (0.39)	
06076+2420AB	9.16 (0.01)	162.6 (0.09)	
06076+2420BC	6.26 (0.04)	246.9 (0.33)	
06076+2424	8.81 (0.02)	10.8 (0.07)	Α?
06077+2412	4.62 (0.22)	14.6 (0.75)	
06078+2424	10.42 (0.03)	29.6 (0.08)	
06079+2423	11.24 (0.02)	346.8 (0.07)	В?
06079+2435	4.16 (0.12)	264.4 (1.28)	Binary
06080+2413	11.96 (0.01)	126.8 (0.09)	В
06080+2425	11.55 (0.01)	232.1 (0.06)	A & B
06081+2422AB	12.53 (0.01)	206.7 (0.05)	
06081+2422AC	9.23 (0.02)	6.5 (0.07)	
06083+2428	12.09 (0.01)	133.2 (0.05)	
06083+2429	11.83 (0.03)	339.1 (0.11)	А
06084+2410	11.57 (0.03)	199.6 (0.09)	
06085+2414	5.7 (0.07)	75.9 (0.4)	A & B, Binary
06085+2417	8.57 (0.14)	94.1 (0.28)	А

8.83 (0.03)	166.5 (0.07)	
14.91 (0.01)	349.9 (0.02)	A & B
22.43 (0.02)	44.6 (0.06)	А
7.67 (0.04)	143.7 (0.16)	
5.63 (0.06)	269.4 (0.37)	В
11.96 (0.01)	176.0 (0.03)	А
11.83 (0.01)	355.7 (0.06)	В
8.28 (0.01)	182.0 (0.06)	В
13.88 (0.02)	323.0 (0.02)	В
11.41 (0.01	165.8 (0.05)	А
7.01 (0.04)	53.0 (0.20)	А
12.68 (0.02)	150.1 (0.05)	А
3.60 (0.3)	41.3 (2.15)	
4.2 (0.19)	194.3 (0.46)	
10.65 (0.02)	68.9 (0.13)	А
	14.91 (0.01) 22.43 (0.02) 7.67 (0.04) 5.63 (0.06) 11.96 (0.01) 11.83 (0.01) 8.28 (0.01) 13.88 (0.02) 11.41 (0.01 7.01 (0.04) 12.68 (0.02) 3.60 (0.3) 4.2 (0.19)	14.91 (0.01) 349.9 (0.02) 22.43 (0.02) 44.6 (0.06) 7.67 (0.04) 143.7 (0.16) 5.63 (0.06) 269.4 (0.37) 11.96 (0.01) 176.0 (0.03) 11.83 (0.01) 355.7 (0.06) 8.28 (0.01) 182.0 (0.06) 13.88 (0.02) 323.0 (0.02) 11.41 (0.01 165.8 (0.05) 7.01 (0.04) 53.0 (0.20) 12.68 (0.02) 150.1 (0.05) 3.60 (0.3) 41.3 (2.15) 4.2 (0.19) 194.3 (0.46)

Table 1 Our measurements for rho and theta for the pairs observed. The 4th column indicates if either or both of the stars are members of the M35 open cluster. Systems that are true binaries are also here indicated.

Discussion

To investigate whether any of these systems are physical, we plotted our measurements together with the historical measurements provided by Matson (2023). These plots were generated with Plot Tool (Harshaw 2020) for all our observed systems. For 30 stars, the first observation dates from 1926, while the remainder generally have a first observation dating to 1998. In many cases, we found that less than 1" of motion has been observed, sometimes over the course of a century or so, which makes it difficult to assess the physicality of the systems from the historical measurements alone. We find that in general, the historical measurements from 2009 tend to be outliers. This may be because the 2009 measurements were taken by the space-based Wide-field Infrared Survey Explorer (WISE) mission (Wright et al. 2010), and it is

possible that there was some systematic offset in correlating the astrometry of that mission with ground-based astrometry.

Figure 2 shows plots of historical measurements, together with our new measurement, for 4 of the stars we observed. The top two panels, for WDS 06080+2425 and WDS 06073+2437, show linear relations for the motions of these stars over the course of the last century. Many of the systems we observed show such linear relations, although these relations may not mean much in cases where the observed motion is less than 1 arcsec.

In the bottom two panels we show examples of the plots where the motion is harder to interpret. WDS 06076+2416 AC shows several outliers, the most discrepant of which is the measurement from 2009. The bottom right panel for WDS 06078+2424 is typical of those whose reported measurements make it difficult to discern the actual motion of the star. The 2009 measurement again appears to be discrepant, as does the 2010 measurement. In these panels we again see an apparent motion of less than 1." Clearly, the historical measurements alone would not be sufficient to characterize the nature of these systems.

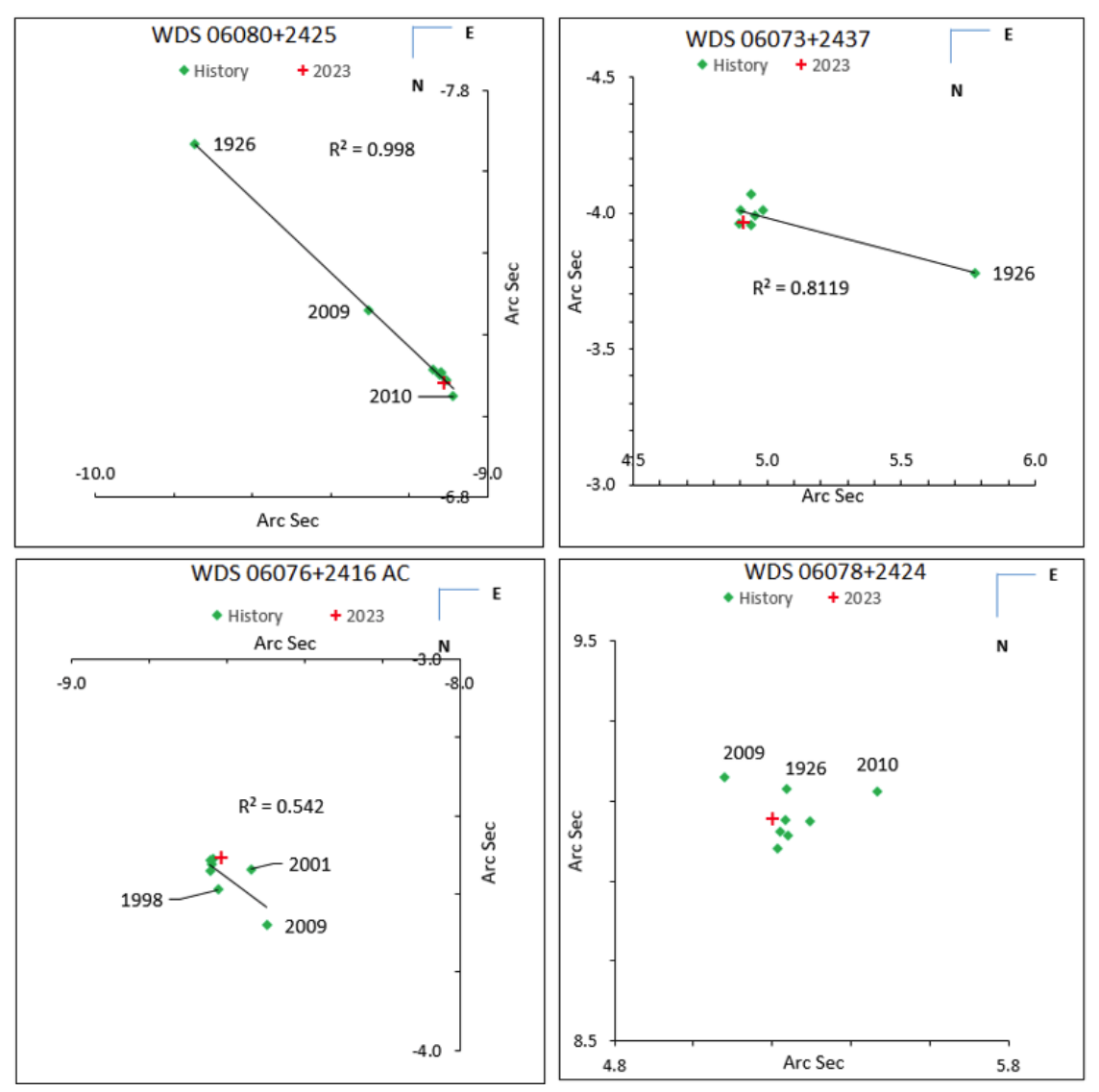


Figure 2 Plots of historical measurements (generated using Plot Tool) for 4 representative systems. Although the top two seem linear, they show less than 1" of motion over ~100 years. The bottom two are less clear, but again less than 1" of motion is seen.

To further assess whether our observed systems are physical, we extracted parallax and proper motion data from Gaia DR3. This was also used to examine whether the stars we observed are members of the M35 cluster. Several values for the parallax and proper motion of this cluster are provided in the literature. Dias et al. (2021) used Gaia DR2 data to derive a parallax of 1.127 with a measurement error of 0.07 mas, while Poggio et al. (2021) used Gaia EDR3 data to generate a parallax of 1.152 with a measurement error of 0.039 mas. As for proper motion, Dias et al. (2021) report a pm-ra of 2.299 (±0.567) and a pm-dec of -2.905 (±0.251), with Poggio et al. (2021) reporting a pm-ra of 2.256 (±0.201) and a pm-dec of -2.889 (±0.197). Based on these values, we have indicated in Table 1 probable cluster members stars whose parallax lie within the range 1.025 - 1.149 and whose pm-ra lies within the range 1.4 - 2.7 and whose pm-

dec is between -3.19 and -2.34. In the paragraphs that follow, we discuss the properties of each system in the context of the historical measurements, our new observation, and the Gaia parallax and proper motions. The "goodness" of the Gaia data is measured with RUWE (Lindegren 2018). For good measurements, the RUWE should be near 1. In the discussion that follows, all Gaia measurements are near this value, unless otherwise noted.

06071+2419

It is difficult to interpret the motions of this pair, as there are three apparent outliers in the data. The observations do not appear to be consistent with either orbital or linear motion. However, the system has seen less than 0.5" of motion over the past century, which is true for many of the systems in this field. The Gaia data clarify the nature of the system, with the A component at a distance of 1,600 pc and the B component at 2,700 pc. This would explain why so little motion has been seen, and would also indicate that this pair is not physical.

06071+2427

Past measurements of these stars are hard to analyze due to their scattered nature. Measurements from 2009 and 2010 appear to be outliers, and there is no strong linear relationship between the pair. However the Gaia data indicate that the stars are not physical, although the errors on the parallax are somewhat elevated, at 17% for the A component and 8% for the B component. The distances corresponding to these parallaxes are 4,400 - 6,200 pc for the primary and 1,600 - 1,900 pc for the secondary. This suggests that these stars are not physically related.

06071+2432

The historical observations are incredibly linear, with R^2 = 0.95. Our measurement fits well into this line of movement. It is unlikely that these two stars are related to each other, as the Gaia data indicate that the primary is at 1,750±75 pc away, while the secondary is at a distance of 872±17 pc. This distance and the proper motion are consistent with the secondary being a member of M35. However, this star is ~30' from the center of the cluster, indicating that if it is indeed a cluster member it must be only weakly bound.

06073+2418

This system is faint, complicating measurement. Additionally, the measurements taken in 2001 and 2009 seem to be outliers. The system has seen less than 0.5" of motion in a century, so we turn to the Gaia data for help. The proper motions are dissimilar, and the stars appear to be quite distant, with the primary at 3,650±400 pc and the secondary at 5,500±1,100 pc. Clearly these parallax measurements have very large errors, although the RUWE for both stars is near 1. Nevertheless, it seems evident that these stars are not physical.

06073+2435

These stars are bright, meaning we can be more confident in the data we have collected. There are measurements starting in 1926, and including all data there is a moderate linear association (R^2 =0.51). However, 2001 and 2009 are both outliers, and once they are removed, the linear

association becomes very strong (R^2 = 0.95), and our data point sits at the end of this line. This isn't a very meaningful association, however, as there is less than 1 arcsec of motion in the last century. Parallax measurements tell us that the two stars are very far apart, with the primary star at 3,500 pc and the secondary at 1,500 pc. This, along with the great dissimilarity between the proper motions, confirms that the stars are not physically associated.

06073+2437

Because of the stars' brightness and location at the edge of our field of view, we have a somewhat elevated standard deviation in our measurements. There are no outliers in the plot of historical measurements, and there is a strong linear relation between them ($R^2 = 0.81$). Referring to the Gaia data, we see that the stars have dissimilar proper motions and parallaxes, with the primary star being at a distance of 4,000 pc, and the secondary at 1,600 pc. This tells us that the stars are probably not physically associated.

06075+2411

The plot for these two stars doesn't indicate a linear relationship, and our data point is in the middle of the measurements. Remarkably there has been almost no motion in the last century, with the separation varying by less than 0.25" since 1926. The Gaia data are helpful, which indicate that the primary is at a distance of 1,000 pc, and the secondary is at 870 pc. Clearly they are not physical, although the proper motions of the secondary indicate that it is a member of M35. However this star is 23' from the center of the cluster, suggesting that it is probably loosely bound.

06076+2411

These stars are faint, which resulted in marginally elevated standard deviations, especially for our measurement of θ . With such little movement in the separation over the last 100 years, it is hard to get a clear picture of the star's motion. The Gaia data suggest that the stars are not physical, as the primary is at a distance of 2,540±200 pc and the secondary is at a distance of 3,400±340 pc. The proper motions are dissimilar, which suggests that these stars are not physical.

06076+2416 AB

These stars have a nice baseline of observations dating to 1926. However there has been very little motion in that timespan, which makes it difficult to interpret the historical observations. The Gaia data is more helpful, as the primary is at a distance of 824±8 pc and the secondary is even closer at 730±7 pc. The parallax and proper motion of the primary are consistent with its membership in M35, although at nearly 20' from the center of the cluster it may be only loosely bound.

06076+2416 AC

As with the A and B components, there has been little change in θ and ρ in the past century. The C component is at a distance of 2,035±184 pc, and is unrelated to the A component.

However, the RUWE for the C component is somewhat elevated, at 1.45. As noted above, the A component appears to be a member of M35.

06076+2416 CD

These stars are quite faint, leading to increases in our reported standard deviations. With little change in separation and position angle, it is hard to interpret the historical measurements. The Gaia data appear to be more straightforward though, as the C component is at a distance of 2,035±184 pc and the D component is at a distance of 571±6 pc. Along with this, their proper motions are dissimilar, indicating that these stars are not physically associated.

06076+2420 AB

This system was first observed in 1926, but there has been less than 0.1" of motion since then. The observation from 2009 seems to be an outlier, with the remaining data appearing very linear. This has little meaning however, in the context of such little movement. Looking at the Gaia data, we see that the distance between the stars is quite large, with star A being at 3,400 pc and star B at 1,700 pc. Along with this, their proper motions are quite dissimilar, so we can say that they are not physical.

06076+2420 BC

As with the AB components, these show very little motion, albeit over a smaller time span as the first observation of this pair dates to 1998. They are faint, which contributes to the higher errors we report. The Gaia parallax data suggests that they are not physical, with the B component at a distance of 1,740±52 pc and the C component at a distance of 1,027±31 pc. Their proper motions are quite different, consistent with this pair not being physical.

06076+2424

With less than 0.5" of motion over the course of a century, it is hard to interpret the historical observations. The Gaia data may not be of great help either, as the RUWE for the primary component is quite large, at 2.67. The Gaia distance to the primary is 728 pc and the secondary is 925 pc. Although the proper motion of the primary is consistent with it being a member of M35, its inconsistent distance and large RUWE prevent us from determining this with any certainty. Finally, if the A component is indeed a cluster member, it is quite near the edge of the cluster, 30' from the center.

06077+2412

This pair is very close together and rather faint. This produced larger than ideal errors in our measurements, especially regarding the angle. As with the others, very little motion has been observed since the first measurement in 1998. The Gaia data suggests that they are well separated, with the primary at 3,700 pc and the secondary at 7,500 pc, although the errors on both are quite high.

06078+2424

Although first observed in 1926, this pair exhibited less than 0.1" of motion in that time. This makes it quite difficult to interpret the historical measurements. The Gaia data indicate that this

is not a binary, as the primary is at a distance of 864 pc while the secondary is at 1,640 pc. While this distance would suggest that the primary is a member of M35, the proper motion is inconsistent with cluster membership.

06079+2423

Less than 1" of motion has been observed for this pair since observations began in 1926. The Gaia parallax indicates that the A component is at a distance of 2,950 pc while the secondary is at 975 pc. This, together with the star's very different proper motions, indicates that this is not a physical binary. The proper motion of the B component is consistent with M35 cluster membership, but its distance is somewhat larger than that of the cluster. This makes it difficult to say whether this is a cluster member.

06079+2435

These two stars are quite close together, which contributed to the uncertainty of our measurement. There has been little to no motion since the first observation in 1998. Happily, these stars are quite nearby, with Gaia-derived distances of 289±3 and 287±6 pc. They also have very similar proper motions, indicating that these are indeed a physical pair. A longer baseline of observation is clearly needed to observe the orbital motion.

06080+2413

Although this pair seems to show linear motion, it has moved less than 1" in a century. The distance derived from the Gaia parallax for the primary is 3,000±150pc, while the secondary is at 865±17 pc. The proper motion of the secondary, together with its parallax, is consistent with M35 cluster membership.

06080+2425

The plot for this pair is remarkably linear, with R²=0.998. However there is less than 1" of motion, so this linearity must be interpreted with caution. The Gaia data suggests that both stars are cluster members, and may be a physical pair as well. The distance for the A component is 848±17 pc while the B component is at a distance of 862±9 pc. Their proper motions are also quite similar, with both stars having pm-ra = 2.1, while the DECcomponents are somewhat different, at -2.714 and -3.145. These differences in DEC suggest that they may not be physically bound, but are certainly members of M35.

06081+2422 AB

As is typical, little motion has been observed since the first observation, making it hard to interpret the stars' motions. Still, what little motion that has occurred appears to be linear in nature. The Gaia data is somewhat helpful, indicating that the primary is at a distance of 2,500 pc and the secondary is at 2,100 pc. However, the RUWE for the secondary is quite large (5), which means that perhaps these measurements are not to be trusted. Taken together, this suggests that this pair is not physical.

06081+2422 AC

In contrast to almost every other star observed, this pair shows more than 6" of motion over the last 100 years. Perhaps the initial 1926 observation was in error, as the first reported separation was 3", while the next observation, in 1998, was 9.2". This is a greater change than seen for any other stars we observed. Still, the historical measurements are quite linear, with R²=0.98. The Gaia data confirm that this pair is not physical, with the primary at a distance of 2,550±100 pc and the secondary at a distance of 940±19 pc. Their proper motions are also quite different.

06083+2428

Very little motion has been observed in the past century, making it hard to interpret the plot of historical measurements. Compounding the problem is the fact that the B component appears to be itself a double, and indeed there are two adjacent Gaia objects there. The proper motions of these two are similar, but their parallaxes suggest that they are not physical. In contrast the A component lies at a distance of only 575 pc, so we can conclude that it is not related to the B component.

06083+2429

These stars are somewhat faint, affecting our reported errors. With a first observation in 1926, there has been approximately 1" of motion since then. The 2009 observation may be an outlier, although a line fitted to the data has R²=0.91. The Gaia data indicate that the A component is a member of M35, with a distance of 850 pc and proper motion consistent with that of the cluster. In contrast, the B component is at a great distance of 4,800±773 pc. Clearly these stars are not physical.

06084+2410

Unfortunately this pair was near the bottom edge of our frame, which may have affected our measurements. This pair has also shown little movement over the last 100 years, which makes it challenging to interpret the historical measurements. Nevertheless, our reported numbers are broadly consistent with them. Turning to the Gaia data, we see that the stars are probably not physical, as the primary is at a distance of 1,600 pc while the secondary is at a distance of 900 pc. The RUWE for the secondary is quite large, at 3.692, which means its parallax must be treated with some caution.

06085+2414

The first observation of this pair only dates to 1998, so little motion has been observed. It is not clear from these few historical measurements how the stars are moving. Furthermore they are close together, which has slightly elevated our reported errors. The Gaia data however indicates that both stars are cluster members, with the A component at a distance of 874±9 pc and the B component at a distance of 876±9 pc. Their proper motions are also quite similar, suggesting that in addition to being part of M35, this pair is probably physical.

06085+2417

Like many of the other stars we observed, this one has exhibited less than 0.5" of movement over the past century. There is no clear trend in the historical measurements over such a short time span. The Gaia data clarify the nature of this system, as the primary is at a distance of 922 pc while the secondary is at a distance of 1,800 pc. The proper motions suggest that the A component is a member of M35, and indeed this star is within 10' of the cluster center.

06085+2418

The first observation for this system dates to 1998, and as with other such systems, there has been very little (<0.2") motion since then. The Gaia data indicate that they are not physical, as the A component is at a distance of 490 pc and the secondary is much further away at 1,600 pc.

06085+2419 AB

There is a nice baseline of observations for this system, dating back to 1898. However, it is unclear from these observations how the stars are moving. The data don't show a curved trend, nor are they linear. There has been less than 0.3" of motion since the first observation. Turning to the Gaia data, we see that these two are probably part of M35, as the primary is at a distance of 879±9 pc and the secondary is at 861±9 pc. Their proper motions are also consistent with cluster membership.

06085+2419 AC

With less than 0.25" of motion since the first observation in 1998, it is difficult to understand from the historical measurements alone the motion of this system. The Gaia data indicates that they are not physical, with the primary being at a distance of 879±9 pc and the secondary at a distance of 2,070±100 pc. Their proper motions are also unrelated, and it appears that the A component is a member of M35.

06085+2419 CD

These stars are rather faint, which resulted in larger errors in our reported measurements. The first observation was recorded in 1998, and there has been less than 0.25" of motion since then. The Gaia data suggest that the stars are at a similar distance, with the primary at 2,070±100 pc and the secondary at 1,980±80 pc. However their proper motions are quite dissimilar, so they don't seem to be part of a moving group.

06086+2419

These stars are quite close together, which makes them hard to measure and has resulted in a somewhat elevated standard deviation for our reported θ and ρ . Unfortunately, the first measurement only dates to 1998, and there has been no reported change since then. The Gaia data suggest that they are not physical, as the proper motions are quite different, and the primary is at a distance of 1,700 pc and the secondary is at a distance of 925 pc. Based on its proper motion, it is likely that the B component is a member of M35.

06086+2423

Once again, less than 0.5" of motion has been seen for this pair in the last century. The data seems a bit scattered, but the Gaia data is helpful in that it indicates that the A component is at a distance of 830 pc and is a cluster member, while the B component is even closer, at 740 pc.

06086+2427

Like many of the other double stars in this field, this system has seen very little motion in the past century. Although the 2009 and 2010 observations appear to be outliers, it is hard to interpret the remaining data. Luckily, the Gaia data indicate that this pair is not physical, with the primary at a distance of 1,360 pc and the secondary at 900 pc. Based on this distance as well as its proper motion, we conclude that the secondary is a member of M35.

06086+2436

This system was first observed in 1926, and has 9 observations total. The measurements from 2010 and 2009 are outliers. If these are removed and a line is fitted, it has R²=0.9. Nevertheless, there has been very little (<0.5") motion in the past century, so the astrometry alone is not helpful. The Gaia data suggests that they are not physical, with the primary at a distance of 1,200 pc and the secondary at a distance of 875 pc. This distance, together with its proper motion, suggests that the B component is a cluster member.

06087+2415

This system has 9 observations dating to 1926. The data does not appear to have a clear trend, but there has been less than 0.5" of movement in the past century. The Gaia data indicate that the system is not physical, with the A component at a distance of 1,200 pc and the secondary at a distance of 880 pc. This distance, together with its proper motion, suggests that the B component is a member of M35.

06088+2432

The first observation for this star dates to 1926, and has 7 historical measurements in total. It seems that the observations dating to 2010 and 2009 may be outliers, and if they are removed and a line is fitted, that line has R^2 =0.94. Looking at the Gaia data, we see that they are not physical, as the proper motions do not match and they are quite far from each other. The primary is at a distance of 876 pc, suggesting that it is a cluster member, and the secondary is at a distance of 2,800 pc.

06089+2420

This star has 11 historical measurements, although there is no clear pattern in the data. The 2009 measurement appears to be discrepant, as does two from 2015. Removing these gives a line with R²=0.7. The Gaia data suggest that the stars are not physically associated, with the A component at a distance of 880 pc and the B component at a distance of 1,440 pc. This distance, together with its proper motion, suggests that the A component is a member of M35.

06089+2423

This system seems quite linear, although 2009 could be an outlier. If that observation is removed, then the R² becomes 0.997. The RUWE for the primary is quite poor at 8.9, although it is near 1 for the secondary. The Gaia parallax gives a distance of 880 pc for the primary, and a distance of 1400 pc for the secondary, indicating that this is not a physical system. However, based on its proper motion and parallax, the A component is probably a member of the M35 cluster.

06089+2424

These are quite close together (<4") and faint, which produced a relatively large standard deviation. Still, our measurement appears to be in line with the historical measurements, except for 2009, which may be an outlier. The Gaia measurements suggest that the system is not linear, as the A component is at a distance of 1,400 pc while the B component is at 2,900 pc. However, the RUWE is somewhat high (1.6) for the A component. In any case, this is probably not a physical system.

06089+2427

This system is interesting because there are three stars in a line, which makes measuring difficult. This is compounded by the small separation (4") and relative faintness of the stars. Still, our measurement appears to be linear with the previous ones, although 2009 seems to be an outlier. There are only 3 historical data points, the earliest of which dates to 1998. The Gaia data indicate that the A and B components are not physical, with the A component at a distance of 1,360 pc and the B component at a distance of 900 pc. The third C component is likely physical with the B component, as they are at a similar distance and have similar proper motions.

06090+2419

This pair is near the extreme left side of our images, and are also somewhat faint, which may affect the accuracy of our measurement. The plot suggests that 2009 is an outlier, but the measurements seem rather linear. However, the proper motions and parallaxes are quite different, with the primary at a distance of about 860 pc and the secondary much further away at 1,430 pc. The A component's parallax and proper motion are consistent with it being a member of M35.

Acknowledgements

This research made use of AstroImageJ, Astrometry.net, and the Washington Double Star Catalog maintained by the U.S. Naval Observatory. This work has made use of data from the European Space Agency (ESA) mission Gaia (https://www.cosmos.esa.int/gaia), processed by the Gaia Data Processing and Analysis Consortium (DPAC,

https://www.cosmos.esa.int/web/gaia/dpac/consortium). Funding for the DPAC has been provided by national institutions, in particular the institutions participating in the Gaia Multilateral Agreement.

References

Anselmo, Dallas, et al., 2018, Journal of Double Star Observations, 14 (3).

Cantat-Gaudin, T, Anders, F. (2020), *Clusters and mirages: cataloguing stellar aggregates in the Milky Way,* Astronomy & Astrophysics, 633, id.A99.

Collins, K. A., Kielkopf, J. F., Stassun, K. G., & Hess man, F. V., (2017), The Astronomical Journal, 153(2), 77.

Dias, W. S, et al. (2021). *Updated parameters of 1743 open clusters based on Gaia DR2.*Monthly Notices of the Royal Astronomical Society. 504, 1, 356.

- Gaia Collaboration, T. Prusti, J.H.J. de Bruijne, et al. (2016b). *The Gaia mission*. Astronomy & Astrophysics, 595, pp.A1.
- Gaia Collaboration, Vallenari, A., Brown, A. G. A., et al. (2023j). *Gaia Data Release 3:*Summary of the content and survey properties. Astronomy & Astrophysics, 674, pp.A1.
- Harshaw, R. 2020, Journal of Double Star Observations, 16(1), 386-400.
- Lang, Dustin, et al., 2010, The Astronomical Journal, 139, 5, 1782.
- Lindegren, L. 2018, technical note GAIA-C3-TN-LU-LL-124, http://www.rssd.esa.int/doc_fetch.php?id=3757412
- Matson, Rachel, 2023, The Washington Double Star Catalog, Astronomy Department, U.S. Naval Observatory.
- Poggio, E., et al. (2021). *Galactic spiral structure revealed by Gaia EDR3*. Astronomy & Astrophysics, 651, id.A104,10.
- Wright, E. L., Eisenhardt, P. R. M., Mainzer, A. K., et al. (2010). *The Wide-field Infrared Survey Explorer (WISE): Mission Description and Initial On-orbit Performance*, The Astronomical Journal, 140, 1868.

Measurements of WDS 20310-2700 and WDS 20313-2707

Tyler D. Scott¹, Sarah Grace Bogle¹, Kathryn M. Boeckers¹ Grace College, Winona Lake, Indiana; scottt@grace.edu

Abstract

We conducted a study on two double star systems, WDS 20310-2700 (DAM 1042) and WDS 20313-2707 (SKF 2086), using the Las Cumbres Observatory (LCO) global telescope network. The goal of the study was to determine separation and position angles of the double stars and possibly determine whether the systems are gravitationally bound. Our separation and position angle for WDS 20310-2700 were 10.73 \pm 0.03" and 1.78.9 \pm 0.22°, respectively. Our separation and position angle for WDS 20313-2707 were 6.84 \pm 0.11" and 303.9 \pm 0.56°, respectively. Future observations are required to establish whether these systems are binary or not.

1. Introduction

To identify interesting star systems to study, we searched the Stelle Doppie database (Sordiglioni, 2023), looking for double stars whose nature was "uncertain." We focused on stars with separation between 5-15" and those that had not been observed since 2015. We also looked for systems with a primary star magnitude brighter than 13 and a magnitude difference between primary and secondary less than 3.

As a result of this search, we decided to observe and analyze WDS 20310-2700. The primary star (Gaia Designation 6799650892560759040) is located at a right ascension of 20h 31m 02.72s and declination of -27° 00′ 27.93″ and has a G-band mean magnitude of 12.6 (Gaia Collaboration, 2023). The secondary star (Gaia Designation 6799750892560757760) is located a right ascension of 20h 31m 0274s and declination of -27° 00′ 38.73″ and has a G-band mean magnitude of 13.6 (Gaia Collaboration, 2023). The system is located in the constellation Capricornus. This system was first observed in 1998 (DENIS Consortium, 2003) and last observed in 2000.

After taking images of this system, however, we found that the field of view of the images included a second double star system, WDS 20313-2707. This system was first observed in 1977 (Skiff, 2014) and last observed in 2016 (El-Badry et. al., 2021). Also in the constellation Capricornus, the primary star (Gaia Designation 6799737354823802368) is located at a right ascension of 20h 31m 20.31s and declination of -27° 07′ 11.57″ and has a G-band magnitude of 9.9 (Gaia Collaboration, 2023). The secondary star (Gaia Designation 6799737354823803648) is located at a right ascension of 20h 31m 19.88 s and declination of -27° 07′ 07.39″ and has a G-band magnitude of 13.8 (Gaia Collaboration, 2023). Therefore, this paper will include an analysis of both systems.

2. Equipment and Methods

We used the Las Cumbres Observatory global telescope network (LCO) to capture 10 images of these stars. Specifically, a 0.4-m telescope at the Cerro Tololo Observatory in Chile with a SBIG STL-6303 CCD was used with a V-band filter on 24 October, 2023 (2023.81) between 23:54:09 and 23:58:29 UTC. Image reduction was done by LCO using the BANZAI pipeline. Each image had a 10-s exposure time.

To analyze the images, we used Afterglow Workbench (Afterglow Access, 2023) to determine separation in arcseconds and position angle E of N. Two screenshots of the measurements are shown in Figure 1.

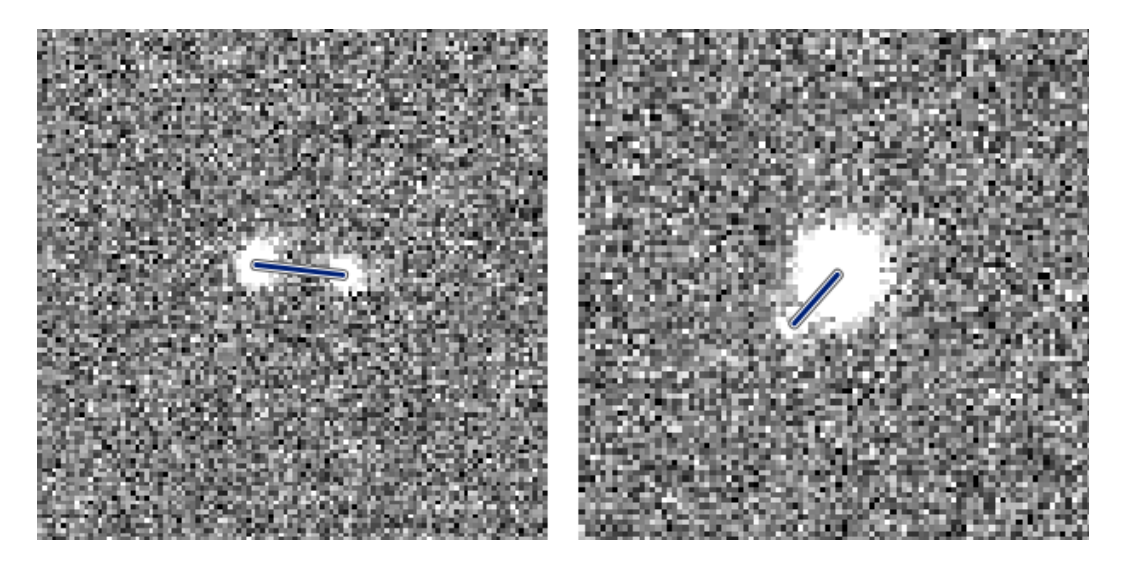


Figure 1: Afterglow Workbench measurement of WDS 20310-2700 (left) and WDS 20313-2707 (right)

We obtained parallax, proper motion, and magnitude data from the Gaia data release 3 (Gaia Collaboration, 2023). We obtained historical separation and angle data directly from the United States Naval Observatory (USNO).

3. Data

In Table 1, we include the measurements of separation in arcseconds and position angle in degrees for each of our 10 images of WDS 20310-2700. The table also includes the average values, the standard deviation, and the standard error of the mean for both separation and position angle.

Table 1: Current measurements and calculations of separation and position angle of WDS 20310-2700 (DAM 1042).

File Name	Sep (arcsec)	PA (deg)
lsc0m409-kb98-20231024-0057-e91.fits.fz	10.72	178.8
lsc0m409-kb98-20231024-0058-e91.fits.fz	10.84	179.1
lsc0m409-kb98-20231024-0059-e91.fits.fz	10.57	179.6
lsc0m409-kb98-20231024-0060-e91.fits.fz	10.67	178.5
lsc0m409-kb98-20231024-0061-e91.fits.fz	10.61	178.9
lsc0m409-kb98-20231024-0062-e91.fits.fz	10.78	177.7
lsc0m409-kb98-20231024-0063-e91.fits.fz	10.79	180.2
lsc0m409-kb98-20231024-0064-e91.fits.fz	10.90	178.7
lsc0m409-kb98-20231024-0065-e91.fits.fz	10.79	179.1
lsc0m409-kb98-20231024-0066-e91.fits.fz	10.66	178.2
Average	10.73	178.9
Std. Dev.	0.10	0.69
Std. Err. of Mean	0.03	0.22

In Table 2, we include the measurements of separation in arcseconds and position angle in degrees for each of our 10 images of WDS 20313-2707. The table also includes the average values, the standard deviation, and the standard error of the mean for both separation and position angle.

Table 2: Current measurements and calculations of separation and position angle of WDS 20313-2707 (SKF 2086).

File Name	Sep (arcsec)	PA (deg)
lsc0m409-kb98-20231024-0057-e91.fits.fz	6.77	303.9
lsc0m409-kb98-20231024-0058-e91.fits.fz	6.46	305.1
lsc0m409-kb98-20231024-0059-e91.fits.fz	7.02	305.6
lsc0m409-kb98-20231024-0060-e91.fits.fz	6.57	302.7
lsc0m409-kb98-20231024-0061-e91.fits.fz	7.01	302.7
lsc0m409-kb98-20231024-0062-e91.fits.fz	7.54	302.4
lsc0m409-kb98-20231024-0063-e91.fits.fz	6.97	306.5
lsc0m409-kb98-20231024-0064-e91.fits.fz	6.53	305.2
lsc0m409-kb98-20231024-0065-e91.fits.fz	7.11	304.1
lsc0m409-kb98-20231024-0066-e91.fits.fz	6.43	300.7
Average	6.84	303.9
Std. Dev.	0.35	1.76
Std. Err. of Mean	0.11	0.56

4. Discussion

To get the bigger picture of these two star systems, we have obtained historical data from USNO. These data are shown in Tables 3 & 4.

Table 3: Historical Separation and Position Angle Data from the USNO and the current study for WDS 20310-2700 (DAM 1042).

Date	Sep. (arcsec)	PA (deg)
1998.7258	10.84	178.7
1998.7366	10.82	178.7
1998.74	10.83	178.7
1999.50	10.814	178.5
1999.52	10.80	178.6
2000.0	10.76	178.6
2023.81	10.734	178.88

Table 4: Historical Separation and Position Angle Data from the USNO and the current study for WDS 20313-2707 (SKF 2086).

Date	Sep. (arcsec)	PA (deg)
1977.67	7.99	306.8
1999.50	7.060	305.8
1999.52	7.07	305.7
2010.5	6.88	303.4
2015.0	7.091	305.987
2015.5	7.08885	305.984
2016.0	7.08945	305.98
2023.81	6.84	303.9

The separation and position angle values found in this study are similar to the historical data. We converted the separation ρ and position angle θ to right ascension (RA) and declination (Dec) to rectangular coordinates with the following equations:

$$RA = \rho \sin \theta$$

$$Dec = -\rho \cos \theta$$

The results for WDS 20310-2700 are shown in Figure 2. While the USNO data included six data points (shown in Table 3). The data do not give us enough information to calculate an orbit. We only have 25 years of observations for this star system.

The results for WDS 20313-2707 are shown in Figure 3. The USNO data included seven data points. While there is more data and a longer time interval (46 years), they do not show a trend that can be fit to an orbit.

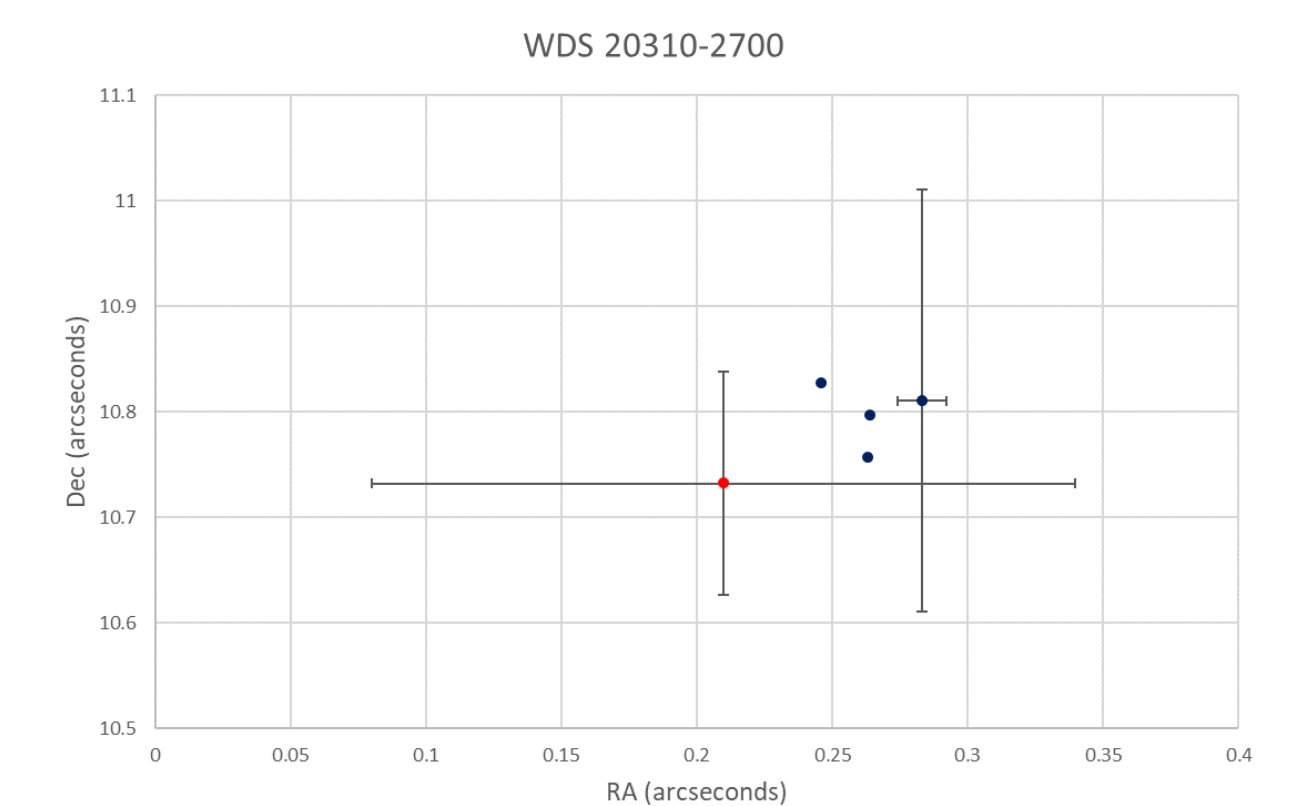


Figure 2: Plot of historical data (blue) and our observation (red) for WDS 20310-2700. The separation and position angle have been converted to right ascension and declination coordinates. Error bars are included when available.

WDS 20313-2707

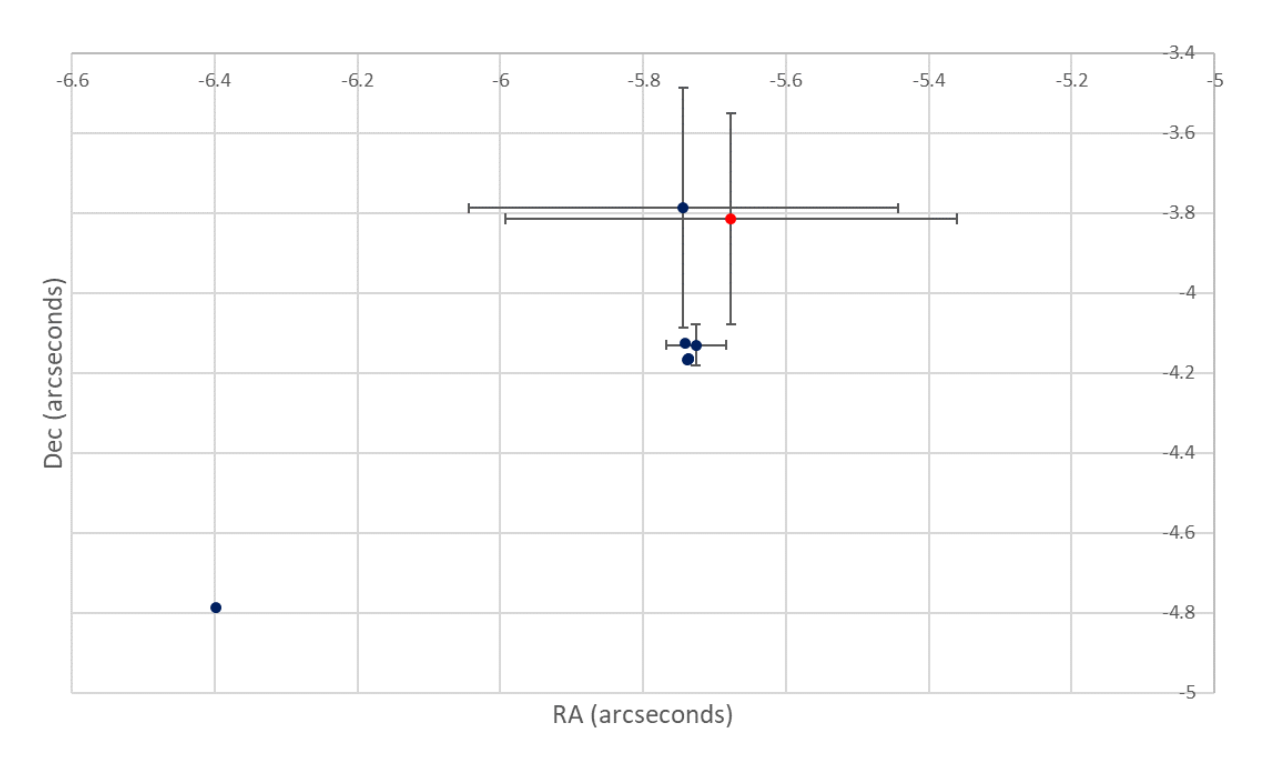


Figure 3: Plot of historical data (blue) and our observation (red) of WDS 20313-2707. The separation and position angle have been converted to right ascension and declination coordinates. Error bars are included when available.

Since an orbit cannot be calculated, an important question is whether the two stars are even near each other. Therefore, parallax and proper motion data were obtained from Gaia data release 3. In Tables 5 & 6, parallax data were used to calculate a distance to the stars using the equation $D = 1/\theta$, where D is the distance to the star in parsecs and θ is the parallax in arcseconds.

Table 5: Parallax from Gaia Data Release 3 with calculated distance for WDS 20310-2700.

Star	Parallax (mas)	Distance (pc)
Primary	1.594 ± 0.016	627.2 ± 6.1
Secondary	1.545 ± 0.016	647.2 ± 6.6

Table 6: Parallax from Gaia Data Release 3 with calculated distance for WDS 20313-2707.

Star	Parallax (mas)	Distance (pc)
Primary	9.31 ± 0.17	107.4 ± 1.9
Secondary	9.243 ± 0.018	108.2 ± 0.2

The stars of WDS 20313-2707 are very near each other. Distance to the stars calculated by parallaxes are within the uncertainty range of each other. The stars of WDS 20310-2700 are much further apart, around 20 parsecs from each other.

Another tool we used to help determine the nature of these double stars is the "rating" calculation of Harshaw (2014). Using proper motion data from Gaia Data Release 3, the statistic was calculated for each system and is reported in Table 7 (for WDS 20310-2700) and Table 8 (for WDS 20313-2707). The resulting value for WDS 20313-2707 (0.5%) indicates a common motion pair and therefore likely to be a binary system. A "rating" of 18.4% for WDS 20310-2700 is at the end of the range for star systems with known orbits (Harshaw, 2014). However, it is closer to the ratings of binary systems than to those with linear solutions.

Table 7: Proper motion from Gaia Data Release 3 with calculated proper motion "rating" (Harshaw, 2014) for WDS 20310-2700.

Star	Proper Motion RA (mas/yr)	Proper Motion Dec (mas/yr)	Mag. of PM Diff. (mas)	Sum of PM Mags. (mas)	Rating (%)
Primary	18.708 ± 0.015	-21.331 ± 0.012	0.07	40.22	10.4
Secondary	16.699 ± 0.016	-12.486 ± 0.013	9.07	49.22	18.4

Table 8: Proper motion from Gaia Data Release 3 with calculated proper motion "rating" (Harshaw, 2014) for WDS 20313-2707.

Star	Proper Motion RA (mas/yr)	Proper Motion Dec (mas/yr)	Mag. of PM Diff. (mas)	Sum of PM Mags. (mas)	Rating (%)
Primary	-74.67 ± 0.17	-47.341 ± 0.14	0.012	177.6	0.5
Secondary	-75.469 ± 0.019	-48.100 ± 0.014	0.913	177.6	0.5

5. Conclusions

We used our observations to measure separation and position angles for two double star systems. In both cases, our observations are similar to those in the historical record.

Parallax and proper motion data for WDS 20313-2707 indicated a very high likelihood that this system is binary. However, the 46 years of data are not enough to calculate an orbit. More observations in the future are needed to obtain orbital information.

For WDS 20310-2700, only 25 years of data exist. Without more data, an orbit cannot be calculated. The parallax and proper motion data are more ambiguous for this system. The stars are relatively close to each other on the cosmic scale, but are very far compared to most binary systems. The proper motion "rating" is nearer to known binary systems than to those that are only optical double star systems (Harshaw, 2014).

But it is also high compared to most known binary systems. The nature of this system must remain unknown until more data is available.

Acknowledgements

This research has made use of the Washington Double Star Catalog maintained at the U.S. Naval Observatory. Also, this work has made use of data from the European Space Agency (ESA) mission Gaia (https://www.cosmos.esa.int/gaia), processed by the Gaia Data Processing and Analysis Consortium (DPAC, https://www.cosmos.esa.int/web/gaia/dpac/consortium). Funding for the DPAC has been provided by national institutions, in particular the institutions participating in the Gaia Multilateral Agreement. This research has also made use of the VizieR catalog access tool, CDS, Strasbourg, France (DOI: 10.26093/cds/vizier). The original description of the VizieR service was published in 2000, A&AS 143, 23.

We would also like to thank Rachel Freed for her help during the research and writing process.

References

El-Badry, K., Rix, H. W., & Heintz, T. M. (2021). A million binaries from Gaia eDR3: sample selection and validation of Gaia parallax uncertainties. Monthly Notices of the Royal Astronomical Society, 506(2), 2269-2295.

DENIS Consortium (2003). The DENIS database (Version 12-Jun-2017) [Data set]. Centre de Donnees astronomique de Strasbourg (CDS). https://cds.unistra.fr//denis.html

Gaia Collaboration (2023). Gaia DR3 Part 1. Main Source (Version 08-Aug-2023) [Data set]. Centre de Donnees astronomique de Strasbourg (CDS). https://doi.org/10.26093/cds/vizier.1355

Harshaw, R. (2014). Another Statistical Tool for Evaluating Binary Stars. Journal of Double Star Observations, 10(1), 32-51.

Skiff, Brian A. (2014). Common-Motion Pairs and Other Doubles Found in Spectral Surveys - 9. Survey Work for 2014. The Webb Deep-Sky Society Double Star Section Circular, 23, p. 49.

Sordiglioni, Gianluca (2021, October). Stelle Doppie - Double Star Database. https://www.stelledoppie.it/index2.php?section=1

Afterglow Access (2023). Retrieved November 15, 2023 https://afterglow.skynetjuniorscholars.org/en/workbench

WDS18338+1744: Speckle Analysis of a Quadruple in Hercules

¹John Major, Elias Faughn², Bradley Brungardt³, and Paul McCudden³
¹Bud Werner Memorial Library, Steamboat Springs, CO; major.john.robert@gmail.com

²Glenwood HS, Glenwood Springs, CO

³ Colorado Mountain College, Steamboat Springs, CO

Abstract

Using data collected from the historic 60" telescope at the Mount Wilson Observatory on 2023.4873 (June 27, 2023), the position angle and separation of the multiple system WDS 18338+1744 were calculated using Speckle Tool Box and compared with previous measurements. The AB system's mean position angle was found to be 90.055° and the mean separation was 0.2057". The CD system's mean position angle was found to be 264.071° and the mean separation was 0.478". The AB system measurements exhibited a standard error of .001 for ρ and .109 for θ , and the CD system had an error of .005 for ρ and .082 for θ . Data for the AB system is compatible with the published orbit, while data for the CD system is inconclusive.

1. Introduction

In June 2023, 53 Known Binaries selected from a list merging the WDS and 6th Orbit Catalog and Ephemerides (McCudden, et al; 2022) were observed using the historic 60" telescope at Mount Wilson Observatory (MWO). From those binaries, WDS 18388+1744 (HU322, HD 171365, STF 2339, SAO 103853, HIP 90996, Tycho 2: 1574-01293-1, Gaia DR2 4523973547779600384) was selected for analysis due to its abundant past observations, including several speckle ones, and its quadruple nature. Images from Digital Sky Survey II and a sample speckle image from MWO are featured in Figures 1 and 2, respectively.

WDS 18338+1744 was also chosen to test the Speckle Toolbox software on stars with separation values between the AB and CD stars that differ by a factor of 10, and to compare the measurements with ample data gleaned from larger instruments using a variety of other methods, including spectroscopic, short-exposure CCD imaging, Hipparcos, and Tokovinin "HRCam" methods (see Tables 1 and 2). The speckle technique was pioneered by Antoine Labeyrie and "freezes" the effect of atmospheric distortion by "stacking" the images, offering a clear distinction between even very close members of a multiple system (Labeyrie 1970).

The AB (HU322 AB) system has an estimated period of 42.4 years and a distance of 183.49 parsecs (598.54 light years). The A member has an apparent magnitude of 7.74 and the B member's apparent magnitude is 8.91. The primary is spectral class F6V. This grade 2 double is physically related, and the orbit was first calculated in 2012 (Rica Romero 2012). Select data from the USNO is listed in Table 1. The table includes measurements from 1.5 m telescopes or larger.

Table 1. USNO Double Star data for WDS18338+1744AB

			r		
Date	ρ (")	θ (°)	Observer		
1958.60	0.14	78.4	van den Bos, W.H. 1960		
1958.61	0.12	70.2	Van Biesbroeck, G. 1960		
1976.301	0.15	93.4	Walker, R.L. 1985		
1983.4194	0.218	87.2	McAlister, H.A. 1987		
1983.7144	0.221	88.3	McAlister, H.A. 1987		
1984.3751	0.233	90.0	McAlister, H.A. 1987		
1984.3833	0.228	91.7	McAlister, H.A. 1987		
1985.4835	0.229	88.0	McAlister, H.A. 1987		
1987.7552	0.225	89.0	McAlister, H.A. 1989		
1991.3182	0.211	84.9	Hartkopf, W.I. 1994		
1992.3094	0.202	84.5	Hartkopf, W.I. 1994		
1992.6076	0.201	89.1	Balega, I.I. 1999		
1995.5996	0.169	83.1	Hartkopf, W.I. 1997		
1996.4214	0.152	81.5	Hartkopf, W.I. 2000		
1996.6918	0.155	80.9	Hartkopf, W.I. 2000		
1997.3904	0.148	81.2	Balega, I.I. 1999		
1997.3932	0.144	80.7	Balega, I.I. 1999		
1998.653	0.115	71.6	Scardia, M. 2000		
1998.7754	0.128	79.9	Balega, I.I. 2002		
2001.7535	0.077	73.5	Balega, I.I. 2006		
2001.7535	0.076	73.7	Balega, I.I. 2006		
2001.7535	0.075	73.6	Balega, I.I. 2006		
2001.7535	0.077	73.5	Balega, I.I. 2006		
2009.2592	0.0570	91.3	Tokovinin, A. 2010		
2009.2592	0.0481	81.0	Tokovinin, A. 2010		
2009.2592	0.0561	91.3	Tokovinin, A. 2010		
2017.4294	0.1378	94.3	Tokovinin, A. 2018		
2018.2539	0.1650	90.7	Tokovinin, A. 2019		
2019.5363	0.1744	92.3	Tokovinin, A. 2020		

The CD (WAK21 CD) system shares the AB spectral class, but is somewhat fainter with apparent magnitudes of 9.3 and 9.56 for the C and D members, respectively. The 28 observations available from the USNO reflect an increasing ρ and θ since 1975, but it is not known whether the system is physically related. There is no 6th Orbit Catalog plot for the system, and there is no consensus on its distance, but the two stars

do have identical proper motions (Mason 2023, Rica Romero 2012). Select data from the USNO is listed in Table 2. The table includes measurements from telescopes of aperture greater than 1.5 m.

Table 2	USNO	Double	Star data	for	WDS18338+174	4CD
raute 2.	COLIC	Double	Star data	101	11 DOIO330 1 1 / T	Των

Date	ρ (")	θ (°)	Observer
1976.301	0.16	248.4	Walker, R.L. 1985
1985.4836	0.319	256.7	Hartkopf, W.I. 2000
1996.4214	0.395	260.2	Hartkopf, W.I. 2000
1997.3803	0.406	258.9	Balega, I.I. 1999
1997.3932	0.405	259.0	Balega, I.I. 1999
1998.653	0.409	261.7	Scardia, M. 2000
1998.7754	0.414	260.3	Balega, I.I. 2002
2005.8651	0.409	262.5	Mason, B.D. 2009
2007.5878	0.454	260.2	Mason, B.D. 2009
2009.2592	0.4651	261.2	Tokovinin, A. 2010
2017.4294	0.4920	262.5	Tokovinin, A. 2018
2018.2539	0.4920	262.5	Tokovinin, A. 2019
2018.3985	0.4932	263.1	Tokovinin, A. 2019
2019.5363	0.4921	263.3	Tokovinin, A. 2020



Figure 1. WDS 18338+1744 from Aladin

2. Equipment and Methods

Data on WDS 18338+1744 AB and CD was collected by the historic 60-inch (1.52m) telescope at MWO on June 28, 2023 (2023.490 or JD 2460124.747). The telescope was used in its bent Cassegrain mode. One thousand 20 ms images of the target were taken with a ZWO ASI 6200MM Pro camera fitted with an Astronomik ProPlanet 642 BP 2850002585 (IR pass) filter with a midpoint transmission at 750 nm. A sample speckle image is shown in Figure 2. Five hundred images, also with 20 ms exposures were taken of HD 176938 to be used as a reference in the Speckle reduction. Dave Rowe's PlateSolve software (Rowe & Genet, 2015) was used to determine the pixel scale of 0.0306 arcseconds/pixel and rotation angle of 178.997° of the camera/optical train.

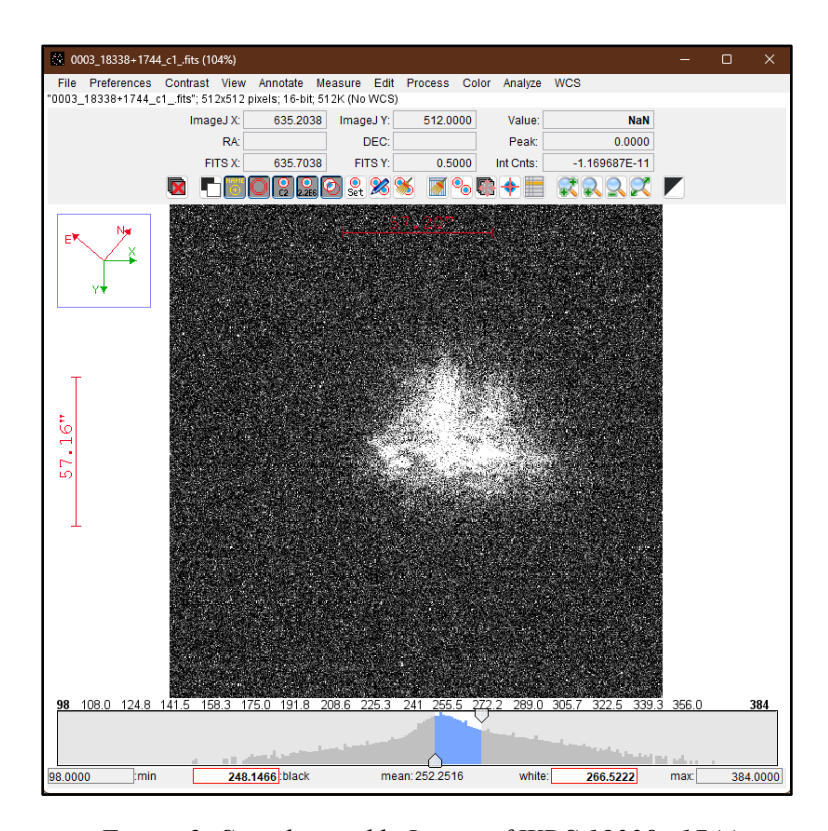


Figure 2: Sample speckle Image of WDS 18338+1744

3. Data

Five reductions each of both the AB and CD stars at 128, 256 and 512 pixel sized images using Speckle ToolBox (Rowe, 2017) were taken by each author, and the mean ρ , mean θ , standard deviation and standard error were calculated and are shown in Table 3.

Table 3. Measured values for WDS 18338+1744AB

Pixel size	ΑΒρ(")	Standard Deviation	AB θ (°)	Standard Deviation	CD ρ (")	Standard Deviation	CD θ (°)	Standard Deviation
128	0.206	0.00620	90.004	0.73667	0.468	0.00825	263.628	0.71638
256	0.205	0.00713	90.410	0.91310	0.493	0.00288	264.234	0.46406
512	0.206	0.0106	89.751	0.87987	0.472	0.09941	264.352	0.73651
Average	0.2057	0.00798	90.055	0.84321	0.478	0.03685	264.071	0.63898

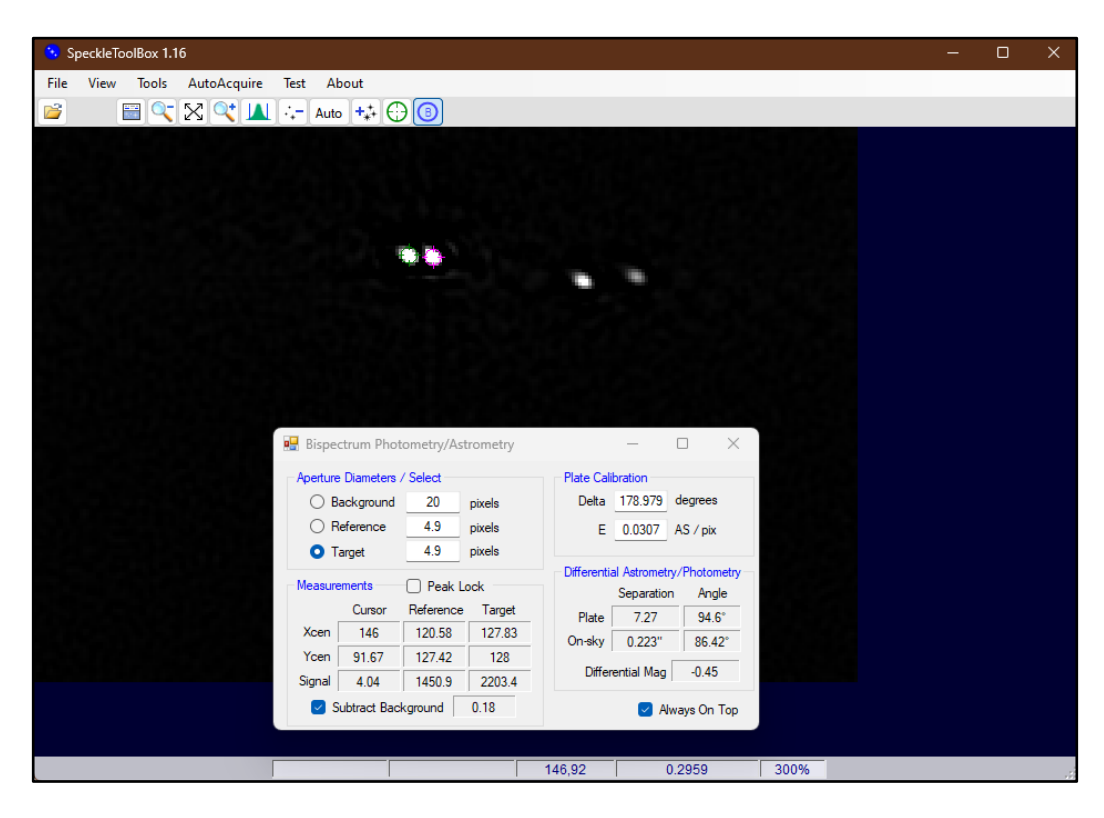


Figure 3: Sample Bispectrum Image from Speckle Toolbox of WDS 18338+1744, showing both the AB and CD stars

	ρ (")	θ (°)
Extrapolated 6th Orbit value	0.215	90.5
Our Measurements	0.20507	90.055
Standard Deviation	0.00798	0.84321
Standard Error	0.00178	0.18855

Table 4 - Current measurements of WDS 18338+1744AB compared to 6th Orbit extrapolated values

Our data is plotted along with recent large aperture speckle observations, with observation dates indicated in parentheses in Figure 4 using the commercial program Desmos. The published orbit (Rica Romero, 2012) is indicated by the dotted line. Our data is indicated as "MWO 2023 (2023.6)."

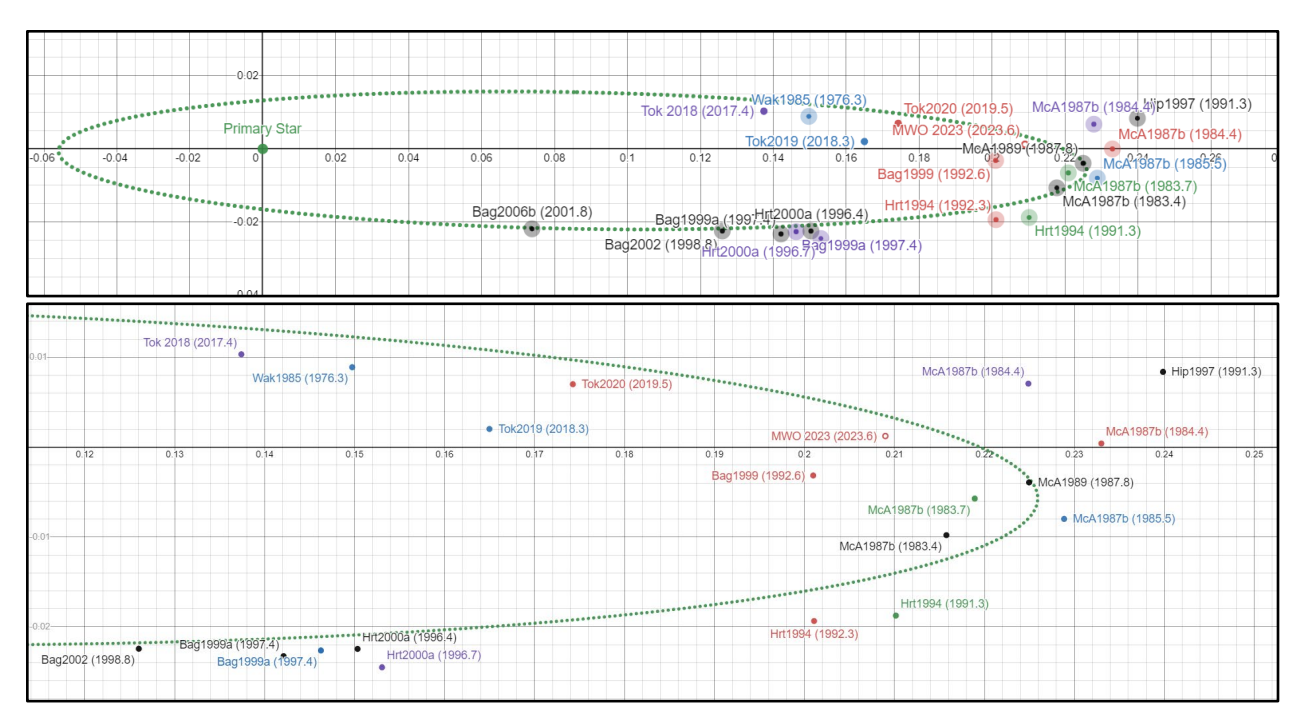


Figure 4- Speckle Observations of 18338+1744 (AB). Current Observation is labeled as MWO2023 (2023.6)

4. Discussion

Our observation fits well with the published orbital plot from the 6th Orbit Catalog (see Figure 4), although there is significant variation in previous measurements (e.g., the Hip1997 data point). Our ρ deviated from the extrapolated 6th Orbit Ephemeris value by .77% and the θ by 2.78%. Other recent speckle observations deviate from the calculated orbit by even larger margins, despite this being a Grade 2 orbit. The CD system was plotted using our observation and historical observations but showed no observable trend that would indicate a gravitationally bound system despite sharing an identical proper motion (Rica Romero 2012).

Further information on the CD system is lacking so it can not be concluded whether the pair is gravitationally bound to the AB system. Measurements taken on the AB system had a standard error of .001 for ρ and .109 for θ and the CD system had an error of .005 for ρ and .082 for θ . Such low error indicates that STB can simultaneously provide precise measurements on systems with ρ values that differ by a factor of 10.

Using the new orbit plotting tool in STB 10.01, and only confirmed, large aperture (>3m) Speckle data, including recent data that was not available to calculate the currently published orbit (FMR 2012b), we removed outlier points (including the 1991 Hipparchos measurement and ones later retracted (Tok2010)) and then fitted an orbit to the remaining data. It is possible (see Figure 5) that a new orbit calculation is necessary.

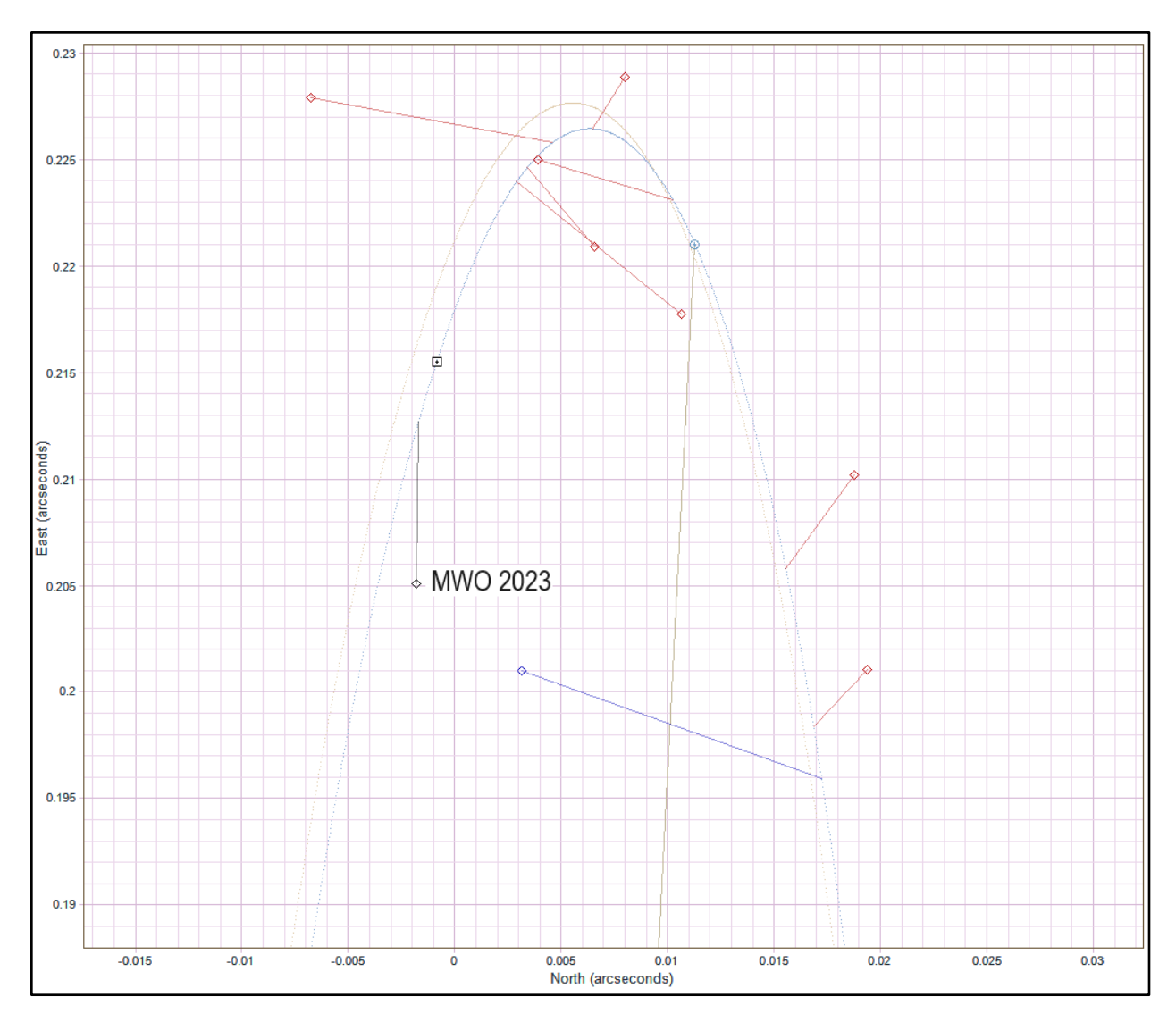


Figure 5. Published Orbit for WDS18338+1744AB in brown (FMR2012b) and recalculated orbit using STB 10.01 in blue. Current measurement (MWO 2023) is labeled.

5. Conclusion

Speckle interferometry via the STB software has become a valuable, powerful tool in the hands of researchers and amateur observers. Automated and amateur-sized telescopes can provide large amounts of data on known and suspected binaries that can easily and quickly be analyzed to further refine known orbits of double stars. These tools and methods can provide valuable data to nail down higher grade orbits, in an efficient and accessible fashion. Future use of software like Speckle Toolbox may compel revisions of published orbits for Known Binaries. In this case, we were able to use our measurements, add the most recent observations for WDS18338+1744 AB, and wield new tools to offer a modified orbital plot.

Acknowledgements

This research has made use of the Washington Double Star Catalog maintained at the U.S. Naval Observatory.

This work used the SIMBAD service operated by Centre des Donnees Stellaires (Strasbourg, France), biblio-graphic references from the Astrophysics Data System maintained by SAO/NASA

This research made use of the Stelle Doppie database, maintained by Gianluca Sordiglioni.

The authors are grateful to the Colorado Mountain College Foundation for supporting student travel and research.

Thanks to Rachel Freed and the Institute for Student Astronomical Research for funding instrument time at MWO, and to Tom Meghini and MWO staff.

References

- Gili, Rene et al. Measurements of visual binaries with PISCO2 at the Nice 76-cm refractor in 2011-2012. Astronomische Nachrichten, Volume 342, Issue 6, pp. 865-886. July 2021
- Labeyrie A. (1970) Attainment of Diffraction Limited Resolution in Large Telescopes by Fourier Analysing Speckle Patterns in Star Images. Astron. & Strophys. 6, 85-87. https://adsabs.harvard.edu/pdf/1970A%26A....6...85L
- Mason, B.D., Wycoff, G.L. and Hartkopf, W.I., The Washington Double Star Catalog https://crf.usno.navy.mil/wds/ (accessed November 26, 2023)
- McCudden, P., Genet, R., Willie, E, Dugan, L., Risin, S. Known Binaries Excel Spreadsheet. The Journal of Double Star Observations, Volume 18, Number 4, October (2022).
- Rica Romero, F.M. & Zirm, H. International Astronomical Union Commission 26 (Double Stars) Information Circular No. 176. Feb. 2012
- Rowe, D. & Genet, R. M. 2015. User's guide to PS3 speckle interferometry reduction program. Journal of Double Star Observations, 1S, 89.
- Rowe, David (2017). The Speckle Toolbox: A Powerful Data Reduction Tool for CCD Astrometry. Journal of Double Star Observations, 13 (1), p.52-67. http://www.jdso.org/volume13/number1/Harshaw 52 67.pdf
- Tokovinin, Andrei; Mason, Brian D.; Hartkopf, William I. Speckle Interferometry at the Blanco and SOAR Telescopes in 2008 and 2009. The Astronomical Journal, Volume 139, Issue 2, pp. 743-756 February 2010. https://iopscience.iop.org/article/10.1088/0004-6256/139/2/743/pdf.

Observation and measurements for the Double Star System - HJ3203

Sofia A. Osorio Correa¹, Jeremy L. Curry Romero¹, Alondra S. Gonzalez Agosto¹, Fabian G. Rivera Rivera¹, Devon M. Rivera Moran¹, Carmen A. Pantoja Pantoja¹, Mayra E. Lebrón¹, Lisa Storrie-Lombardi² Edward Gomez², Alice Hopkinson², Sabrina Stierwalt³, Rachel Freed⁴

¹University of Puerto Rico-Río Piedras Campus, San Juan, Puerto Rico; sofia.osorio@upr.edu

²Las Cumbres Observatory, Goleta, California

³Occidental College, Los Angeles, California

⁴InStAR, Tucson, Arizona

Abstract

The double system WDS 23352+1133 HJ 3203 was observed on October 17, 2023, with a 0.4m optical telescope from Las Cumbres Observatory (LCOGT). We compare the historical data with our measurements of position angle (PA) and separation (SEP).

1. Introduction

The observation of binary star systems is a key factor when studying stellar evolution, as they are used to determine the masses of stars (Fraknoi et al., 2022). This information can be acquired from observing and measuring their orbital dynamics (e.g. Genet et al., 2018). Our goal was to observe the double system HJ 3203 and make measurements of PA and SEP to contribute to having a more accurate determination of the nature of this system. In this paper we present a graph of a possible orbit, a table of historical data of the system and our new measurement of PA and SEP.

We selected HJ 3203 using the program Stelle Doppie and considering double star systems with apparent magnitudes between 9 < m < 11 and $\Delta m < 3$. In 187 years 19 observations have been made of this system. The earliest observation was made in 1830 by the well-known English astronomer John Herschel, and the last observation was made in 2017. Table 1 shows the coordinates (2000.0) of HJ3203 and the apparent magnitudes of the stars in this system. Figure 1 shows an image of HJ3203 from the Digitized Sky Survey (DSS) obtained from the Stelle Doppie program. Figure 2 shows an example of the measurements made using AstroImageJ.

Table 1. Basic data of HJ 3203 system.

Name	RA (2000.0)	DEC (2000.0)	m_1	m ₂
HJ 3203, WDS J23352+1133AB, Tycho 1172-00633-1, Gaia DR3 276227830582570880	23h 35m10.365s	+11°32'42.8"	10.23	10.20

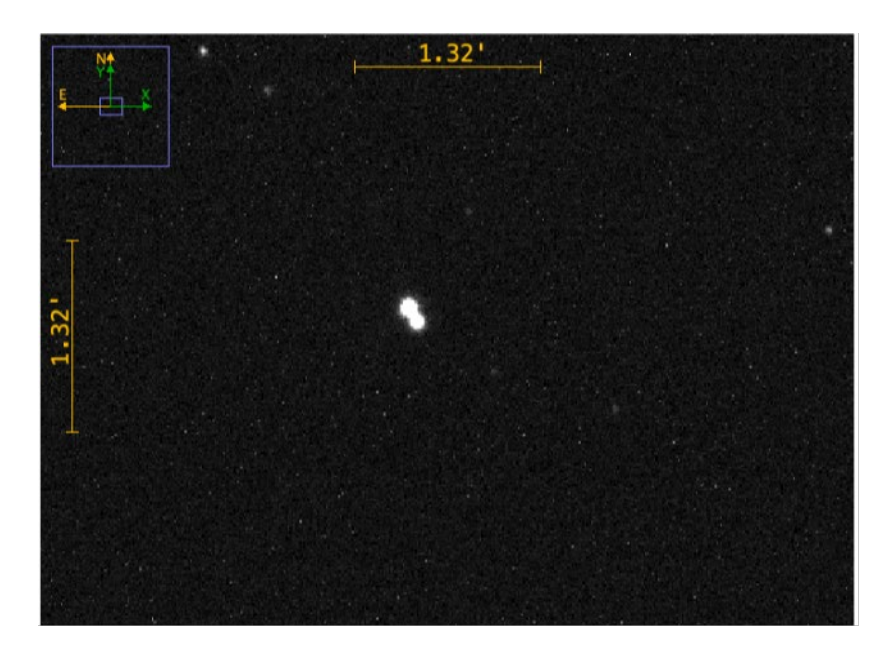


Figure 1: Image of HJ 3203 taken with a 0.4m optical telescope operated by LCOGT

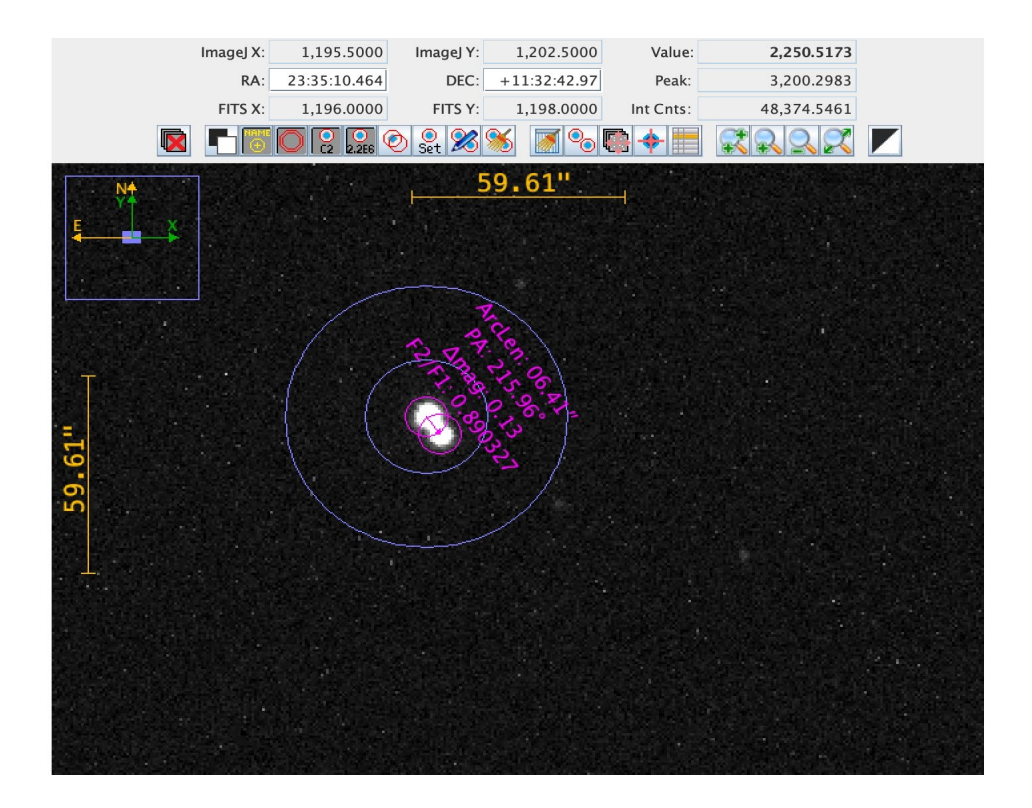


Figure 2: Example of measurements of HJ 3203 made using AstroImageJ

2. Equipment and Methods

The astrometric images of HJ 3203 were taken using a 0.4m optical telescope from LCOGT at the South African Astronomical Observatory (SAAO) and Haleakala nodes using a DeltaRho 350+QHY600 camera (field view of 30'x30'). The observations were submitted using the LCOGT observing portal.

3. Data

Table 2 presents the measurements of PA in degrees and SEP in arcsec for the images obtained with LCOGT. All images were taken with a Bessell-V filter and 2 seconds of exposure time.

Date PA (deg) SEP (arcsec) oct.18.2023 207.57 6.04 oct.18.2023 212.89 6.48 oct.18.2023 211.38 5.79 oct.18.2023 214.12 6.71 207.56 oct.18.2023 6.59 215.96 oct.18.2023 6.41 oct.18.2023 215.4 6.06 oct.18.2023 215.96 4.27 215.12 oct.18.2023 5.89 oct.18.2023 211.38 6.52 Average 213 6.1 Standard deviation PA 3 (degrees) Standard deviation SEP 0.7 (arcsec)

Table 2. Data of system HJ 3203 observed with LCOGT.

4. Discussion

We searched SIMBAD for information about the system, shown in Table 3. The primary star is also known as Tyc 1172-633-1 and Gaia DR3-2764227830582570880 in the Gaia DR3 catalog. We present in column 1 Parallax (mas), column 2 shows the error in Parallax (mas), column 3 contains the Proper Motion (PM) in RA (mas/yr), column 4 presents the error in PM in RA (mas/yr), column 5 is the PM in DEC (mas/yr), column 6 shows the error in PM in DEC (mas/yr) and column 7 contains the distance (pc). No information about the secondary star was found in Gaia DR3.

In Table 4 we present the PA and SEP for the historical data for the system HJ 3203. Column 1 lists the date, column 2 is the PA (degrees), column 3 is the SEP (arcsec), column 4 is the RA (arcsec) calculated as SEP x sin(PA), column 5 shows the DEC(arcsec) calculated as –SEP x cos(PA), column 6 is the aperture of the telescope (m) and column 7 shows the number of nights.

In Figure 3 we present the historical data plotted as a cartesian plot with the primary star at the origin and the secondary star represented by dots (blue is the historical data and red is our measurement). The x-axis is the RA (arcsec) and the y-axis is the DEC (arcsec). The plot suggests a curvature but shows a lot of scatter. The blue line is a second order polynomial fit to the data, the value of R2= 0.7. In Figure 3 we have labeled the four oldest observations: 1830.78, 1910.68, 1910.68, 1910.74. They all lie above the blue line with two of them very close to the polynomial fit (1830.78, 1910.74).

To explore the effect of the oldest points on the data we present Figure 4. It shows the motion as a cartesian plot with the primary star at the origin but it excludes the three earliest data recorded (1830.78, 1910.68, 1910.74). The plot in Figure 4 shows much more scatter and a lower correlation coefficient value (R²=0.6). This is probably due to the oldest two points being very close to the polynomial fit in Figure 3.

A further test is shown in Figure 5 which shows the historical data excluding the 5 earliest data recorded (1830.78, 1910.68, 1910.68, 1910.74, 1912.85, 1912.93 excluded). The resulting polynomial fit has an $R^2 = 0.7$. Those 5 data points correspond to observations taken with 0.5m and 0.3m telescopes.

For our analysis of the system it is more appropriate to include all the historical data (the two oldest observations were made with 0.5m telescopes). Our results in Figure 3 indicate our double star system is consistent with a physical system.

It was found that the measurements obtained with AstroImageJ were sometimes different even using the same presets that can be modified in the Aperture Photometry Settings section of the AstroImageJ program. We found that when using the AstroImageJ program to determine data from the binary system, systematic errors on the part of the observer may be present. Factors such as the image quality can influence the observer's perception of the binary system. For binary pairs that are this close together, it can be more difficult to measure the separation.

Parallax	Error Parallax	PM in RA	Error for PM	PM in DEC	Error for	Distance
(mas)	(mas)	(mas/yr)	in RA (mas/yr)	(mas/yr)	PM in DEC	(pc)
7.2030	0.0229	21.377	0.028	3.625	0.018	135.5746

Table 3: Data for Gaia DR3-2764227830582570880 – (HJ 3203)

Table 4: Historical data HJ 3203 from the WDS catalog.

Date	P.A. (degrees)	Sep (arcsec)	RA (arcsec)	DEC (arcsec)	Aperture (m)	#Nights
1830.78	206.4	5	-2.223	4.479	0.5	1
1910.68	209.1	6.55	-3.185	5.723	0.5	2
1910.74	207.1	5.484	-2.498	4.882	0.3	1
1912.85	209.2	6.661	-3.250	5.815	0.3	1
1912.93	209.7	6.865	-3.401	5.963	0.3	1
1986.8	210.8	5.57	-2.852	4.784	0.6	2
1988.924	212.8	6.52	-3.532	5.480	0.7	2

2000.72	211.3	6.54	-3.398	5.588	1.3	1
2000.814	211.1	6.5630	-3.390	5.620	1.2	4
2010.5	211.5	6.42	-3.354	5.474	0.4	1
2010.837	211.2	6.59	-3.414	5.637	0.7	2
2013.953	211.36	6.525	-3.396	5.572	0.2	3
2014.752	211.41	6.555	-3.416	5.594	0.2	8
2015	211.366	6.57	-3.420	5.610	1	1
2015.5	211.377	6.5721	-3.422	5.611	1	1
2016	211.38	6.573	-3.423	5.611	1	1
2016.826	210.9	6.586	-3.382	5.651	1	1
2016.924	210.7	6.54	-3.339	5.623	0.7	1
2017.9342	211.71	6.621	-3.480	5.632	0.3	1
2023.8	213	6.1	-3.322	5.116	0.3	1

Historical Data Plot

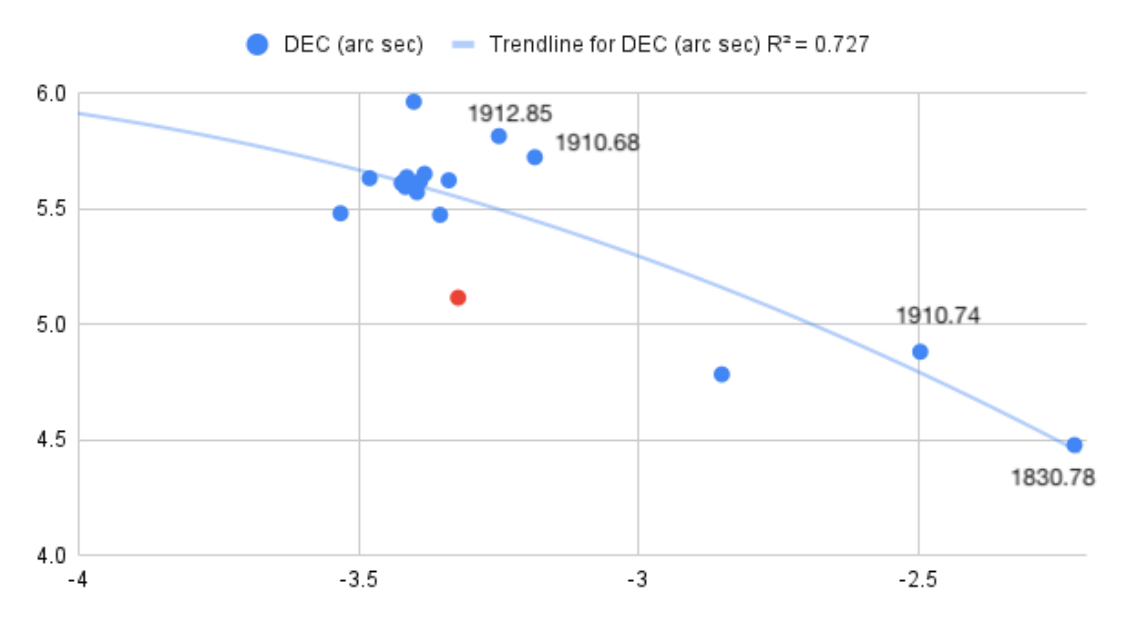


Figure 3: Plot for the historical data of HJ 3203 in a cartesian plane with the primary star in the origin. The horizontal axis represents the RA in arcseconds, and the vertical axis is the DEC in arcseconds. Blue is the historical data and Red represents our measurement. The oldest 4 observations have been labeled.



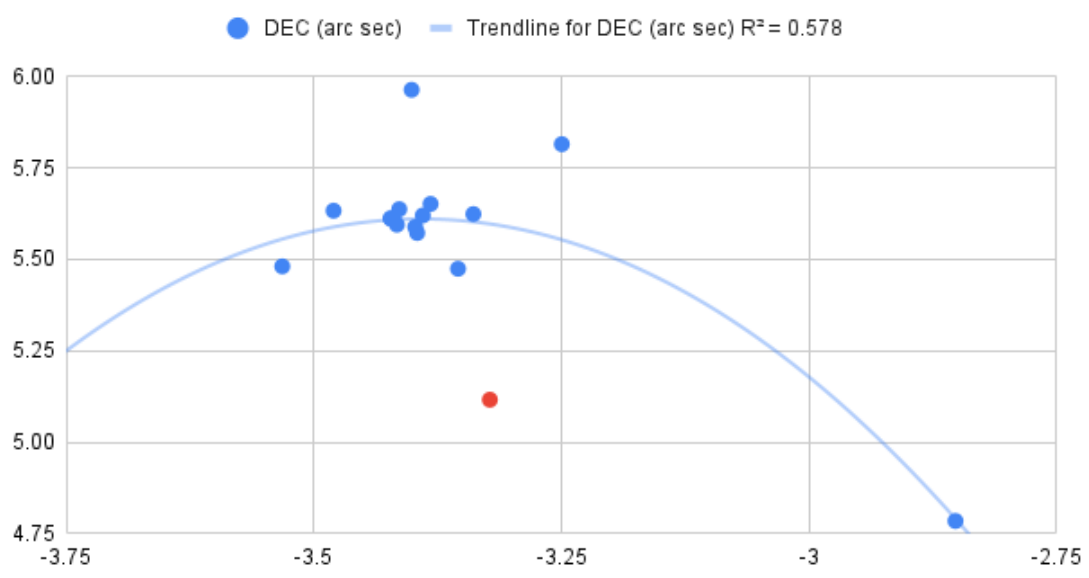


Figure 4: Plot for the historical data of HJ 3203 without the three oldest observations. The horizontal axis represents the RA in arcseconds, and the vertical axis is the DEC in arcseconds. Blue is the historical data and Red represents our measurement

Historical Data Plot 1986-2023

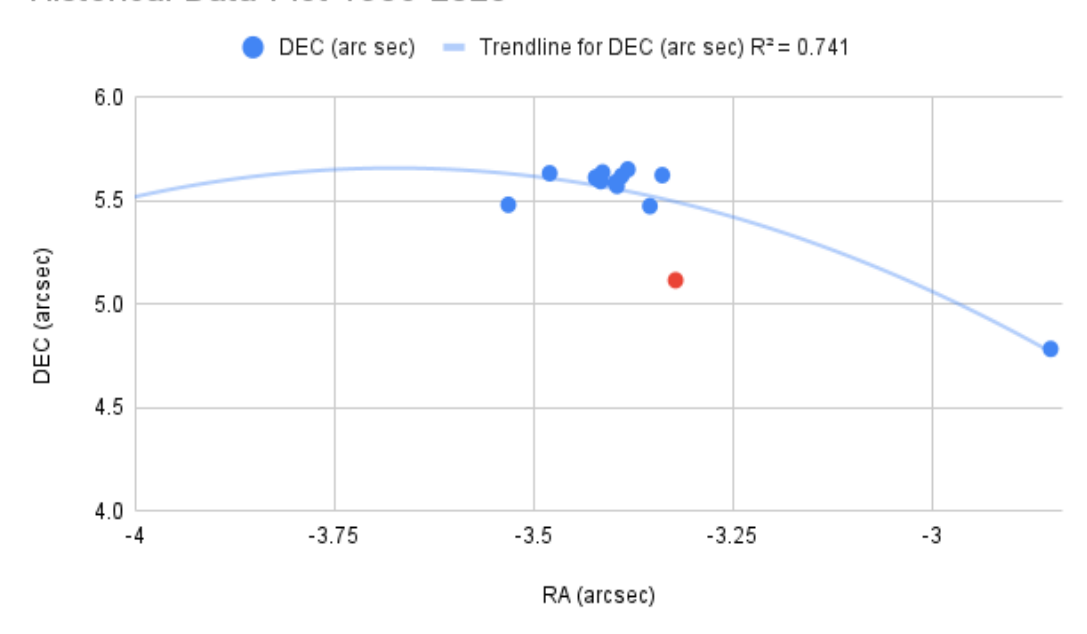


Figure 5: Plot for the historical data of HJ 3203 without the five oldest observations (time period 1986-2023). The horizontal axis represents the RA in arcseconds. Blue is the historical data and Red represents our measurement.

5. Conclusions

HJ 3203 seems to be a physical pair. More observations of the system would help prove that hypothesis. Our results in Figure 3 show a second order polynomial fit with $R^2 = 0.7$ moderately consistent with a physical system. Gaia DR3 catalog only had information regarding the primary star. Further observations are required to determine a more precise orbit for this binary system in which the stars have a small separation. More information about the secondary star is needed as well in order to determine and confirm the nature of HJ 3203 double star system.

6. Acknowledgements

This research has made use of the Washington Double Star Catalog maintained at the U.S. Naval Observatory. We would like to thank Rachel Matson from the USNO for providing the historical data for this work. This work makes use of observations from the Las Cumbres Observatory global telescope network. This research has made use of the SIMBAD database, operated at CDS, Strasbourg, France. We acknowledge the use of www.stelledoppie.it maintained by Gianluca Sordiglioni. This research has made use of the Stellarium planetarium. This research has made use of the open-source software AstroImage J. This work has made use of data from the European Space Agency (ESA) mission Gaia (https://www.cosmos.esa.int/gaia), processed by the Gaia Data Processing and Analysis Consortium (DPAC, https://www.cosmos.esa.int/web/gaia/dpac/consortium). Funding for the DPAC has been provided by national institutions, in particular the institutions participating in the Gaia Multilateral Agreement.

7. References

The Washington Double Star Catalog. (2023). Washington Double Star Catalog. https://crf.usno.navy.mil/wds.

Collins, K. A., Kielkopf, J. F., Stassun, K. G., & Hessman, F. V. (2017). ASTROIMAGEJ: Image Processing and Photometric Extraction for ULTRA-PRECISE ASTRONOMICAL Light Curves Commander, Naval Meteorology and Oceanography Command. (2022). U.S. Naval Observatory. Retrieved from https://www.cnmoc.usff.navy.mil/usno/

"Las Cumbres Observatory Global Telescope Network", Brown, T. M. et al., Publications of the Astronomical Society of the Pacific, 2013, Volume 125, issue 931, pp.1031-1055

Stelle Doppie - Double Star Database. (2022). Stelle Doppie, from https://www.stelledoppie.it/index2.php Genet, R. M., Buccheim, R., Johnson, J., Harshaw, R., & Freed, R. (Eds.). (2018). Star: Small Telescope Astronomical Research Handbook (First). Sheridan Books.

Fraknoi, A., Morrison, D., & Wolff, S. (2022). Astronomy 2e (Second). Openstax. Gaia Collaboration et al. (2016b): The Gaia mission (provides a description of the Gaia mission including spacecraft, instruments, survey and measurement principles, and operations)

Gaia Collaboration et al. (2023): Gaia DR3: Summary of the contents and survey properties.

Orbit Determination and Astrophysical Study of the Binary System HU 481 (= HD 147442)

F. M. Rica, 1*

¹ Federación Extremeña de Astronomía, C/José Ruíz Azorín, 14, 4° D, Mérida E-06800, Spain

ABSTRACT

I present a revised orbital solution for the binary WDS 16212+2259 = HU 481, composed of stars with V magnitudes 8.1 and 9.9, separated by 0.5 arcsec. The methodology employs the "three-dimensional grid search method" for orbital computation as originally outlined by Hartkopf, McAlister, & Franz (1989).

Conducting an astrophysical investigation, fundamental parameters for each stellar components of HU 481 are derived classifying the component as F6V and G9V stars. To achieve this, I utilize a tool constructed by the author. This tool was designed for the deblending of the entire observed multiband photometry, enabling the separation into individual fundamental and photometric parameters. The methodology is rooted in the application of PARSEC isochrones.

Key words: (stars:) binaries: general — binaries: visual - stars: fundamental parameters.

1. INTRODUCTION

This paper continues the investigation line of previous work published in Rica et al. (2017) and Rica and Zirm (2020).

The binary star WDS 16212+2259 = HU 481, also catalogued as HD 147442 and HIP 80117, consist of two stars with V magnitudes of 8.1 and 9.9, separated by approximately 0.5 arcsec. While Hartkopf and Mason (2010) previously calculated a grade 3 orbital solution, recent measures have revealed astrometric residuals, necessitating an improved orbital solution for this binary system.

This paper conducts a thorough orbital study, refining the existing orbital solution. The "three-dimensional grid search method," originally outlined by Hartkopf, McAlister, & Franz (1989), is employed for orbital computation.

In addition to the dynamical study, I undertook an astrophysical investigation utilizing combined multiband photometric data and trigonometric parallax information sourced from the literature. This approach enables me to extract individual photometric data and fundamental parameters for each component.

2. METHOD OF ORBITAL CALCULATION

The orbital computation employed in this study utilizes the three-dimensional grid search method as initially detailed by Hartkopf, McAlister, & Franz (1989) and subsequently refined following the modifications described by Mason, Douglass, & Hartkopf (1999). This methodology commences with three known elements (orbital period (P), epoch of periastron (T), and eccentricity (e)) to iteratively determine the geometric elements a (semimajor axis), i (inclination), Ω (ascending node) and ω (argument of periastron) through the method of least squares.

In practical terms, a space of potential values for *P*, *T*, and *e* must be defined. For each set of values, we compute a corresponding orbital solution, selecting the one with the smallest residuals. Additionally in cases where refinement is deemed necessary, a least squares approach is applied using the formula for differential corrections in rectangular coordinates (Heintz 1967a). Notably, this refinement method demonstrates efficacy even when dealing with a relatively short and linear observational arc.

.

^{*} frica0@gmail.com

Formal errors (1 σ uncertainty intervals) for the orbital elements are computed using the covariance matrix. The covariance matrix is a square matrix that contains the covariances between all pairs of orbital elements. The formal errors are calculated by taking the square root of the diagonal elements of the covariance matrix.

Prior to commencing any computations, the observed θ values must be corrected by the precession equinox effect, ensuring that all astrometric measurements are expressed for the 2000 equinox. However, not all the θ values reauire correction. Digital observational techniques (e.g., CCD, speckle, adaptive optics, lucky imaging) that utilized reference binaries to calibrate the orientation of CCD images are exempt from this correction owing to the use of ephemerides based on the 2000 equinox. On the other hand, θ values from digital astrometric points that employ slit masks to calibrate the orientation, must be corrected, because it uses the Earth's rotation. Moreover, θ values obtained from astrometric catalogues (e.g., Hipparcos, 2MASS, Gaia) do not require θ correction since they are referenced to the 2000 equinox or equivalent astrometric frame (that is ICRS).

We applied a data-weighting scheme to astrometric measures, following the guidelines outlined in Rica et al. (2012). This involved considering various criteria, including observational method, telescope aperture, observer experience, and the number of nights observed. Initially, for visual measures, we set θ weights four times larger than p weights, a practice proposed by Heintz (1978) and corroborated by Geoffrey & Worley (1992). Any measures with residuals exceeding 3σ within their respective groups, primarily determined by the observational technique, were assigned zero weight. Subsequently, non-zero weight measures underwent re-weighting based on the methodology described by Irwin et al. (1996).

2. PROCEDURE FOR DETERMINE FUN-DAMENTAL PARAMETERS AND ASTROPHYSICAL PROPERTIES

We performed an astrophysical analysis, utilizing combined (that is, sum of the light for both stellar

¹ **CMD** is a service maintained at the Osservatorio Astronomico di Padova, composed by a set of routines that provide interpolated isochrones in a grid, together with derivatives such as luminosity functions, simulated star clusters, etc. The photometry can be

components) multiband photometric trigonometric parallax, and Vmagnitudes between the stellar components retrieved from the literature. My methodology included applying evolutionary isochrones to decompose the combined observed UBVIJHK photometry of the binary systems, predominantly sourced from the Hipparcos, Tycho-2, and 2MASS catalogs. This procedure led to the extraction of synthetic photometry fundamental parameters for each individual component.

For our isochronal analysis, I utilize the CMD 3.3 evolutionary isochrones online tool¹, based on PARSEC release v1.2S + COLIBRI S_35 (Bressan et al. 2012, Chen et al. 2014, 2015, Tang et al. 2014, Marigo et al. 2017, Pastorelli et al. 2019). This tool facilitated the acquisition of the necessary isochrones for the investigation.

To do this task in this paper, I use a tool I built called Binary Deblending v5.0 which integrates *UBVIJHK* synthetic photometry from PARSEC isochrones, spanning a diverse range of ages and metallicities [Fe/H].

The "Binary Deblending" tool performs a search algorithm to find two distinct entries within each evolutionary isochrones, minimizing the χ^2 between the combined observational photometry and the PARSEC model's prediction. The output encompasses synthetic photometry in *UBVIJHK* bands, spectral types, and fundamental parameters (masses, effective temperature, surface gravity, luminosity, and radius) for each component.

The tool produces a comparative table that juxtaposes the combined observed photometry with the corresponding combined model photometry. Furthermore, it provides fundamental parameters for each component of the binary system.

I determined the line-of-sight reddening by utilizing the maps provided by Schlafly and Finkbeiner (2011). The derived values are scaled to the *Hipparcos* or *Gaia* distance using the formula presented by Anthony-Twarog and Twarog (1994). In addition, I employ the Stilim web tool (https://stilism.obspm.fr/), which generates 3D maps of the local InterStellar Matter (ISM). These maps are constructed based on measurements of starlight absorption by dust

produced for many different broad- and intermediateband systems, including non-standard ones. Online tool: http://stev.oapd.inaf.it/cgi-bin/cmd

¹ <u>https://stilism.obspm.fr/</u>

(resulting in reddening effects) or gaseous species (revealed through absorption lines or bands). The current map originates from the inversion of reddening estimates towards 71,000 target stars.

I also undertook a kinematic study to approximate the stellar ages based on galactocentric velocity (Przybylski 1962) represented as (U, V, W). The Eggen diagrams (1969a, 1969b; see Figure 1 in both papers) were utilized. These diagrams offer valuable insights, applicable to stars of all types, assisting in discriminating between young and old stars.

In addition to the Eggen diagrams, I incorporated the kinematic age parameter introduced by Grenon (1987), designated as fG. Bartkevicius & Gudas (2002) establishing a correlation between fG and age, thus allowing us to distinguish between different age groups. Their statistical analysis suggests that stars with fG < 0.20 belong to the young-middle age group (with an age less than 3-4 Gyr) within the thin disk population. Stars with 0.20 < fG < 0.35 are associated with the old (with an age of 3-10 Gyr) thin disk population. Those with 0.35 < fG < 0.70 are linked to the thick disk population (age greater than 10 Gyr), while stars with fG > 0.70 belong to the halo population.

3. THE BINARY STAR WDS 16212+2259 = HU 481 = ADS 10017

The binary star HU 481 (= HD 147442 = HIP 80117) was discovered by Hussey at Lick Observatory (1902), utilizing a 0.9 telescope. It consists of two stars with *V* magnitudes of 8.1 and 9.9 separated approximately by 0.5 arcsec. Since its discovery, this binary system has been observed on 86 occasions covering about one revolution although less than half of a revolution it is covered by speckle astrometric measures. Hartkopf & Mason (2010) calculated the last orbital parameters, but the more recent astrometric measures start to show astrometric residuals. Therefore, this binary star needs an improved orbital solution.

3.1 Astronomical literature

HD 147442 is a star located at 66 pc (*Hipparcos*) poor in metallicity with a combined spectral type of F8 (Cannon & Pickering 1928-1924) and with an age similar to the Sun or younger. The *Hipparcos* catalogue lists a parallax of 15.11 \pm 0.84 mas while *Gaia* DR3 lists an object with a higher parallax (18.84 \pm 0.36 mas) and with a

RUWE parameter of 8.75, indicating an issue with the single-star astrometric model. This high RUWE value is likely caused by the presence of the close secondary as pointed out by Belokurov et al. (2020).

The RUWE parameter in Gaia Catalog

The RUWE (Renormalized Unit Weight Error) is a measure of the quality of astrometric data for a source in the Gaia catalog. It is calculated as the ratio between the observed astrometric error and the expected astrometric error for a source of that magnitude and position. A RUWE value close to 1 indicates that the data fit well to a simple model of a star, while a value greater than 1 indicates that the data may be from a more complex object, such as a binary system, a variable star, or an extragalactic object.

To determine if one of these parallaxes are not realistic, I calculated the dynamical total mass utilizing the orbital period (*P*) and the semimajor axis (*a*) published by Hartkopf & Mason (2010). If we use the *Gaia* DR3 parallax, a dynamical total mass of 1.1 solar masses is obtained, which is not a realistic total mass. While using the *Hipparcos* parallax, the dynamical total mass is 2.0 solar masses, much in agreement with the expected mass. Therefore, in this work I will utilize the *Hipparcos* parallax.

Related with metallicity, Table 1 lists the values found in the literature:

Table 1. Metallicity data for HD 147442

[Fe/H]	Reference
-0.32	Marsakov & Shevelev (1995)
$-0.14^{+0.21}_{-0.14}$	Ammons et al. (2006)
-0.32	Holmberg et al. (2009)
-0.28	Casagrande et al. (2011)
-0.10	Gontcharov (2012)

Holmberg et al. (2009) determined a galactocentric velocity (U, V, W) of (-5, -20, -17) km s⁻¹ which corresponds to a star within the young-medium (3-4 Gyr) stellar population in the thin Galactic disk, in agreement with other references.

Tokovinin et al. (2010) estimated a differential magnitude for the stellar components of 2.0 (for wavelengths of about 550 nm, that is,

Table 2. Comparison of observed and synthetic phptometries for HU 481

Photometric band	Observed photometry	Source	Synthetic photometry	Difference
В	8.41 ± 0.05	Hipparcos	8.41	0.00
V	7.87 ± 0.04	Hipparcos	7.88	-0.01
I	7.27 ± 0.05	Hipparcos	7.26	0.01
J	6.84 ± 0.03	2MASS	6.84	0.00
H	6.58 ± 0.03	2MASS	6.60	-0.02
K	6.54 ± 0.02	2MASS	6.53	0.01
B - V	0.54 ± 0.03	Hipparcos	0.52	0.02
V-I	0.60 ± 0.02	Hipparcos	0.62	-0.02
V - K	1.33 ± 0.04		1.35	-0.02
J - H	0.26 ± 0.04	2MASS	0.24	0.02
H - K	0.04 ± 0.04	2MASS	0.07	-0.03
J - K	0.26 ± 0.04	2MASS	0.24	0.02

near the visible wavelength). Using all the visual measures from the WDS catalogue, I estimate a Δ mag = 1.76 ± 0.31 mag. The *Hipparcos* Δ mag converted to ΔV is used for the analysis (1.81 ± 0.16 mag.).

Using the *Hipparcos BVI* photometry, the 2MASS *JHK* photometry as well as magnitude difference (ΔV), I employ *Binary Deblending v5.0* which minimum χ^2 solution gives individual spectral types of F6V and G9V. The difference between the synthetic photometry and the unreddening and combined observed photometry

Table 3. Astrophysical data for the binary HU 481.

Data	A	В	
Vo	8.08	9.86	
(B - V)0	0.48	0.77	
Mv	3.97	5.76	
Mass [M _{sun}]	1.11	0.84	
$T_{\rm eff}$ [$^{ m o}$ K]	6380	5411	
$\log g$	4.33	4.59	
$\log L/L_{\rm sun}$	0.28	-0.39	
$R/R_{\rm sun}$	1.13	0.73	
SpT	F6V	G9V	
Distance [pc]	66.2		
Age [Gyr]	2.8		

are listed in **Table 2** while the fundamental parameters and others astrophysical data for each components are listed in **Table 3** for the first time.

Literature reports only combined astrophysical data and no paper determined the astrophysical data for the stellar components. The effective temperature $(T_{\rm eff})$ spectral types obtained this paper, are consistent with the literature, that reports a $T_{\rm eff}$ of

6100 K from Ammons et al. (2006), 6067 K from Holmberg et al. (2009), and 6131 K from Casagrande et al. (2011).

My study gives a minimum χ^2 solution for [Fe/H] = -0.16 and an age of 2.8 Gyr. Although the 68% confidence interval is from -0.29 to +0.05 for metallicity (in moderated agreement with the values listed in Table 1) and \leq 4.8 Gyr for the age.

3.2 New Orbital solution

Hartkopf and Mason (2010) calculated a grade 3 orbital solution, but the more recent measures start to show astrometric residuals. Therefore, this binary star needs an improved orbital solution. Utilizing the three-dimensional grid search method orbital methodology, I compute a new orbital solution that was refined with a differential correction method using rectangular coordinates. The new orbital solution is very similar to the previous one, but the RMS residuals are reduced significantly. The orbital parameters, with the formal errors, for the new orbital solution is listed in **Table 4**. For comparison, the previous orbit is also listed.

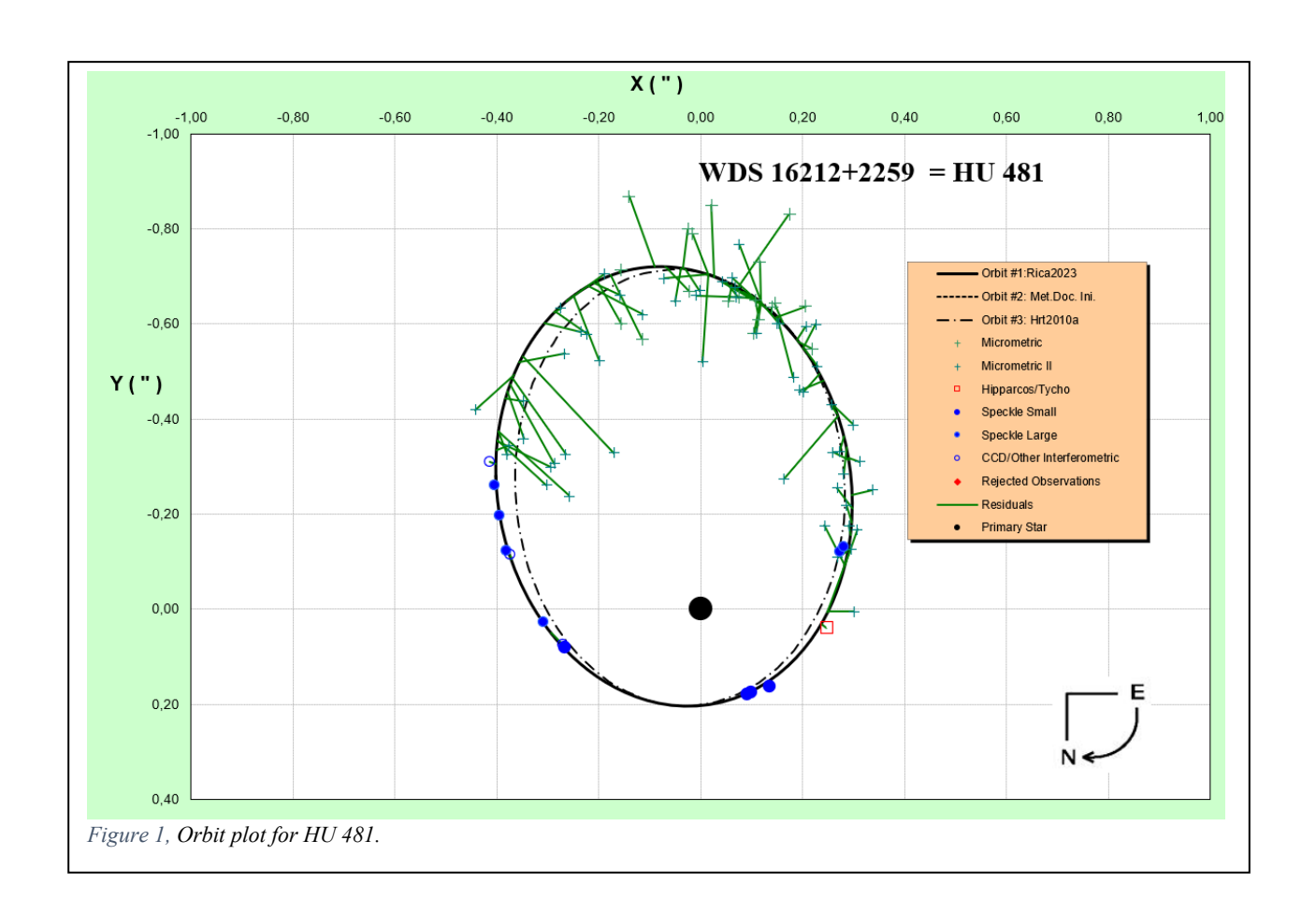
Figures 1-3 show the orbit plot in addition to the θ and ρ evolution against time. The black solid thick ellipse is the new orbit, and the dashed and dotted ellipse is the previously calculated orbit in the literature. North is down and East is right. The filled black circle is the main stellar component at (0,0) coordinate. Astrometric measures are

Table 4. New orbital solution for HU 481

	This wo	rk	Hrt2010
P [yr]	122.49 ±	0.89	119.500
To [yr]	1997.83 ±	0.07	1997.950
e	$0.569 \pm$	0.003	0.567
a [arcsec]	0.466 ±	0.004	0.464
i [deg]	154.4 ±	1.2	146.8
ω [deg]	165.0 ±	2.8	160.5
Ω_{2000} [deg]	178.0 ±	2.8	172.6
RMS(9) [deg]	0.99		2.34
RMS(ρ)[arcsec]	0.009		0.026
χ2 red [arcsec]	1.2		7.3
Σmass [M _{sun}]	1.96	2.03	

represented by green "+" (micrometric measures), red square (the *Hipparcos* and Tycho-2 measures), large blue circle (speckle measures), small blue circle (photographic and CCD measures). Rejected measures are plotted with red "X".

I can see those micrometric distances (ρ) measured before the year 1940, seem to show a systematic residual of -0.08 arcsec.



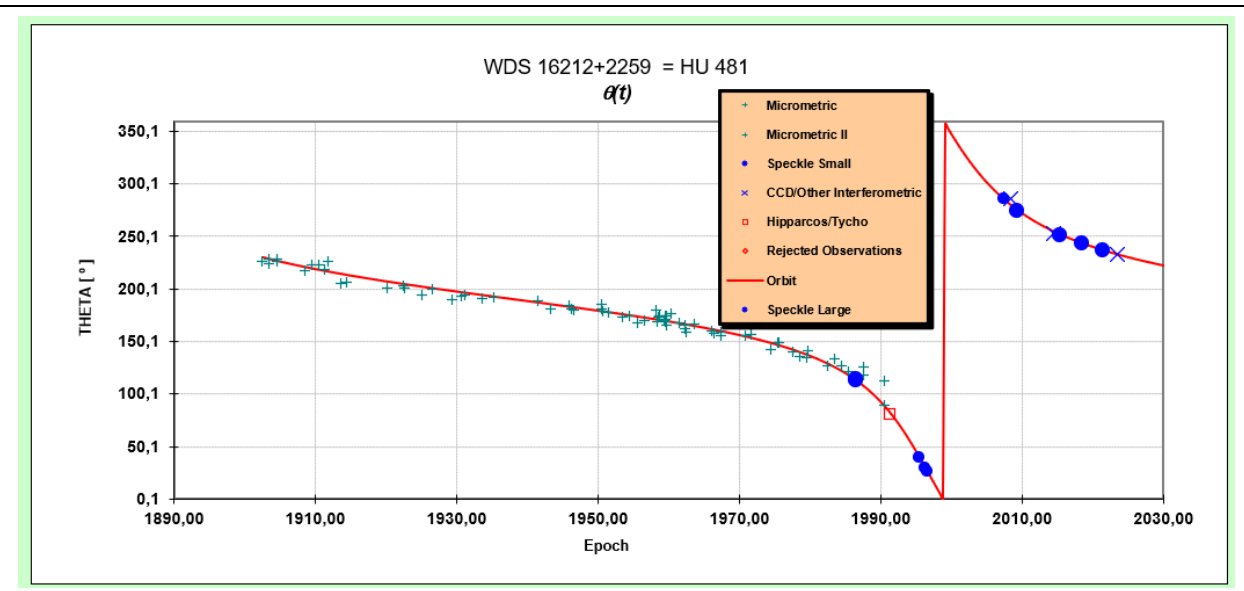


Figure 2. Position angles as a function of epoch for HU 481.

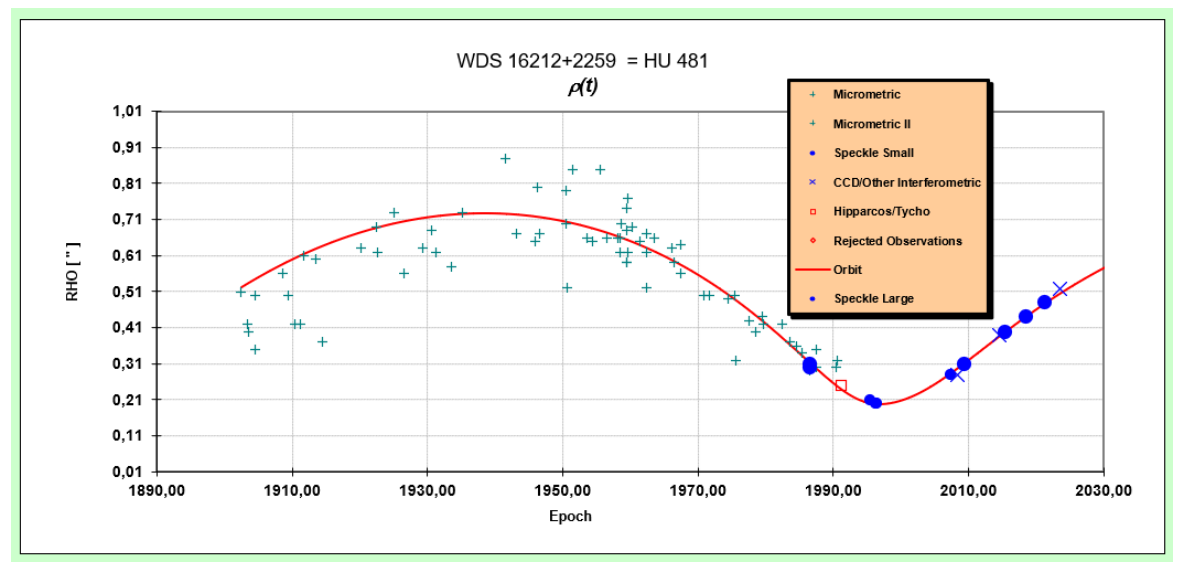


Figure 3. Angular distance as a function of epoch for HU 481.

REFERENCES

Ammons S.M., Robinson S.E., Strader J. et. al, 2006, ApJ, 638, 1004A

Anthony-Twarog B. J., Twarog B. A., 1994, AJ, 107, 1577

Bartkevicius A., Gudas A., 2002, Baltic Astron., 11, 153

Belokurov, V. et al., 2020, MNRAS, 496, 1922Bressan A., Marigo P., Girardi L., Salasnich B.,Dal Cero C., Rubele S., Nanni A., 2012,MNRAS, 427, 127

Cannon A. J., Pickering E. C., VizieR Online
Data Catalog, III/135A, https://vizier.u-strasbg.fr/viz-bin/VizieR?-source=III/135A&-to=3

Casagrande L., Schoenrich R., Asplund M. et al, 2011, A&A, 530A, 138C

Chen Y., Girardi L., Bressan A., Marigo P., Barbieri M., Kong X., 2014, MNRAS, 444, 2525

Chen Y., Bressan A., Girardi L., Marigo P., Kong X., Lanza A., 2015, MNRAS, 452, 1068

Eggen O. J., 1969a, PASP, 81, 741

Eggen O. J., 1969b, PASP, 81, 553

Geoffrey G. Douglass & Charles E. Worley, 1992 (IAU Coloquium 135, ASP Conference Series, Vol 32)

Gontcharov G.A., 2012, PAZh, 38, 860G

Grenon M., 1987, JAp&A, 8, 123

Hartkopf, McAlister, Franz, 1989, AJ, 98, 1014

Hartkopf, W. I. & Mason, B. D., 2010, IAUDS, 170, 1H

Heintz W. D., 1967a, Acta Astr., 17, 311

- Heintz W. D., 1978, Double Stars (Dordrecht: Kluwer)
- Holmberg J., Nordstrom B., Andersen J., 2009, A&A, 501, 941H
- Hussey, W.J., 1902, LicOB, 1, 161H
- Irwin A. W., Yang S. L. S., Walker G. A. H., 1996, PASP, 108, 580
- Marigo et al., 2017, ApJ, 835, 77
- Marsakov V.A., Shevelev Yu.G., 1995, BICDS, 47, 13M
- Mason D. M., Douglass G. G., Hartkopf W. I., 1999, AJ, 117, 1023M
- Pastorelli G. et al., 2019, MNRAS, 485, 5666P

- Przybylski A., 1962, PASP, 1962, 74, 230P Rica F. M. & Zirm H., JDSO, 2020, 16, 30
- Rica F. M., Barrena R., Vázquez G., Henríquez J. A., Hernández F. et al., 2012, MNRAS, 419, 197R
- Rica F. M., Barrena R., Henríquez J. A., Pérez F. M., Vargas P., 2017, PASA, 34, 4R
- Schlafly E. F. & Finkbeiner D. P., 2011, ApJ, 737, 103
- Tang J. et al., 2014, MNRAS, 445, 4287T Tokovinin, A., Mason, B., & Hartkopf, W., 2010, AJ, 139, 743T

Observation of the Double Star System HD 21599

Gabriela R. Santiago Rodriguez¹, Alanys S. Pizarro Vélez¹, Carmen A. Pantoja Pantoja¹, Mayra E. Lebrón Santos¹, Edward Gomez², Lisa Storrie-Lombardi², Alice Hopkinson², Rachel Freed³, Sabrina Stierwalt⁴

¹Universidad de Puerto Rico-Río Piedras, gabriela.santiago35@upr.edu

²Las Cumbres Observatory; Goleta, California

³InStAR; Arizona

⁴Occidental College; Los Angeles, California

Abstract

This study focuses on observing and analyzing the HD215990 double star system to contribute a measurement of position angle (PA) and separation (SEP) that will help in obtaining a precise orbit in the future. We selected this double star system utilizing the Stelle Doppie program. We combine our measurements with the historical data from the Washington Double Star Catalog (WDS).

1. Introduction

The objective of this research is to be able to observe and analyze the HD215990 double star system to obtain a new value for PA and SEP. We used the Stelle Doppie program to select a double with a magnitude difference (Δm) of 3, an apparent magnitude within the range of 9 < m < 11, a SEP between 5 and 10 arcseconds, and a requirement of 12-25 recorded observations. We selected HD 215990. The name of the primary star is TYC 3222-1938-1 with a magnitude of 9.91 and the name of the secondary star is HD 215990 with a magnitude of 10.07.

2. Equipment and Methods

Table 1 provides basic data of the double star system HD 215990. Column 1:name, from Stelle Doppie: columns 2,3: RA (2000.0), DEC (2000.0), Column 4: Apparent magnitude, from SIMBAD: column 5: spectral type, from Gaia DR3: column 6: parallax (mas), column 7: parallax error (mas), column 8: proper motion in RA (mas/yr), column 9: error of proper motion in RA (mas/yr), column 10: proper motion in DEC (mas/yr), column 11: error proper motion in DEC (mas/yr).

Name	RA (2000.0) (h,m,s)	DEC (2000.0) (°,','')	m	Spectral type (quality)	pe parallax error		pmRA (mas/yr)	error pmRA (mas/yr)	pmDEC (mas/yr)	error pmDEC (mas/yr)
HD 215990	22 48 34.97	+41 35 42.8	10.07	F5 E	3.4261	0.0137	-14.256	0.008	-5.798	0.014
TYC 3222- 1938-1	22 48 34.23	+41 35 38.3	9.91	A2 D	3.5423	0.0602	-15.277	0.034	-5.231	0.058

Table 1. Binary System HD 215990.

In Figure 1 we show an image of HD215990 taken from Stelle Doppie (Digitized Sky Survey).

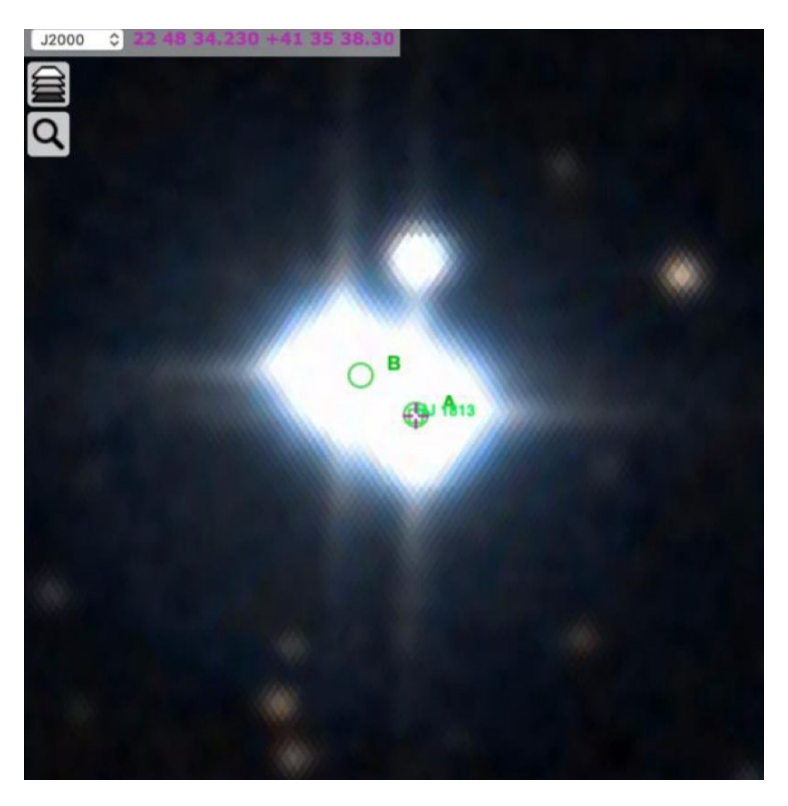


Figure 1: Photo of the binary system, taken from Stelle doppie. Star A is the primary star called TYC 3222-1938-1 and its pair, Star B, is called HD215990

The observations made were conducted utilizing a robotic telescope from Las Cumbres Observatory (LCOGT) telescope network. The chosen camera was 0m4 SCICAM QHY600, with an exposure count set at 1s for the preliminary test. Each exposure had a duration of 2s and used a Bessell-V filter.

3. Data

Table 2 provides our measurements of position angle and separation for 9 images taken with a 0.4m robotic telescope from Las Cumbres Observatory (LCOGT). All nine observations were taken on October 19, 2023, with a Bessell-V filter. Both stars exhibited a circular appearance in the images. We measured the PA and SEP using AstroImageJ. We obtained an average $PA = 61^{\circ}$ and standard deviation = 1°. We found an average PA = 9.3° and standard deviation = 0.4°.

Table 2. Observation of HD 215990 with 0.4m telescope.

Exp Time (s)	PA (deg)	SEP (arcsec)
0.999	61.52	9.32
0.999	60.54	9.41
1	61.33	8.49
1	61.52	9.32
0.999	62.48	8.81
1	60.39	9.12
0.999	62.93	10
1	59.87	9.39
1	62.78	9.58

4.Discussion

A request was made to Dr. Brian Mason for the historical data pertaining to the double star system HD 215990. Table 3 lists column 1: date, column 2: PA (degrees), column 3: SEP (arcsec), column 4: telescope aperture (m), column 5: PA (radians), column 6: the number of nights and column 7: reference from WDS. This data was used to generate the plot in Figure 2

Table 3. Historical Data for HD 215990.

Date	PA (degrees)	SEP (arcsec)	telescope aperture (m)	PA (Radians)	RA (arc sec)	DEC (arc sec)	number of nights	reference
1828	64.7	5.5	0.5	1.129228026	4.9724540231	-2.350468249	2	HJ_1831
1895.91	65.4	9.101	0.3	1.141445331	8.274957828	-3.78857149	1	WFC1998
1895.99	62.1	9.532	0.3	1.083849465	8.424053986	-4.46030699	1	WFC1998
1904.98	61.6	9.36	0.4	1.075122819	8.233510642	-4.451842597	2	Es_1906a
1906.02	61.8	9.45	1	1.078613478	8.328317622	-4.465604728	1	Bu_1906
1916.72	60.9	9.13	0.5	1.062905514	7.977540396	-4.440242023	2	Doo1923
1917.74	62.3	9.75	0.3	1.087340124	8.632587851	-4.532209946	3	Ptt1921
1919.74	60.9	9.25	0.2	1.062905514	8.082393063	-4.498602269	2	Frk1919a
1929.67	61.8	9.154	0.2	1.078613478	8.0674518	-4.325729702	1	WFC1958a
1958.72	61.6	9.245	0.2	1.075122819	8.132351056	-4.397145813	1	WFC1975
1991.63	61.2	9.45	0.3	1.068141502	8.281098126	-4.55257222	1	TYC2002
1998.77	61.3	9.4	1.3	1.069886831	8.245173939	-4.514100876	1	TMA2003
2002.707	61.3	9.418	0.2	1.069886831	8.26096257	-4.522744899	4	UC_2013b
2005.574	61.3	9.38	0.2	1.069886831	8.227631016	-4.504496406	1	Arn2006f
2006.737	61.2	9.4	0.2	1.068141502	8.237282792	-4.528484537	3	Spn2007

2010.5	61.4	9.43	0.4	1.071632161	8.279379458	-4.51406422	1	WIS2012
2012.777	61.51	9.403	0.2	1.073552023	8.264300266	-4.485281499	5	UR_2015
2013.733	61.28	9.422	0.2	1.069537766	8.262891245	-4.527550362	12	UR_2015
2014.776	61.31	9.417	0.2	1.070061364	8.260874582	-4.52082295	9	UR_2015
2015	61.275	9.423	1	1.069450499	8.263373046	-4.528752024	1	Kpp2018m
2016.88	61.1	9.438	0.7	1.066396173	8.262634206	-4.561219133	1	WSI2017b

Historical data plot

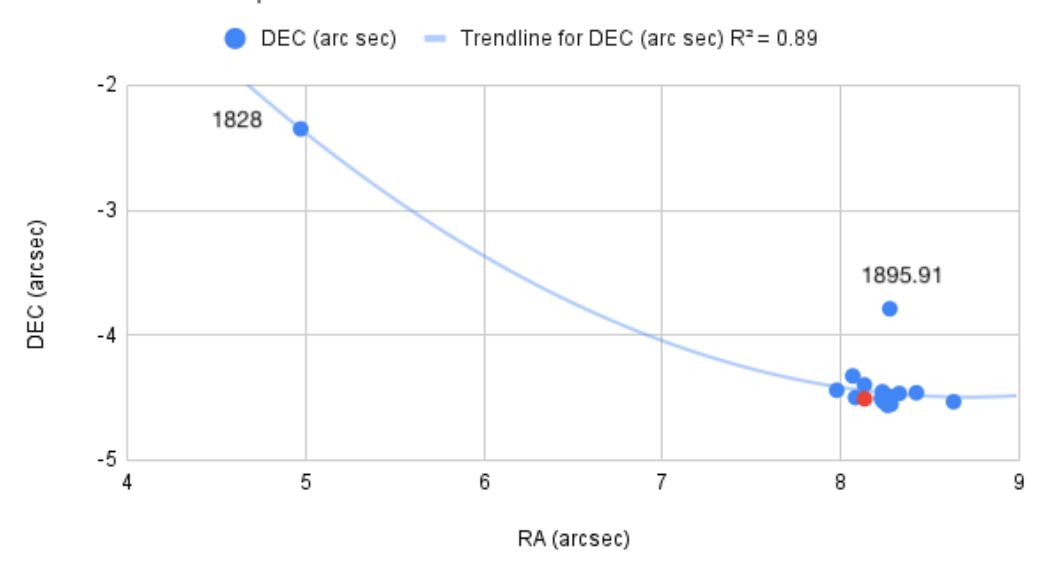


Figure 2: Shows a graph of the historical data of HD 215990. Blue dots are the historical data, and the red dot is our measurement. The blue line is a second order polynomial fit of the data

The reported spectral types for the primary star TYC 3222-1938-1: A2 D and the secondary star HD215990: F5 E, provided by SIMBAD. The proper motion data of HD215990 is consistent with a physical pair. The primary star is 920.55 ly away and the secondary star is 955.34 ly away.

5. Conclusions

Our observations allowed us to provide two new measurements of PA and SEP for HD 215990. The available data of the system (proper motion and parallax) supports that this is a physical pair. This system would benefit from more observations to obtain a more precise orbit.

Acknowledgements

This research has made use of the Washington Double Star Catalog maintained at the U.S. Naval Observatory. This research has made use of the SIMBAD database operated at CDS, Strasbourg, France. We acknowledge the use of www.stelledoppie.it created and maintained by Gianluca Sordiglioni.

References

Fraknoi, A., Morrison, D., & Wolff, S. C. (2022). Astronomy 2E. Openstacks.

Las Cumbres Observatory. (n.d.). https://lco.global/

Simbad: Basic query. SIMBAD Astronomical Database - CDS (Strasbourg). (n.d.). https://simbad.u-strasbg.fr/simbad/sim-fbasic

Stelle Doppie - Doble Star Database. (2023). Retrieved September 2023, from https://www.stelledoppie.it/index2.php

Washington Doble Star Catalog - Doble Star Catalog. (2023). Retrieved September 2023, from http://astro.gsu.edu/wds/

Astrometric Measurements of Four Physical Double Star Systems

Corbin Breeden, Zoe Schurman, Michael Pylypovych, Atria Freeman, Kalée Tock Stanford Online High School, Redwood City, California; corbin.breeden@gmail.com

Abstract

Images of four Washington Double Star systems, WDS 06065-4705 TVB 115, WDS 06404+1423 TVB 139, WDS 08494-1711 POC 3, and WDS 10019+7334 STF 1393 were taken and reduced in AstroImageJ to evaluate the position angle and separation, current for 2024.0. The resulting astrometric measurement is presented, along with a historical data plot and a comparison of relative three-dimensional space velocity to system escape velocity. All four systems are found to exhibit common proper motion, meaning they are moving in almost the same way. The data plot and measurements, combined with the Gaia Data Release 3 information suggest that TVB 115 could be a gravitationally bound binary star system, while TVB 139, POC 3, and STF 1393 are physical double star systems.

1. Introduction

Binary star systems fall under the umbrella term of a "physical" system, which move together in space but may or may not be gravitationally bound and in orbit around one another. While binary systems receive substantial focus, other types of physical relationships between stars are just as intriguing. Physically related stars often share an origin, and studying the nature of these relationships and origins can indirectly inform us about the nature of this galaxy and its history. The following paper investigates the physicality of four double star systems.

When selecting targets from the Washington Double Star (WDS) catalog, several parameters were employed. First, the target needed to have an RA between 5 and 13 hours so it would be visible in midwinter when observations were to be made. Second, the secondary star's magnitude needed to be less than 13, to ensure both stars would be bright enough to be resolved on a Complementary Metal-Oxide Semiconductor (CMOS) image with 0.35 m telescopes. The third requirement was a difference in magnitude (Δ mag) of less than 3. If the star system had a Δ mag greater than 3, it would be challenging to capture both stars in the system in the same image. Fourth, the two stars needed to have a separation between 5 and 15 arcseconds. A double star system with a separation of less than 5" would not be easily resolved, due to the closeness of the two stars in the image. Systems with a separation of greater than 15" are less likely to have a strong physical relationship. The final parameter was that the star system needed to be classified as a physical double. Ultimately, the systems TVB 115, TVB 139, POC 3, and STF 1393 were selected.

To find the spectral classes of the stars in each system, we used the measurements from Gaia DR 3 about their BP-RP color and Gaia G-filter magnitude corrected for parallax (absolute G magnitude). These measurements were used to plot the star on Gaia's Hertzsprung-Russell Diagram (Babusiaux, 2023; Prusti, 2016; Vallenari, 2023). The stars' positions on this diagram were then used to estimate their spectral types

and corresponding masses (Morgan, S. 2023; Mamajek, 2022). Figure 1 shows the stars' HR-diagram positions; Table 1 shows the data used to plot those positions, plus the resulting mass estimates. All four systems are listed as "physical" in Stelle Doppie and are located in winter constellations: TVB 115 and POC 3 in Puppis, TVB 139 in Gemini, and STF 1393 in Draco.

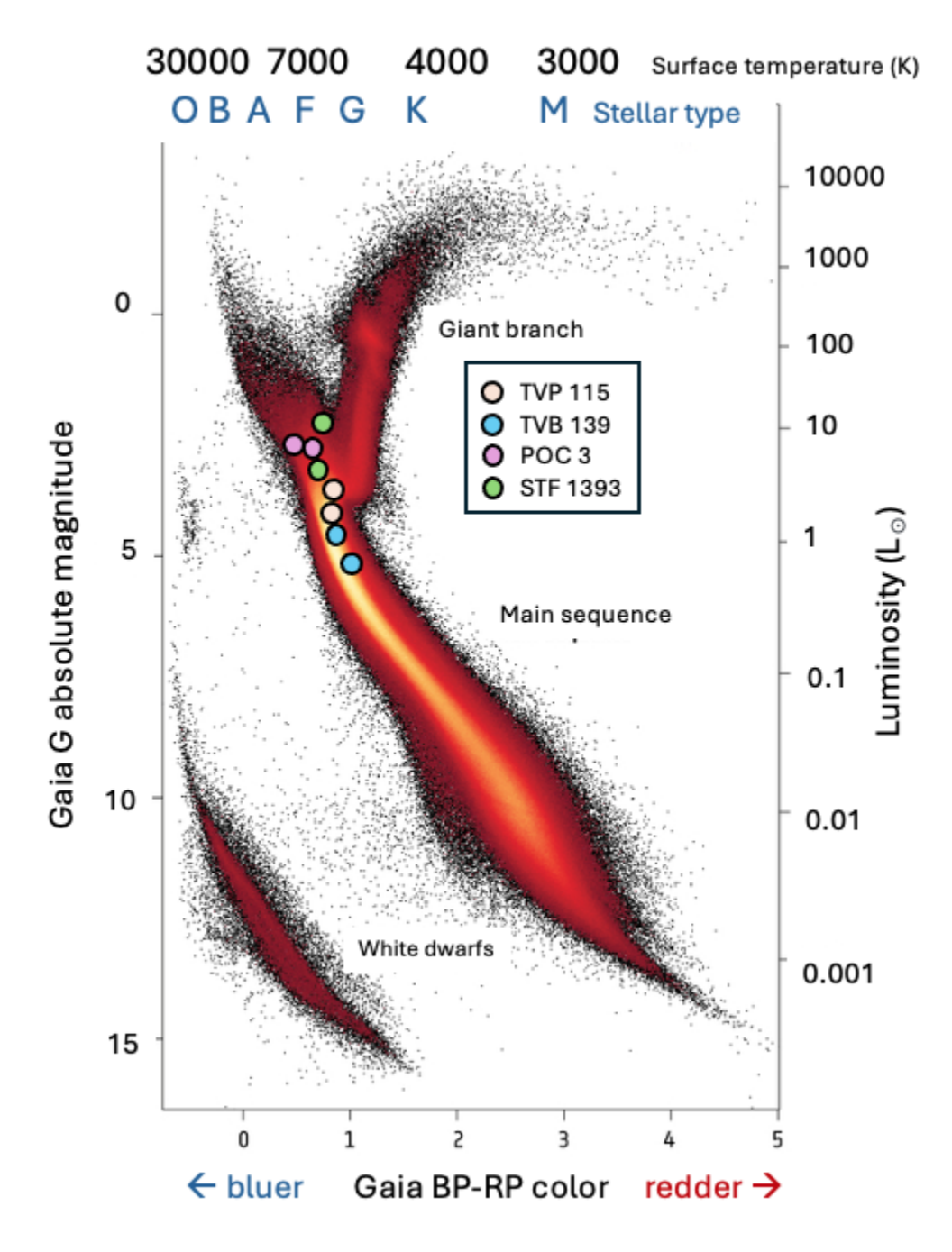


Figure 1: Gaia CMD diagram with each system's stars plotted according to their Gaia G absolute magnitude and Gaia BP-RP color

Table 1. Coordinate, Magnitude, Colors, and Estimated Masses.

System	Coordinates	Absolute Gaia Gmag (Primary)	Absolute Gaia Gmag (Secondary)	Colors (Bp-Rp) Primary	Color (Bp-Rp) Secondary	Primary Est. Mass (Solar Masses)	Secondary Est. Mass (Solar Masses)
TVB 115	06h 06m 29.06s -47° 05' 08.7"	3.80	4.13	0.86044 0.83652		0.9	1.1
TVB 139	06h 40m 22.89s +14° 23' 16.5"	4.52	5.24	0.84646 0.83931		1.5	0.8
POC 3	08h 49m 22.61s -17° 11' 29.6"	3.06	3.37	0.57963	0.69653	1.4	1.4
STF 1393	10h 01m 56.54s +73° 34' 07.1"	3.80	4.14	0.70094	0.64310	1.21	1.6

¹The primary star for STF 1393 has a spectral type of F8 (Brandt, 2021), implying a mass of 1.2 solar masses. It is the only star for which there is a known spectral type.

2. Instruments Used

All images were taken by a Planewave Delta Rho 350 + QHY600 CMOS camera. The telescope has an aperture of 0.35m and a focal length of 1050mm. The QHY600 CMOS camera has an angular pixel size of 0.73", and an FOV of 1.9° x 1.2°, cut down to 30' x 30' for the default imaging "central mode" of these Las Cumbres Observatory Global Telescope (LCOGT) instruments. Two different LCOGT sites were used: Teide and Siding Spring. The LCOGT Teide Observatory Aqawan A #1 is located on the island of Tenerife in Spain's Canary Islands, at an altitude of 2390m. The LCOGT Siding Spring Observatory is in Coonabarabran, New South Wales, Australia, at an altitude of 1164m. The two filters used were Bessell-V and PanSTARRS-w (Bessell, 1990; Tonry, 2012). Date of observation, exposure time, images taken, and filter used are shown in Table 2.

Table 2. Observation data for the set of double star systems.

System	LCOGT Observatory	Decimal Date of Observation	Images Taken	Exposure Time (sec)	Filter Used
TVB 115	Siding Spring	2024.0329	10	30	Bessell-V
TVB 139	Teide	2024.0192	11	25	PanSTARRS-w
POC 3	Teide	2024.0301	10	5	Bessell-V
STF 1393	Teide	2024.0301	10	8.75	Bessell-V

3. Measurements

All images for TVB 115, TVB 139, and STF 1393 were well-resolved, with clearly separated stars and minimal blurring. Images of POC 3 initially seemed to have stars blended together, but after adjusting brightness and contrast, the stars were well defined. Additionally, while TVB 115 has a smudge next to it, this third star is not in the system - according to Gaia data, it has a parallax far different from TVB 115. Measurements were made with AstroImageJ's multi-aperture photometry tool. Examples of the measurement process for each system are shown in Figure 2. The individual measurements of position angle in degrees and separation in arcseconds can be found in Appendix A.

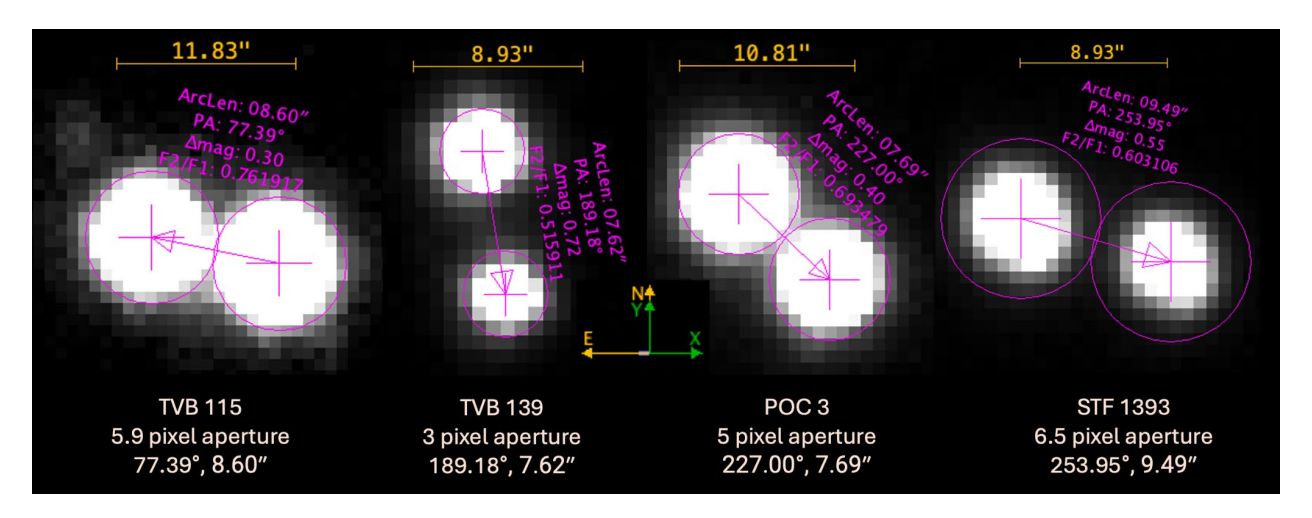


Figure 2: Example of the measurement process for each system

The individual measurements of the images were averaged, with average position angle and separation and accompanying standard errors depicted in Table 3.

Table 3. Average measurement	s, standard deviation	, and standard error	of the mean average.
------------------------------	-----------------------	----------------------	----------------------

System	Position Angle (°)	Standard Deviation on PA (°)	Standard Error PA (°)	Separation (")	Standard Deviation Separation (")	Standard Error Separation (")
TVB 115	77.1	0.48	0.17	8.56	0.116	0.041
TVB 139	189.2	0.07	0.02	7.63	0.023	0.007
POC 3	227.3	0.24	0.08	7.72	0.044	0.014
STF 1393	254.1	0.22	0.07	9.47	0.023	0.007

4. Results and Discussion

To assess the radial proximity of the stars in each pair to each other and the degree to which their motion is synchronized, Gaia DR3 parallax and proper motion measurements are tabulated in Table 4. The proper motion ratio (rPM) is calculated by taking the ratio of the magnitude of the relative proper motion vector to the magnitude of the longer proper motion vector of the two stars (Harshaw, 2016). Double star systems are considered to display common proper motion if the rPM value is less than 0.2, as all of these are.

Table 4. Parallax and proper motion data for the set of double star systems, including the proper motion ratio (rPM). Data taken from Gaia DR3.

System	Parallax of Primary (mas)	Parallax of Secondary (mas)	Proper Motion of Primary (mas/yr)	Proper Motion of Secondary (mas/yr)	rPM
TVB 115	2.89 ± 0.011	2.90 ± 0.011	$(-9.97 \pm .01,$ $-6.2 \pm .01)$	$(-9.97 \pm .01,$ $-6.17 \pm .01)$	0.001
TVB 139	2.92 ± 0.014	2.94 ± 0.023	$(12.1 \pm 0.02, \\ -27.4 \pm 0.02)$	$(12.5 \pm 0.03, \\ -27.04 \pm 0.03)$	0.017
POC 3	5.77 ± 0.014	5.96 ± 0.024	$(1.00 \pm 0.01, \\ -33.9 \pm 0.01)$	$(0.68 \pm 0.02, \\ -34.3 \pm 0.02)$	0.015
STF 1393	2.81 ± 0.014	2.81 ± 0.015	$(14.02 \pm 0.01, -7.0 \pm 0.02)$	$(15.8 \pm 0.02, \\ -7.4 \pm 0.02)$	0.106

One study which included POC 3 (identifier HD 75423) concluded that stars with >1 parsec (pc) separation cannot be easily distinguished as genuine wide binaries (binary systems set relatively far apart) instead of moving groups, contamination from randomly aligned stars, or ionized former binary systems (former binaries that have become gravitationally unbound). The study instead suggests that stars with <1 pc separation are high-confidence candidates for being a binary (Andrews, et al., 2017). The three-dimensional separation of POC 3 is calculated using the separation and the parallaxes of the stars and is greater than 5 pc, so POC 3 is unlikely to be gravitationally bound according to the Andrews criterion. Despite likely not being gravitationally bound, POC 3 shows common proper motion even at >5 pc separation.

The three remaining systems have both common proper motion and similar parallaxes between their two stars, suggesting a stronger physical relationship.

Another way to assess the physical relationship of double star systems is the comparison of system escape velocity to relative three-dimensional space velocity. The stars in a system whose three-dimensional space velocity is less than the system escape velocity are likely to be gravitationally bound. We calculated system escape velocity (in m/s) using the following equation:

$$v_{escape} = \sqrt{\frac{2G(m_1 + m_2)}{r}}$$

where m_1 is the estimated mass of the primary star, m_2 is the estimated mass of the secondary star, and G is the gravitational constant. In this equation, the variable r is either the transverse separation in space when the stars' parallaxes overlap within uncertainty or r is the three-dimensional spatial separation when the stars' parallaxes do not overlap within uncertainty (Bonifacio 2022). Transverse separation (in parsecs) is calculated using the following equation:

$$Sep_{pc} = \frac{Sep_{arcseconds} \times \frac{1deg}{3600''} \times \frac{2\pi \ rad}{360deg}}{parallax''}$$

Three-dimensional spatial separation (in parsecs) is calculated by converting the parallaxes into parsecs and taking the difference in radial distance between the two stars, then applying the Pythagorean Theorem to the transverse separation and radial separation to account for all three dimensions. POC 3 was the only system whose stars' parallaxes do not overlap within uncertainty, necessitating use of the three-dimensional spatial separation when calculating the escape velocity.

To find the relative three-dimensional space velocity to compare with the system escape velocity, we again applied the Pythagorean Theorem to the relative transverse motion through space and the relative radial motion through space. The relative transverse motion through space (in m/s) was found by dividing the magnitude of the relative proper motion vector by the parallax of the primary star (this assumes that the two stars are close to the same distance from Earth). The relative radial motion through space (in m/s) was calculated by taking the absolute value of the difference between the Gaia primary and secondary radial velocities when given. POC 3 was the only system for which Gaia did not have a radial velocity value for the secondary star, so relative space velocity was taken to be the same as the relative transverse motion through space. Masses were roughly estimated with Gaia BP-RP values and Gaia G magnitude values, or with the spectral type if it was known, as described previously and listed in Table 1. The relative and escape velocities computed as described here are presented in Table 5.

Table 5. Separation calculations, system escape velocity, and relative space velocity.

System	Transverse separation (pc)	System escape velocity (m/s)	Gaia radial velocity of primary (km/s)	Gaia radial velocity of secondary (km/s)	Transverse velocity (m/s)	Relative 3D space velocity (m/s)
TVB 115	0.014	1065	25.22	25.70	14	488
TVB 139	0.013	1243	108.76	106.71	842	2217
POC 3	5.781	65	-13.32	N/A	423	423
STF 1393	0.017	1196	-47.95	-49.25	3118	3380

¹The italicized transverse separation for POC 3 indicates the three-dimensional spatial separation that incorporates transverse and radial separation, used when the stars' parallaxes do not overlap with uncertainty. The three-dimensional spatial separation was used to calculate the system escape velocity for POC 3 only. The other systems used transverse separation.

Having estimated the system escape velocity, we compared it to the calculated relative three-dimensional space velocity. TVB 115 has a relative space velocity less than its system escape velocity suggesting that the stars may be gravitationally bound. For TVB 139 and STF 1393, the escape and relative velocities are the same order of magnitude, which problematizes a definitive conclusion. For POC 3, however, the relative space velocity is more than six times greater than the escape velocity, as might be expected for a system whose components are so widely separated.

While POC 3's components likely have a weaker physical relationship, the spectral type analysis paper from Houk and Smith-More in 1988 suggests that the secondary star in POC 3 may itself have a very faint companion of Type G or K. When POC 3's coordinates are queried in both Simbad and Gaia DR3, three stars appear. The Gaia DR3 listing appears in Figure 3. Because Gaia's angular resolution limit is 0.4 arcseconds, and the difference between the secondary and possible tertiary star in Simbad is less than 0.4 arcseconds, Gaia was not able to accurately resolve the third star, which explains the lack of color, parallax, proper motion, and other data points (Luri, 2018). The Gaia DR3 listed G magnitude of 20.44 explains why the possible third star does not appear in any images. Further measurements and analyses of POC 3 are recommended to better describe this possible third star.

The 10 closest stars in order of proximity to 08h49m22.61-17d11m29.6s are:

PA	•	•	•			•		•		•		•		•		•	
164.37777	•		•			•		•		•		•		•			
344.94487		5.21541		20.4426								1					
227.13756		7.75106	ĺ	9.56644	0.69653		5.76561		0.02434		0.67755		0.02303		-34.33953		0.02341

Figure 3: Gaia DR3 listing for POC 3 with the primary star in the first row, secondary star in the third row, and possible tertiary star in the second row with many data points missing

5. Plots

Using historical position angle and separation data obtained from the United States Naval Observatory, as well as Gaia DR3 measurements and our measurements, the positions of the secondary stars with the primary stars at the origins over time are plotted in Figure 4.

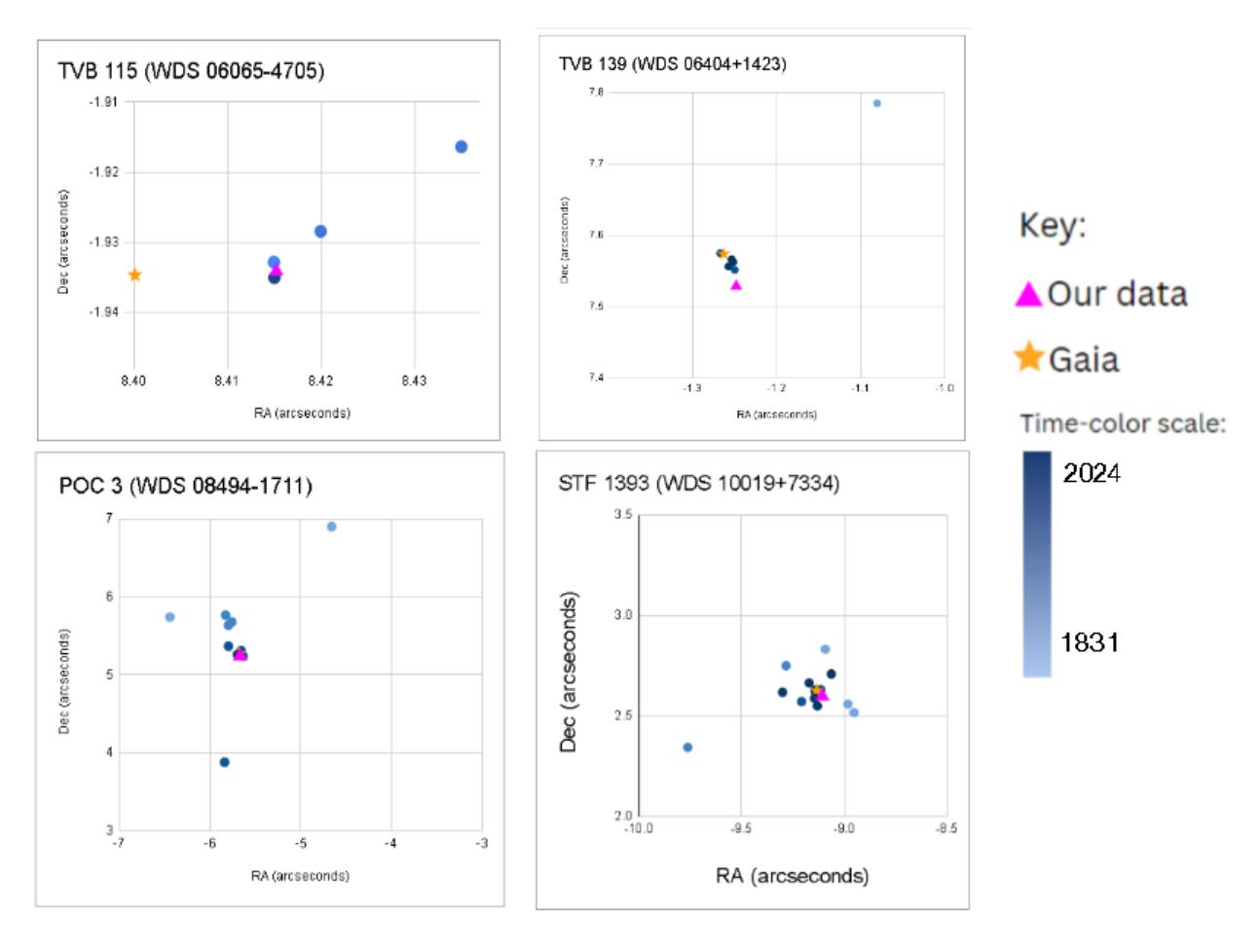


Figure 4: Position of secondary star in RA and Dec of TVB 115, TVB 139, POC 3, STF 1393 with respect to primary with labeled measurements from Gaia and this study. The first two data points of TVB 115 from 1902.94 are out-of-bounds at (8.05, -2.07) and (8.58, -1.81). The first data point of STF 1393 from 1831.84 is out-of-bounds at (-11.69, 2.70)

The data plotted above is from the historical data requested from the Washington Double Star Catalog. None of these systems have a published orbit or linear solution. Despite the fact that the component stars of TVB 115 have a lower relative velocity than escape velocity, the erratic temporal dependence of the data in Figure 4 does not suggest an orbital solution.

The historical data plot of TVB 139 differs in general shape from the plots of TVB 115, POC 3, and STF 1393. We propose that the outlier at (-1.08, 7.78) in TVB 139 be deprioritized as it is from the oldest known measurement and could therefore be subject to more uncertainty than the more recent ones. The graph of TVB 139 is unique in its shape because it shows promising signs of a curve relative to the origin. TVB 139 is worth further study to assess whether this trend continues.

There appears to be a lack of a trend over time in systems POC 3 and STF 1393. In POC 3, the distribution for historical data points in POC 3 is erratic and is likely to have no association between time and data points. It is important to note that the purple triangle representing the observations done in this study on POC 3 is obscuring the orange star corresponding to the Gaia data point in the graph. There is a similar

story in STF 1393. The first data point from 1831 is off the graph to the upper left, the furthest left visible point is the 6th observation from 1930. Meanwhile, the two furthest right points are from 1894 (-8.95, 2.52) and 1911(-8.98, 2.55). Furthermore, the 2015 Gaia DR3 data point is clumped in the middle of the graph along with the most recent 2024 data point. Both a fitted 2nd degree polynomial trendline that includes the out-of-bounds data point and the same trendline that only includes the visible data points fail to encompass the origin.

6. Conclusion

The measurements within this study were consistent with historical observations of the four systems. All four stars have common proper motion, classifying them as physical systems. Systems TVB 115 and STF 1393 could have long-period orbital solutions that don't show up in the timespan of the observations conducted so far. Based on escape velocity calculations, TVB 115 is the likeliest candidate for a long-period orbital solution. However, TVB 139 is the only system that shows some indication of curvature in the historical data plot. With the exception of TVB 115, the systems have escape velocities lower than their relative space velocity, implying that they are not gravitationally bound, though the data is significantly less conclusive for TVB 139 and STF 1393 and does not fully rule out the idea of any of these systems being binary. Given the parallax of the stars in POC 3 (>5 pc), the system is unlikely to be gravitationally bound. Further observation is recommended for all four of these physical double star systems.

Acknowledgements

This research was made possible by the Washington Double Star catalog maintained by the U.S. Naval Observatory, the Stelle Doppie catalog maintained by Gianluca Sordiglioni, Astrometry.net, and AstroImageJ software which was written by Karen Collins and John Kielkopf.

This work has made use of data from the European Space Agency (ESA) mission Gaia (https://www.cosmos.esa.int/gaia), processed by the Gaia Data Processing and Analysis Consortium (DPAC, https://www.cosmos.esa.int/web/gaia/dpac/consortium). Funding for the DPAC has been provided by national institutions, in particular the institutions participating in the Gaia Multilateral Agreement.

This work makes use of observations taken by the Planewave Delta Rho 350 + QHY600 CMOS camera systems of Las Cumbres Observatory Global Telescope Network located in Tenerife, Spain.

The Las Cumbres Observatory's education network telescopes were upgraded through generous support from the Gordon and Betty Moore Foundation.

This research has made use of the SIMBAD database, operated at CDS, Strasbourg, France (Wenger et al. 2000).

References

- Andrews, J. J., Chanamé, J., & Agüeros, M. A. (2017). Wide binaries in Tycho-Gaia: search method and the distribution of orbital separations. *Monthly Notices of the Royal Astronomical Society*, 675–699. https://doi.org/10.1093/mnras/stx2000
- Bessell, M. S (1990). Publications of the Astronomical Society of the Pacific, 102, 1181-1199. https://adsabs.harvard.edu/full/1990PASP..102.1181B
- Brandt, T. D (2021). The Hipparcos-Gaia Catalog of Accelerations: Gaia EDR3 Edition. The Astrophysical Journal Supplemental Series, 254(2). https://simbad.cds.unistra.fr/simbad/simref?bibcode=2021ApJS..254...42B
- Bonifacio, B., C. Marchetti, R. Caputo, and K. Tock. (2020). Measurements of Neglected Double Stars. Journal of Double Star Observations, 16(5), 411–423. http://www.jdso.org/volume16/number5/Bonifacio 411 423.pdf
- Evans, D. W, et. al (2018). Gaia Data Release 2 Photometric content and validation. A&A 616, A4. https://www.aanda.org/articles/aa/full html/2018/08/aa32756-18/aa32756-18.html
- Gaia Collaboration, A. Vallenari, A. G. A. Brown, et al. (2022k). Gaia Data Release 3: Summary of the content and survey properties. arXiv e-prints, https://arxiv.org/abs/2208.00211
- Gaia Collaboration, C. Babusiaux, F. Van Leeuwen, et al. (2018). Gaia Data Release 2: Observational Hertzsprung-Russell diagrams. A&A 616, A10. https://www.aanda.org/articles/aa/full html/2018/08/aa32843-18/aa32843-18.html
- Gaia Collaboration, T. Prusti, J.H.J. de Bruijne, et al. (2016b). The Gaia mission. A&A 595, A1. https://www.aanda.org/articles/aa/full-html/2016/11/aa29272-16/aa29272-16.html
- Gaia Collaboration, X. Luri, A. G. A. Brown, et al. (2018). Gaia Data Release 2: Using Gaia Parallaxes/arXiv e-prints, https://arxiv.org/abs/1804.09376
- Harshaw, Richard (2016). CCD Measurements of 141 Proper Motion Stars: The Autumn 2015 Observing Program at the Brilliant Sky Observatory, Part 3. Journal of Double Star Observations, 12(4), 394–399. http://www.jdso.org/volume12/number4/Harshaw 394 399.pdf
- Mamajek, E. (2022). A Modern Mean Dwarf Stellar Color and Effective Temperature Sequence.

 Department of Physics and Astronomy: University of Rochester.

 https://www.pas.rochester.edu/~emamajek/EEM dwarf UBVIJHK colors Teff.txt
- Morgan, S. (Jan. 2023). Spectral Type Characteristics. https://sites.uni.edu/morgans/astro/course/Notes/section2/spectraltemps.html
- Tonry, J.L. et al. (2012). The Pan-STARRS1 Photometric System. The Astrophysical Journal, 750(2), 99. https://iopscience.iop.org/article/10.1088/0004-637X/750/2/99/pdf
- Wenger, M. et al. (Apr. 2000). "The SIMBAD astronomical database. The CDS reference database for astronomical objects". In: Astronomy and Astrophysics Supplement 143, pp. 9–22. DOI: 10.1051/aas: 2000332. arXiv: astro-ph/0002110 [astro-ph].

Appendix A:

Table 6. Measurements from image reductions for each image and system.

PA for	Sep for	PA for	Sep for	PA for	Sep for	PA for	Sep for
TVB 115	TVB 115	TVB 139	TVB 139	139 POC 3 POC 3		STF 1393	STF 1393
(°)	(")	(°)	(")	(°)	(")	(°)	(")
76.46	8.51	189.18	7.62	227.00	7.69	253.95	9.49
77.93	8.65	189.27	7.61	227.04	7.72	254.12	9.48
76.58	8.8	189.1	7.62	227.06	7.73	254.32	9.48
76.79	8.51	189.23	7.63	227.36	7.72	254.15	9.47
76.96	8.55	189.17	7.62	227.55	7.72	253.96	9.44
77.1	8.36	189.07	7.64	227.37	7.62	253.83	9.48
76.95	8.55	189.16	7.63	227.34	7.78	253.93	9.49
77.85	8.59	189.06	7.69	226.87	7.71	254.07	9.48
77.04	8.62	189.18	7.61	227.57	7.75	253.87	9.47
76.87	8.49	189.17	7.62	227.38	7.76	254.56	9.42
		189.07	7.65				

Astrometric Measurements and Physical Likelihood Assessments for HJ 4258, STF 1106, and VNI 1

Maiya Qiu¹, Nicholas Peh¹, Eden (Songxiao) Li¹, Kalée Tock¹ Stanford Online High School, Redwood City, CA 94063; <u>maiyaq6487@gmail.com</u>

Abstract

In this study, we analyze historical data and present new astrometric measurements of the position angle and separation of double star systems HJ 4258, STF 1106, and VNI 1 using 10 images for each system. A comparison of HJ 4258's components' relative motions to the computed system escape velocity supports classifying it as a gravitationally bound binary, but the trend in the relative position of its secondary star does not support this, and further research would be needed for confirmation. Similar analysis of STF 1106 and VNI 1 suggests a physical, but not binary, relationship between the component stars of these two systems.

1. Introduction

Double star systems with similar parallax may be gravitationally bound or have some other type of physical relationship. For example, stars in such a pair may have originated from the same nebula, or may share a trajectory in the past or future. Wide double stars systems may also provide information about the structure and evolution of the galaxy and potential gravitational effects of dark matter (Banik et al., 2024). Furthermore, binary systems allow for determination of the mass of each of the stars, which is valuable in refining the mass-luminosity relation, a fundamental tool of astrophysics. In this study, we examine the relationship between the primary and secondary stars for three double star systems whose stars exhibit similar parallax and proper motion.

The systems of this study were chosen from Stelle Doppie, a search engine to the Washington Double Star Catalog, according to several criteria:

- The Right Ascension (RA) of the star was constrained to be within the optimal RA of 3 to 13 hours at the time of measurement in January.
- The secondary star was constrained to have a magnitude less than 13 in order to be detectable with the equipment used.
- The difference in the magnitude of the two stars (Δmag) was constrained to be less than 3 so that both stars could be captured in the same image.
- The constraint for the lower bound of the two star's separation was 5 arcseconds so that the two stars could be resolved, and the constraint for the upper bound was 15 arcseconds as it is more likely for two stars close together to be related in some way.
- Systems marked as "physical" according to Stelle Doppie were selected because these are more likely to have a similar parallax and proper motion.

Table 1 provides the Discoverer code, WDS number, and astrometric measurements for the three systems, along with colors and apparent Gaia G-filter magnitudes from Gaia Data Release 3 (DR3), and estimated spectral types and masses. The latter are estimated by plotting the stars' colors and absolute Gaia G-magnitudes (computed from apparent G-magnitude and parallax according to Equation 1) on the Gaia HR-

Diagram in Fig. 1 (Gaia Collaboration, 2023, 2016b, 2023j). Note that the parallax values cited in Fig. 1 are listed with their uncertainties in Table 5.

Table 1. Double Star System	m Summary Data.
-----------------------------	-----------------

System	WDS	Star (Primary / Spectral Mass (s		Estimated Mass (solar masses)	Last Observation Date	Last observed PA (deg)	Last observed Sep (arcsecs)	
НЈ 4258	09448	Primary	F7 ¹	1.2	2016 ²	163	8.62	
HJ 4258	-7554	Secondary	F^1	1.1	2010	103	8.02	
STF 1106	07313	Primary	F0	1.4	2017.222 ³	33.9	10.68	
311 1100	+1619	Secondary	F0	1.3	2017.222	33.7		
VNI 1	04534	Primary	K	0.66	2015.5	51.67	9.65	
VNI 1	+0452	Secondary	M	0.46	2013.3	31.07		

¹ Houk et al. (1975)

The mass of the two stars of each system was estimated by plotting the absolute magnitude and color on a CMD diagram. The absolute magnitude was calculated using Eq. 1 and the parallax, magnitudes (gmag), and color (BP-2P) were taken from Gaia DR3 (Collaboration, 2023, 2016b, 2023j).

Table 2. Gaia DR3 data of double star systems.

Syste	em	Plx (mas)	gmag	BP-RP
HJ	pri	4.57	8.95	0.93
4258	sec	4.57	9.67	0.84
STF	pri	6.66	9.26	0.74
1106	sec	6.55	9.32	0.71
VAIL 1	pri	16.97	10.28	1.23
VNI 1	sec	17.07	12.02	1.89

$$M = m + 5 \cdot log(p+1)$$

Equation 1: Gaia G absolute magnitude (M) from gmag (m) and parallax (p)

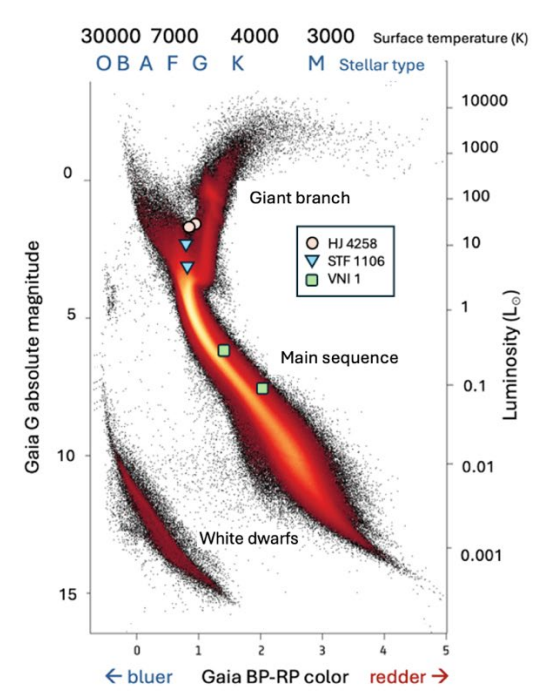


Figure 1: Information from Gaia DR3 of the double star systems HJ4258, STF1106, and VNI1

² El-Badry et al. (2021)

³ Mason et al. (2018)

The stars of HJ 4258 are high proper motion stars (Wenger et al., 2000) of approximately solar mass. When plotted on Gaia's CMD diagram, the stars of HJ 4258 are found to be close to the main sequence turnoff point. The stars of VNI 1 are still definitively on the main sequence, while STF 1106's position relative to the giant branch is inconclusive.

Notably, STF 1106 is the only system of this study considered to have wide (> 1 pc) separation, at 2.54 pc. This is the 3D spatial separation as shown in Table 6, calculated through the process described in Sec. 4. Past studies have shown that it is difficult to distinguish whether comoving double stars with > 1 pc separation are genuine binaries, separated former binaries, moving groups, or contamination from randomly aligned stars (Andrews et al., 2017).

Finally, VNI 1 is the only system studied with significantly different masses—the secondary star mass is 30% less than that of the primary star whereas the mass difference for the pairs of stars of STF 1106 and HJ 4258 are both less than 10%, using the estimated masses from Table 1. The two stars of VNI 1 also have the highest parallax within the study of 16.97 and 17.07, meaning the two stars are within 60 parsecs of Earth.

None of the systems studied have a published orbital or linear solution. Therefore, in addition to contributing to astrometric data and using the computed system escape velocities to classify each system, we aim to examine the historical data to ascertain whether either of these solution types are relevant.

2. Equipment and Methods

Images were requested from telescopes in the Las Cumbres Observatory Global Telescope (LCOGT) network (Brown, 2013). All telescopes were DeltaRho 350 telescopes with aperture 0.35m using a QHY600PH CMOS camera. The camera's field of view is 1.9 x 1.2 degrees, but this is cut down to 30' x 30' in the central mode used for imaging to minimize file size. Pixel size is 3.76 microns covering 0.73" per pixel. Images were taken using a V filter (Bessell, 1990). Observing site, decimal date, and exposure time are listed in Table 3.

Observation Date System Telescope Location Exposure Time per image (s) HJ 4258 Sutherland, South Africa 2024.0301 3.80 STF 1106 Texas, USA 2024.0356 4.00 Siding Spring, Australia 7.78 VNI 1 2024.0342

Table 3. Telescope Observing Parameters.

10 telescope images of each system were reduced to determine astrometric position angle (PA, in degrees) and separation (Sep, in arcseconds) by centroiding in AstroImageJ. Plotting these measurements along with historical data reveals trends in relative motion (Fig. 2).

Fig. 2 below depicts an example of a resolved image of each system using AstroImageJ.

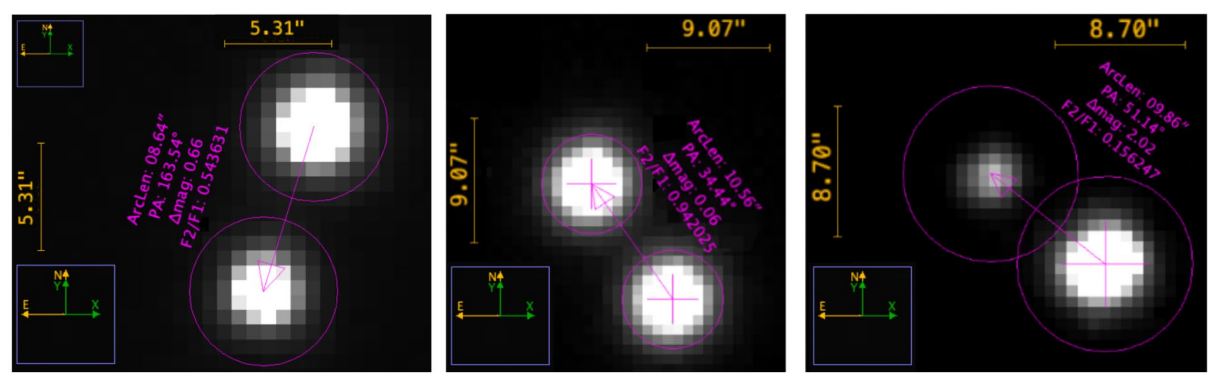


Figure 2: Example measurements in AstroImageJ of PA and Sep for systems from left to right: HJ 4258 (measurement aperture radius 5 pixels), STF 1106 (5 pixels), and VNI I (8 pixels)

3. Data

Table 3 below shows measurements of 10 images for each of the double star systems HJ 4258, STF 1106, and VNI 1. All image reductions were performed using AstroImageJ.

Table 3. Astrometric Measurement of Position Angle and Separation of Star Systems.

	Н	IJ 4258	S	TF 1106	VNI 1		
Image #	PA (deg)	Sep (arcsecs)	PA (deg)	Sep (arcsecs)	PA (deg)	Sep (arcsecs)	
1	163.0	8.65	34.1	10.68	51.0	9.53	
2	163.5	8.56	33.9	10.68	50.2	9.58	
3	162.9	8.62	34.1	10.69	51.1	9.71	
4	163.0	8.61	34.0	10.69	51.2	9.11	
5	163.5	8.61	34.1	10.67	51.3	9.72	
6	163.2	8.59	34.5	10.60	50.9	9.59	
7	163.4	8.92	34.4	10.56	50.2	9.66	
8	163.1	8.63	33.9	10.72	50.5	9.79	
9	163.2	8.62	34.1	10.68	53.1	9.74	
10	163.2	8.65	34.2	10.64	53.7	9.66	

Table 4 shows summary statistics for the measurements above, including the mean, standard deviation (SD), and standard error (SE) for the position angle and separation of the three double star systems.

System	Date of Measurement	Number of Images	Position Angle (°)	Standard Deviation of Position Angle	Standard Error of Position Angle	Separation (")	Standard Deviation of Separation	Standard Error of Separation
НЈ 4258	2024.0301	10	163.2	0.19	0.060	8.65	0.10	0.032
STF 1106	2024.0356	10	34.1	0.20	0.063	10.66	0.05	0.015
VNI 1	2024.0342	10	51.3	1.18	0.373	9.61	0.19	0.061

Table 4. Summary of Measurements of HJ 4258, STF 1106, and VNI 1.

4. Escape Velocity versus Relative Velocity

The masses shown in Table 1 were used to calculate an escape velocity for each double star system. The formula for escape velocity (Eq. 2) is derived by finding the relative velocity of orbit such that the total mechanical energy of the system is 0 (Bonifacio et al., 2020). In Eq. 2, M is the sum of the masses of the two stars, with units converted from solar masses to kg. r is the 3D spatial separation between the two stars, with units converted from parsecs to meters. Hence the escape velocity is in meters per second.

$$\mathrm{v}_{escape} = \sqrt{rac{2GM}{r}}$$

Equation 2: Escape velocity

The 3D spatial separation (r) in Eq. 2 was calculated from the stars' angular astrometric Sep (Table 4) and radial separation computed by taking the difference of the inverted Gaia DR3 parallaxes in arcseconds (Table 5). The angular separation (in arcseconds) was converted into physical separation (Sep_{pc} in parsecs) through the following formula, where parallax is abbreviated as Plx, and separation is abbreviated as Sep_{arcsec}.

$$ext{Sep}_{pc} = rac{ ext{Sep}_{arcsec} \cdot rac{1(ext{deg})}{3600(")} \cdot rac{2\pi (ext{rad})}{360(ext{deg})}}{ ext{Plx}(")}$$

Equation 3: Transverse separation in parsecs

For each system, the parallax used to compute the transverse separation in Eq. 3 was the Gaia DR3 primary star parallax shown in Table 5. The 3D separation was computed as the transverse and radial separation combined via the Pythagorean Theorem. Since the parallax uncertainties for HJ 4258 were overlapping, the 3D separation was taken as the transverse separation without any radial component. Table 5 shows the parallax, proper motion in right ascension (RA) and declination (Dec), and radial velocity for each star (Gaia Collaboration, 2023, 2016b, 2023j).

Table 5. Gaia DR3 Parallaxes, Proper Motions, and Radial Velocities.

Star Parallax (mas) Proper Motion RA (mas/yr) Proper Motion Dec (mas/yr 4.57 ± 0.011

System Radial Velocity (km/s) Primary -56.77 ± 0.015 27.92 ± 0.014 N/A HJ 4258 Secondary 4.57 ± 0.023 -57.45 ± 0.030 28.37 ± 0.027 -1.14 ± 0.0266 Primary 6.66 ± 0.020 16.92 ± 0.024 -21.16 ± 0.019 -10.51 ± 6.271 STF 1106 6.55 ± 0.015 Secondary 17.89 ± 0.019 $\text{-}21.49 \pm 0.015$ -2.74 ± 0.300 16.97 ± 0.019 Primary -43.83 ± 0.024 -65.82 ± 0.017 14.08 ± 0.206 VNI 1 17.07 ± 0.017 Secondary -65.63 ± 0.015 -45.59 ± 0.019 15.26 ± 0.376

The proper motions in Table 5 were also used to compute the relative 3D space velocity of the system for comparison with the escape velocity. The 3D space velocity is calculated with the Pythagorean theorem from the radial velocity (where available) and proper motion changes from angular to physical units via Equation 3. As shown in Table 6, HJ 4258 has a slower relative velocity than escape velocity according to this analysis and therefore is likely to be gravitationally bound. Although unlikely to be bound, STF 1106 and VNI 1 are physically related, as evidenced by their low relative proper motion ratio (rPM). The rPM is calculated as the ratio of the relative proper motion to the longer proper motion vector magnitude of the two stars. A small ratio indicates that the motion of the secondary star with respect to the primary is small compared to the movement of the system as a whole, so the two stars are mostly moving together. A double star system is classified as Common Proper Motion (CPM) if its relative proper motion ratio is between 0 and 0.2, as is the case for all of these systems (Harshaw, 2016).

Table 6. System Separation and Classification based on Relative Proper Motion Ratio.

System	3D Spatial Separation (pc)	System Escape Velocity (m/s)	3D Relative Velocity (m/s)	Relative Proper Motion (rPM) ratio	Classification based on rPM
HJ 4258	0.01	1473	842	0.013	СРМ
			-		
STF 1106	2.54	96	7805	0.04	CPM
VNI 1	0.31	175	1279	0.022	CPM

Figure 3 below shows the historical data plots of the relative position in right ascension and declination of the secondary star with respect to the primary for star systems HJ 4258, STF 1106, and VNI 1. In these plots, the primary star is located at the origin of the RA/Dec coordinate system. The blue square represents the data point calculated from this study using the 10 images, and the red circle represents Gaia DR3 data (epoch 2016.0). Time is shown on a gradient from purple to yellow, with most recent measurements yellow and the earliest purple. Two outliers were removed from the plot of STF 1106 because they had a PA of 75 where all other data points had a PA in the value range from 25 to 35, and a separation of 8.24 where all other measurements were in the range from 10 to 11.5.

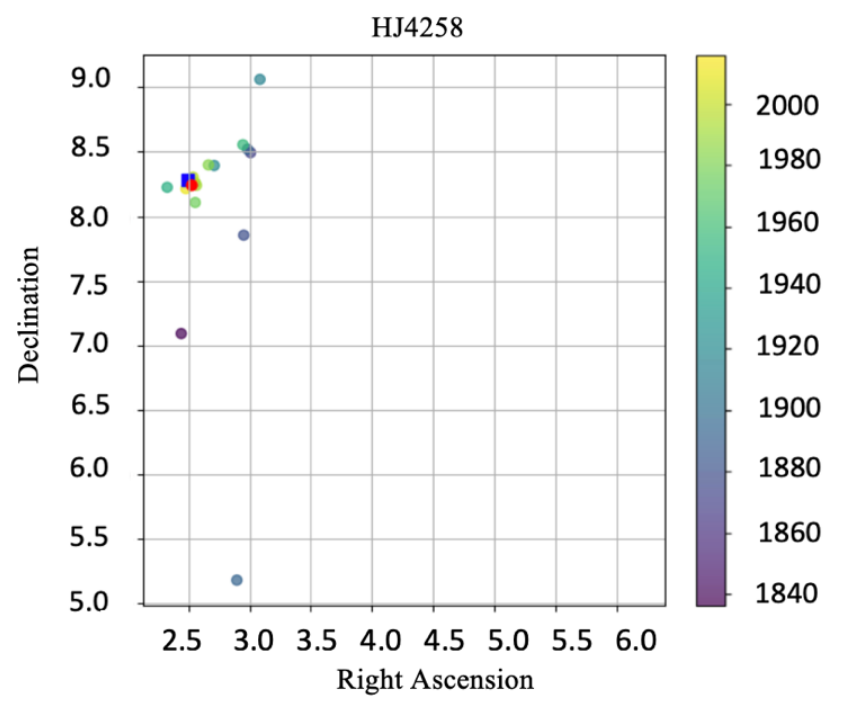


Figure 3a: Relative position of secondary star with respect to the primary of HJ 4258

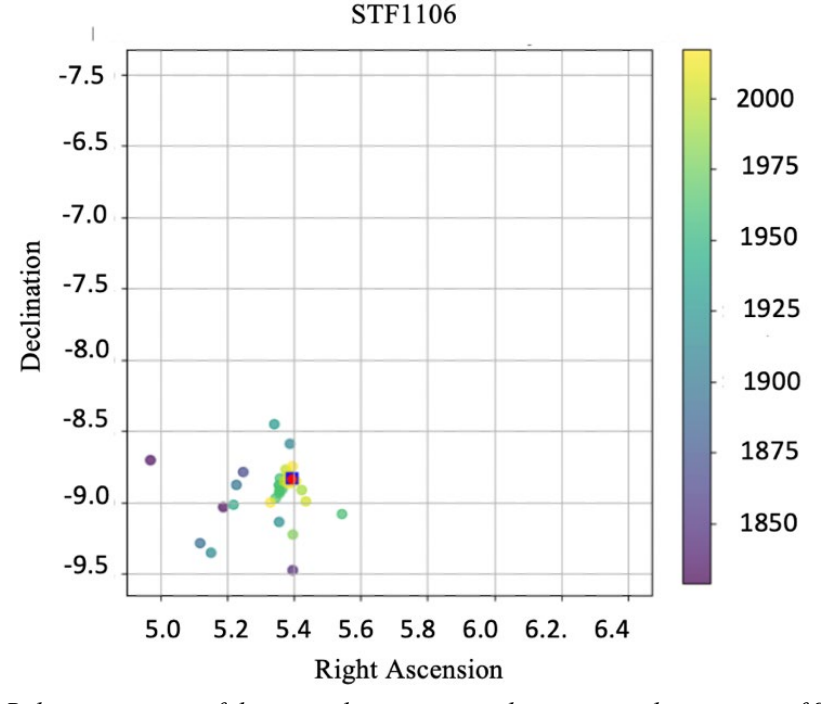


Figure 3b: Relative position of the secondary star in with respect to the primary of STF 1106

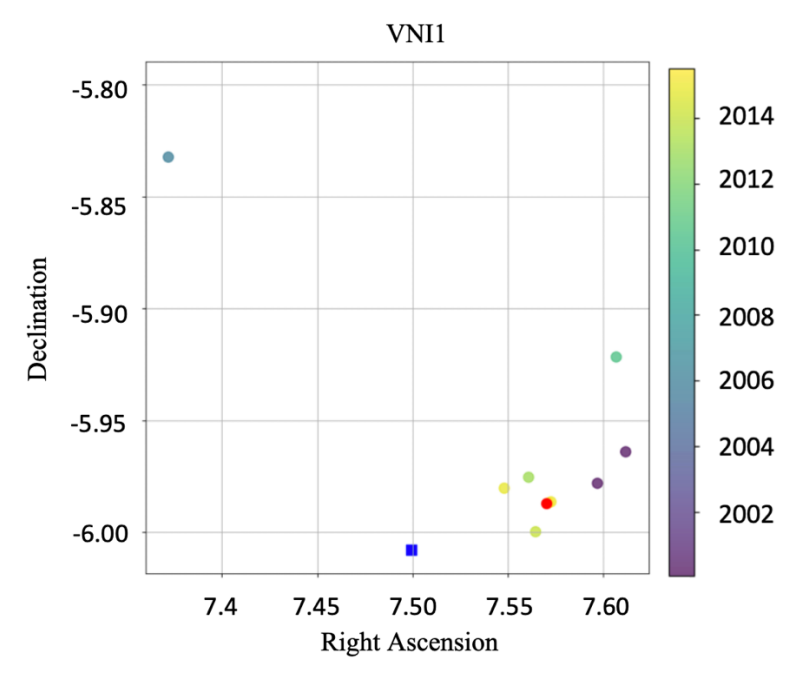


Figure 3c: Relative position of the secondary star with respect to the primary star of VNI 1

5. Discussion

In the plot of HJ 4258 (Fig. 3a), although many of the older measurements are sparse and show high imprecision, varying from each other in an unlikely manner, the measurements could be interpreted to suggest a possible elliptical orbit going from the bottom of the graph upwards to the upper right, and turning back left and down. However, when scaling the axes to include the origin, this possible elliptical orbit does not appear to contain the origin, so it would not be a reasonable orbital path as the origin represents the primary star's location. Assuming that the oldest measurements were inaccurate, there would be a trend of decreasing Dec and gradually decreasing RA in the more recent measurements, which may indeed represent an orbit around the primary star. The newest measurement of this study does continue the recent trend of moving generally leftward in the plots. There may be some slight curvature downward to the origin, but this would require future measurements to confirm.

Most of the recent measurements of STF 1106 (colored green and yellow in the second plot of Fig. 3b) are clumped together while older measurements exhibit no trend. Similar to the data points of HJ 4258, this may be due to lack of precision of older measurements. However, over time, the secondary star tends to move in the positive direction in both Dec and RA. As shown in Fig. 3b, older data points tended to be to the left and bottom (more negative Dec and smaller RA) while the more recent data tended to be more upwards and to the right, and this study's measurement is at the center of a clump of recent measurements.

For VNI 1, notably are three overlapping data points at where the red circle is marked. The three measurements were all taken in 2015. When 11 data points were plotted, there is a general trend of the relative position of the secondary star decreasing in Right Ascension and Declination, implying that the secondary star is moving nearer to the primary star.

The historical data of all three systems indicate trends in the relative position of the secondary star, but no conclusive orbital path. There is also currently no published orbital solution for any of the three double star systems, suggesting more measurements are needed to determine how the secondary star's relative position changes over time. Using the measurements from Table 6, only HJ 4258 has a relative 3D space velocity which does not exceed its escape velocity. The other two systems, STF 1106 and VNI 1, each have a relative velocity which exceeds the system escape velocity by 2 orders of magnitude, so they are unlikely to be gravitationally bound. This makes HJ 4258 the only system in this study where an orbital relationship is likely.

However, while only HJ 4258 is likely to have an orbital relationship, all three double star systems exhibit common proper motion. STF 1106, with its physical separation of 2.54pc (Table 6), is considered a comoving pair of stars with a wide separation (> 1 pc) by Oh et al., 2017. Therefore, it may be a separated former binary, and could be potentially used to measure the star formation and evolution in the solar neighborhood (Oh et al., 2017).

6. Conclusion

Astrometric data analysis shows that all three systems studied here exhibit common proper motion, suggesting a physical relationship between the primary and secondary star of each system. Escape velocity calculations and comparisons with 3D space velocity indicate that only HJ 4258 is likely to be gravitationally bound, though there is no evidence of this in its historical data plot. The components of VNI 1 and STF 1106 are likely to be physically related (despite STF 1106's wide separation of 2.54pc) but not gravitationally bound. The measurements presented in this paper plot close to Gaia DR3 measurements, and continue temporal trends identified for VNI 1 and STF 1106. Further observations over time are recommended for all three systems.

Acknowledgements

This research was made possible by the Washington Double Star catalog maintained by the U.S. Naval Observatory, the Stelledoppie catalog maintained by Gianluca Sordiglioni, Astrometry.net, and AstroImageJ software which was written by Karen Collins and John Kielkopf.

This work has also made use of data from the European Space Agency (ESA) mission Gaia (https://www.cosmos.esa.int/gaia), processed by the Gaia Data Processing and Analysis Consortium (DPAC, https://www.cosmos.esa.int/web/gaia/dpac/consortium). Funding for the DPAC has been provided by national institutions, in particular the institutions participating in the Gaia Multilateral Agreement.

This work makes use of observations taken by the Planewave Delta Rho 350 + QHY600 CMOS camera systems of Las Cumbres Observatory Global Telescope Network located in Coonabarabran, Australia; Texas, USA; and Sutherland, South Africa.

References

Andrews, J. J., Chanamé J., Agüeros, M. A. (2017). Wide binaries in Tycho-Gaia: search method and the

- distribution of orbital separations, *Monthly Notices of the Royal Astronomical Society*, Volume 472, Issue 1, Pages 675–699, https://doi.org/10.1093/mnras/stx2000
- Banik, I., Pittordis, C., Sutherland, W., Famaey, B., Ibata, R., Mieske, S., & Zhao, H. (2024). Strong constraints on the gravitational law from Gaia DR3 wide binaries, Monthly Notices of the Royal Astronomical Society, Volume 527, Issue 3, Pages 4573–4615, https://doi.org/10.1093/mnras/stad3393
- Bessell, M.S. (1990). UBVRI Passbands. Publications of the Astronomical Society of the Pacific, 102, 1181-1199. https://iopscience.iop.org/article/10.1086/132749
- Bonifacio, B., Marchetti, C., Caputo, R., & Tock, K. (2020). Measurements of Neglected Double Stars. Journal of Double Star Observations, 16(5), 411–423. http://www.jdso.org/volume16/number5/Bonifacio 411 423.pdf
- Brown, T. M., et al. (2013). Las Cumbres Observatory Global Telescope Network. Publications of the Astronomical Society of the Pacific, 125(931), 1031–1055. https://iopscience.iop.org/article/10.1086/673168/meta
- El-Badry, K., Rix, H., & Heintz., T. M. (2021). A million binaries from Gaia eDR3: sample selection and validation of Gaia parallax uncertainties. Monthly Notices of the Royal Astronomical Society, 506(2), 2269-2295. 10.1093/mnras/stab323
- Gaia Collaboration, Babusiaux, C., Fabricius, C., Khanna, S., et al. (2023). Gaia Data Release 3. Catalogue validation. A&A 674, pp. A32. https://arxiv.org/abs/2206.05989
- Gaia Collaboration, Prusti, T., de Bruijne, J.H.J., et al. (2016b). The Gaia mission. A&A 595, A1. https://www.aanda.org/articles/aa/full-html/2016/11/aa29272-16/aa29272-16.html
- Gaia Collaboration, Vallenari, A., Brown, A.G.A., et al. (2023j). Gaia Data Release 3. Summary of the content and survey properties. A&A 674, pp. A1. https://arxiv.org/abs/2208.00211
- Harshaw, R. (2016). CCD Measurements of 141 Proper Motion Stars: The Autumn 2015 Observing Program at the Brilliant Sky Observatory, Part 3. Journal of Double Star Observations, 12(4), 394–399. http://www.jdso.org/volume12/number4/Harshaw_394_399.pdf
- Houk, N., Cowley, A.P. (1975). University of Michigan Catalogue of two-dimensional spectral types for the HD stars. Volume 1. Declinations -90 to -53_f0. Ann Arbor, MI (USA): Department of Astronomy, University of Michigan, 19 + 452 p.
- Mason et al., (2018). Speckle Interferometry at the U.S. Naval Observatory. XXIII, The Astronomical Journal, 156 (5), 240. 10pp. https://iopscience.iop.org/article/10.3847/1538-3881/aae484/pdf
- Oh, S., Price-Whelan, A. M., Hogg, D. W., Morton, T. D., & Spergel, D. N. (2017). Comoving Stars in Gaia DR1: An Abundance of Very Wide Separation Comoving Pairs. The Astronomical Journal, 153(6), 257. https://doi.org/10.3847/1538-3881/aa6ffd
- Wenger, M., et al. (2000). The SIMBAD Astronomical Database. Astronomy and Astrophysics Supplement Series, 143(1). https://doi.org/10.1051/aas:2000332

New Measurements of Some Double Stars in the Constellation Vulpecula

Zsolt Szamosvari Hungarian Astronomical Association Double Star Section H-2500 Esztergom, Hungary. szamos.photo@gmail.com

Abstract

The purpose of these research is to measure rarely observed double stars in the constellation Vulpecula, especially members of multiple systems. During work, were managed to observe 59 pairs as a primary target and 89 pairs as a secondary target. Were also found 2 new possible binary stars and more new members for seven system. All observed pairs were processed using Harshaw's method and the probability of gravitational bonding was established.

1. Introduction

The Washington Double Star Catalog (WDS) contains many visual double stars that have been rarely observed, leaving few measurements available for further investigation. That is why were chose the re-observation of neglected pairs as the subject of our research. First was selected the constellation Vulpecula, which is in a good position in summer for observations. To select the targets, were used the special search engine of the Stelle Doppie website (Sordiglioni, 2023). Table 1 shows the search criteria. When defining the

criteria, also were considered the technical characteristics of the instrument to be used, the T21 telescope of the iTelescope network.

i	
Mag. primary	between 7-11
Δ mag	< 3
Separation	between 5" - 50"
Last observation	< 2015
Number of obs.	between 3-15
Members of system	> 3
Gaia ID	yes

Table 1. Search criteria

The results of filtering, 16 pairs, are shown in Table 2.

G 1	WDCN	т ,	01	D		3.61	3.60	
Coord	WDS Name	Last	Obs	Pa	Sep	M1	M2	Δ mag
20 32 51 +29 02 35	ARY 27 BC	2015	14	50	35.3	8.32	10.89	2.57
20 22 48 +27 09 09	ARN 50 CD	2015	15	186	25.9	8.85	9.1	0.25
20 18 17 +25 39 15	BU 985 CD	2015	13	67	8.6	10.87	13.6	2.73
19 48 55 +25 49 48	BKO 740 AB	2015	13	38	15.9	10.32	10.75	0.43
21 06 29 +26 55 05	STF 2756 AB	2015	11	48	11.9	10.2	12.3	2.1
21 04 29 +24 57 04	SLE 520 AB	2015	10	346	34.3	9.73	11.62	1.89
20 47 39 +25 18 00	POU 4996 DH	2015	8	127	12	10.78	13.4	2.62
20 46 19 +27 40 47	MLB 712 AB	2015	10	43	8.5	10.49	12	1.51
20 33 04 +28 51 48	ES 507 AB	2015	11	295	7.1	8.78	11.4	2.62
20 30 47 +26 57 35	OPI 25 AC	2015	9	324	27	10.03	12.5	2.47
20 30 11 +26 50 34	LMP 45 AF	2015	10	252	43.7	10.5	13.1	2.6
20 18 38 +28 31 59	HJ 1501 AB	2015	10	355	12.9	10.18	11.1	0.92
19 38 36 +24 54 32	POU 3973 AC	2015	10	230	7.6	10.53	11.5	0.97
19 36 23 +25 03 51	DOO 76 AB	2015	14	145	24.4	8.66	11.3	2.64
19 28 13 +20 12 60	WAL 113 AC	2015	14	327	36.8	10.1	11.47	1.37
19 23 13 +22 09 53	HJ 886 AB	2015	15	45	8.2	10.41	11.4	0.99

Table 2. List of targets

2. Equipment and Methods

The images of the double stars were acquired by the T21 telescope, located in Beryl Junction Utah, USA, at an elevation of 1,570 meters. The CCD camera for T21 is an FLI-PL 6303E with a resolution of 0.96" per pixel, housing a pixel array 3072 by 2078, with a FOV of 32.8 by 49.2 arcminutes. The CCD camera is mounted on a Planewave 17 Corrected Dirk-Kirkham (CDK) OTA, with a focal length of 1,940 mm with an aperture of 431 mm and a focal ratio of f/4.5. Exposure times of 60 s with a luminance filter were taken fir 10 images. Figure 1 shows the instrument (source: iTelescope.net).

For measurements, were used AstroImageJ (Collins et al, 2017) software. The FITS files were calibrated using *astronomy.net key* within the software. At this point, the program shows the images with the correct skyline, and allows for accurate separation and position angle measurement. Were adjusted the brightness and aperture sizes individually to get the best results.

Astrometric data were obtained from GAIA DR3 via the Aladin interactive sky atlas (Bonnarel et al, 2000) and the Simbad database (Wenger et al, 2000). These were stored in a new spreadsheet based on the Rowe-Harshaw Excel spreadsheet (Harshaw, 2018). From the GAIA coordinates of the members, were calculate the position angles and separations for the 2016 epoch (Buchheim, 2008). Were requested historical data of pairs from USNO, which were supplemented with calculated GAIA positions and the new measurements. The detailed analysis of the pairs was performed in the Plot Tool Excel spreadsheet (Harshaw, 2020).

To establish binary probability, were considered several indicators: the *Harshaw Rating* (the distance between two stars and their proper motion, the relationship between total velocity and escape velocity), the relationship between maximum orbital velocity and observed velocity, the limit of the gravitational bond derived from the mass of the primary star, and the limit of the gravitational bond derived from the total masses of the two stars.

The mathematical formulas for calculating total velocity and escape velocity are known from previous works, which I will not describe further. The maximum orbital velocity and



Figure 1.: the T21 telescope

observed orbital velocity are more interesting. It was first used by Sinachopoulos and Mouzourakis to establish gravitational bonds in 1992.

To calculate the maximum orbital velocity, the equation "vis viva" is applied:

$$v_{orb_max} = \sqrt{G(M+m)\left(\frac{2}{s} - \frac{1}{a}\right)}$$
 (1)

where M is the primary, m is the mass of the secondary star in M_0 , s is the distance between the two stars in parsec, a is semi-major axis in parsec, G is the gravitational constant.

The observed orbital velocity is calculated according to the formulas (Rica, 2011):

$$\Delta u = \sqrt{\left(\rho \frac{\Delta \theta}{\Lambda t}\right)^2 + \left(\frac{\Delta \rho}{\Lambda t}\right)^2} \tag{2}$$

 Δu is displacement of the secondary around the primary, ρ is the last separation, $\Delta \Theta$ is difference of the position angle, $\Delta \rho$ is the difference of the separation, Δt is the difference of the time.

$$v_{obs} = 0.0474 d \Delta u \tag{3}$$

where d is the distance of the system from Earth, in parsec. If the v_{obs} is smaller than v_{orb_max} , then a gravitational bond is possible.

The advantage of this calculation over total velocity calculation is that it can be calculated from historical data, whereas in many cases the radial velocity required for total velocity is missing from GAIA's DR3 database.

To calculate gravitational bond limits of stars, were used the following formulas (Rica Romero, 2010):

$$d_{\text{max}}AU = 2500(M_A)^{1,54}$$
 (4)

where d_{max} is the primary limit in AU, M_A is the mass of the primary in M_O.

$$a_{\text{max}} = 1000 \left(\frac{M_{\text{tot}}}{0.185} \right)$$
 (5)

where a_{max} is the limit of the combined gravitational bond of the two stars, M_{tot} is the sum of the masses of the two stars in M_O (Rica Romero, 2010).

The various indicators were weighted. Harshaw Rating gets 90% weight, speeds get 5% weight, gravity limits get 2.5% weight, and Plot tool R2 gets 2.5% weight. That's 100% in total. To evaluate binary probability, Harshaw's limits were used, which are summarized in Table 3 (Harshaw, 2018).

3. Data summary

The target 16 pairs are part of 16 multiple systems. Each member of these systems was measured and analyzed including historical data using the Plot tool spreadsheet. In the end, were obtained new measurement results for 59 pairs, which are summarized in Table 5. Were called these systems the primary targets. The findings of their detailed analysis are shown in Table 4 and Figure 2.

It can be concluded that out of 59 pairs, a total of 30%, 18 pairs, *Figure 2.: Distribution of primary targets* turned out to be physical double stars, the rest are of questionable physicality. In many cases, this is due to the low number of observations. Some 22 pairs are questionable, and 17 pairs are surely optical double.

In addition to the primary systems, 89 other binary systems were found by examining the images. These are called secondary targets. The measurement results of the secondary targets are included in Table 6. The results of them detailed analyses are shown in Table 4 and Figure 3.

Among the secondary targets, 89 pairs are members of 42 systems. 47% of these pairs turned out to be physical double stars. This is already a better ratio than in the case of primary targets.

Threshold (%)	Class
>85	Physical
85 - 65	Physical?
65 - 50	Maybe
50 - 35	??
35 - 0	No

Table 3.: Thresholds

Type	Primary	Secondary
Unk	2	4
No	17	17
??	11	13
Maybe	11	13
Y?	8	27
Y	10	15
Sum	59	89

Table 4.: Summary of targets



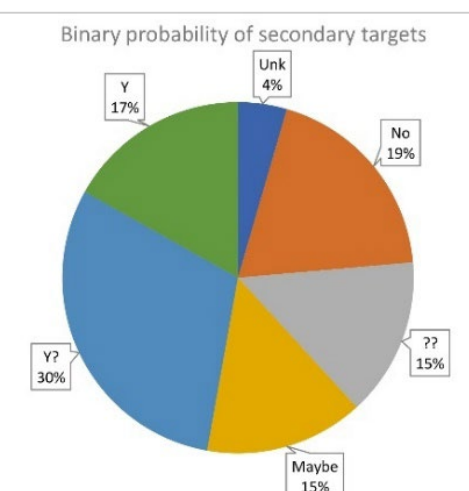


Figure 3.: Distribution of secondary targets

As a function of absolute magnitude and effective temperature, were also plotted the stars on the Hertzsprung-Russel Diagram (HRD). From Figure 4. it can see that the stars do not cover the entire HRD, but part of the main sequence and the giant arm are nicely drawn. Most of the stars are clustered at the base of the main sequence and giant arm. The compaction can be explained by looking at the spectral distribution of stars. Here were include only the spectral classes estimated by the Plot tool, since there are very few spectral types for individual stars found in different catalogs (Figure 5).

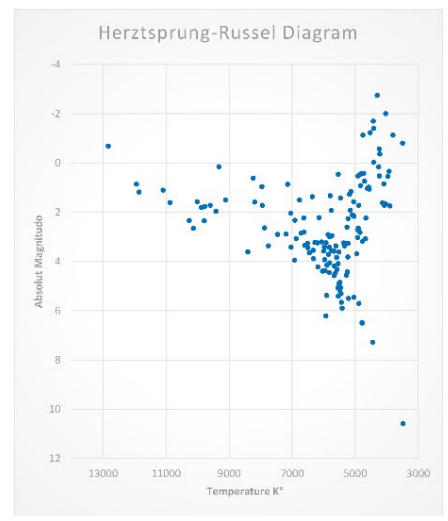


Figure 4.: Observed stars on HRD

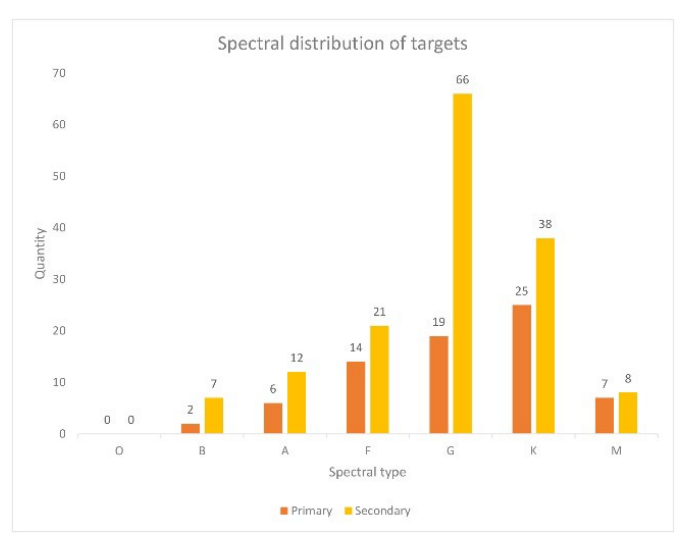


Figure 5.: Spectral type of stars

4. Measurement data

Explanation for the following tables. The WDS and Disc columns contain double identifiers. The Comp column contains component markings. In the Separation and Position Angle and Δ mag columns, the AVG columns represent the measurement averages, and the STD columns contain the standard errors. The Date column shows the date of observation. The Binary Probability column shows the probability of physicality. Possible new binary stars are marked CND (candidate) in the Disc column.

3.10	HIDG.	ъ:	G	Separat	tion	Position	Angle	Δm	nag	ъ.	Binary	3.7
Nº	WDS	Disc	Comp	AVG	STD	AVG	STD	AVG	STD	Date	Proba- bility	Notes
1	20229+2708	ARN50	AC	85.07	0.14	330.62	0.02	0.19	0.01	2023.582	55.22%	1
2	20229+2708	ARN50	AD	65.63	0.1	318.1	0.09	0.42	0.02	2023.582	93.66%	
3	20229+2708	ARN50	CD	25.36	0.13	184.72	0.08	0.23	0.03	2023.582	56.78%	
4	20183+2539	HJ1499	AC	21.6	0.33	353.65	0.77	1.12	0.05	2023.585	76.05%	
5	20183+2539	WAL131	AE	122.68	0.09	151.2	0.03	0.42	0.01	2023.585	72.83%	
6	20183+2539	BU985	CD	8.77	0.18	67.56	1.5	2.9	0.06	2023.585	49.69%	
7	21065+2655	STF2756	AB	11.79	0.04	49.37	0.23	1.82	0.06	2023.59	No Px	2
8	21065+2655	STF2756	AC	75.02	0.03	287.94	0.04	1.18	0.02	2023.59	No Px	2
9	21045+2457	SLE520	AB	34.58	0.05	345.78	0.05	1.72	0.01	2023.599	23.77%	
10	21045+2457	SLE520	AC	43.5	0.04	144.49	0.05	2.23	0.01	2023.599	47.93%	
11	21045+2457	SLE520	BD	17.92	0.01	117.63	0.08	2.12	0.01	2023.599	31.76%	
12	20327+2903	ARY47	AB	128.13	0.03	107.56	0.04	0.04	0	2023.601	45.91%	
13	20327+2903	ARY27	ВС	35.35	0.03	49.13	0.08	2.23	0.02	2023.601	23.12%	
14	20327+2903	ARY27	BD	89.93	0.05	178.3	0.01	0.99	0.01	2023.601	62.22%	
15	20331+2852	ES507	AB	7.24	0.19	294.89	1.79	1.52	0.03	2023.601	93.45%	
16	20331+2852	ES507	AC	36.27	0.04	345.85	0.04	0.86	0.01	2023.601	46.44%	
17	20331+2852	ES507	AD	36.9	0.03	223.67	0.06	1.04	0.01	2023.601	16.18%	

18	20331+2852	FMY137	AE	42.74	0.02	101.18	0.05	5.7	0.03	2023.601	50.49%	
19	20331+2852	FMY137	AF	23.14	0.29	176.41	0.21	5.52	0.02	2023.601	15.40%	
20	20331+2852	FMY137	AG	32.69	0.05	299.18	0.08	5.58	0.04	2023.601	41.93%	
21	20331+2852	ES507	DS	16.06	0.03	145.96	0.04	2.79	0.03	2023.601	51.58%	
22	19489+2550	BKO740	AB	15.91	0.03	37.4	0.1	0.46	0	2023.602	47.33%	
23	19489+2550	BKO740	AD	18.83	0.02	92.33	0.15	3.16	0.02	2023.602	61.50%	
24	19489+2550	BKO740	ВС	7.93	0.16	263.89	0.32	2.93	0.01	2023.602	72.86%	
25	19489+2550	BKO740	DE	2.79	0.16	314.89	2.25	0.9	0.19	2023.602	55.26%	
26	20478+2519	BUP218	AB	49.65	0.02	36.6	0.03	0.12	0.01	2023.641	49.42%	
27	20478+2519	BUP218	AC	102.87	0.02	98.86	0.01	1.15	0.01	2023.641	8.83%	
28	20478+2519	BUP218	AD	153.76	0.03	252.51	0.02	0.61	0	2023.641	28.08%	
29	20478+2519	DAM514	AF	44.21	0.04	99.46	0.02	1.94	0.02	2023.641	61.54%	
30	20478+2519	WSI49	BE	5.32	0.53	141.1	1.18	3.46	0.15	2023.641	37.68%	
31	20478+2519	POU4996	DH	11.85	0.08	128.27	0.36	2.86	0.02	2023.641	75.98%	
32	20478+2519	BKO856	FG	9.13	0.03	178.83	0.36	0.32	0.01	2023.641	16.70%	
33	20463+2740	MLB712	AB	8.54	0.08	42.3	0.4	2.72	0.06	2023.672	57.53%	
34	20463+2740	MLB712	AC	23.96	0.04	125.47	0.04	0.92	0.05	2023.672	48.52%	
35	20463+2740	BRT3362	CD	6.07	0.22	84.86	0.7	1.72	0.02	2023.672	94.12%	
36	19365+2502	DOO76	AB	24.54	0.07	145.43	0.13	3.07	0.08	2023.624	57.53%	
37	19365+2502	DOO76	AC	43.39	0.09	167.55	0.06	1.47	0.05	2023.624	86.13%	
38	19365+2502	FYM82	AE	15.26	0.27	316.57	0.16	4.54	0.05	2023.624	31.34%	
39	19365+2502	FYM82	AF	21.47	0.06	201.59	0.15	4.76	0.11	2023.624	34.56%	
40	19365+2502	DOO76	CD	2.23	0.18	259.61	3.05	0.34	0.12	2023.624	91.94%	
41	19386+2455	POU3975	AB	4.35	0.34	104.34	1.51	2.8	0.17	2023.624	34.31%	
42	19386+2455	POU3973	AC	7.52	0.11	229.61	0.49	0.86	0.03	2023.624	54.05%	
43	19386+2455	POU3974	AD	21.37	0.05	225.69	0.12	1.53	0.02	2023.624	25.17%	
44	19232+2209	HJ886	AB	8.2	0.04	45.34	0.23	0.84	0.02	2023.627	91.40%	
45	19232+2209	SLE939	AC	31.8	0.08	199.52	0.13	0.39	0.02	2023.627	90.68%	
46	19232+2209	SLE939	AD	57.17	0.08	144.65	0.06	0.31	0.02	2023.627	89.63%	
47	19282+2013	STF3132	AB	7.56	0.12	38.64	1.02	0.73	0.05	2023.627	92.98%	
48	19282+2013	WAL113	AC	36.26	0.14	325.78	0.3	1.61	0.04	2023.627	45.83%	
49	19282+2013	WAL113	AD	56.28	0.13	307.35	0.23	1.85	0.03	2023.627	23.02%	
50	20186+2833	HJ1501	AB	12.86	0.04	354.04	0.11	0.99	0.02	2023.643	19.00%	
51	20186+2833	HJ1501	AC	57.18	0.04	349.2	0.03	1.09	0.01	2023.643	74.52%	
52	20186+2833	HJ1501	CD	20.35	0.02	12.31	0.07	1.61	0.03	2023.643	18.84%	
53	20302+2651	BUP213	AC	9.91	0.04	324.28	0.27	2.92	0.02	2023.61	84.16%	3
54	20302+2651	BUP213	AD	92.21	0.05	281.92	0.03	1.06	0.02	2023.61	83.87%	
55	20302+2651	BUP213	ΑE	1342.03	0.32	92.97	0.01	0.38	0.02	2023.61	82.98%	
56	20302+2651	LMP45	AF	42.37	0.02	253.14	0.03	3.42	0.02	2023.61	87.48%	
57	20307+2657	OPI25	AB	14.19	0.04	29.85	0.15	3.71	0.02	2023.643	46.47%	
58	20307+2657	OPI25	AC	27.12	0.02	325.07	0.09	2.68	0.01	2023.643	23.70%	
59	20307+2657	OPI25	AD	103.88	0.06	357.33	0.03	1.86	0.02	2023.643	26.14%	

Table 5.: Measurements of primary targets

Notes:

- 1. 20229+2708 AB I couldn't measure it because it didn't separate.
- 2. 21065+2655 there isn't parallax of the primary.
- 3. 20302+2651 I couldn't measure it because it didn't separate.

				Separa	ition	Position Angle		Δ mag			Binary	
Nº	WDS	Disc	Comp	AVG	STD	AVG	STD	AVG	STD	Date	Probabil- ity	Notes
1	17503-2621	DAM371	AB	6.18	0.02	58.77	0.34	0.22	0.01	2023.578	92.15%	
2	17503-2620	HJ4986	AB	10.58	0.02	225.67	0.23	2.03	0.05	2023.578	92.90%	
3	17503-2620	HJ4986	AC	23.33	0.03	3.53	0.07	4.33	0.05	2023.578	28.32%	
4	17503-2620	HJ4986	AD	27.18	0.03	58.96	0.16	3.24	0.06	2023.578	13.84%	
5	19478+2615	BRT201	AB	2.92	0.16	359.89	0.76	0.02	0.03	2023.589	33.92%	
6	19478+2612	SCA200	AB	2.90	0.20	138.66	2.08	0.02	0.03	2023.589	33.29%	
7		CND41	AB	43.64	0.05	42.79	0.05	0.73	0.02	2023.589	48.35%	1
8		CND41	AC	41.38	0.02	91.98	0.10	3.43	0.04	2023.589	80.23%	1
9		CND41	ВС	35.45	0.02	160.71	0.04	2.70	0.05	2023.589	76.88%	1
10		CND42	AB	38.08	0.02	146.81	0.02	0.59	0.03	2023.589	68.85%	2
11	21030+2457	BKO482	AB	5.97	0.08	358.72	0.41	1.06	0.02	2023.599	27.80%	
12	21033+2454	BKO483	AB	8.42	0.10	71.89	0.28	0.14	0.01	2023.599	80.61%	
13	21050+2458	GRV411 POU5110	AB	45.84	0.04	348.66	0.04	0.68	0.00	2023.599	80.79%	
14	21030+2458 21032+2453	POU5110 POU5114	AB AB	12.43 2.29	0.03	146.01 338.06	0.17 2.20	0.36	0.01	2023.599	21.48% 73.66%	
16	21032+2433	POU5114 POU5126	AB	20.20	0.12	141.79	0.26	0.36	0.03	2023.599	77.47%	
17	21042+2449	POU5133	AB	6.20	0.07	311.30	0.20	0.65	0.01	2023.599	74.84%	
18	21047+2504	POU5134	AB	14.07	0.03	201.27	0.09	0.30	0.00	2023.599	41.07%	
19	21047+2446		AB	19.93	0.06	178.14	0.13	0.48	0.02	2023.599	76.91%	
20	21047+2446	CND43	AC	3.92	0.17	15.57	0.69	0.24	0.02	2023.599	52.86%	3
21	21051+2454		AB	15.54	0.02	346.10	0.13	1.00	0.01	2023.599	19.75%	
22	21051+2454	POU5142	AC	17.72	0.16	327.79	0.85	1.45	0.05	2023.599	18.53%	
23	21051+2454	POU5142	ВС	6.03	0.10	268.93	0.80	0.55	0.01	2023.599	92.01%	
24	21053+2444	POU5144	AB	16.53	0.04	331.48	0.16	1.52	0.01	2023.599	40.20%	
25	21053+2447	POU5145	AB	9.88	0.02	150.19	0.24	0.22	0.01	2023.599	18.17%	
26	21056+2510	POU5149	AB	16.64	0.03	275.40	0.10	0.60	0.01	2023.599	43.74%	
27	21059+2458		AB	12.43	0.05	27.88	0.14	1.00	0.00	2023.599	75.98%	
28	21060+2451	POU5153	AB	5.30	0.39	20.98	2.10	1.94	0.08	2023.599	55.92%	
29	21063+2457	POU5156	AB	5.40	0.43	280.43	1.54	2.18	0.13	2023.599	42.65%	
30	21063+2449	POU5157	AB	4.51	0.18	87.53	1.24	1.00	0.03	2023.599	68.35%	
31	20312+2855	ES506	AB	4.88	0.28	302.66	1.62	0.70	0.13	2023.601	91.72%	
32	20320+2915	GRV349	AB	33.18	0.02	42.49	0.02	2.38	0.01	2023.601	43.84%	
33	20346+2914	J565	AB	6.95	0.06	47.51	0.38	1.55	0.03	2023.601	58.19%	
34	20346+2914	J565	AC	16.31	0.27	208.00	0.21	3.86	0.02	2023.601	25.62%	
35	17069+2254 20487+2507	KUI123 BKO862	AB AB	7.93	0.03	298.00 57.88	0.11 3.34	1.32	0.01	2023.602	41.32% 88.98%	
37	20487+2307	BKO862 BKO864	AB	9.21	0.35	314.77	1.92	3.65	0.27	2023.641	26.86%	
38	20491+2509	BKO865	AB	9.02	0.33	101.16	0.71	0.41	0.10	2023.641	78.07%	
39	20500+2508	BKO874	AB	12.48	0.10	254.24	0.65	0.89	0.08	2023.641	28.76%	
40	20462+2513	POU4972	AB	13.80	0.14	279.76	0.22	0.41	0.03	2023.641	64.06%	
41	20462+2526	POU4974	AB	17.25	0.08	106.71	0.11	1.53	0.03	2023.641	64.18%	
42	20465+2506		AB	7.37	0.07	145.44	0.94	0.49	0.03	2023.641	28.39%	
43	20465+2506		AC	12.95	0.10	105.51	0.49	0.52	0.06	2023.641	58.82%	
44	20480+2504	POU5001	AB	7.77	0.08	197.65	0.71	0.70	0.03	2023.641	64.46%	
45	20482+2508	POU5003	AB	14.58	0.08	208.03	0.26	3.17	0.06	2023.641	30.32%	

% % % % % ***
% %
%
X
%
%
%
%
%
%
%
%
% 4
% 4
% 4
%
%
% 5
%
%
%
%
%
%
%
X
X
%
% 6
%
%
%
%
%
х
%
%
%
%
% 7
% 7
%
%

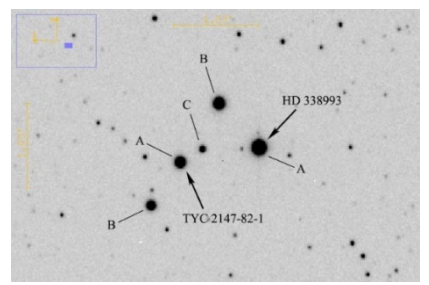
Table 6.: Measurements of secondary targets

Notes:

The explanation for the following plots. The *SZM* notation is my measurement (my own name code in WDS), the red arrow is the predicted resultant motion vector, the green arrow is the measured motion vector. The dashed arrow is a trend line.

1. CND41: HD 338993, new possible triple system at coordinates: 19h48m19.45s +26°23'02.25"

The astrometric data for the new triple system are presented in Table 8. Its measurement results can be seen in rows 7-9 of Table 6. Plots in Figure 7.



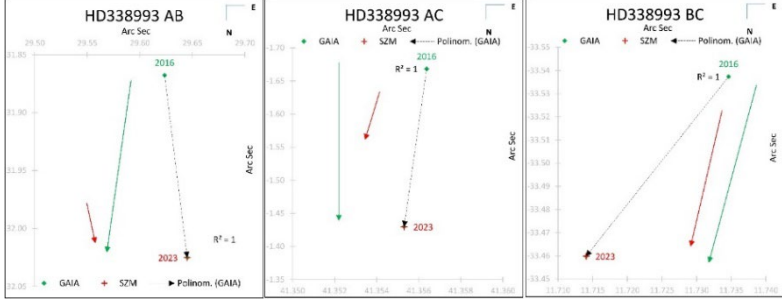


Figure 6.: Two new possible systems, CND 41 and CND 42

Figure 7.: Plots of new triple system

Comp	Simbad ID	Gaia ID	PM RA	PM Dec	Px	G mag	Rad(O)	Mass(O)	Lum(O)	Spect
A	HD338993	2027782604544202368	-2.54	-5.73	1.29	9.88	5.97	2.90	58.39	A0
В	TYC 2147-138-1	2027782707624110720	2.40	-4.67	1.96	10.78	3.62	1.82	10.98	K
С	No ID	2027782707623403648	0.42	3.96	1.56	13.61	1.22	1.06	1.27	K

Table 8.: Astrometric data of CND41

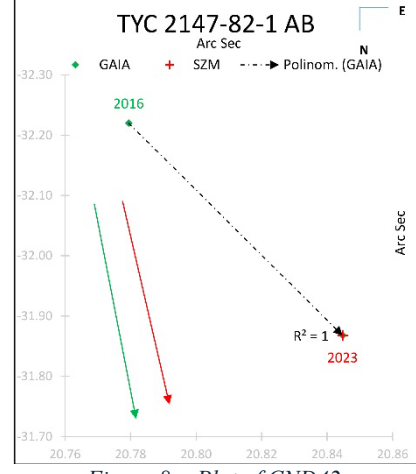
3. CND42: TYC 2147-82-1, new possible double stars at coordinates: 19^h48^m19.45^s +26°23'02.25".

See the Figure 6. The astrometric data for the new double is presented in Table 9. Its measurement results can be seen in row 10 of Table 6. Plot in Figure 8.

Since the two new systems are close to each other, we wondered if they could form a system, but the analysis did not show a positive result. So, they were considered two separate systems.

Comp	Simbad ID	Gaia ID	PM RA	PM Dec	Px	G mag	Rad(O)	Mass(O)	Lum(O)	Spect
A	TYC 2147-82-1	2027781951709153152	-27.78	-22.83	4.02	11.28	1.29	1.13	1.62	G
В	TYC 2147-116-1	2027781882994843136	-17.36	23.75	3.21	11.90	1.23	1.44	1.44	G

Table 9.: Astrometric data of CND42





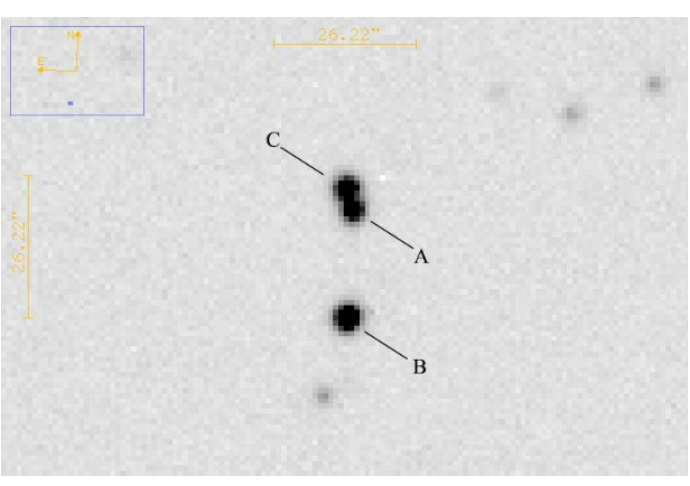


Figure 9.: 21047+2446 (POU5135)

3. CND43: New member of the 21047+2446 (POU5135). See the Figure 9.

The new possible C member appears close to the primary. The analysis showed that there was a 52.86% possibility of physicality. Its measurement result is shown in row 20 of table 6. The astrometric data of members A and C are summarized in Table 10, Figure 10 shows the plots of the system. So, it may be more of a triple system.

Comp	Simbad ID	Gaia ID	PM RA	PM Dec	Px	G mag	Rad(O)	Mass(O)	Lum(O)	Spect
A	No ID	1841192217111877248	5.63	-2.72	0.94	14.64	1.20	1.08	1.37	G
С	No ID	1841192217111877632	-18.69	-15.38	1.57	14.30	0.82	0.90	0.66	G

Table 10.: Astrometric data of 21047+2446 AC

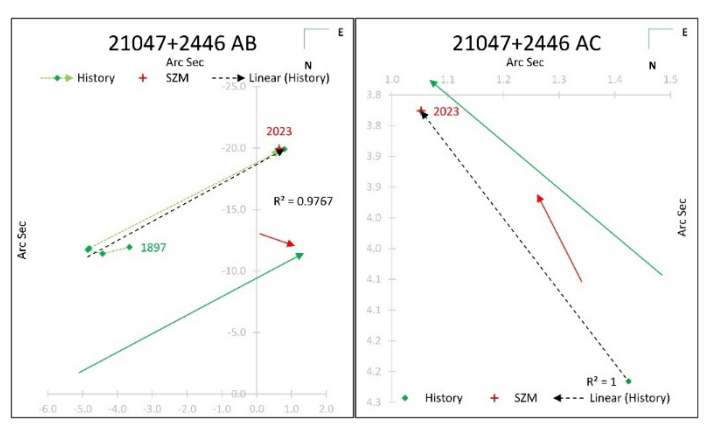


Figure 10.: Plots of 21047+2446 (POU5135)

4. CND44: New members of the 19399+2447 (BKO430). See the Figure 11.

When measuring the system, were noticed the nearby stars, and looked at their Gaia data. Analysis showed that this is a system of five stars. Astrometric data of stars are shown in Table 11, plots are shown in Figure 12. Its measurement results in rows 59-61 of Table 6. The T_{eff} value of star B is missing.

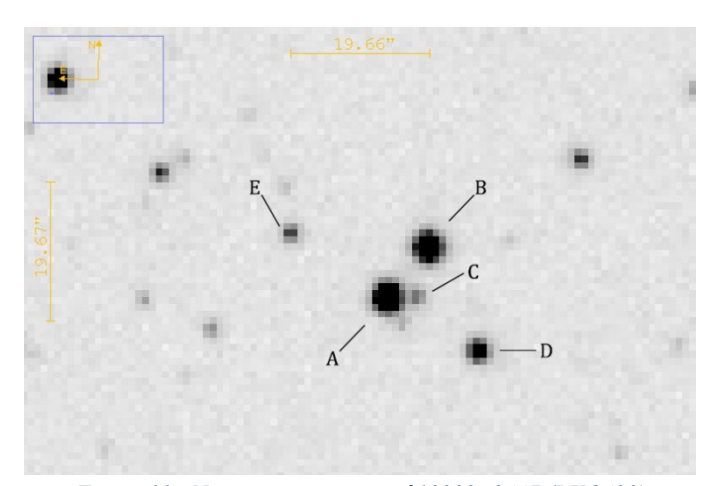


Figure 11.: New quinary system of 19399+2447 (BKO430)

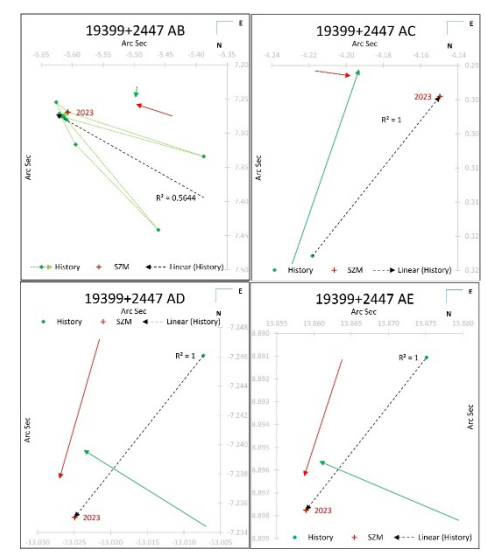


Figure 12.: Plot of 19399+2447 (BKO 430)

Comp	Simbad ID	Gaia ID	PM RA	PM Dec	Px	G mag	Rad(O)	Mass(O)	Lum(O)	Spect
A	No ID	2021196289405496832	-1,28	-4.42	0.38	13.03	6.67	2.55	37.23	K
В	No ID	2021199244342997888	-1.97	-6.49	0.39	13.53	?	2.56	37.61	?
С	No ID	2021196289405497472	-1.43	-5.48	0.33	16.22	1.68	1.26	2.55	G
D	No ID	2021194811936748032	-1.90	-6.53	0.30	14.94	2.37	1.78	10.00	В
Е	No ID	2021196289405495680	-1.93	-6.47	0.33	16.05	1.46	1.33	3.09	A

Table 11.: Astrometric data of 19399+2447 (BKO460)

5. CND45: New member of the 19387+2444 (POU3978), see Figure 13.

While measuring the system, were noticed the fainter star next to the primary. A detailed analysis using GAIA data showed the possibility of a physical relationship between star A and star C. Astrometric data of stars are shown in Table 12, plots are shown Figure 14. The measurement data are shown in row 64 of Table 6.

Comp	Simbad ID	Gaia ID	PM RA	PM Dec	Px	G mag	Rad(O)	Mass(O)	Lum(O)	Spect
A	No ID	2021238891137062016	-1.27	-2.93	0.41	14.12	3.66	1.83	11.67	G
С	No ID	2021239101642812416	-2.55	-7.76	0.47	16.71	0.91	0.95	0.80	G

Table 12.: Astrometric data of 19387+2444 AC

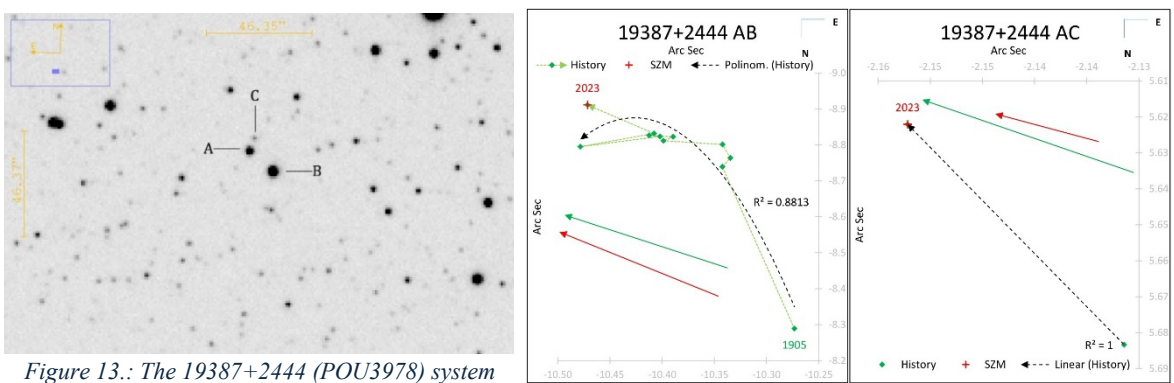


Figure 14.: Plots of 19387+2444 (POU3978)

6. CND46: New member of the 19399+2455 (POU3998). See Figure 15.

In the image, next to the primary, another star was closely visible. Detailed analysis revealed a possible physical relationship between the two stars. Astrometric data are shown in Table 13, plots are shown in Figure 16. The results of measurements are presented in row 75 of Table 6. Unfortunately, the DR3 database missing the T_{eff} value for stars A and C.

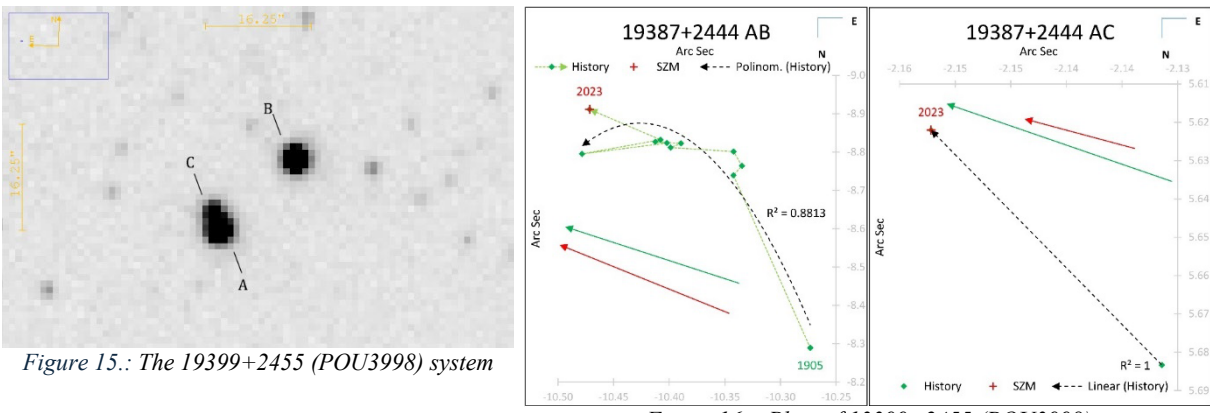


Figure 16.: Plots of 13399+2455 (POU3998)

Comp	Simbad ID	Gaia ID	PM RA	PM Dec	Px	G mag	Rad(O)	Mass(O)	Lum(O)	Spect
A	UCAC4 575-095440	2021201099769213952	-0.11	-1.01	0.63	13.19	?	1.82	11.38	?
С	No ID	2021201099722583552	0.07	-1.33	0.45	15.25	?	1.36	3.43	?

Table 13.: Astrometric data of 19399+2455 AC

7. CND47: Two new members of the 20291+2700 (DOO86). See the Figure 17.

During the measurement, were looked at the data of the stars next to the double in the DR3 database. Were found that C and D stars may have a physical relationship with the primary. Astrometric data are shown in Table 14, plots in Figure 18. The measurement results are shown in rows 86 and 87 of Table 6.

Comp	Simbad ID	Gaia ID	PM RA	PM Dec	Px	G mag	Rad(O)	Mass(0)	Lum(O)	Spect
A	TYC 2164-550-1	1856917363707093376	3.17	-4.37	0.56	12.21	5.10	2.52	35.79	A
С	No ID	1856905612676566272	-4.96	-14.23	0.49	15.98	1.27	1.10	1.46	G
D	No ID	1856917363707090560	0.51	-6.81	0.54	15.28	1.37	1.23	2.26	F

Table 14 Astrometric data of 20291+2700 (DOO86)

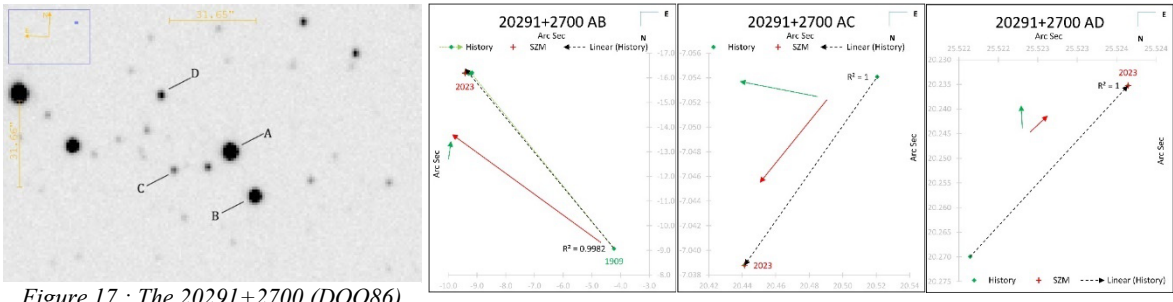


Figure 17.: The 20291+2700 (DOO86) system

Figure 18.: Plots of 20291+2700 (DOO86)

5. Acknowledgements

Thanks Rachel Matson of the USNO for providing the historical data for this work. I also acknowledge that this work uses the Washington Double Star Catalog maintained at the US Naval Observatory, the SIMBAD database, and the ALADIN sky atlas. This work also used data from the European Space Agency (ESA) Gaia mission (https://www.cosmos.esa.int/gaia) processed by the Gaia Data Processing and Analysis Consortium (https://www.cosmos.esa.int/web/gaia/dpac/consortium). The financing of DPAC was provided by national institutions, especially those participating in the Gaia Multilateral Agreement. Thanks to Richard Harshaw for the Plot tool.

6. References

- Buchheim R. K., "CCD Double-Star Measurements at Altamira Observatory in 2007", JDSO, Vol 4, No. 1, 27-31. Winter 2008.
- Bonnarel, F. et al., "The ALADIN interactive sky atlas. A reference tool for identification of astronomical sources", Astronomy and Astrophysics Supplement, v.143, p.33-40. April 2000.
- Collins, K. A., Kielkopf, J. F., Stassun, K. G., and Hessman, F. V. "AstroImageJ: Image Processing and Photometric Extraction for Ultra-Precise Astronomical Light Curves", Astronomical Journal, 153(77). February 2017.
- Harshaw, R., "Gaia DR2 and the Washington Double Star Catalog: A tale of two databases", JDSO, Vol. 14 No. 4. Page 734-740. October 1, 2018.
- Harshaw, R., "Using Plot Tool 3.19 to Generate Graphical Representations of the Historical Measurement Data", JDSO, Vol. 16 No. 4. Page 386-400. September 1, 2020.

- Rica, F. M., "Determining the Nature of a Double Star: The Law of Conservation of Energy and the Orbital Velocity", JDSO, Vol. 7, No. 4; 254-259. October 1. 2011.
- Francisco Rica Romero, "Criteria to Determine the Nature of Double Stars: the Stellar Masses", JDSO. Vol. 6, No. 2; 156-159. April 1. 2010.
- Sinachopoulos&Mouzourakis, "Searching for Optical Visual Double Stars", Complementary Approaches to Double and Multiple Star Research, IAU Colloquium 135., ASP Conference Series, Vol. 32, 1992 Harold A. McAllister and William I. Hartkopf (eds).
- Gianluca Sordiglioni's (SDG) StelleDoppie: https://www.stelledoppie.it/
- The Washington Double Star Catalog, 2023: http://www.usno.navy.mil/ USNO/astrometry/optical-IR-prod/wds/WDS.
- Wenger, M. et al., "The SIMBAD astronomical database. The CDS reference database for astronomical objects", Astronomy and Astrophysics Supplement, v.143, p.9-22. April 2000.

A New Approach to Determine Orbits of Wide Binary Stars Case: WDS 19377+3022 BU 144

Richard Nugent
International Occultation Timing Association
RNugent@wt.net

Abstract

Astrometric, photometric and other data have been acquired for the double star WDS 19377+3022 BU 144, previously not considered to be a binary star system. Analysis of the data using new methods provides considerable evidence that BU 144 is a gravitationally connected binary star system. With the new methods, the data suggests a physical separation range of 1,075 - 1,100AU, an orbital inclination angle of $\approx 50^{\circ}$, and an orbital period ranging from 9,800 - 10,330 years.

1. Introduction

The Washington Double Star Catalog (WDS) system 19377+3022 BU 144 has 46 position angle and separation measurements dating from 1873 to the present. The Gaia DR3 G-band apparent magnitudes (Vallenari, A., et. al. 2022) of the components are +9.20 and +9.33 for the primary and the secondary. During the 149 year measurement history position angles (PA) changed by just 5.29° and the separations (SEP) by less than 0.4". With the limited range of PA and SEP data, BU 144 was not considered as a gravitationally bound binary star system hence it is not listed in the *Sixth Catalog of Orbits of Visual Binary Stars* (Matson, et. al., 2022). Further, with a Gaia distance of 49.1pc, BU 144 is not listed in The *General Catalog of Trigonometric Stellar Parallaxes Fourth Edition* (van Altena, et. al., 1995). This parallax catalog has stellar distances to 650 pc and higher, however the accuracies of distances beyond 150pc (which were measured with ground based telescopes) are highly questionable. It is not the objective of this paper to determine all seven orbital elements $(a, e, i, \omega, \Omega, T_0, P)$ that define an orbit. Instead, all the available Gaia and observational data is used here as a starting point to derive the best estimates of physical separation, the orbit's orientation angles with respect to the Sun and its orbital period.

2. Data Acquisition

New measurements of position angle and separation were made using the video drift method and the author's Meade 14-inch LX200 telescope located in Ft. Davis, Texas. The observations were made under good seeing conditions with the target within 30 minutes of its passage across the local meridian. Astrometric observations should always be made with the target as close to the meridian as possible to minimize the amount of atmosphere the telescope/camera system is observing through.

Using a *Watec 902H Ultimate* video camera, (this camera typically used for occultations due to its highly sensitive chip) the scale factor was 0.56"/pixel using the telescope/camera/focal length system. The video drift method (Nugent and Iverson 2018, and other papers in the series) has the advantage of very little human intervention in determining the position angle and separation of the components.

The video drift method works as follows: The component stars are placed on the video camera chip corresponding to the far eastern part of the field of view (FOV). The telescope's motor drive is then turned off. As the components drift across the FOV, they will move precisely in the west direction (position angle 270°). In 25-30 seconds, (duration of the video depends on the focal length of the telescope/camera system) the stars will drift out of the FOV. The video is then saved. The components are re-positioned back at the east side of the camera chip and the process is repeated several times resulting in several 25-30 second videos.

Data from the videos are generated using the software program Limovie (Miyashita 2006). Limovie was written for occultation videos to measure brightness changes of stars during an occultation. In addition to brightness information, Limovie also outputs (x,y) Cartesian coordinates of each component for each video frame. With a 30 frame/sec video recording rate, a 25 second video outputs 750 video frames resulting in 750 pairs of individual (x,y) coordinates for each component. The software program VidPro (written by this author) analyses the (x,y) coordinates for each video frame and computes a position angle and separation for each video frame. All of the video frame output data are then combined resulting in a single position angle and separation along with statistical results.

An example on how the video drift method works using the software programs *Limovie* and *VidPro* is demonstrated in this YouTube video: https://www.youtube.com/watch?v=rlg_mrxnvU0.

The new position angle and separation for BU 144 is presented in Table 1. The Gaia Early Data Release 3 (Gaia Collaboration, A. Vallenari, A. G. A. Brown, et al. 2022) parallaxes, proper motions, radial velocities and associated errors of the components are in Table 2.

PA°	error°	SEP"	error"	Date	Mag Pri	Mag Sec	Nights
356.5	1.57	5.81	0.14	2022.65	+9.20	+9.33	1

Table 1. WDS 19377+3022 BU144 measurements using the video drift method. Measurements are from Equator and Equinox of date.

							Radial	
	Parallax	error	pmra	pmra error	pmdec	pmdec error	velocity	error
	(mas)	mas	mas/yr	mas/yr	mas/yr	mas/yr	km/sec	km/sec
Primary	20.37438	0.011583	71.41078	0.009319	39.21757	0.010964	-32.73	0.374
Secondary	20.37068	0.012532	76.72102	0.010137	35.24491	0.011941	-33.762	0.428

Table 2. Gaia ERD3 data for WDS 19377+3022 BU 144. Gaia Source IDs for Primary: 2032516891133712000, Secondary: 20325168954291291136

The Centre de Données astronomiques de Strasbourg (CDS) VizieR tables derived from Gaia EDR3 also contains data on each component's effective temperature ($T_{\rm eff}$), radius and mass. These tables reveal the component's masses ranging from $0.78M\odot$ - $0.80M\odot$. The average component mass from the various VizieR data sets is listed in Table 3.

	Temp °K	Radius R_{\odot}	Mass M _⊙
Primary	5,038	0.83	0.795
Secondary	4,965	0.81	0.795

Table 3. VizieR (based on Gaia ERD3) effective temperature, radius and average mass.

Using the new measured separation angle along with the Gaia EDR3 distances, the physical separation between the components was derived using the law of cosines. The calculated physical separation between the components is 1,879AU and this value uses the Gaia mean parallaxes and not the errors. Taking into account the errors in the parallaxes, the physical separation between the components ranged from 285AU to 13,819AU.

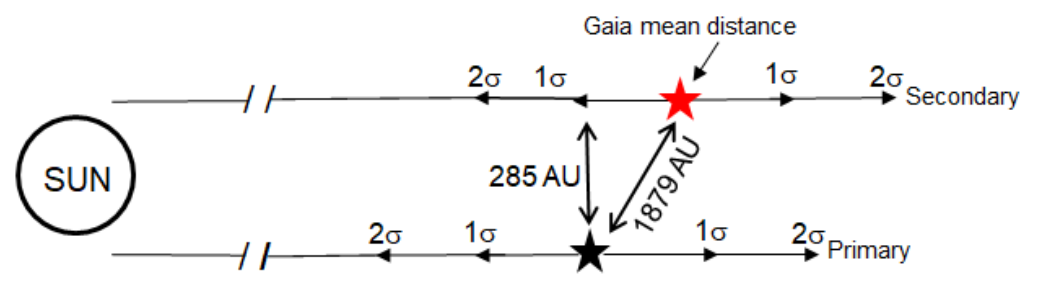


Figure 1. Gaia distances of components from the Sun including errors for WDS 19377+3022 BU 144. The 1σ and 2σ points show the standard deviations in distance at the 68% and 95% confidence levels. Diagram not to scale.

The separation 285AU would be the minimum distance between the primary and secondary and this assumes that both components are equidistant from the Sun. There is substantial overlap in the component distances from the Table 2 parallax errors shown in Figure 1 amounting to 10,148AU. The method used to derive the 1,879AU separation with the associated errors, hereinafter will be referred to the "Law of Cosines" method.

3. Proper Motions and Radial Velocity

The Gaia EDR3 proper motions were plotted on the Digital Sky Survey 2 (DSS2) blue image using the *Aladin Sky Atlas Version 11* interactive software program (Figure 2). The proper motions of the component stars are nearly identical in direction and magnitude (see Table 2). To confirm, Harshaw's (Harshaw 2016) calculation was used to determine if the components share a common proper motion. The derived value was 7.8%.

From Harshaw's reasoning, values < 20% = common proper motion (CPM) pair, 20% < value < 60% = similar proper motion (SPM) pair and a value > 60% = different proper motion (DPM) pair. BU 144's 7.8% value is an expected result with the physical separation of the components being very close as the stars are moving through space together.

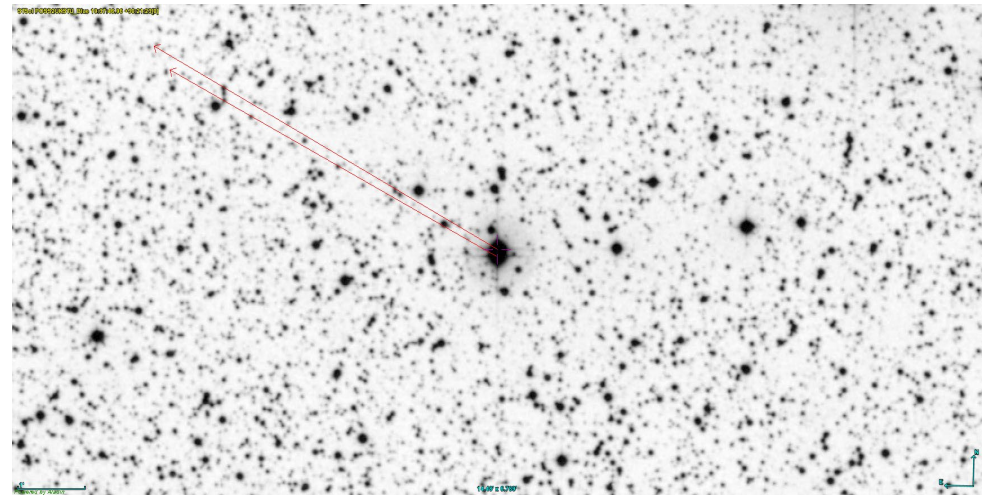


Figure 2. Gaia proper motions of components BU 144 overlaid on DSS2 blue image. DSS2 image date: July 14, 1988.

The radial velocities V_R of the components from Gaia ERD3 are: V_R primary: -32.73 ± 0.374 km/sec and V_R secondary: -33.76 ± 0.43 km/sec. The similar radial velocities, proper motions and close separation provide evidence that BU 144's components are moving through space together as a binary star system.

4. Estimating Absolute Magnitude, Bolometric Correction, Mass and Orbital period

Assuming the estimated physical separation of the component stars of BU 144 is 1,879AU, it may be a gravitationally connected binary star system. The orbital period of a binary is historically derived using Newton's version of Kepler's 3rd law:

$$P^{2} = \left[\frac{4\pi^{2}a^{3}}{G(Mass_{pri} + Mass_{sec})} \right]$$
 [1]

In equation [1], P is the period, π the mathematical constant, G the gravitational constant, $Mass_{pri}$, $Mass_{sec}$ are the masses of the primary, secondary and a is the semi-major axis of the orbit. Estimates for the component masses in solar mass units were computed from the empirical mass-luminosity relation (Lang, 1992, p. 116),

$$Mass_{\odot} = 10^{0.48 - 0.105 Mbol}$$
 [2]

where M_{bol} is the absolute bolometric magnitude. The bolometric magnitude is the magnitude of a star from its total radiation over all wavelengths. Equation [2] is only valid for stars with absolute bolometric magnitudes from $-8 < M_{\text{bol}} < +10.5$. The bolometric magnitude is traditionally derived from:

$$M_{\text{bol}} = M + BC, \tag{3}$$

where M is the absolute magnitude and BC is the bolometric correction. The absolute magnitude M is derived using the distance modulus:

$$m - M = 5 \log R - 5 \tag{4}$$

where m is the apparent Gaia G-band magnitude and R is the known distance to the components in parsecs. From the tables in Pecaut and Mamajek (2013), Gaia effective temperatures ($T_{\rm eff}$) were used to estimate the bolometric correction BC: Primary:-0.286mag, secondary: -0.317mag. With M and BC known for each component, equation [3] was used to get $M_{\rm bol}$. The absolute bolometric magnitudes were then used in equation [2] to derive the mass of the components. The results are primary: $0.80M\Theta$ and secondary: $0.79M\Theta$ where both are nearly identical to the VizieR tabular values in Table 3. These nearly equal masses provide evidence that BU 144's components may be in a circular orbit.

Using the estimated masses from equation [2], and the 1,879AU physical separation, equation [1] was used to calculate the orbital period of the system: 22,813 years. From the Gaia range of physical separation (285AU – 13,840AU), the period ranges from 1,350 – 456,000 yrs. The long orbital period based on 1,879AU physical separation could explain the small changes of position angle observed over the 149 year measurement history.

The WDS catalog lists the spectral type for the primary component as K0V and no spectral type for the secondary. With the Gaia DR3, the $T_{\rm eff}$ are listed as primary: 5038°K and secondary: 4965°K. These temperatures are consistent with spectral types of the components as K2V – K3V. With nearly identical $T_{\rm eff}$ and spectral types, these stars may have formed and evolved together at some point in the galaxy's history.

5a. Developing an Orbit: Deriving Space Velocity

The computation of an orbit of a visual binary usually requires a large change of observed PA values over the measurement history along with the corresponding angular separations. Typical PA changes for orbits in the Sixth Orbit Catalog span 25°–50° and larger. There are very few exceptions. These exceptions systems

have large separations approaching 2,000AU - 3,000AU hence they have long periods and small changes in PA.

We begin by assuming BU 144 is a gravitationally connected binary star system. From the previously derived nearly identical masses of the components it will also be assumed that BU 144 has a circular orbit revolving around a common center of mass. It is proposed that the component space velocity differences ($\Delta V_{\rm space}$) can be used to estimate the orbital velocity. With the orbital velocity known of either component along with their physical separation, the period can be determined.

The $V_{\rm space}$ is found from combining the radial velocity $V_{\rm R}$ and proper motions. Proper motions represent tangential velocity as they are the projected velocity across the celestial sphere. The $V_{\rm space}$ is the actual velocity of the components (with respect to the Sun) through space in a given direction. See Figure 3 parts 1-4. The $V_{\rm space}$ is computed from the following formula:

$$V_{\text{space}} = \sqrt{V_{\text{R}}^2 + (4.74 \ \mu''/\pi'')^2}$$
 [5]

In equation [5], V_R is the radial velocity in km/sec, μ is the total proper motion in arcsec/yr, and π is the parallax of component in arcseconds.

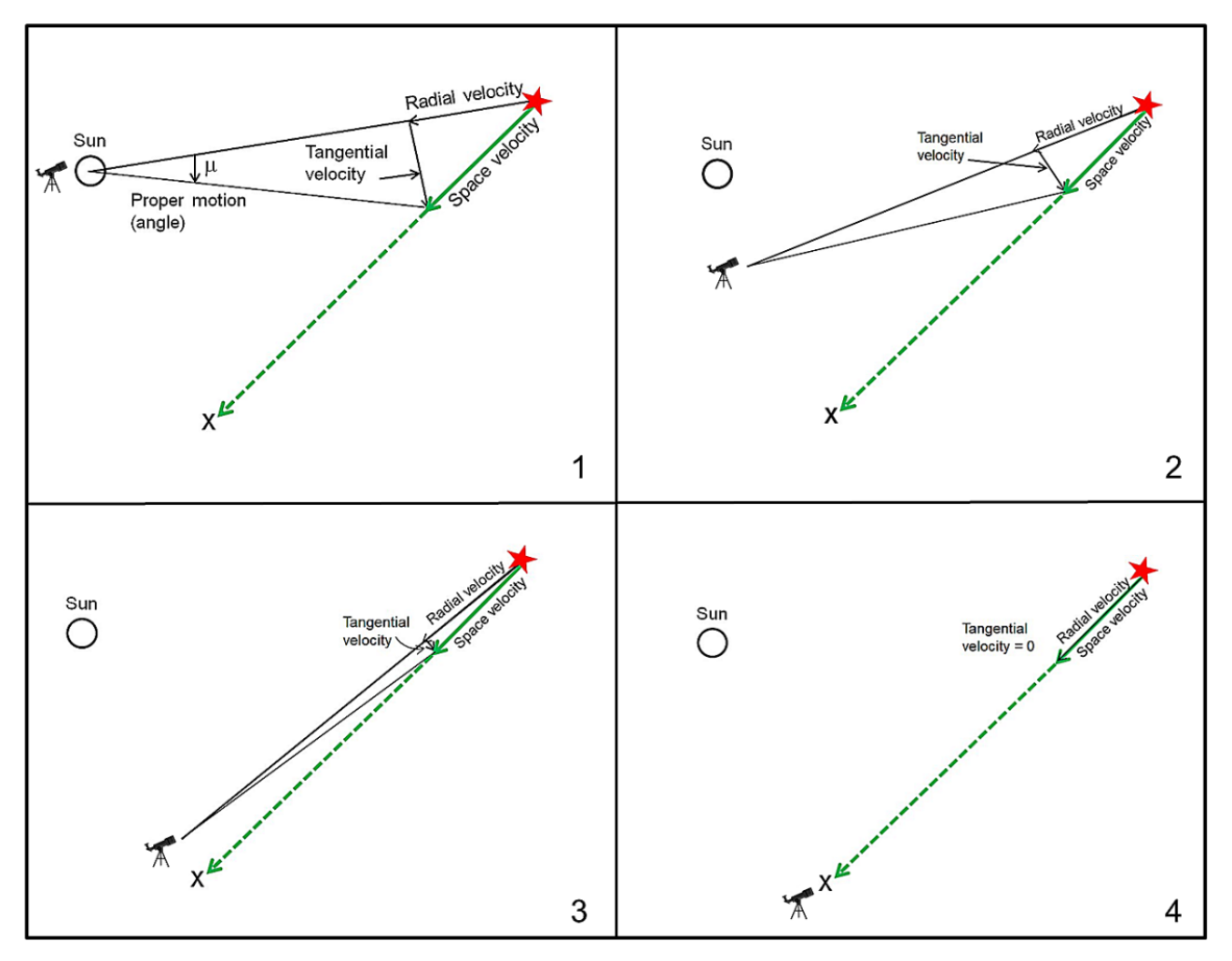


Figure 3. Part 1: The Observer at the Sun sees proper motion, radial velocity and computes $V_{\rm space}$ (space velocity) of the components. Parts 2, 3 and 4: The Observer is moved away from the Sun to the point "X" where the proper motions equal zero. At this point "X", the Observer views only the $V_{\rm space}$ which is the radial velocities of the components.

In Figure 3, the Sun and the point X are at different positions in the galaxy. Figure 3 illustrates that if an observer moves from the Sun at part 1 toward the point X (as shown in parts 2, 3 and 4), this reduces the tangential velocity (proper motion) to zero. Thus the observer at the point X in part 4 only sees the actual space velocity V_{space} of the components, which is their individual radial velocities at point X. The orbit viewed from the position X eliminates the space velocity projection effect seen from the Sun/Earth perspective. For the case of BU 144, the point X is 24.8 pc from the Sun. This creates a 30° angular separation on the sky between the Sun and point X as viewed from the BU 144 components.

5b. Orbital Velocity from Space Velocity

To illustrate the orbital velocity computation, we first assume that the orbit of BU 144 is edge on (inclination = 90°) to the line of sight as seen from the point X as shown in Figure 4. For an observer at the position of X in Figure 4 the space velocity V_{space} of the components is the radial velocity. Then any difference in V_{space} of the components can be attributed to orbital motion. For example, if the primary's V_{space} is +5 km/sec and the secondary's V_{space} is -5 km/sec at the point X, then each component's orbital velocity would be 5 km/sec (Figure 4 only). The Observer would see an *absolute difference* in V_{space} of 10 km/sec: +5 - (-5) = 10. Thus, the orbital velocity of each component is one-half of the absolute difference, in this example: 5 km/sec.

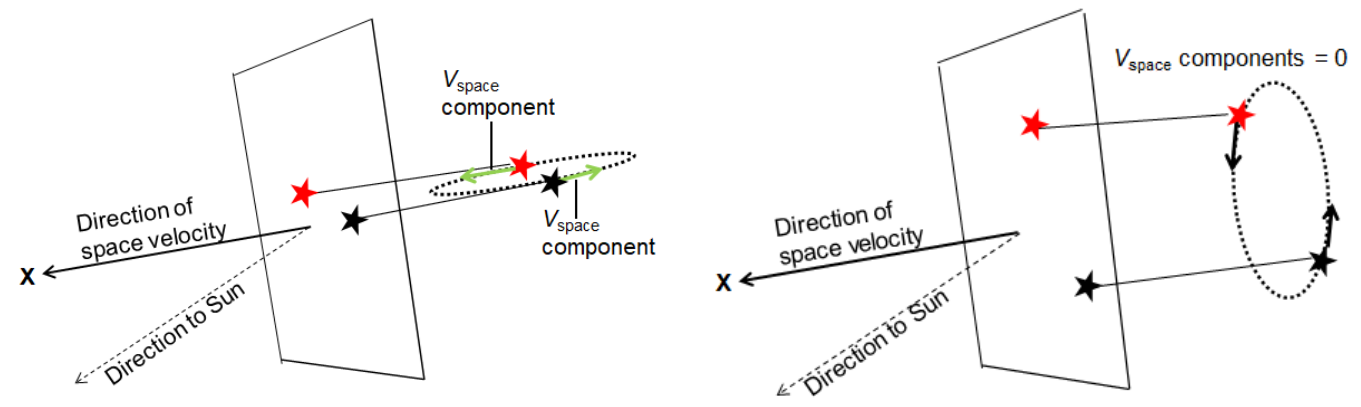


Figure 4. Net observed orbital/space velocities in opposite directions from X.

Figure 5. $V_{\text{space}} = 0$ at the point X

If the orbit was oriented as shown in Figure 5 (inclination = 0° , face on to our line of sight) there would be no measureable difference in the radial (V_{space}) velocity seen at point X.

BU 144's derived space velocities are primary: -37.82 ± 0.37 km/sec and secondary: -39.06 ± 0.43 km/sec, the absolute difference 1.24 ± 0.40 km/sec. As reasoned above this absolute difference in $V_{\rm space}$ can be interpreted that one component is moving toward us and the other component away from us. Figure 6 illustrates this. The $V_{\rm space}$ velocity of each component is ½ of the absolute difference or 0.62 ± 0.40 km/sec. Taking into account the errors, the range of projected component $V_{\rm space}$ is 0.22 km/sec -1.02 km/sec. As Figure 6 shows, the actual orbital velocity will depend on the orientation (inclination angle, i) of the orbit as viewed from the observer at the point X. Note that the orbital velocity derived from this method is independent of the physical separation of the components.

5c. Orbital Period from Orbital Velocity and Inclination

Now consider the case where the orbit is inclined by 45° as viewed from point X, (not from the Sun), as shown in Figure 6. The orbital velocity can be computed from the space velocity:

Orbital velocity =
$$\frac{V_{\text{space}}}{\cos 45^{\circ}}$$
 [6]

Using the range of projected $V_{\rm space}$, 0.22-1.02 km/sec, the actual orbital velocities along the 45° inclined orbit will vary from 0.31 to 1.44 km/sec.

Assuming a circular orbit, and a 1,879 AU separation, the circumference of the orbit is 5,903 AU. From the range of derived orbital velocities from equation [6], the components will make one complete revolution of 5,903 AU in 19,419 – 90,441 years.

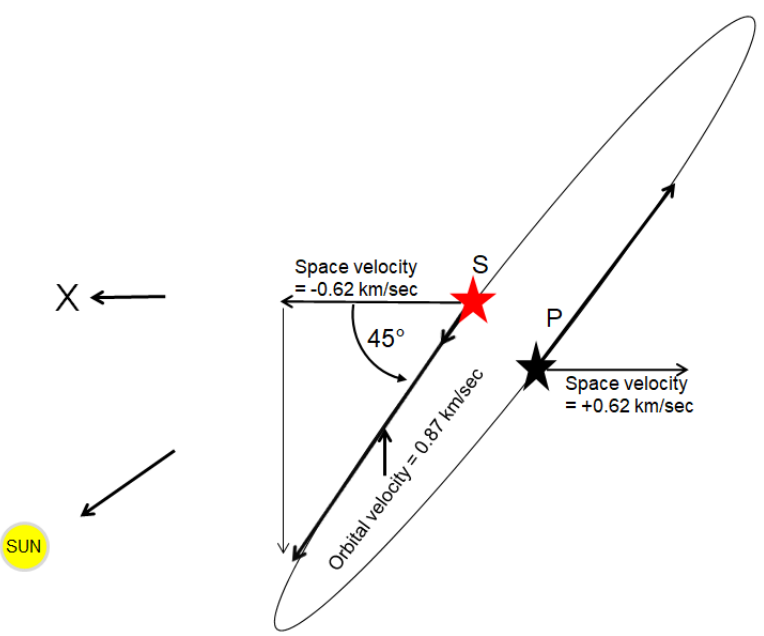
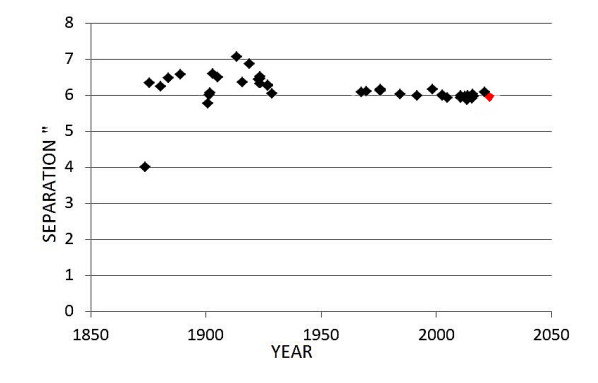


Figure 6. With inclination = 45° , the projected space velocity of the components = 0.62 km/sec. The resulting actual orbital velocity = 0.87 km/sec. Different inclination angles result in different orbital velocities.

6. Historical Measurements: Orbital Period from Position Angle

The angular separation change of BU 144 over its 149 year measurement history is 5.29°. Figure 8 shows the historical PAs. (PA values in 1913: 359.3°, 1928: 356° and 1984: 357.7° are several degrees different from the surrounding values and are outliers). Ignoring the physical separation, if the components moved 5.29° in 149 years, extrapolating to 360°, one full orbit would take 10,139 years. This orbital period is substantially smaller than the period from the $V_{\rm space}$ /inclination method above which derived an orbital velocity and used the 1,879AU separation. This result indicates that a smaller separation would be needed to match the extrapolated period from the historical PA's.



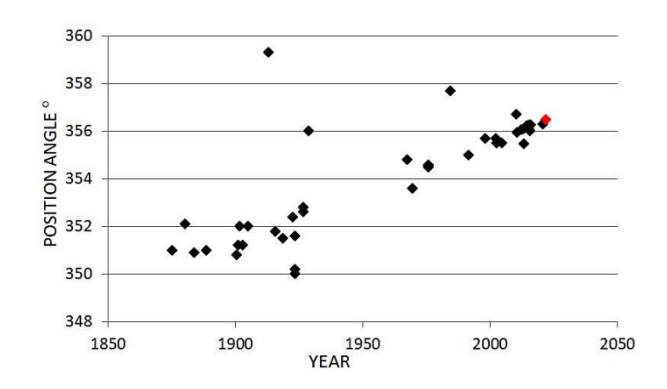


Figure 7. Historical separations. Red data point from this author.

Figure 8. Historical position angles. Red data point from this author.

7. Historical Measurements: Angular Separation

Historical angular separation measurements for BU 144 are shown in Figure 7. Over the 149 year history there is a trend showing a slight decrease in separation amounting to less than 0.4". The 1873–1928 measurements have a 1" scatter of ranging from 6.0"–7.0". This large scatter is likely due to personal error from the visual techniques used to make the measurements. The first reported separation in 1873 was 4". Compared to the remaining measurements, this observation is an outlier. After a nearly 40-year gap in measurements (1928-1967), the separations were again measured with more refined instruments and techniques. They remained similar, ranging from 5.9" to 6.15".

For a circular orbit with an inclination = 90° (or close to it, Figure 4), the angular separations will decrease and increase over time as the stars appear to approach and recede from one another in a periodic manner over the time scale of the orbit. This is analogous to eclipsing binaries. The PAs would only have two values 180° apart as the components pass each other twice per orbit. The historical data does not support this as the PA is changing and the SEP is remaining relatively constant. The opposite is also true. From Figure 5, for a circular orbit with an inclination = 0°, the PA's would be changing in a periodic manner and the SEP's would remain constant. The historical PA and SEP measurements demonstrate this. Along with Gaia data, this provides evidence that BU 144 is a binary system whose orbit is similar to Figure 6.

8. Estimating Longitude of the Ascending Node Ω

The 5.29° position angle change from the 149 year measurement history could be a projected position angle change, as shown in Figure 9. If the orbit is rotated in a left-right manner as shown in Figure 9, this will result in a smaller (projected) observed position angle change in the apparent orbit compared to the actual position angle change. In the terminology of orbit calculations, this rotation angle would be the longitude of the ascending node, Ω .

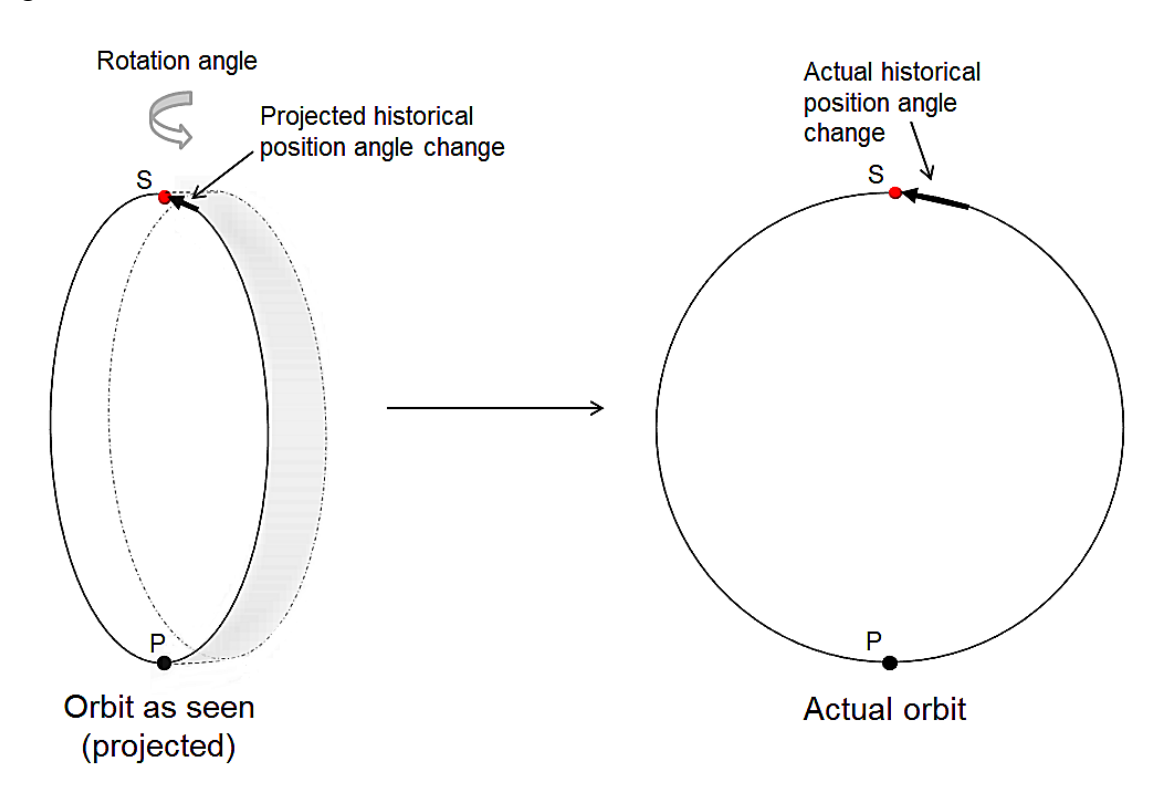


Figure 9. **Left:** Projected historical position angle change from a left-right rotation. **Right:** Actual historical position angle change in the true orbit. P = Primary, S = Secondary.

Using the historical PA change of 5.29°, a 0° rotation angle is the equivalent to the actual orbit on the right side of Figure 9: period = 10,139 years. A 5° rotation angle = 10,101 year period (5.31° actual PA change), 15° rotation angle = 9,794 year period (5.47° actual PA change) and a 25° rotation angle = 9,189 year period (5.84° actual PA change). This rotation angle (longitude of the ascending node Ω) is from the point X in space, not as viewed from the Sun. From the Sun, a 30° correction to the rotation angle (Ω) derived in Section 5a above will have to be applied.

The historical PA change and the rotation angle Ω described above place limitations on the orbital period. These two methods indicate an orbital period of approximately 10,000 years, which is inconsistent with the periods obtained from Kepler's 3rd law and the inclination/ $V_{\rm space}$ methods using the 1,879AU separation. From trial and error, the upper limit of the $V_{\rm space}$ (1.02 km/sec) at various inclination angles with smaller physical separations, provides orbital periods in good agreement with the historical PA/ rotation angle methods.

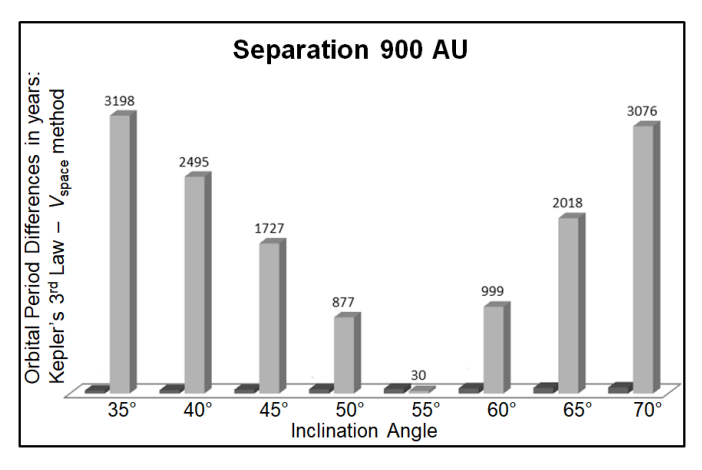
Using the 3 methods outlined above: Kepler's 3^{rd} law period, inclination/ V_{space} period and the PA/rotation angle period, we can proceed to determine the best match of orbital periods as follows:

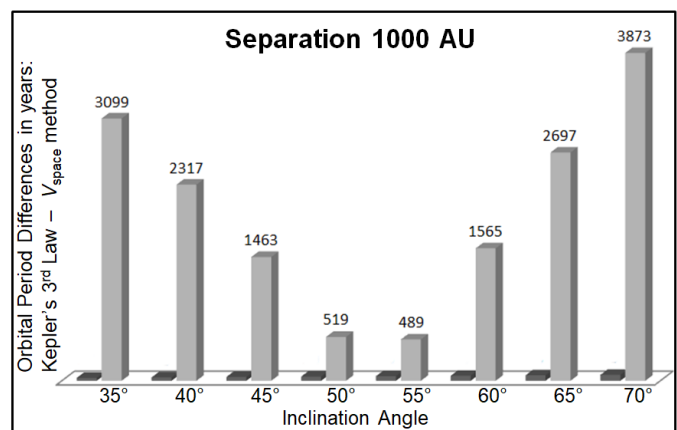
- 1. For a given physical separation in AU's, equation [1] (Kepler's 3rd law), compute a period. The masses of the components (*Mass_{pri}* + *Mass_{sec}*) remain constant.
- 2. For a given physical separation, adjust the inclination angle (inclination/ $V_{\rm space}$ method) to provide an orbital period for BU 144.
- 3. Compare Kepler's 3^{rd} law period with the inclination/ V_{space} method period and note the differences.
- 4. By trial and error, we can minimize the orbital period differences between Kepler's $3^{\rm rd}$ law method and the inclination/ $V_{\rm space}$ method by adjusting the inclination angle and physical separation.
- 5. The historical PA's /rotation angle methods provide limitations on the range of orbital periods, thus a "best match" of physical separation, inclination angle and orbital period can be obtained.

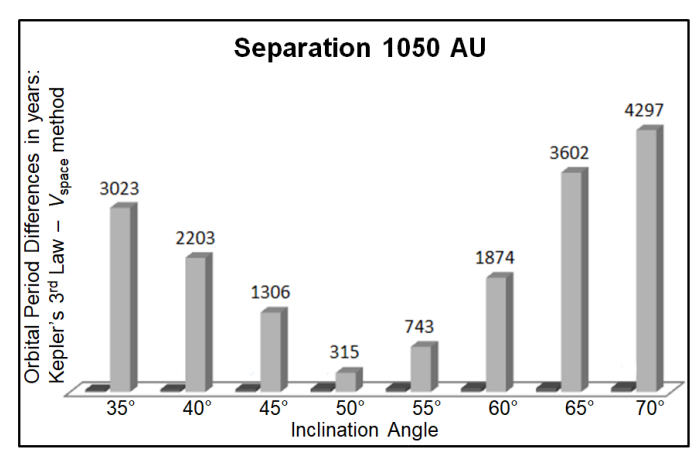
9. Comparison of Techniques in Estimating Physical Separation and Orbital Period

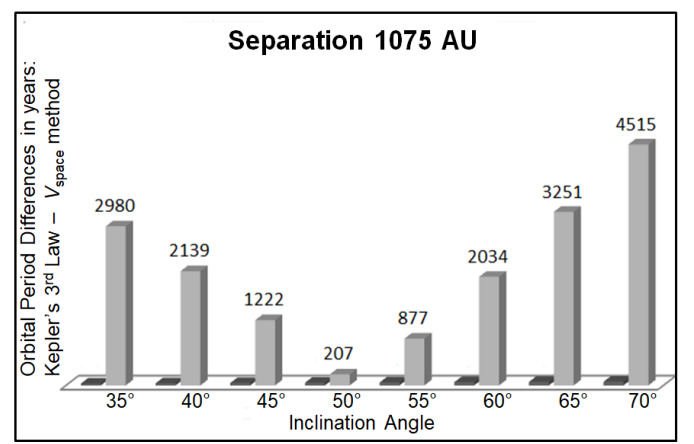
Figure 10 illustrates for a given physical separation in AU's, the differences between the orbital periods from Kepler's 3^{rd} law and the inclination/ V_{space} method.

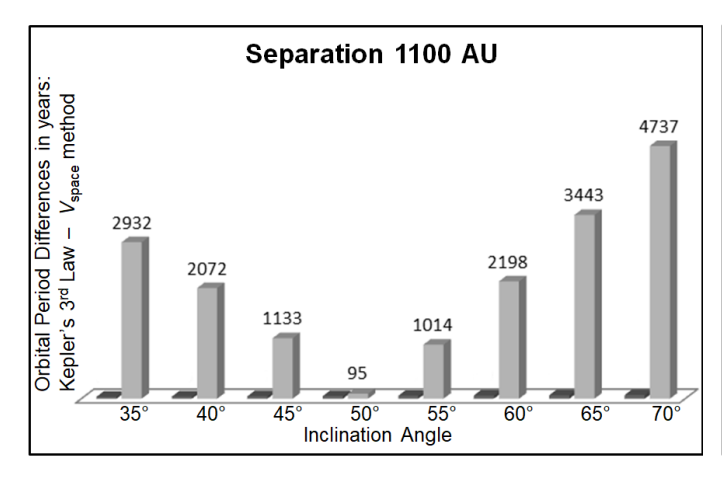
Table 4 combines the three methods used for estimating the orbital period of BU 144: Method 1: Gaia parallaxes-Law of Cosines, Method 2: Inclination angle/ $V_{\rm space}$, and Method 3: Rotation angle (Ω)/historical PA change. Taking into account the smallest differences from Figure 10, the best matches from the three methods for separation, inclination angle/ $V_{\rm space}$, historical PA's and rotation angle are highlighted in Table 4.











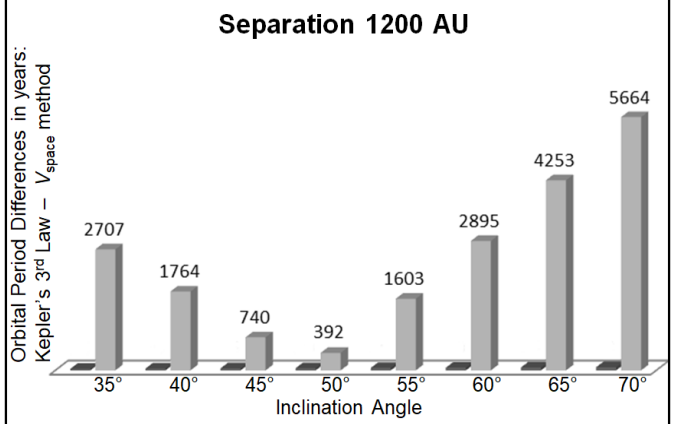


Figure 10. Orbital period differences in years from Kepler's 3^{rd} law – inclination/ V_{space} method for various inclinations. As stated in the text, the larger V_{space} of 1.02 km/sec was used to derive orbital velocities.

Metho		Metho		Method	
Law of c	cosines	Inclination-Space	e/Orb. Velocity	Historical PA/	Rot. angle
Gaia Sep	Period	Inclination	Period	Rotation	Period
AU	yrs	Angle ⁰	yrs	Angle ^o	yrs
900	7,574	45	9,301	0	10,140
	•	50	8,451	5	10,101
		55	7,543	10	9,985
		60	6,574	15	9,794
			•	20	9,528
1000	8,871	45	10,334		-
		50	9,390	Rotation angles are	
		55	8,381	for the 29deg angula	
		60	7,305	from the Sun to poir	nt X
1050	9,544	45	10,851		
		50	9,860		
		55	8,801		
		60	7,670		
1075	9,887	45	11,110		
		50	10,095		
		55	9,010		
		60	7,583		
1100	10,234	45	11,368		
		50	10,329		
		55	9,220		
		60	8,035		
1200	11,661	45	12,401		
		50	11,268		
		55	10,058		
		60	8,766		

Table 4. Three methods in deriving the orbital period. The best matches for separation, inclination angle/ $V_{\rm space}$, historical PA's and rotation angle are highlighted.

The results from the three methods in Table 4 show that the following quantities make a "best match" for BU 144's basic orbital elements:

Separation: 1,075 - 1,100 AU Period: $10,065 \pm 265$ yrs Inclination angle: $\approx 50^{\circ}$

Rotation angle/Longitude Ascending Node Ω : 0° to 5° (plus a correction of 30° for the angle at point X - see

Figure 3)

10. Discussion

Prior to the Gaia data releases, BU 144 was not considered a gravitationally bound binary system. This is due to the small historical position angle change of just 5.29°. Gaia's DR3 parallaxes have now given accurate distances to the components resulting in a physical separation range of 285AU–13,819AU. This data justified a new look at BU 144's possible binary status. Considering parallax errors, the component separations have an overlap of over 10,000AU. The radial velocities and proper motions give accurate space

velocities, and for specific cases, this provides an orbital period. The inclination angle/space velocity method provides an independent technique of estimating the orbital period. Figure 10 shows that the orbital period differences from Kepler's 3^{rd} law and the inclination/ V_{space} methods for the various separations are minimized as the inclination angle approaches 50° .

Is it possible that BU 144's components are just passing each other and by chance are close to each other on the celestial sphere? This is highly unlikely as the data shows: 1) the radial velocities are very similar, 2) the proper motions are very similar, 3) the space velocity of the components are very similar showing they are moving through space together in the same direction and 4) the masses and spectral types of the component stars are nearly identical. If BU 144's components were just passing by each other in space, the radial velocities, space velocities and proper motions would be quite different.

It is certainly possible that one of BU144's components captured the other millions of years ago. Over time, with their nearly identical masses, it is possible that the orbit would have stabilized into a nearly circular orbit.

Acknowledgements

An anonymous referee provided many helpful suggestions which were incorporated into the final version of this paper. Dr. Rachel Matson kindly provided the historical data from the *Washington Double Star Catalog* maintained at the US Naval Observatory. This work has made use of data from the European Space Agency (ESA) mission Gaia https://www.cosmos.esa.int/Gaia, processed by the Gaia Data Processing and Analysis Consortium, DPAC. Also acknowledged is the *Aladin Sky Atlas* interactive software program, the *SIMBAD Database* (updated daily) and the *VizieR* catalog (updated daily) http://vizier.cds.unistra.fr/viz-bin/VizieR-4 all maintained by the Center de Données Astronomiques in Strasbourg, France. The second *Palomar Observatory Sky Survey* (DSS2) was made by the California Institute of Technology with funds from the National Science Foundation, the National Geographic Society, the Sloan Foundation, the Samuel Oschin foundation, and the Eastman Kodak Corporation.

REFERENCES

Gaia Collaboration Vallenari, A., Brown, A.G.A., et.al., 2022, "Gaia Data Release 3: Summary of the Content and Survey Properties", Astronomy & Astrophysics No. AA4394-022 https://arxiv.org/pdf/2208.00211.pdf

Harshaw, R., 2016, "CCD Measurements of 141 Proper Motion Stars: The Autumn 2015 Observing Program at the Brilliant Sky Observatory, Part 3", Journal of Double Star Observations, Vol. 12, No. 4, pp. 394-399

Lang, K., 1992, "Astrophysical Data: Stars and Planets", Springer-Verlag, New York. ISBN 0-387-97104-2, p. 116.

Matson, R., Williams, S., Hartkopf, W., Mason, B., 2022," *Sixth Catalog of Orbits of Visual Binary Stars*", U.S. Naval Observatory, Washington, D.C., (updated frequently), http://www.astro.gsu.edu/wds/orb6.html

Miyashita, K. 2006, *Limovie*, *Light Measurement Tool for Occultation Observation Using Video Recorder*, https://ui.adsabs.harvard.edu/abs/2006RNAOJ...9....1M/abstract

Nugent R. and Iverson E., 2018, "Double Star Measures Using the Video Drift Method XI", Journal of Double Star Observations, Vol 14, No. 3, pp. 566-576

Pecaut, M., Mamajek, E., 2013, "Intrinsic Colors, Temperatures and Bolometric Corrections of Pre-Main Sequence Stars", Astrophysical Journal Supplement Series, 208:9

van Altena, W., Truen-liang Lee, Hoffleit, D. E., 1995, "The General Catalogue of Trigonometric Stellar Parallaxes", Fourth Edition, Yale University Observatory.

Measurements of 40 Neglected Stars - Report of December 2023

Joseph L. Carro Cuesta College, San Luis Obispo, California

Abstract

The position angles and separations of 40 neglected double stars were measured from photographs taken remotely. A neglected star is defined as a star which has at least one component with 10 or fewer measurements. The double stars were selected from the Washington Double Star Catalog, which is published by the United States Naval Observatory. When possible, comparisons were made with published data. The photographs were taken at the Open University located on the Canary Islands, Spain. The WDS data was current as of 1 November 2023. The data analyses were done by the author.

This research made use of the SIMBAD database operated by CDS, in Strasbourg, France, and the Washington Double Star Catalog maintained by the United States Naval Observatory.

Data about the Open University site

The observatory is in the Canary Islands, Spain at a latitude of 28 ° 17 '59 "N, a longitude of 16 ° 30' 30" W, and an altitude of 2,360 meters. on the island of Tenerife. The telescope is a 17" f/6.8 corrected Dall-Kirkham Astrograph equipped with an FLI Proline KAF-0900 CCD camera with broadband and narrow band filters mounted on a GM-4000.

Methodology

The photographs were reduced by the author using SKY X version 10.5.0 build 13479, a product of Bisque Software. Several factors, namely ambient temperature, humidity, wind, and visibility were not reported by the observatories. Not all photographs were useful, and the number of possible measurements for each star is reported. A literature search was performed for each star and the data sources were reported.

Report

The information included in this report consists of the WDS identifier, the constellation code, the discoverer code, the components, the position angle with standard deviation and standard error of the mean, the separation with standard deviation and standard error of the mean, the number of measurements, and the date of the most recent measurement. When no calculations were possible, the term "na" was used.

WDS/Constellation	Code/Component	PA / SD/ SEM	Sep / SD/ SEM	# of Obs	Date
08111+6952 UMA ¹	TDS 5604 AB	324.01/0.51/0.3	2.4/0.11/0.07	3	2023.9095
WDS		325	2.3	1	1991

08138+6306 UMA	LDS 2564 AB	112.59 na	245.1 na	1	2023.8658
WDS		113	244.5	10	2016
	RAO 60 BC	37.39	12.6	1	2023.8658
GAIA DR2 v3		36.76	12.78		2018
JDSO (Knapp) ³		36.652	12.833		2018
WDS		37	12.9	8	2015

08147+6326 UMA ¹	LDS 2565 AB	256.54 na	4.7 na	1	2023.8685
GAIA DR2 v3		256.14	4.77		2018
WDS		256	4.8	5	2016

Page 223

MDC/Constallation	6-1-16	DA /CD/CENA	Car / CD / CENA	11 - C Ol	D-1-
WDS/Constellation	Code/Component	PA / SD/ SEM	Sep / SD/ SEM	# of Obs.	Date
08158+6023 UMA	STF 1192 AD	193.7 na	98.6 na	1	2023.8685
WDS		194	98.4	4	2015
	T	1		T	1
08160+6907 UMA ¹	LDS 1674 AB	289.48 na	99.1 na	1	2023.8685
JDSO (Curelaru, +)		289.7	98.66		2011.780
WDS		290	98.8	8	2015
08167+6808 UMA ¹	LDS 2567 AB	103.51 na	5.6 na	1	2023.8685
GAIA DR2 v3		103.95	5.45		2018
WDS		104	5.4	5	2015
08169+6435 UMA ¹	LDS 2570 AB	92.35 na	35.1 na	1	2023.8685
WDS		93	35.4	8	2015
	•	•	•	•	
08188+6806 UMA	LDS 2571 AB	47.56 na	6.4 na	1	2023.8685
GAIA DR2 v3		48.15	6.33		2018
WDS		49	6.2	7	2015
08204+6549 UMA ¹	MLB 1072 AB	114.02 na	8.3 na	1	2023.8685
GAIA DR2 v3	-	114.38	8.35		2018
JDSO (Knapp)		114.272	8.407		20187
WDS		114	8.4	8	2015
		1 :			
08207+6236 UMA ¹	LDS 2573 AB	79.07 na	13.1 na	1	2023.8685
GAIA DR2 v3	250 2070 715	78.77	12.94	_	2018
WDS		79	12.9	7	2015
***************************************		7.5	12.5	,	2013
08236+6757 UMA ¹	LDS 2275 AB	246.45 na	20.1 na	1	2023.8685
WDS	LDS ZZ7 5 AD	248	19.7	7	2015
VVDS		240	15.7	/	2015
08239+6610 UMA ¹	GAT 1 AB	94.45/0.58/0.34	4.3/0.05/0.03	3	2023.9425
GAIA DR2 v3	GATTAB	92.60	4.2	3	2023.9423
		93.45	4.030		2012.079
JDSO (Gatewood, +)				4	
WDS		93	4.2	4	2015
00220 - 6750 - 1844	LDC 227C AD	227.54	12.2	4	2022 0005
08239+6750 UMA ¹	LDS 2276 AB	227.51 na	12.3 na	1	2023.8685
WDS		231	12.0	6	2015
24	1		1	T_	T
08244+6544 UMA ^{2,4}	LDS 2277 AB	48.37/0.09/0.06	14.8/0.01/0.006	3	2023.9425
GAIA DR2 v3		48.40	14.84		2018
JDSO (Knapp)		48.383	14.852		2018
WDS		48	14.8	6	2015

WDS/Constellation	Code/Component	PA / SD/ SEM	Sep / SD/ SEM	# of Obs.	Date
08259+6541 UMA	LDS 2278 AB	194.18/0.38/0.22	38.2/0.1/0.006	3	2023.9425
WDS		194	38.2	5	2015
	LDS 2278 BC	63.53/.0.23/0.13	4.2/0.2/0.11	3	2023.9425
GAIA DR2 v3		64.08	4.16		2018
WDS		64	4.2	5	2015
08266+6212 UMA ¹	LDS 2279 AB	330.71/1.08/0.62	9.9/0.17/0.1	3	2023.9507
GAIA DR2 v3		329.34	9.84		2018
WDS		329	9.8	7	2015
					<u>.</u>
08278+6653 UMA ¹	LDS 2281 AB	116.27/0.12/0.07	12.4/0.06/0.03	3	2023.9425
GAIA DR2 v3		116.44	12.47		2018
WDS		116	12.5	9	2016
08287+6350 UMA	UC 1677 AB	111.57/0.48/0.28	15.3/0.31/0.18	3	2023.9425
WDS		112	15.1	9	2016
				•	
09227+7020 UMA	TDS 529 AB	342.38/0.13/0.07	0.8 na	3	2023.8233
GAIA DR2 v3		341.93	0.81		2018
Tycho2		337.9	0.815		1991
WDS		342	0.8	3	2015
	DAM 1609 AC	119.25/0.21/0.12	4.5/0.06/0.03	3	2023.8233
WDS		119	4.5	1	2015
					_
09255+5055 UMA	TOI 1770 AB	32.39/0.07/0.04	4.9/0.06/0.03	3	2023.8575
WDS		32	4.9	1	2015
09327+5114 UMA	MTR 4 AB	16.21/0.06/0.04	11.7/0.1/0.06	3	2023.8233
WDS		16	11.7	1	2018
09593+4350 UMA	GIC 91 AB	88.36/0.52/0.30	22.9/0.17/0.10	3	2023.8548
JDSO (Knapp)		89.375	23.111		2018
WDS		89	23.1	9	2016
10084+6620 UMA	LDS 1235 Aa,Ab	166.21/0.17/0.1	3.7/0.05/0.03	3	2023.8233
WDS		167	3.6	3	2016
10269+6311 UMA ¹	TDS 7276 AB	131.83/0.46/0.23	2.7/0.13/0.06	4	2023.9397
WDS		133	2.7	1	1991
10339+4158 UMA	ES 1396 AB	190.11 na	5.6 na	1	2023.8795
GAIA DR2 v3		190.19	5.54		2018
JDSO (Schlimmer)		190.2	5.58		2180.340
•	•			ı	

WDS		190	5.6	11	2018
	l		l .		
WDS/Constellation	Code/Component	PA / SD/ SEM	Sep / SD/ SEM	# of Obs.	Date
11055+4332 UMA	VBS 18 AB	124.12 na	32.6 na	2	2023.8236
JDSO (Knapp)		125.484	32.26727		2020
WDS		125	32.0	11	2017
	1		T		1
11061+4253 UMA	GIC 97 AB	17.06 na	17.9 na	2	2023.8230
WDS		18	17.9	9	2016
	WND 25 AC	292.25 na	37.9 na	2	2023.8230
WDS		291	37.9	5	2015
	WND 25 BD	294.85 na	33.4 na	2	2023.8230
WDS		290	33.1	5	2015
	WND 25 CD	33.25 na	17.0 na	2	2023.8230
WDS		33	17.3	1	2016
44000,5344,1844	1DC 2020 AD	200.00 = -	75.4	2	2022 0222
11068+5214 UMA ¹	LDS 3028 AB	296.98 na	75.4 na	2	2023.9233
WDS		298	75.0	1	1960
11161+3329 UMA	GMZ 187 AB	116.02 na	4.4 na	2	2023.9233
WDS	GIVIZ 187 AB	116	4.5	1	2023.9233
VVD3		110	4.5	1	2010
11282+3313 UMA ¹	SEI 524 AB	153.83 na	7.9 na	2	2023.9233
WDS		154	8.1	1	1894
				,	
11381+3246 UMA ³	ES 2285 AB	331.41/0.65/0.37	10.6/0.36/0.21	3	2023.9233
GAIA DR2 v3		332.23	10.70		2018
JDSO (Schlimmer)		331.2	10.78		2022.416
JDSO (Knapp)		331.476	10.776		2018
Tycho2		336.2	10.38		1991
WDS		332	10.7	19	2015
	SIN 65 AC	156.95/0.72/0.42	16.6/0.15/0.08	3	2023.9233
WDS		1596	16.8	1	1989
	SIN 65 AD	2.06/0.10/0.06	74.3/0.2/0.11	3	2023.9233
WDS		3	73.8	1	1989
11571+2855 UMA ¹	TDS 8136 AB	309.16/0.11/0.06	3.8/0.03/0.03	3	2023.9507
Tycho2	103 0130 AD	309.10/0.11/0.00	3.75	, ,	1991
WDS		310	3.8	1	1991
VVDJ		310	5.0	-	1331
11590+2642 COM	UC2243 AB	168.31/0.08/0.05	44.7/0.1/0.06	3	2023.9425
WDS		169	44.4	10	2015
	•		•		
WDS/Constellation	Code/Component	PA / SD/ SEM	Sep / SD/ SEM	# of Obs.	Date
vv D3/ COHStellation	code/component	TA / JU/ JEIVI	Jeh / Ju/ JEIM	# 01 005.	Date

20152+1357 DEL ⁴	J 3066 AB	333.69/0.55/0.31	4.5/0.1/0.06	3	2023.8411
GAIA DR2 v3		333.48	4.53		2018
JDSO (Knapp)		336.580	4.394		2018
WDS		333	4.5	6	2016
	J 3066 AC	215.66/1.03/0.60	9.4/0.15/0.08	3	2023.8411
GAIA DR2 v3		215.83	9.31		2018
WDS		216	9.3	4	2015
	<u> </u>		•		
20155+1455 DEL ¹	BKO 544 AB	29.17 na	2.6 na	2	2023.7616
GAIA DR2 v3		29.41	2.59		2018
WDS		29	2.6	2	2015
	<u> </u>				
20156+1526 DEL	HDS 2887 AB	244.54/1.01/0.58	4.9/0.06/0.03	3	2023.7616
Tycho2		243.8	4.72		1991
WDS		244	4.7	2	1991
	CHE 246 AC	85.19/0.09/0.05	`	3	2023.7616
GAIA DR2 v3		85.60	15.99		2018
JDSO (Nugent)		87.0	15.9		2017
WDS		87	15.9	11	2016
	CVP 1 AD	340.04/0.39/0.27	40.2/0.15/0.09	3	2023.7616
WDS		340	39.7	8	2016
	-	1	1	П	
20157+1508 DEL	CHE 249 AB	347.44/0.09/0.05	22.9/0.16/0.07	3	2023.8411
GAIA DR2 v3		348.37	22.81		2018
WDS		349	22.6	6	2018
	-	1	1	П	- 1
20160+1510 DEL ¹	BKO 555 AB	201.49/0.53/0.30	4.6 na	3	2023.8411
GAIA DR2 v3		202.01	4.63		2018
WDS		202	4.6	4	2015
		·			
20166+1606 DEL ¹	CHE 263 AB	139.91/0.59/0.34	3.9/0.12/0.07	3	2023.8575
GAIA DR2 v3		139.58	3.96		2018
WDS		140	4.0	3	2015
	•	•	•	ı	•
20172+1553 DEL	CHE 273 AB	94.82/0.70/0.40	26.3/0.16/0.09	3	2023.8657
GAIA DR2 v3		94.48	26.78		2018
WDS		94	26.8	7	2015
	BKO 560 BC	200.26/0.67/0.39	1.8/0.06/0.03	3	2023.8657
GAIA DR2 v3		201.08	1.84		2018
WDS		199	1.4	1	2008
-	ı		l	1	

Notes

- 1. Stelle Doppie reported that the status of this pair is uncertain.
- 2. Stelle Doppie reported that this pair is not physical.
- 3. Knapp reported that this pair is "almost certainly optical".
- 4. Knapp reported that this pair is "probably optical".

WDS 09593+4350

Components AC, AD and BE could not be identified from two photographs taken with 90 second exposure each.

WDS 10084+6620, 11055+4332

Components AB could not be identified from two photographs taken with 30 second exposure each.

WDS 08120+6907, 08128+6306, 08155+6349, 08160+6907, 08211+6008, 08211+6008, 20155+1455,

20157+1457, 20157+1509, 20158+1510, 20161+1552, 20165+1601, 20232+0957,

20253+0847, 20254+0700, 20258+0818

No pairs were found in two photographs of 30 second exposure each.

WDS 11055+4332, 20157+1508, 20157+1508

Component AC could not be found in two photographs of 30 second exposure each.

WDS 10339+4158, 11381+3246

The values in GAIA for the components AB and AC are identical.

Components AC and AD could not be identified from two photographs taken with 60 second exposure each.

References

Curelaru, L, +, Neglected Double Star Measurements, JDSO, 2012, p204.

GAIA DR2 v3 data catalog as available from http://cdn.gea.esac.esa.int/Gaia/P

Gatewood, G. Gatewood, C., Near IR Measurements of Double Stars, JDSO 2012, p337

Knapp, W., "WDSvsUCAC5 II.xlsx", Journal of Double Star Observations, 2018

Knapp, W., Star Systems in the Solar Neighborhood up to 10 Parsecs Distance, JDSO, 2020, p286

Mason, B., Washington Double Star Catalog http://www.astro.gsu.edu/wds/

Nugent, R., Double Star Measures Using the Video Drift Method, JDSO, 2017, p325

Schlimmer, J., Double Star Measurements Annual Report, JDSO, 2018, p540

Tycho-2 Catalog as published on their websitet

Website of Stelle Doppie http://stelledoppie.it/

Determining the Gravitationally Bound and Optical Components of Quadruple System WDS 18136-1536

Sierra Kasl-Godley¹, Dylana Wagorn², Joshua Curiel³, Shannon Pangalos-Scott^{2,6}, Alexander Vasquez^{2,7}, Dag Harmsen⁴, Bebe Simone Hart², Rachel Freed⁵, Rebecca Chamberlain²

- 1. University of Washington, Seattle, WA
- 2. The Evergreen State College, Olympia, WA
- 3. Los Angeles Mission College, Sylmar, CA
- 4. University of Munster, Germany
- 5. Institute for Student Astronomical Research, Sonoma, CA
- 6. Quadrivium STEAM & Astronomical Society, Olympia, WA
- 7. The Evoked Scion Institute, Lacey, WA

Abstract

Data was collected for the quadruple system, WDS 18136-1536, where according to Stelle Doppie the nature of this system was previously uncertain. New images were obtained using the Las Cumbres Observatory global telescope network. The current separations and position angles were measured with Skynet's Afterglow Access and compared with historical records from the United States Naval Observatory. The AB separation was found to be 2.96 arcseconds and the position angle was found to be 275.74 degrees. Based on the parallax and proper motion values retrieved from the Gaia catalog, it has been determined that the AB pair are likely gravitationally bound, and the C and D components are only optically aligned.

1. Introduction

WDS 18136-1536, is a quadruple system in the constellation of Serpens Cauda, and is located at a right ascension of 18^h 13^m 35.49^s , and at a declination of -15° 35' 54.1''. The research objective was to examine and determine the nature and relationships of the gravitationally bound and optical components of this quadruple system. Historical records of the AB pair were first recorded in 1873 by American astronomer, Sherburne Wesley Burnham. These measurements gave a separation of (ρ) 2.0", with a position angle (θ) of 270° (Burnham, 1873). The primary star of this system has a magnitude of 7.54, the secondary star has a magnitude of 11.75 (Stelle Doppie). In 1880 the tertiary star (C) of this system was discovered, also by Burnham, with an 11.75 magnitude. The AC pair was first recorded with a separation of 7.1", and a position angle of 279°, and a delta magnitude of 4.21. The BC pair was recorded with a separation of 4.6", and a position angle of 278°. Thirty-three years later in 1913, the quaternary star (D) was discovered by Phillip Fox (Fox, 1925), with a magnitude of 12.52. The AD pair was first recorded with a separation of 35.0" and a position angle of 36°. The nature of each of these component pairs is logged in Stelle Doppie (Stelle Doppie) as "Uncertain."

Several of the team researchers attended the "Astronomy and Cosmology: Stars and Stories" program at the Evergreen State College in Olympia, Washington. As part of the astronomy field studies, mentor Alexander Vasquez took the photo shown in Figure 1 of this multiple-star system (circled in red) in Serpens Cauda.

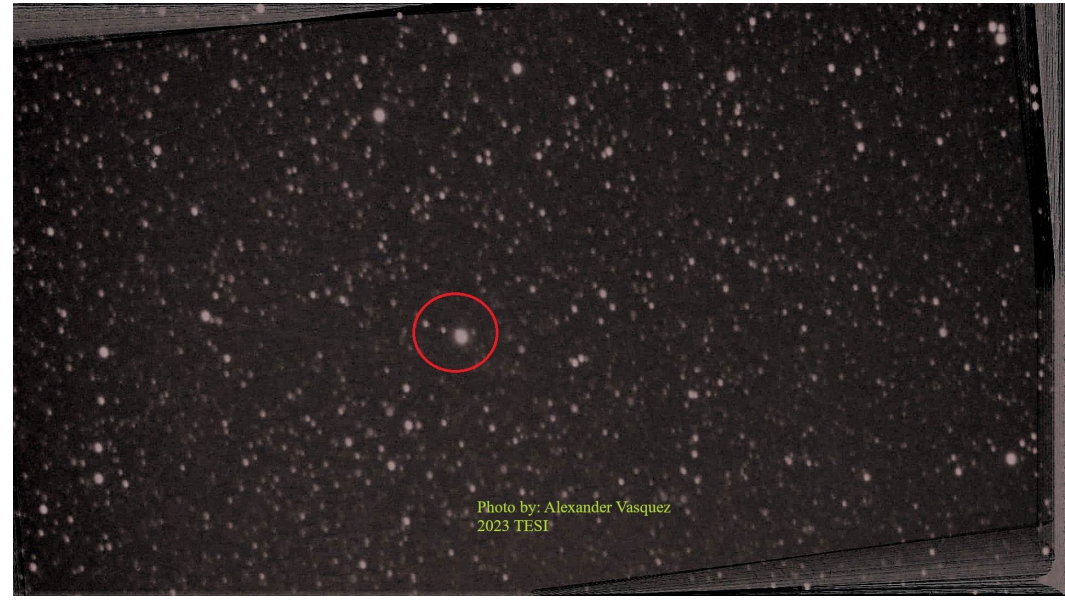


Figure 1: Dwarf2 Digital telescope (Sensor: SONY IMX415 Starvis 8 Megapixel, AD:24mm, FL(equiv.):100mm(675mm) F4.2, FOV:3°) (2*2 binning, FITS, exp:2secs, Gain:70, Shots Taken: 238, Stacked:222) Coords: 47.0730 -122.9762, Bortle:5. Image taken at the Evergreen State College, Olympia, Washington. Alexander Vasquez, 07/27/2023.

2. Equipment and Procedure

WDS 18136-1536 was selected by utilizing the Advanced Search selection tool available through Stelle Doppie, given the parameters specified in Table 1. The search was narrowed through this filter, and it was eventually decided that there was merit in doing further observations of this quadruple star system.

	RA	Dec	Pri. Mag	Sec. Mag	∆ Mag	Sep.	Last Observed
Min.	13h 00m 00s	N/A	9	-	0	5"	Defere 2045
Max.	23h 00m 00s	N/A	11	-	3	10"	Before 2015

Table 1: Parameters used to select WDS 18136-1536 in the Stelle Doppie Database Selection Tool. Declination did not need to be specified because the telescope network has telescopes in the northern and southern hemispheres.

Once a candidate was selected, an observation request for images was submitted to the Las Cumbres Observatory global telescope network (LCO). On July 16, 2023, sample images were requested with a 1-sec., 5-sec., 7-sec., and a 10-sec. exposure time, using a Bessel-V (visible) filter. A 0.4-meter robotic telescope located at the Teide observatory in Tenerife, Canary Islands, Spain provided these images. After evaluation, it was determined that a 1-sec. exposure time would provide optimal contrast with minimal visual noise. On August 22, 2023, ten additional images with a 1-sec. exposure time and a Bessel-V filter were requested. The 0.4-meter telescope at the Haleakala Observatory on the island of Maui, Hawaii, provided these images using the site's SBIG STL6303 CCD camera.

Of these ten images, the FITS files of two were of sufficient resolution and were analyzed with the image analysis software, Skynet's Afterglow Access (Reichart, 2021), to determine the current position angle and separation of the stars within this system. Afterglow Workbench's plotter tool was used for these measurements as shown in Figure 2.

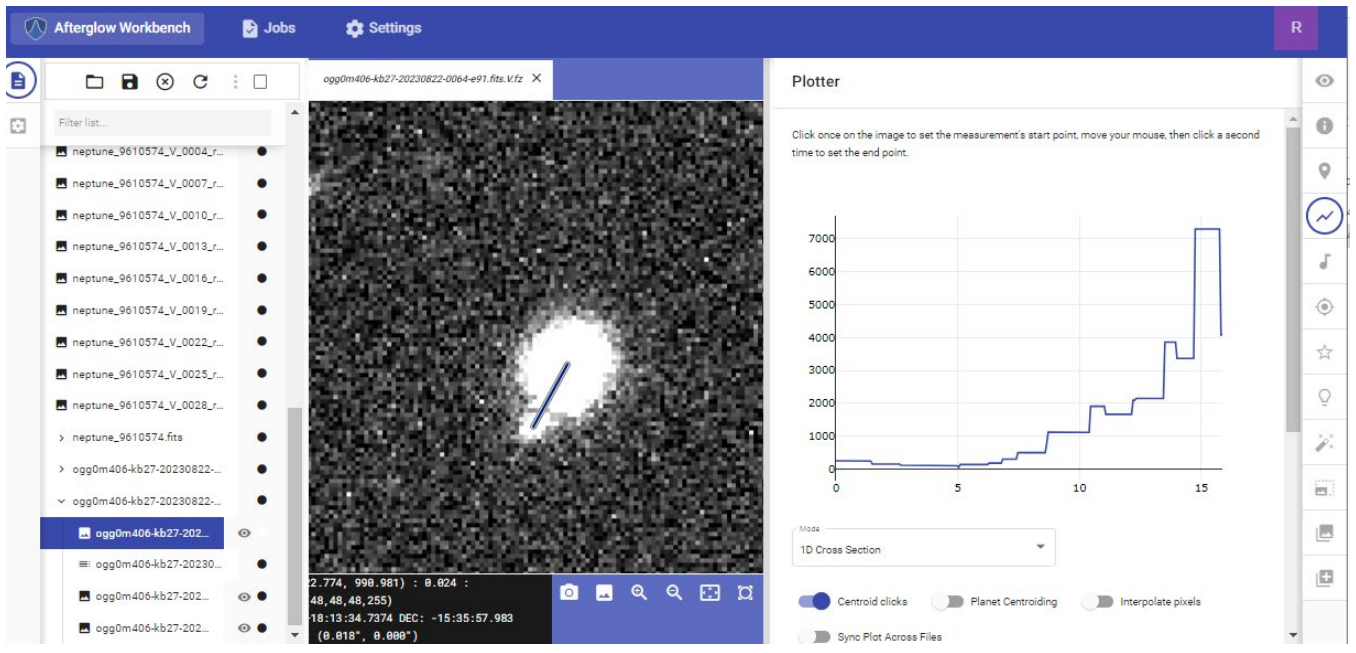


Figure 2: Afterglow Access was used to measure the position angle and separation of the components of WDS 18136-1536.

Though the primary and secondary stars appear unresolved, Afterglow was able to determine the individual centroids in three of the images, as indicated by the measurement line between A's centroid and B's centroid as shown in Figure 3.

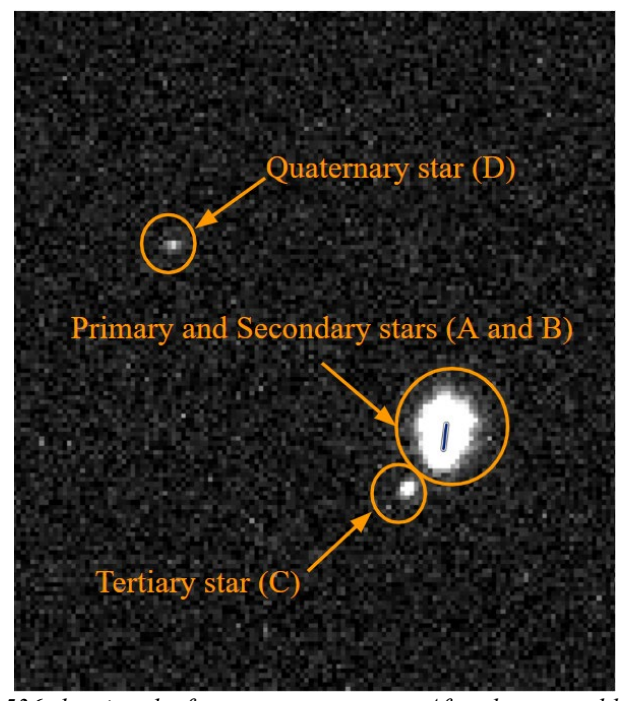


Figure 3: Image of WDS 18136-1536 showing the four component stars. Afterglow was able to determine the individual centroids in several of our images, as indicated by the measurement line between A's centroid and B's centroid.

Historical data for the position angle and separation was requested from Dr. Rachel Matson of the United States Naval Observatory (USNO) and compared to current astrometric measurements. Finally, the VizieR catalog was referenced (Vizier, 2022), and data from the Gaia DR3 for the components of WDS 18136-1536 were retrieved (Table 4). Further information about the components of the quadruple star system was gathered using Simbad's collection of images (Table 4).

3. Results

Images were collected on July 16th and August 22nd, 2023 as shown in Table 2 below.

Image #	File name	Date
1	tfn0m410-kb24-20230716-0116-e91.fits.fz	2023-07-16
2	ogg0m406-kb27-20230821-0058-e00.fits.fz	2023-08-22
3	ogg0m406-kb27-20230821-0061-e00.fits.fz	2023-08-22

Table 2: Summary of images received from LCO, used to determine the current position angles and separations for WDS 18136-1536 and their respective dates.

Data analysis of 3 images resulted in a mean separation of 2.96 arcseconds and a position angle of 275.74 degrees for the AB pair. The standard deviation and standard error of the mean were calculated for all four component pairs and are displayed in Table 3.

АВ	Sep. (arcseconds)	PA (degrees)
Mean	2.96	275.74
St. Dev.	0.15	1.49
Error	0.08	0.86

AC	Sep. (arcseconds)	PA (degrees)
Mean	9.00	301.05
St. Dev.	0.26	0.09
Error	0.15	0.05

ВС	Sep. (arcseconds)	PA (degrees)
Mean	6.45	312.32
St. Dev.	0.13	0.54
Error	0.08	0.31

AD	Sep. (arcseconds)	PA (degrees)
Mean	41.64	33.830
St. Dev.	0.81	0.29
Error	0.47	0.17

Table 3: Summary of data analyzed via Afterglow Access for the four different components.

The current right ascension and declination of the AB pair was plotted with the historical data provided by the USNO by converting measurements from polar to cartesian coordinates (Figure 4). The current data point is indicated in orange.

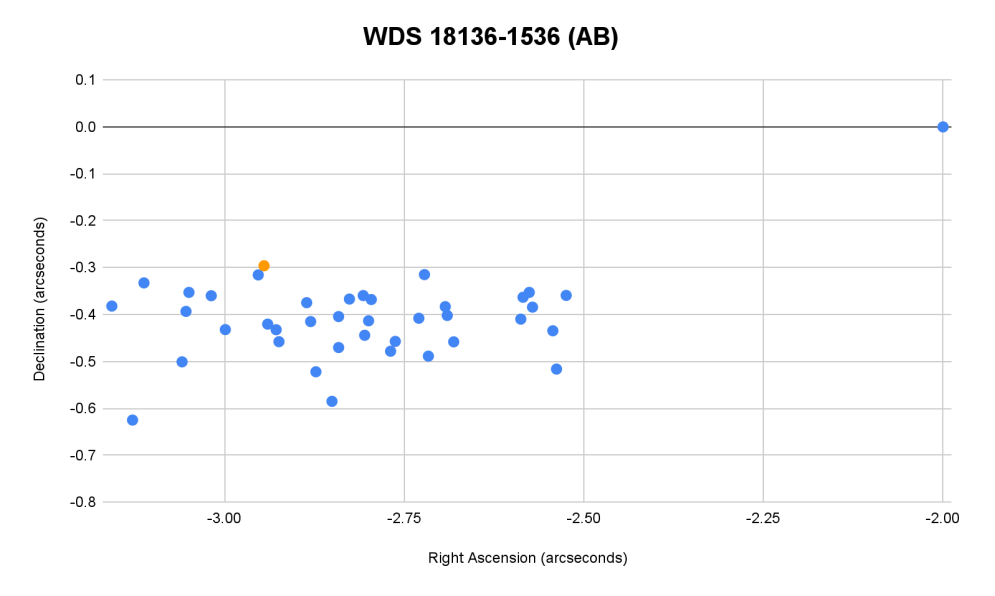


Figure 4: Plot of WDS 18136-1536 (AB) historical data (blue dots) and current data (orange dot).

4. Discussion

AB

The current position angle and separation for the AB components in this system are 275.74 degrees and 2.96 arcseconds. It was concluded that Afterglow Access could not distinguish between the A and B centroids when images were taken with 5-sec. exposures. Images with 1-sec. exposures were of sufficient resolution to distinguish an A and B centroid, and thus a position angle and separation could be measured.

According to the historical data from the USNO, the measurement of the AB components of this star last occurred in 2005. The reported position angle and separation were 276.9 degrees and 3.18 arcseconds, respectively. The current observation—indicated in orange (Figure 5)—does not indicate any major change from the 2005 observation. According to Figure 5, there is a slight overall downward trend in the position angle and a slight overall upward trend in the separation. The current data point matches these overall trends. The initial observation from 1873 does not appear to follow either of these trends, suggesting it is an outlier.

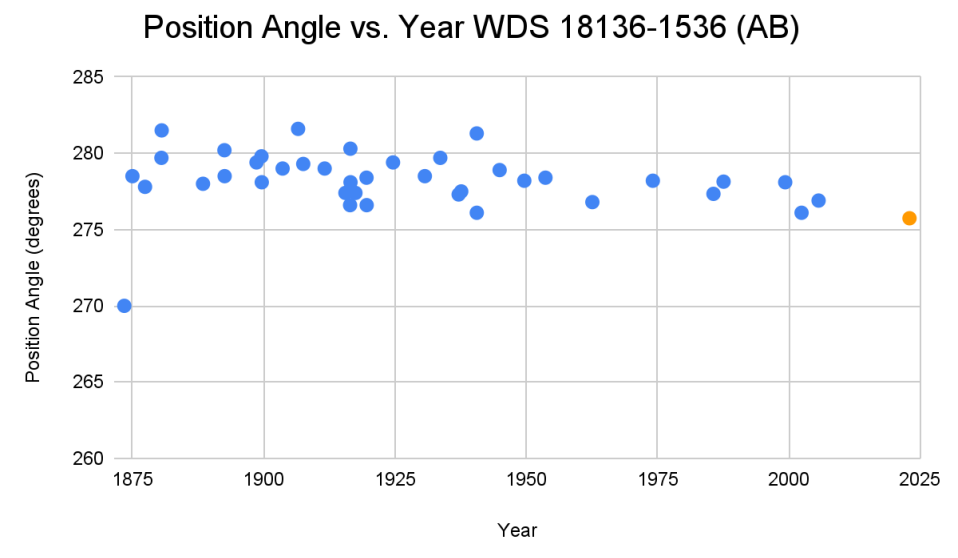
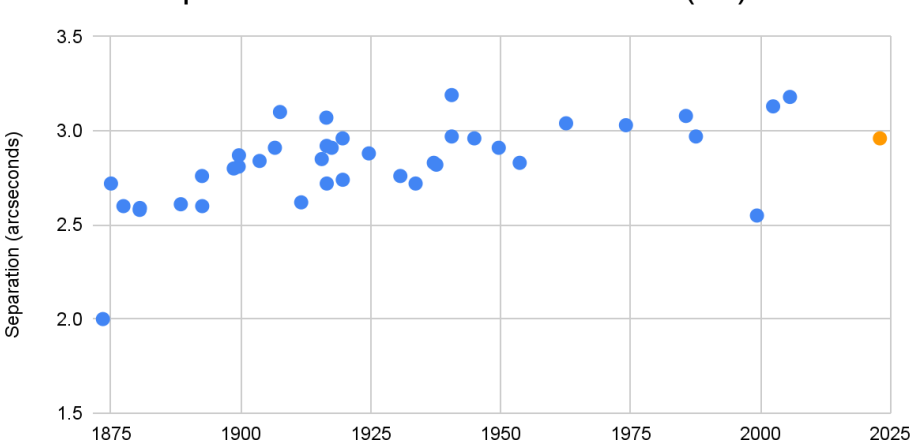


Figure 5: Position angle of WDS 18136-1536 (AB) as a function of time beginning in 1873. The most recent observation from 2023 is indicated in orange.



Separation vs. Year WDS 18136-1536 (AB)

Figure 6: Separation of WDS 18136-1536 (AB) as a function of time beginning in 1873. The most recent observation from 2023 is indicated in orange.

When the parallax values and the proper motions in right ascension and declination of the individual components were compared using Gaia DR3 data, noticeable similarities and differences were analyzed (Table 4). Components A and B are at the same distance from Earth based on their parallax values of 13.55 and 13.81 mas, respectively (Table 4). This suggests that they could be gravitationally bound. Their proper motions in declination are similar, at -29.615 and -30.801 mas/yr, while their proper motions in right ascension differ significantly at 3.58 and 0.74 mas/yr.

Designation in Gaia DR3	A 414581449358 5839744	B 414581449357 2563328	C 414581449358 5843712	D 414581452360 9659520
Parallax (mas)	13.55 ± 0.2	13.81 ± 0.01	0.40 ± 0.03	0.83 ± 0.01
Proper Motion in RA (mas/yr μ)	3.58 ± 0.24	0.74 ± 0.02	-1.04 ± 0.03	3.26 ± 0.02
Proper Motion in Dec (mas/yr μ)	-29.62 ± 0.17	-30.80 ± 0.02	-3.83 ± 0.02	-9.7 ± 0.02

Table 4: Parallax and Proper Motion (μ) data retrieved from the VizieR Catalog and Simbad.

CD

Based on the data retrieved from Gaia for the C and D components, these two stars are not gravitationally bound to the A and B components (Table 3). The parallax values are 0.4048 and 0.8298 mas, respectively, which is too dissimilar from 13 milliarcseconds for these stars to be gravitationally bound. The proper motions in RA are -1.044 and 3.255 mas/yr. The proper motions in declination are -3.825 and -9.695 mas/yr. The parallax values indicate that the C and D stars do not interact with the AB pair (Harshaw, 2018).

5. Conclusions

Analysis of the data obtained from Gaia DR3 put the A and B components at similar distances from Earth, suggesting that they could be a gravitationally bound pair, or at least a common proper motion pair. The C and D components are not at this same distance, making it extremely unlikely for there to be a gravitational interaction between all four components. The current data for position angle and separation of the AB pair align with the overall historical trends and have not changed significantly since the system was previously observed in 2005. Further observation of this system is necessary to clarify the nature of the AB pair.

Acknowledgments

This research was made possible by the continuing support from the Las Cumbres Observatory who provided digital images for our analysis and Dr. Rachel Matson of the U.S. Naval Observatory who provided this system's historical data. The Washington Double Star Catalog, The European Space Agency Gaia Archive, and Stelle Doppie provided technical information on this system's individual star components. We acknowledge our institutions and those who helped us facilitate this research opportunity. From The Evergreen State College, we thank Ryan Geiser, Evergreen student and mentor in "Astronomy and Cosmology: Stars and Stories," who participated in the research.

References

- Burnham, S. W. (1873). A third catalog of 76 double stars discovered with a 6-inch Alvan Clark refractor. Monthly Notices of the Royal Astronomical Society, Vol. 34, p. 59, 34, 59.
- Fox, P. (1925). Measures of Double Stars. Annals of the Dearborn Observatory, 2, 1-219.
- Gaia DR3 content Gaia Cosmos. (2022). GAIA EARLY DATA RELEASE 3 (GAIA DR3). Retrieved July 16, 2023, from https://www.cosmos.esa.int/web/gaia/earlydr3
- Harshaw, R. (2018). Gaia DR2 and the Washington Double Star Catalog: A Tale of Two Databases. Journal of Double Star Observations. Vol 14, No 4.
- Reichart, D. E. (2021). Robotic telescope labs for survey-level undergraduates. The Physics Teacher, 59(9), 728–729. https://doi.org/10.1119/10.0007416
- Stelle Doppie Double Star Database. (2022). Stelle Doppie. Retrieved July 16, 2023, from https://www.stelledoppie.it/index2.php?iddoppia=73722
- VizieR. (2022). VizieR. Retrieved July 16, 2023, from https://vizier.cds.unistra.fr/viz-bin/VizieR

Astrometric Measurements of WDS 18175-1638 HJ 2829 AB, AC

Joseph Leeber, Tristan May Advanced Math and Science Academy Charter School

Abstract

The goal of this research project is to make astrometric measurements of WDS 18175-1638 HJ 2829 AB and AC. By taking photos and making new measurements we found that for pair AB, the new position angle was 320° and the new separation is 4.92 arcseconds. For pair AC, the new position angle that we measured was 168.2° and the new separation of the two stars is 6.2 arcseconds. In the end we found that there is a likely chance of AB being a common proper motion double and that AC may be optical due to the lack of sufficient evidence.

1. Introduction

For this paper we intend to gather information on WDS 18175-1638 HJ 2829 AB and AC to help determine if either pair is a physical or optical double. We chose this star system because the magnitude was sufficient for our observations and the fact that it was a triple star system was interesting because it could contain either two physical or optical doubles or one of each. This triple star system was first observed in 1830 and since then has been observed five additional times including our new observation.

2. Equipment and Methods

After finding a sufficient star system we requested images from Las Cumbres Observatory (LCO) using their 0.4-meter telescope and SBIG 6303 camera at Haleakala Observatory. Utilizing their PanSTARRS-w filter we took ten images with multiple exposure times, with that we found that an exposure time of 4 seconds gave us the best quality images. The images were calibrated with LCO's BANZAI pipeline system and were taken on September 28th, 2023 (2023.945). With these images we used *AstroImageJ* (Collins 2017) to measure our stars' separation (ρ) and position angle (θ) (refer to Figure 1 & 2). We calculated their average values, standard deviation, and standard error (refer to Table 1 & 3).

Vol 20 No 2 April 1, 2024

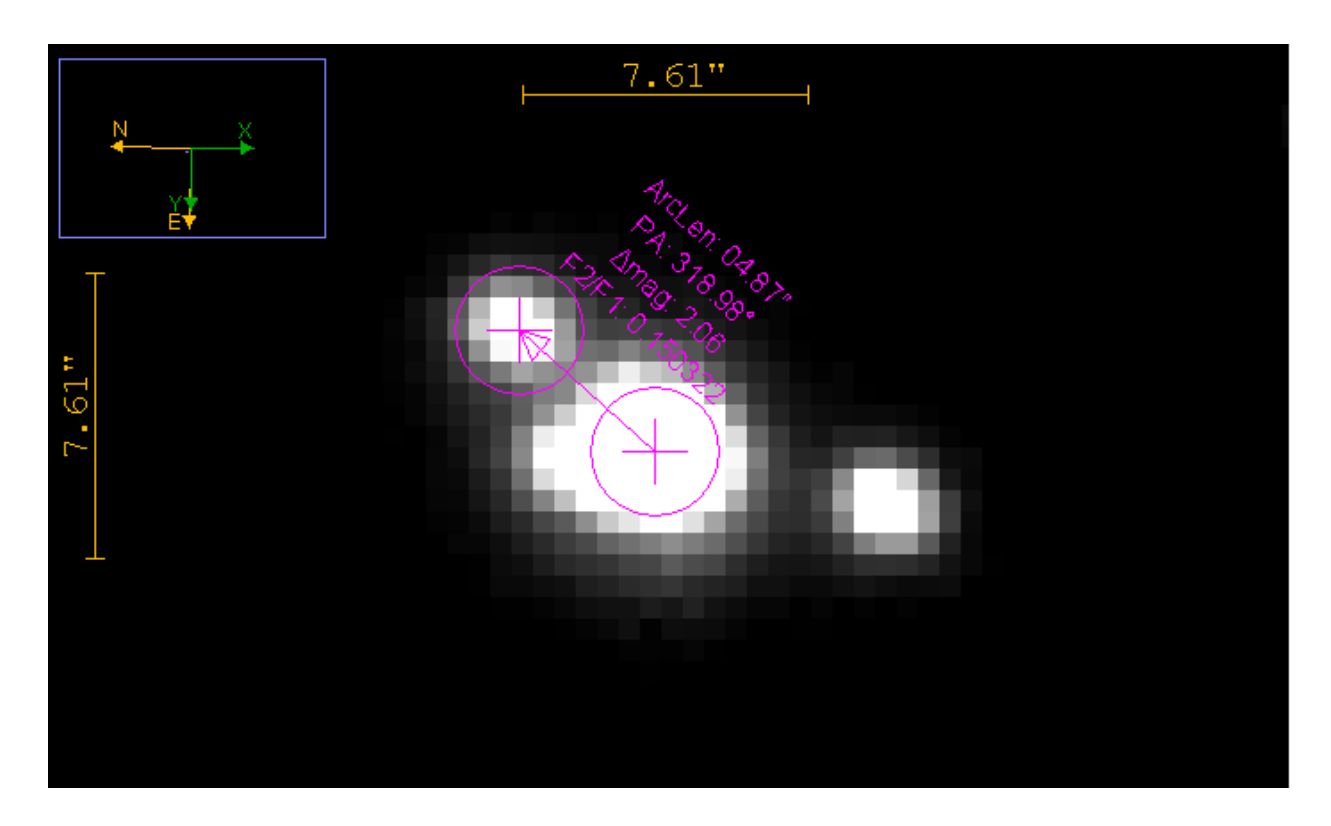


Figure 2: Shown here is an image of our star pair AB in the program AstroImageJ with the program's measurements of the position angle and separation.

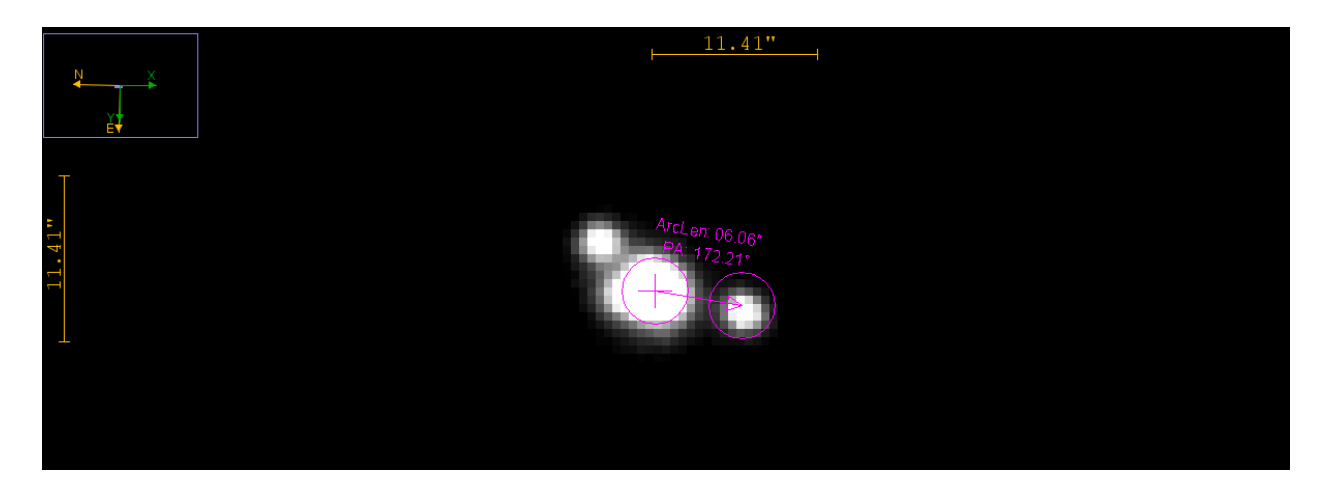


Figure 2: Shown here is an image of our star pair AC in the program AstroImageJ with the program's measurements of the position angle and separation.

3. Data

For the AB pair, the average position angle was 320° and average separation was 4.92 arcseconds. For AC, the average position angle was 168.2° and average separation was 6.2 arcseconds. Also, we requested the historical data (refer to table 2 & 4) for this system from Washington Double Star Catalog. After discarding any incomplete data, we placed it in Plot Tool (Harshaw 2020) and made several graphs based on the data (refer to Tables 1 & 2.) In Figures 3 & 4 we enlarged the graph to get a better look at both stars' paths around the main star.

Table 1: New measurements of WDS 18175-1638 HJ 2829 AB.

Image	Position Angle(°)	Separation (")
1	319.5	4.87
2	321.2	4.98
3	320.3	4.94
4	319.4	4.80
5	320.1	4.90
6	320.1	4.85
7	318.7	4.89
8	320.1	5.11
Average =	320.0	4.92
ST DEV=	0.7	0.16
ST ERROR=	0.2	0.03

Table 2: The historical Data of WDS 18175-1638 HJ 2829 AB.

Year	Position Angle (°)	Separation (")	Made By	Type
1830.57	300	2.5	НЈ-1833с	Mb
1903.57	322.3	5.25	BU-1906	Ma
1999.33	320.1	4.89	TMA2003	E2
2015.0	320.225	4.989	Kpp2018m	Hg
2023.945	319.9	4.92	AMSA	CCD

Table 3: New measurements of WDS 18175-1638 HJ 2829 AC.

Image	Position Angle (°)	Separation (")
1	168.1	6.27
2	168.5	6.24
3	168.1	6.28
4	168.2	6.20
5	168.5	6.25
6	168.4	6.26
7	168.1	6.23
8	167.9	6.234
Average =	168.2	6.2
ST DEV=	0.2	0.02
ST ERROR=	0.1	0.01

Table 4: The historical Data of WDS 18175-1638 HJ 2829 AC.

Year	Position Angle (°)	Separation (")	Made By	Type
1830.57	150.	3.5	HJ_1833	Mb
1903.57	165.2	6.32	Bu_1906	Ma
1999.33	167.3	6.33	TMA2003	E2
2000.262	167.3	6.30	UC_2013	Eu
2015.0	167.406	6.27	Kpp2018	Hg
2023.945	168.3	6.24	AMSA	CCD

Table 5: Data taken from Gaia mission Data Release 3.

Stars	Parallax (mas)	Proper Motion Right Ascension (mas/yr)	Proper Motion Declination (mas/yr)
A	0.5767	0.099	-1.489
В	0.5047	0.108	-1.534
С	0.7419	0.253	-1.203

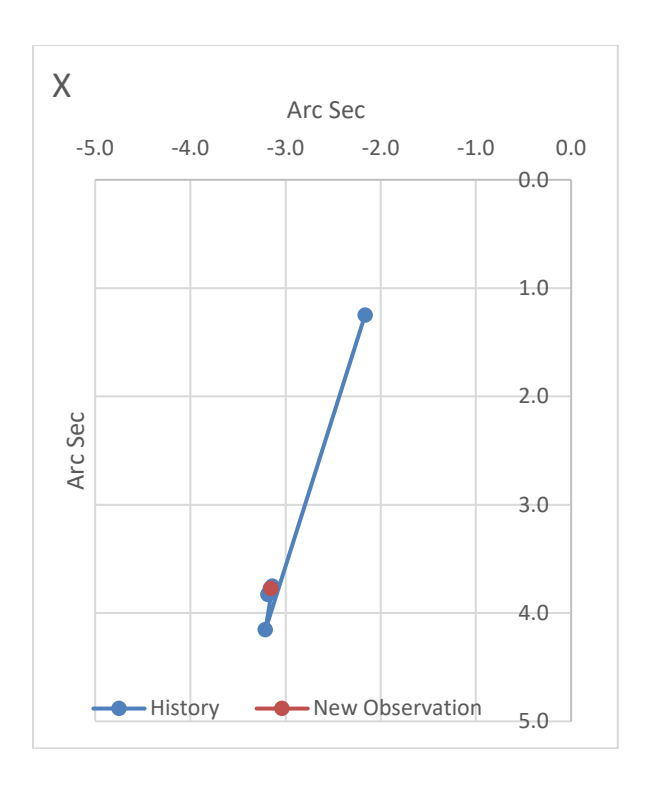


Figure 3: All Historical data and new data of AB presented together. New data represented by the orange dot. The primary star is at (0,0).

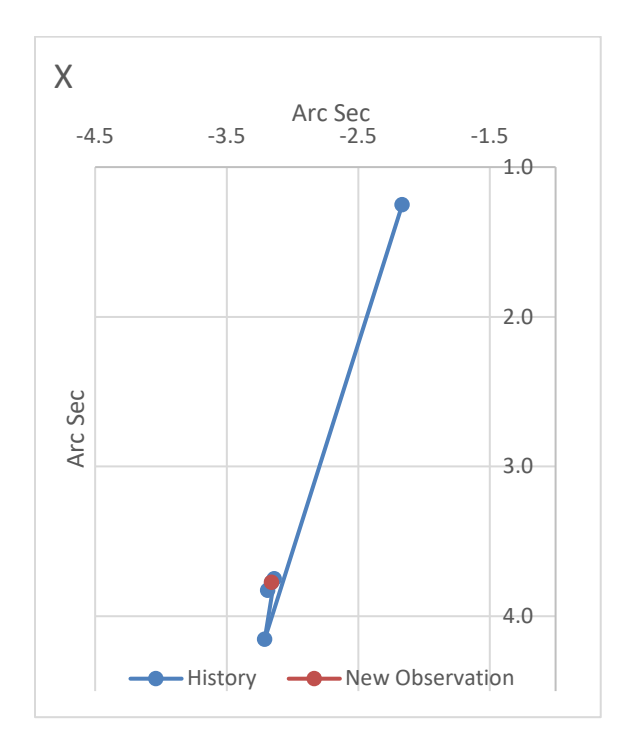


Figure 4: All Historical data and new data of AB presented together zoomed in. New data is represented by the orange dot.

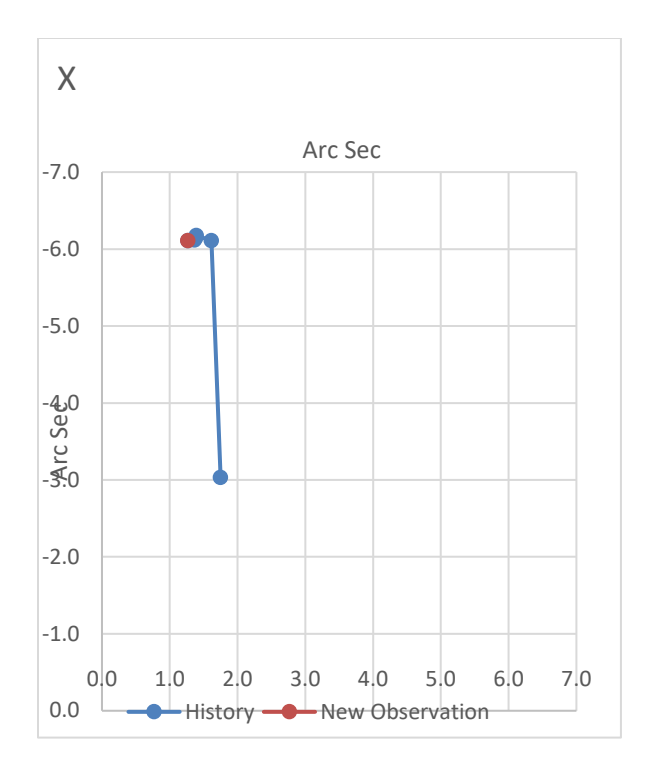


Figure 5: All Historical data and new data of AC presented together. New data represented by the orange dot.

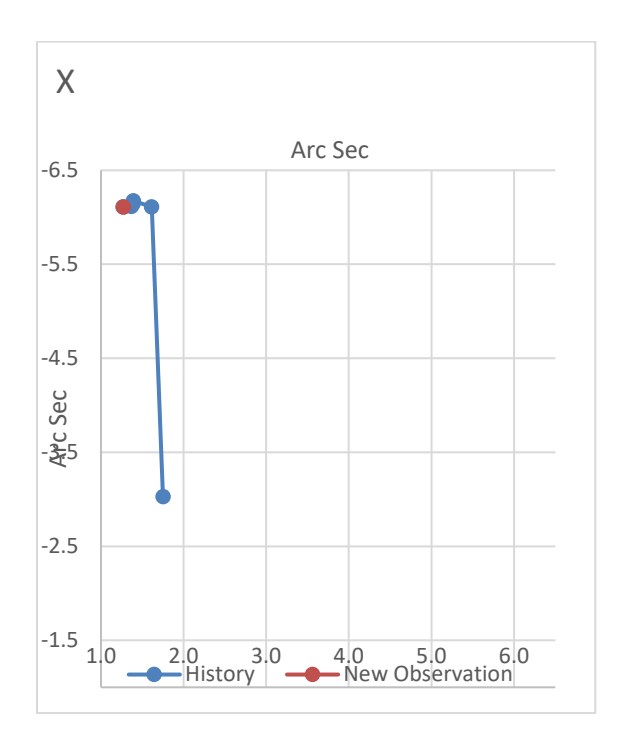


Figure 6: All Historical data and new data of AC presented together zoomed in. New data is represented by the orange dot.

4. Discussion

Both pairs AB and AC have the first data point from 1830, In this time astrometric tools and measurements were less accurate. If the 1830 points are disregarded, both pairs would show less than half an arcsecond of motion in the span of 1900 to 2023. Pair AB shows a slight amount of zig-zag motion in that time, presumably due to measurement error. Pair AC does go in one direction consistently, but it still is only about a half arcsecond in the span of 120 years. In general, neither historical data graph is especially helpful in identifying the nature of these pairs. Still, as both paths appear to be linear this could point to an optical double, a common proper motion double, or an edge-on binary.

The parallax and proper motion data in Table 5 from the Gaia mission was more helpful in providing a plausible answer with how accurate our instruments are today. The parallax and proper motion of stars AB are very close, having a percent difference of 12% parallax, 9% PM right ascension, and 3% PM declination. Pair AC on the other hand has percent differences of 28% parallax, 150% right ascension, 19% declination. For these reasons, we recommend classifying AB as a common proper motion double star system, while AC is probably an optical double.

5. Conclusions

The separation and position angle were measured for WDS 18175-1638 HJ 2829 AB and AC by measuring data given from photos taken. The separation and position angle did not provide any obvious conclusions but the Gaia data advocates for star pair AB to be a common proper motion double (CPMD) and star pair AC to be an optical double. However, we cannot say either of these with a high degree of confidence.

Acknowledgements

This work presents results from the European Space Agency (ESA) space mission Gaia. Gaia data are being processed by the Gaia Data Processing and Analysis Consortium (DPAC). Funding for the DPAC is provided by national institutions, in particular the institutions participating in the Gaia Multilateral Agreement (MLA). The Gaia mission website is https://www.cosmos.esa.int/gaia. The Gaia archive website is https://archives.esac.esa.int/gaia.

This research has made use of the Washington Double Star Catalog maintained at the U.S. Naval Observatory. We would especially like to thank Dr. Rachel Matson who has provided us with data and helped guide us as well. Image taken with 0.4-meter telescope and SBIG 6303 camera at Haleakala Observatory operated by Las Cumbres Observatory.

This research made use of the Stelle Doppie double star database maintained by Gianluca Sordiglioni.

References

Collins, K., Kielkopf, J., Stassun, K., & Hessman, F. (2017) AstroImageJ: Image Processing and Photometric Extraction for Ultra-precise Astronomical Light Curves. Astronomical Journal, 153, 77. Retrieved from https://ui.adsabs.harvard.edu/abs/2017AJ....153...77C/abstract

Harshaw R. (2020) Using Plot Tool 3.19 to Generate Graphical Representations of the Historical Measurement Data. Journal of Double star Observations, 16(4), 386-400. Retrieved from http://www.jdso.org/volume16/number4/Harshaw 386 400.pdf

Measurements of the Position Angle and Separation of Two Pairs in WDS 21406+5419 ES 35, an 11-Fold System

Ian Gifford, Vaishak Pulkayath

¹Advanced Math and Science Academy, Marlborough, Massachusetts

igifford2024@student.amsacs.org

Abstract

New measurements were made for three stars within the 11-fold star system WDS 21406+5419 ES 35. Specifically, we analyzed the AC and the plausibility of a BC pair. By looking at the historical data, new measurements, and graphs of both pairs, we were able to find evidence for the AC pair being a common proper motion double and believe the BC pair is likely not a physical double.

1. Introduction

WDS 21406+5419, Figure 1, is an 11-fold system with a variable primary star possibly consisting of some physical double stars. The size of the system provided a unique prospect for observation. In our images we were able to observe most stars in the system with our eyes. We could make out very faint marking that we assumed were the stars in the system by looking at previous images, but the contrast of our specific images was not large enough for AstroImageJ to analyze all of them. AstroImageJ was able to detect and measure the A, B, and C stars only. The AB pair was first observed in 1900 by British astronomer Rev. T.E. Espin. It was observed 11 times until 2014 and found to not be a physical double as indicated in the WDS catalog. The AC pair was first observed in 1898 by S.E. Urban and T.E. Corbin, and it was observed 18 times until 2014. The nature of the AC pair is uncertain. Most of this paper will be analyzing the AC pair.

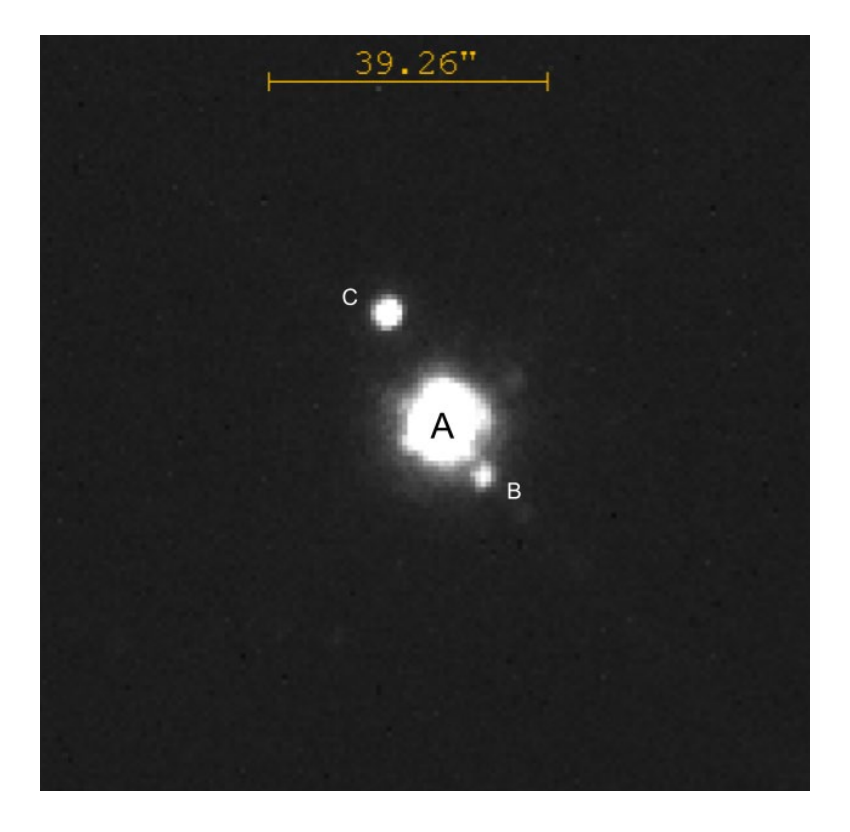


Figure 1: Image of the A, B, and C stars of the WDS 21406+5419 star system from AstroImageJ

2. Equipment and Methods

We took ten images of the star system each with one second of exposure time on 2023.7356 using the Pan-STARRS w filter. We originally tried six and two second exposure times, but the primary star was overexposed. All the images were taken at the Haleakala Observatory through the Las Cumbres Observatory's global network of telescopes. We used a 0.4-meter telescope that has a QHY600 camera system with an FOV of 1.9 x 1.2 arcmin and a pixel size of 0.73 arcsecs. The images were calibrated using the LCO's automatic BANZAI pipeline. Measurements of the separation and position angle were made using AstroImageJ (Collins 2017). After the measurements were made, we calculated the average and standard deviation values. We also requested the historical data of the system from Dr. Rachel Matson at the U.S. Naval Observatory. Finally, we plotted the historical data and our measurements using Richard Harshaw's *Plot Tool* (Harshaw 2022).

3. Data

Tables 1-3 show data for the AC pair. Table 1 shows our ten measurements, Table 2 shows summary statistics, and Table 3 shows the historical data. Tables 4-6 show data for the AB pair. Table 4 shows our ten measurements, Table 5 shows summary statistics, and Table 6 shows the historical data. Table 7 shows the data for all three stars from the Gaia DR3 release (Gaia Collaboration 2023j).

Table 1. WDS 21406+5419 ES 35 AC measurements.

Position Angle (°)	Separation (")
17.8	17.76
17.7	17.69
17.6	17.61
17.7	17.70
17.8	17.79
17.7	17.69
17.6	17.63
17.7	17.73
17.7	17.66
17.8	17.77

Table 2. Average, standard deviation, and error values of WDS 21406+5419 ES 35 AC.

	Position Angle (°)	Separation (")
Average	27.5	17.70
Standard Deviation	0.16	0.054
Standard Error of the Mean	0.048	0.016

Table 3. WDS 21406+5419 ES 35 AC Historical Data.

Year	Position Angle (°)	Separation (")
1898.64	28.6	19.137
1900.16	29.3	18.64
1902.77	28.1	18.083
1903.75	28.2	18.47
1929.66	27.8	17.873
1956.73	27.6	18.128
1962.63	27.3	18.01
1962.72	28.2	18.21
1987.686	28.48	18.32
1991.49	27.8	18.28
1996.728*	28.8	21.3
1996.73*	29.4	21.3
2003.528	27.8	18.227
2006.605	26.9	18.15
2007.607*	29.1	21.23
2009.991	29.29	18.34

2013.63	27.83	18.163
2014.65	27.73	18.203

Rows with asterisks (*) indicate outliers.

Table 4. WDS 21406+5419 ES 35 AB measurements.

Position Angle (°)	Separation (")
217.2	8.76
218.2	8.82
217.8	8.63
218.8	8.70
218.7	8.66
219.4	8.95
217.8	8.88
219.7	8.40
218.7	8.68
217.6	8.84

Table 5. Average, standard deviation, and error values of WDS 21406+5419 ES 35 AB.

	Position Angle (°)	Separation (")
Average	218.4	8.73
Standard Deviation	0.81	0.16
Standard Error of the Mean	0.25	0.049

Table 6. WDS 21406+5419 ES 35 AB Historical Data.

Year	Position Angle (°)	Separation (")
1900.16	223.7	11.1
1902.77	216.8	11.235
1929.66	224	9.958
1956.73	219.9	10.087
1962.63	222.9	9.09
1962.72	220	9.5
1987.686	220.33	9.15
1996.728	219.5	11
1996.73	219.6	10.5
2009.991	217.81	9.99
2014.6	219.37	8.602

Table 7. Gaia proper motion and parallax data for WDS 21406+5419 ES 35 A, B, and C stars.

A R C

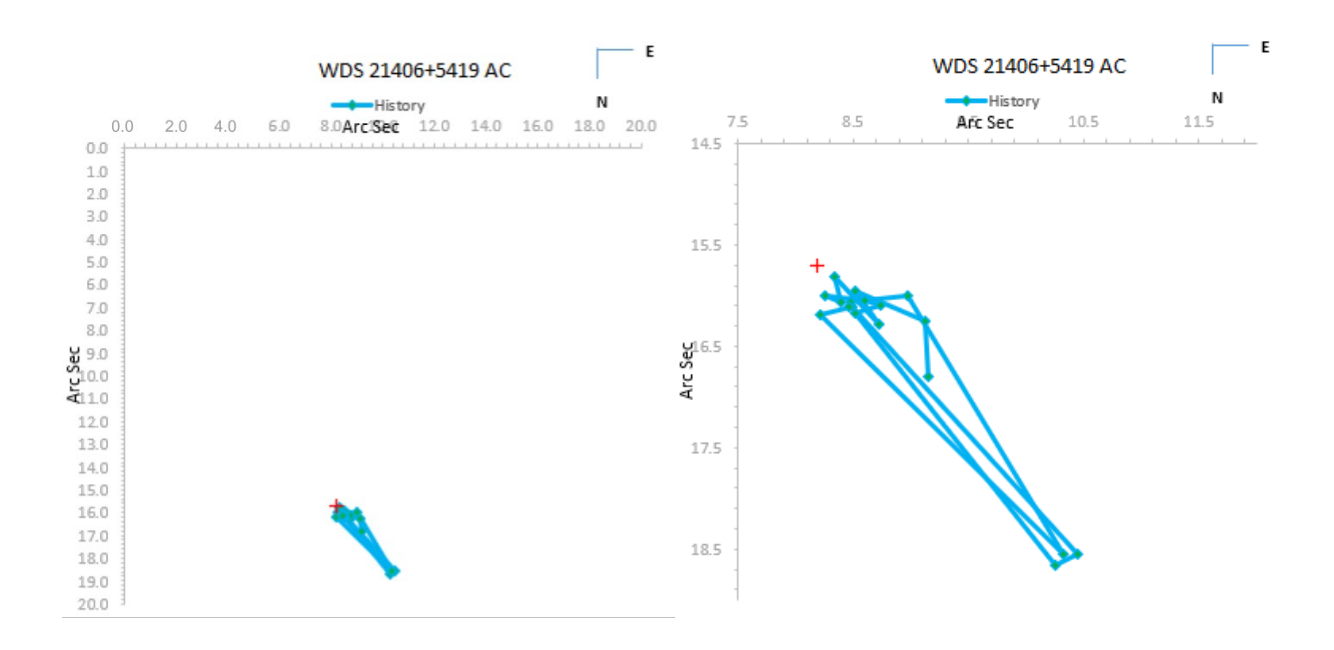
	A	В	С
PM RA ("/yr)	-9.863	3.543	-10.041
PM Dec ("/yr)	-10.522	2.52200	-10.012
Parallax (mas)	1.8144	1.18820	1.7417

4. Discussion

For all pairs we evaluated, we used the *Plot Tool* created by Richard Harshaw to generate graphs for the historical motion with the inclusion of our measurement, denoted by the red + on all graphs.

AC Pair

After creating the graphs, we noticed three outliers from the dates 2007.607, 1996.728, and 1996.73, marked by asterisks in Table 3. It was interesting that these three observations were all about 3 arcseconds away from the rest of the observations. These measurements were taken by different observers, which rules out the possibility of systematic error. Regardless, we decided to remove these points and update our graphs to reflect such to assess if a better timeline of the motion could be established. Figure 2 displays the AC pair motion before the removal, and Figure 3 displays the AC pair motion after the removal. As shown in the new graph, this did not result in a different conclusion. When looking at the Gaia data in Table 7, the proper motions of stars A and C are similar, suggesting that they are a part of a moving group. Also, the parallax values are close. The graph, however, does not contribute to a definitive conclusion, even with the outliers omitted, because of possible atmospheric interference and general uncertainty in the measurements. The largest contributor to this uncertainty of the graph is the fact that there has been less than 1" of motion in the past 125 years. Because of this, we cannot rely heavily on the graph to make definitive conclusions. Despite this, based on the proper motions and parallax values of these stars, there is evidence for the two stars being a moving pair, i.e. a common proper motion double. Future measurements that are more accurate could result in a more definitive conclusion.



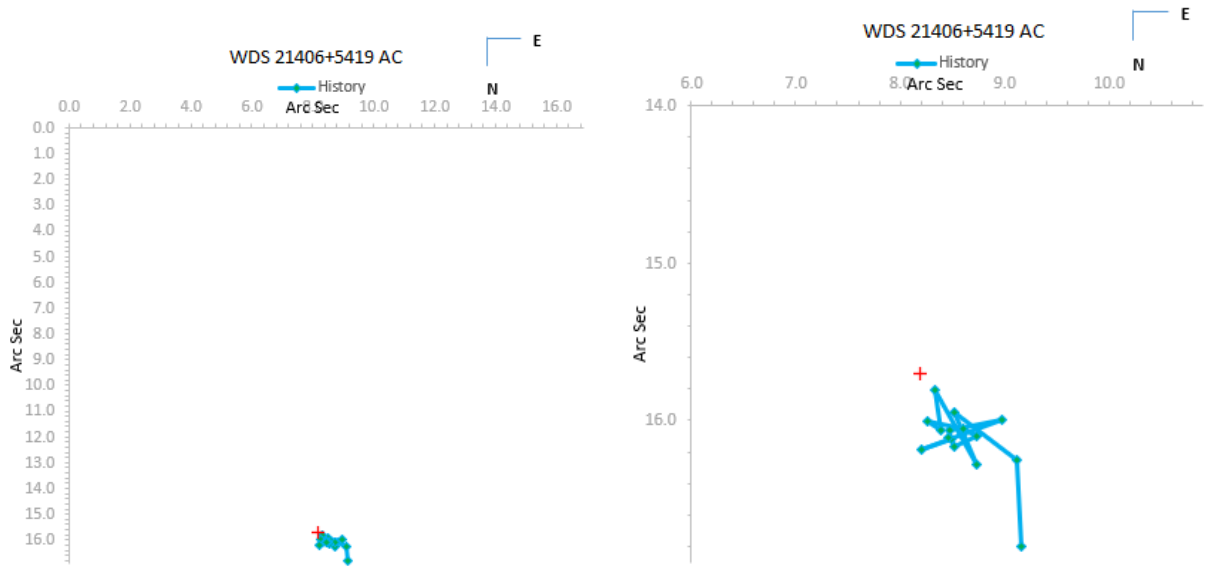


Figure 2: Graphs of historical motion of the AC Pair; Left: origin included; Right: zoomed in.

Figure 3: Graphs of historical motion of the AC Pair with omission of outlying points; Left: origin included; Right: zoomed in.

BC Pair

Since we recorded measurements about the B star and the AB pair is already observed to not be a physical double, we decided to analyze the motion of the B star relative to the C star in order to explore their relationship. To do this, we consulted each star's historical data and removed the entries that do not exist in both star's historical data. Then, in a new spreadsheet, we converted each stars' angle and separation relative to the A star into Cartesian coordinates. Then we transformed the coordinates so that C is the new primary star. We used the new coordinates of B to plot the motion of the B star against the C star. The result of this is shown in Figure 4.

Unfortunately, the graph does not provide any significant information. At a glance, there does seem to be a slight curve in the graph that could possibly suggest the orbiting of the B star around the C star. After further investigation, however, the curve does not move in a single direction over time, meaning this curve could be attributed to inaccuracies in measurements or atmospheric interference. Additionally, the proper motions and parallax values of the stars do not align. Based on these observations, there is no clear evidence that points towards a definite relationship between the B and C stars.

Table 8. Historical data and new measurements of WDS 21406+5419 ES 35 BC pair, transformed to use C as the primary star.

Year	Position Angle (°)	Separation (")
1900.16	214.6655371	29.52062094
1902.77	211.432092	29.23815833
1929.66	213.5821946	27.57590895
1956.73	211.9911004	28.06584159
1962.63	212.5183896	26.87654407
1962.72	212.2395422	27.57775241
1987.686	212.4208371	27.33964359
1996.728	212.4394956	32.17362828

1996.73	212.7638671	31.68865247
2009.991	212.2922885	28.25853888
2014.6	211.4591248	26.68459637
2023.74	211.0901618	26.33022498

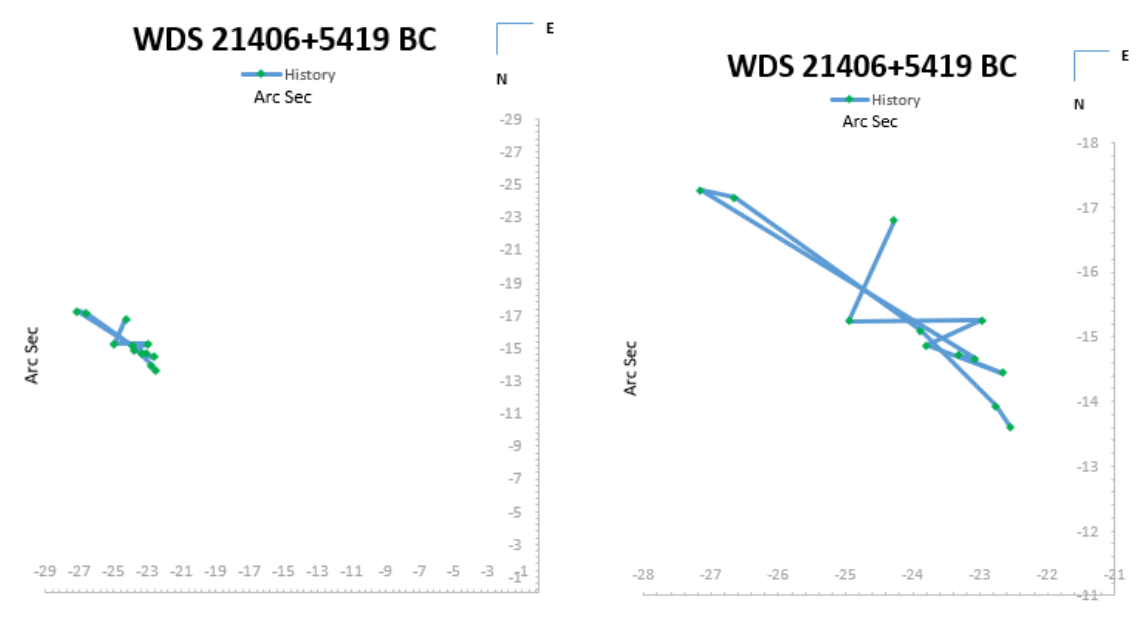


Figure 4: Graphs of historical motion of the BC Pair; Left: origin included; Right: zoomed in

5. Conclusions

After our analysis of the AC pair of the 11-fold system WDS 21406+5419, including the removal of outlying points, we were able to find evidence for A and C being a common proper motion double. The parallax difference between A and C is only 0.0727 mas and the difference between the PM RA and PM Dec values is only 0.51 "/yr. However, additional research is necessary to further confirm the relationship of the AC pair. The AB pair was found to be non-physical in prior analyses by others. After our analysis of the BC pair, we were not able to establish a clear relationship between the B and C stars, due to the nature of the graph, the significant difference in the proper motions of both stars, and the difference in parallax values. Based on this information, the BC pair is likely not a physical double.

Acknowledgements

This research has made use of the Washington Double Star Catalog maintained at the U.S. Naval Observatory. Special thanks to Dr. Rachel Matson for providing us with the historical data for this system. This work has made use of data from the European Space Agency (ESA) mission Gaia (https://www.cosmos.esa.int/gaia), processed by the Gaia Data Processing and Analysis Consortium (DPAC, https://www.cosmos.esa.int/web/gaia/dpac/consortium). Funding for the DPAC has been provided by national institutions, in particular the institutions participating in the Gaia Multilateral Agreement. This research would not have been possible without the use of Stelle Doppie, maintained by Gianluca Sordiglioni. Thank you to Richard Harshaw for the *Plot Tool* which was essential for this endeavor. Thank you to Rachel Freed of the Institute for Student Astronomy Research (InStAR) for funding our telescope usage that made this possible.

References

- Collins, K. A., Kielkopf, J. F., Stassun, K. G., & Hessman, F. V. (2017). AstroImageJ: Image processing and photometric extraction for ultra-precise astronomical light curves. The Astronomical Journal, 153(2), 77. doi:10.3847/1538-3881/153/2/77
- Gaia Collaboration, T. Prusti, J.H.J. de Bruijne, et al. (2016b) The Gaia mission. Astronomy & Astrophysics, 595, A1.
- Gaia Collaboration, A. Vallenari, A. G. A. Brown, et al. (2023j) Gaia Data Release 3. Summary of the content and survey properties. Astronomy & Astrophysics, 674, A1.
- Harshaw, R. (2020). "Using *Plot Tool* 3.19 to Generate Graphical Representations of the Historical Measurement Data." Journal of Double Star Observations, 16(4), 386.
- Las Cumbres Observatory. (n.d.). DeltaRho 350 + QHY600. Las Cumbres Observatory. https://lco.global/observatory/instruments/qhy600-delta-rho-350/

Astrometric Measurements and Analysis of Four Star Systems

Jules Miller, Pierce Arora, Kyler Gandrup, Joe Ross, Kaleé Tock ¹Stanford Online High School, Redwood City, California; <u>jules328@ohs.stanford.edu</u>

Abstract

This paper presents astrometric measurements of double star systems 09483+2410 DAM 1758 AC, 07222-2412 HJ 9002 AB, 05067+5121 SMA 47, and 06440+7218 HJ 2323 AB. New measurements of the systems are presented and are shown to be similar to recent measurements and to listings in Gaia Data Release 3. In addition, each system's historical data are plotted and relative motions are calculated. We find that DAM 1758 AC, HJ 9002 AB, and SMA 47 are physically related, although unlikely to be bound, and that HJ 2323 AB is very likely to be bound.

1. Introduction

Four target double star systems investigated in this study are shown in Figure 1. Gaia Data Release 3 (DR3) magnitude and color data for the component stars are given in Table 1, with Absolute Gaia G-filter magnitudes calculated using Equation 1 (Babusiaux et al., 2023; Prusti et al., 2018; Vallenari et al., 2022).

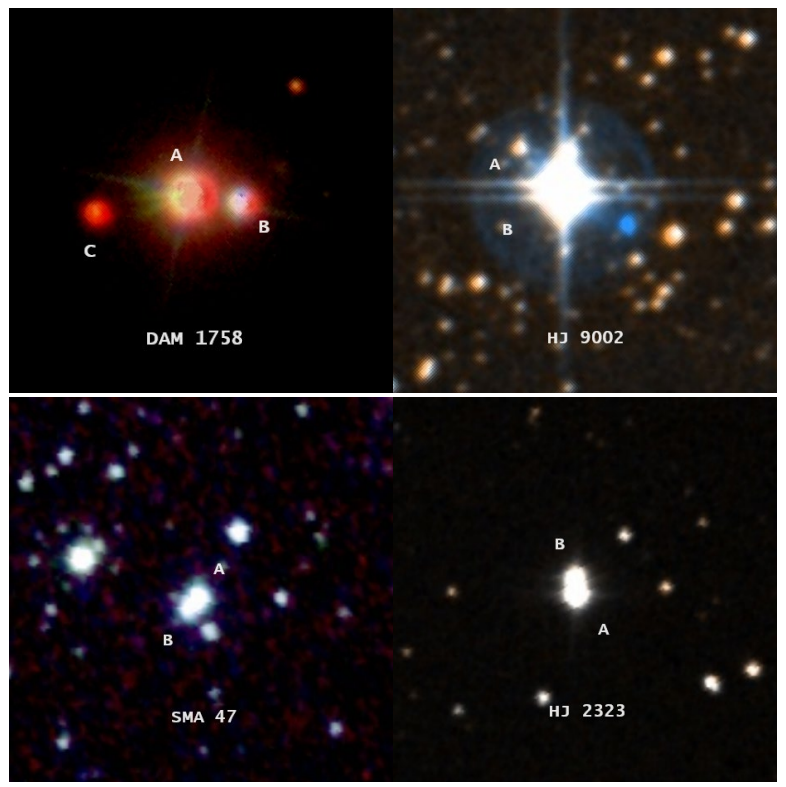


Figure 1: DAM 1758 AC, HJ 9002, SMA 47, and HJ 2323, from the Aladin Lite Sky Atlas.

System	Primary Gmag	Secondary Gmag	Primary Parallax (mas)	Secondary Parallax (mas)	Absolute Primary Gmag	Absolute Secondary Gmag	Primary Color	Secondary Color
DAM 1758 AC	11.3000	16.3889	5.2619	5.2716	4.9	10.0	0.913	2.630
НЈ 9002 АВ	9.3346	9.8578	2.8449	2.8195	1.6	2.1	0.270	0.178
НЈ 9002 АС	*	14.3086	*	0.3228	*	1.8	*	0.961
HJ 9002 AD	*	14.5544	*	0.7958	*	4.0	*	0.790
SMA 47	11.3525	11.8999	0.9090	0.9560	1.1	1.8	0.696	0.548
HJ 2323 AB	10.8307	11.5697	4.1150	4.1054	3.9	4.6	0.712	0.793

Table 1. Gaia DR3 Magnitudes and Parallaxes

Absolute G magnitude in Table 1 above is computed from Equation 1 where p is parallax in milliarcseconds and m is non-absolute G magnitude.

$$M_g = m + 5 \cdot (log(rac{p}{1000}) + 1)$$

Equation 1: Absolute G Magnitude formula

Each of the four systems has noteworthy characteristics. DAM 1758 AC shares a primary star with POU 3058 AB, an optical double. However, as seen in Table 1 above, the primary A star has Gaia G-filter apparent magnitude of 11.3, while C has a G-filter magnitude of 16.38. (Babusiaux et al., 2023; Prusti et al., 2018; Vallenari et al., 2022). This makes DAM 1758 AC a high-delta mag star, which requires use of an infrared filter for the red C star to to be visible in the same image as the blue A star.

Like DAM 1758, HJ 9002 is a physical double with additional optical doubles in its field. The system was first observed in 1835 by John Herschel (Herschel, 1847). Using luminosity and temperature estimates from two studies, the primary star is likely spectral type A1 or A2 and the secondary is spectral type A4 or A5 (McDonald et al., 2012; Zari et al., 2018). The stars have very similar parallaxes and are certainly physically related. However, the tertiary and quaternary stars, SHT 8AC and SHT 8AD, are thousands of parsecs away, as is evident from their parallax values in Table 1. Therefore, they are not physically related to the primary. These two stars were previously thought to be spectral class A0/1 (Shatsky et al., 1999).

Our third system is SMA 47, a pair of stars similar in temperature, magnitude, and color to each other. Combined with the fact that these stars are co-located and co-moving, these similarities may suggest a common origin. The stars' absolute magnitudes in Table 1 above are consistent with main sequence stars of types F3 and F6. From Earth, these stars are seen to be close but not touching and have remained this way for the century that they have been observed (Williams, 2010).

Much like SMA 47, HJ 2323 is a pair of extremely similar stars of near-solar mass and temperature. The pair was identified as a candidate comoving pair by an Astronomical Journal paper in 2017, in their catalog

^{*}HJ 9002 AC and AD share a primary star with AB.

of candidate comoving pairs. (Oh, 2017) Later the same year, in a Monthly Notices of the Royal Academic Society paper, the star was catalogued as a wide binary (Andrews, 2017).

All four pairs are placed on the Gaia HR-diagram in Figure 2 (Babusiaux et al., 2023; Prusti et al., 2018; Vallenari et al., 2022). This placement enables estimation of the stars' spectral types for stars where these are previously unknown. Once spectral types are determined, masses of each system's components are estimated using Dr. Siobahn Morgan's "Spectral Type Characteristics" (Morgan 2023). These estimated masses are tabulated in Table 2.

→ GAIA'S HERTZSPRUNG-RUSSELL DIAGRAM

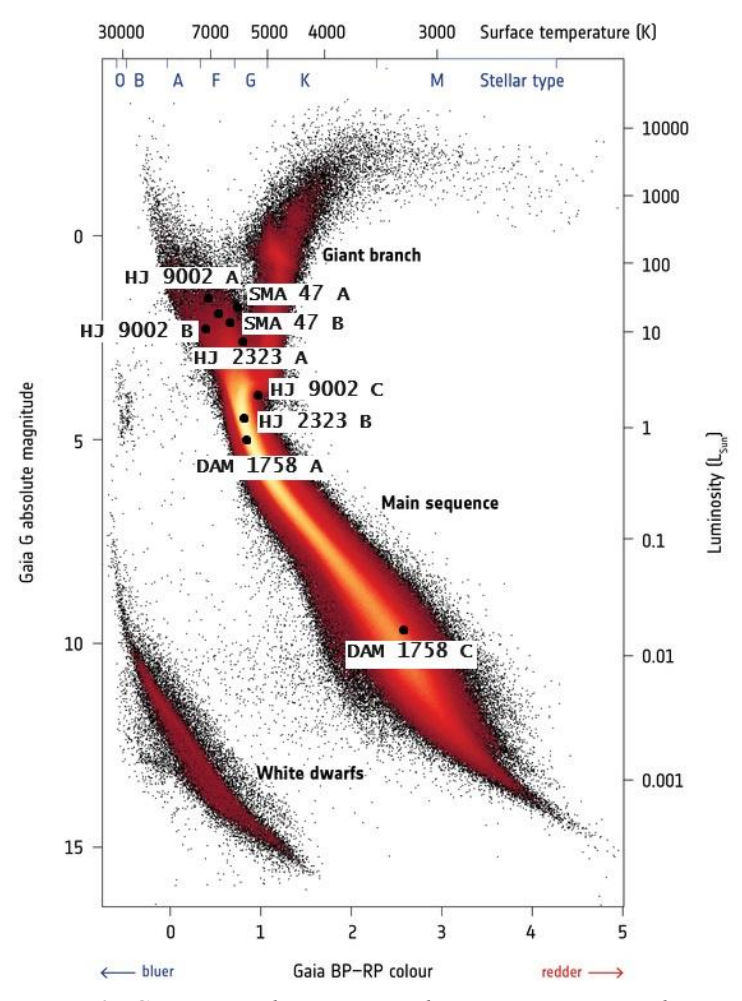


Figure 2: Gaia's HR diagram, used to estimate spectral types

Table 2. Estimated stellar types and masses.

System	Primary Stellar Type	Primary Mass (M⊙)	Secondary Stellar Type	Secondary Mass (Mo)
DAM 1758 AC	G2	1.00	M5	0.40
HJ 9002 AB	A1	2.06	A5	1.73
НЈ 9002 АС	*	*	А3	1.86
НЈ 9002 АД	*	*	F6	1.20
SMA 47	F6	1.20	F3	1.29
НЈ 2323 АВ	G1	1.04	G2	1.00

2. Target Selection

There were several criteria that were used to select this system for study. First, to be visible in the late winter when the images were requested, the system needed an RA between 5 and 13 hours. The astronomical magnitude of the secondary star was intended to be less than 13, to be visible to the 0.35m Delta Rho telescopes at Las Cumbres Observatory Global Telescope (LCOGT) network, and the difference in magnitude was intended to be less than 3 so that the component stars could be exposed together in the same image. Although DAM 1758's secondary star had a V-filter magnitude of 17.4, which did not satisfy the brightness and delta mag criteria, this system was able to be imaged because of the color difference between its red secondary and blue primary. The final criterion was for the stars to have a separation of between 5 and 15 arcseconds, as a small separation also makes it difficult to resolve the individual stars, and a large one would decrease the likelihood of a strong physical relationship.

3. Instruments Used

The images taken for this paper were taken with a 0.35-meter Delta Rho telescope at the Las Cumbres Observatory Global Telescope (LCOGT) site at Siding Spring, New South Wales, Australia, and Teide Observatory at Tenerife, Canary Islands, Spain. This telescope uses a QHY600 CMOS camera. QHY600 CMOS camera in central mode have a field of view (FOV) of 0.5°x0.5° and a pixel size of 0.73".

4. Measurements

Example measurements for each system are in Figure 3. Dam 1758 AC was imaged using a Sloan IR filter (Fukugita, M. et al., 1996). HJ 9002 and SMA 47 were imaged in a Bessel-V filter (Bessell, M. S., 1990). HJ 2323 was imaged in a PanSTAARS-w filter (Tonry, J.L. et al., 2012). Each image had its position angle and separation measured, using the software AstroImageJ. Exposure times are summarized in Table 3, and sample measurements are shown in Figure 3.

System	Exposure time	Filter	Number of images
DAM 1758	42	Sloan IR	10
HJ 9002 AB	3.5	Bessel-V	10
SMA 47	8.28	Bessel-V	10
НЈ 2323	7	PanSTAARS-w	11

Table 3. Image Exposure Times, Filters, and Number of Images.

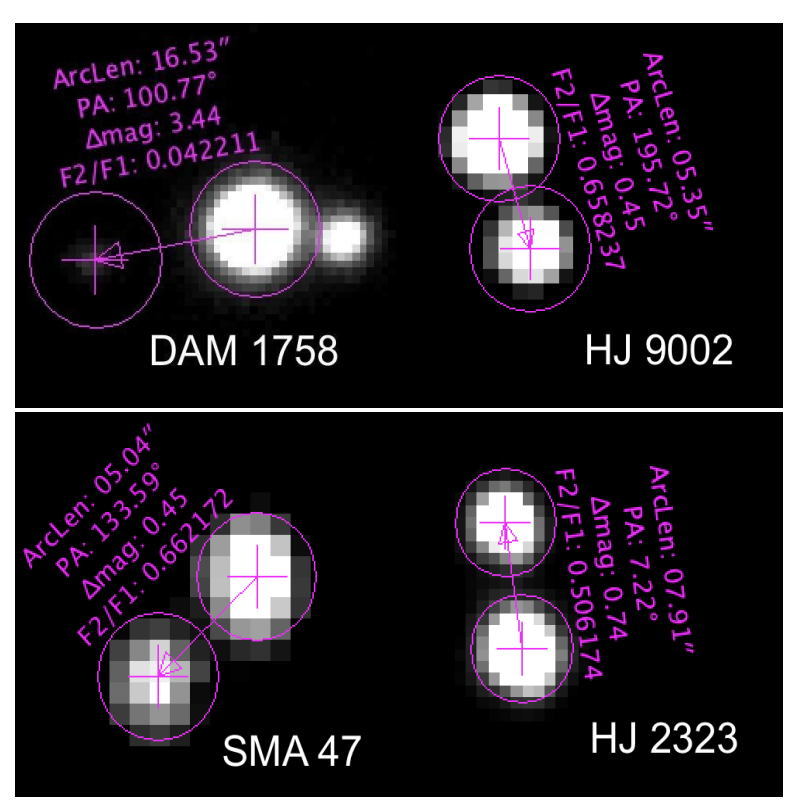


Figure 3: Astrometric measurements of DAM 1758, HJ 9002, SMA 47, and HJ 2323, made in AstroImageJ

5. Results

Table 4 shows the average position angle and separation measurements for each star system, along with the standard errors.

System	Date	Number of Images	PA (°)	Standard Error PA	Sep (")	Standard Error Sep
DAM 1758 AC	2024.052	10	101.032	0.073	16.779	0.024
НЈ 9002 АВ	2024.0327	10	195.107	0.208	5.354	0.022
SMA 47	2023.0414	10	134.758	0.380	5.061	0.081
НЈ 2323 АВ	2024.0246	11	7.337	0.114	7.917	0.019

Table 4. Summary of Position Angle (PA) and Separation (Sep) Measurements.

6. Relative Velocity and Escape Velocity Calculations

Astronomical objects are gravitationally bound if their relative velocity is less than terminal velocity, given by Equation 2, as derived in the appendix of Bonifacio, et. al., 2020.

$$v=\sqrt{rac{2GM}{r}}$$

Equation 2. Escape Velocity Formula

Thus, to determine if a given system is bound, the relative velocity, distance between the stars, and mass must be known.

Relative velocity will be calculated first. To achieve this, both transverse and radial velocity must be known so that total relative velocity can be derived.

Transverse velocity is the vector sum of two component vectors: the relative proper motion in Right Ascension (RA) and relative proper motion declination (Dec). The total relative Proper Motion (PM) vector is calculated as the vector sum of these two perpendicular components, as shown in Equation 3. The pmRA and pmDEC variables stand for the proper motion in RA and Dec respectively, and the subscripts denote the primary or secondary stars. Their vector sum is termed relative proper motion. Proper motion components from Gaia DR3 are tabulated together with the relative proper motion vector magnitudes for each system in Table 5.

$$pm_{relative} = \sqrt{(pmRA_p - pmRA_s)^2 + (pmDEC_p - pmDEC_s)^2}$$

Equation 3: Relative PM Formula

System	Proper Motion RA Primary (mas/yr)	Proper Motion RA Secondary (mas/yr) Proper Motion Dec Primar (mas/yr)		Proper Motion Dec Secondary (mas/yr)	Magnitude of Relative PM Vector (mas / yr)
DAM 1758 AC	-11.40646 ±0.04463	-10.90118 ±0.07278	-27.33307 ±0.03464	-28.65729 ±0.05729	1.42
НЈ 9002 АВ	-2.42788 ±0.00983	-1.90801 ±0.01223	-4.03981 ±0.01682	-2.95131 ±0.02310	1.21
НЈ 9002 АС	-2.42788 ±0.00983	-3.57321 ±0.01077	-4.03981 ±0.01682	3.41594 ±0.01922	7.54
HJ 9002 AD	-2.42788 ±0.00983	$\begin{array}{c} 3.78226 \\ \pm 0.01288 \end{array}$	-4.03981 ±0.01682	1.21226 ±0.02128	8.13
SMA 47	1.62144 ±0.03244	1.37719 ±0.02265	-5.6275 ±0.02723	-5.63733 ±0.01938	0.24
НЈ 2323 АВ	4.05227 ±0.008365	$\begin{array}{c} 4.06422 \\ \pm 0.009548 \end{array}$	-47.27112 ±0.012406	-46.99337 ±0.013053	0.28

Table 5. Relative Proper Motion Data.

Now, to calculate the relative transverse velocity in physical units rather than angular units, the relative PM vector and parallax will be used. Table 6 gives parallaxes from Gaia (Babusiaux et al., 2023; Prusti et al., 2018; Vallenari et al., 2022), which can be used to find the distances using Equation 4:

$$d = \frac{1}{p}$$

Equation 4: Distance-Parallax formula

With the distance from earth, the PM vector can be converted from an angular quantity to a physical one, yielding the relative transverse motion through space. Equation 5 gives the details of the calculation, where rPM_v is the magnitude of the relative proper motion vector and plx is the parallax of the primary. Table 6 displays the numerical calculations, and the parallax of the secondary is also present for later reference.

$$\frac{rPM_{v} \cdot mas}{yr} \cdot \frac{1}{1000 \; mas} \cdot \frac{1}{3600} \cdot \frac{1}{3600} \cdot \frac{2\pi \; rad}{360} \cdot \frac{1}{plx} pc \cdot \frac{3.086 \cdot 10^{13} \; km}{pc} \cdot \frac{1 \; yr}{3.1636 \cdot 10^{7} s}$$

Equation 5: Relative Transverse Motion formula

System	Parallax of Primary (mas)	Parallax of Secondary (mas)	Relative Transverse Motion Through Space (m/s)
DAM 1758 AC	5.2619 ± 0.04048	5.2716 ± 0.06553	1277
НЈ 9002 АВ	2.8449 ± 0.01637	2.8195 ± 0.01905	2010
НЈ 9002 АС	*	0.3228	12568
HJ 9002 AD	*	0.79588	13551
SMA 47	0.9091 ± 0.02670	0.9561 ± 0.01881	1275
НЈ 2323 АВ	5.4391 ± 0.04401	7.1139 ± 0.19454	320

Table 6. Relative Transverse Motions of the Component Stars in Physical Units..

The relative transverse motion is the stars' relative motion in the plane perpendicular to the earth, so to calculate the total relative 3D velocity the relative radial velocity (RV) must also be considered. Gaia supplies the radial velocity of all stars in the systems from which the relative velocity can be calculated as simply the absolute value of the primary's RV minus the secondary's. Then, since the transverse and radial velocity vectors are perpendicular, the total relative velocity can be calculated according to Equation 6, where with the results shown in Table 7 below.

$$\sqrt{(v_{pt}-v_{st})^2+(v_{pr}-v_{sr})^2}$$

Equation 6: Total relative velocity formula, where p stands for primary, s stands for secondary, t stands for transverse, and r stands for radial.

System	Radial Velocity of Primary (km/s)	Radial Velocity of Secondary (km/s)	Relative Radial Velocity (m/s)	Relative 3D Space Velocity (m/s)				
DAM 1758 AC	11.8±0.22	-	-	1277*				
НЈ 9002 АВ	-	3.0**	-	2010*				
НЈ 9002 АС	-	-	-	12568*				
HJ 9002 AD	-	-	-	13551*				
SMA 47	-12.0±3.47	-9.0±5.78	3070	3328				
НЈ 2323 АВ	28.5±0.33	28.8±0.58	-0.271	320				

Table 7. Relative Transverse Motion data.

^{*}Primary star values are the same.

^{*}Radial velocity is assumed to be zero for the sake of calculation because it is unknown.

^{**}Uncertainty not given.

Lastly, to find the escape velocity, the distance between the two stars must be calculated. The separation and distance (as an inverse of parallax) are known and the transverse separation can be calculated by solving for x in Equation 7. This follows because of the trigonometry depicted in Fig. 4, where Sep is the angular separation of the stars, and Transverse Sep is their transverse physical separation in space.

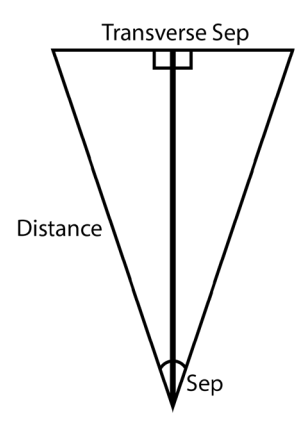


Figure 4: Trigonometric Intuition behind Transverse Sep Calculation

$$sin(rac{sep}{2}) = rac{rac{x}{2}}{D}$$

Equation 7: Transverse Sep formula

Using the small angle approximation listed in Equation 8, this can be rewritten as Equation 9.

$$sin(rac{sep}{2}) pprox rac{sep}{2}$$

Equation 8: Small angle Approximation

$$D \cdot sep = x$$

Equation 9: Simplified transverse separation formula

Radial separation is simply calculated as the difference of distances of the two stars, which, substituting for parallax, is formulated in Equation 10. The radial and transverse distances together combine in a vector sum, yielding the total distance between the two stars. The calculations are summarized in Table 8 and parallax measurements are given from Table 6.

$$R_d = \left| rac{1}{p_p} - rac{1}{p_s}
ight|$$

Equation 10: Radial Distance Formula

Table 8. Star Physical Separations

System	Angular Separation (arcsec)	Transverse Separation (pc)	Radial Separation (pc)	Total Separation (pc)
DAM 1758 AC	16.9	0.016	0.35	0.35
HJ 9002 AB	5.5	0.009	3.17	3.17
HJ 9002 AC	5.5	0.009	2746.39	2746.39
HJ 9002 AD	11.6	0.020	904.97	904.97
SMA 47	5.3	0.028	54.04	54.04
HJ 2323 AB	7.9	0.009	0.57	0.57

Finally, the escape velocity of each of the systems can be compared to the relative velocities and the boundedness of the systems can be determined. Escape velocity is determined via the calculation in Equation 2. If a system is bound, then its relative velocity will be less than the escape velocity. Note the masses and separations are in solar masses and pc, so they must be converted to kg and m respectively.

Table 8. Boundedness Calculation Results

System	Primary Star Mass (solar masses)	Secondary Star Mass (solar masses)	Separation (pc)	Relative Velocity (m/s)	Escape Velocity (m/s)	Bound?
DAM 1758 AC	1.00	0.402	0.35004	1277	840	N
HJ 9002 AB (se.)	1.73	1.97	3.17033	2010	1897	N
HJ 9002 AB (te.)	**	2.06	2746.39093	12568	1923	N
HJ 9002 AB (qu.)	**	1.25	904.96832	13551	1191	N
SMA 47	1.20	1.29	54.04281	3328	19.75	N
НЈ 2323 АВ	1.04	1.00	0.56832	420	1373*	Y

^{*}Using 2D separation, as parallax uncertainties overlap

Although all these quantities have some uncertainty, the data suggests that three out of the four stars are not gravitationally bound. The HJ 2323 AB system is potentially bound, although within parallax uncertainty, there is also a possibility that the star is not gravitationally bound after all. The other three systems may not

^{**}Same values as above

be gravitationally bound, although DAM 1758 AC and HJ 9002 AB likely have strong gravitational influence, due to their high escape velocity. Even SMA 47 could be bound, given that the sum of the parallax uncertainties, 0.0267+0.01881 is almost equal to the difference in parallaxes, 0.95605-0.90908. Thus, if the stars' parallaxes are assumed to be closest within the margin of error, the stars may be closer and more bound than initially suggested by the data.

7. Plots

Figure 10 shows the historical data plots for DAM1758, HJ9002, SMA47, and HJ2323. Given the escape velocities calculated above, the only plot we expect to show evidence of curvature is HJ 2323 AB. However, all four plots have few data points of which many of the earliest measurements are outliers, and are therefore inconclusive, though HJ 2323 AB and SMA 47 do show trends that appear somewhat linear.

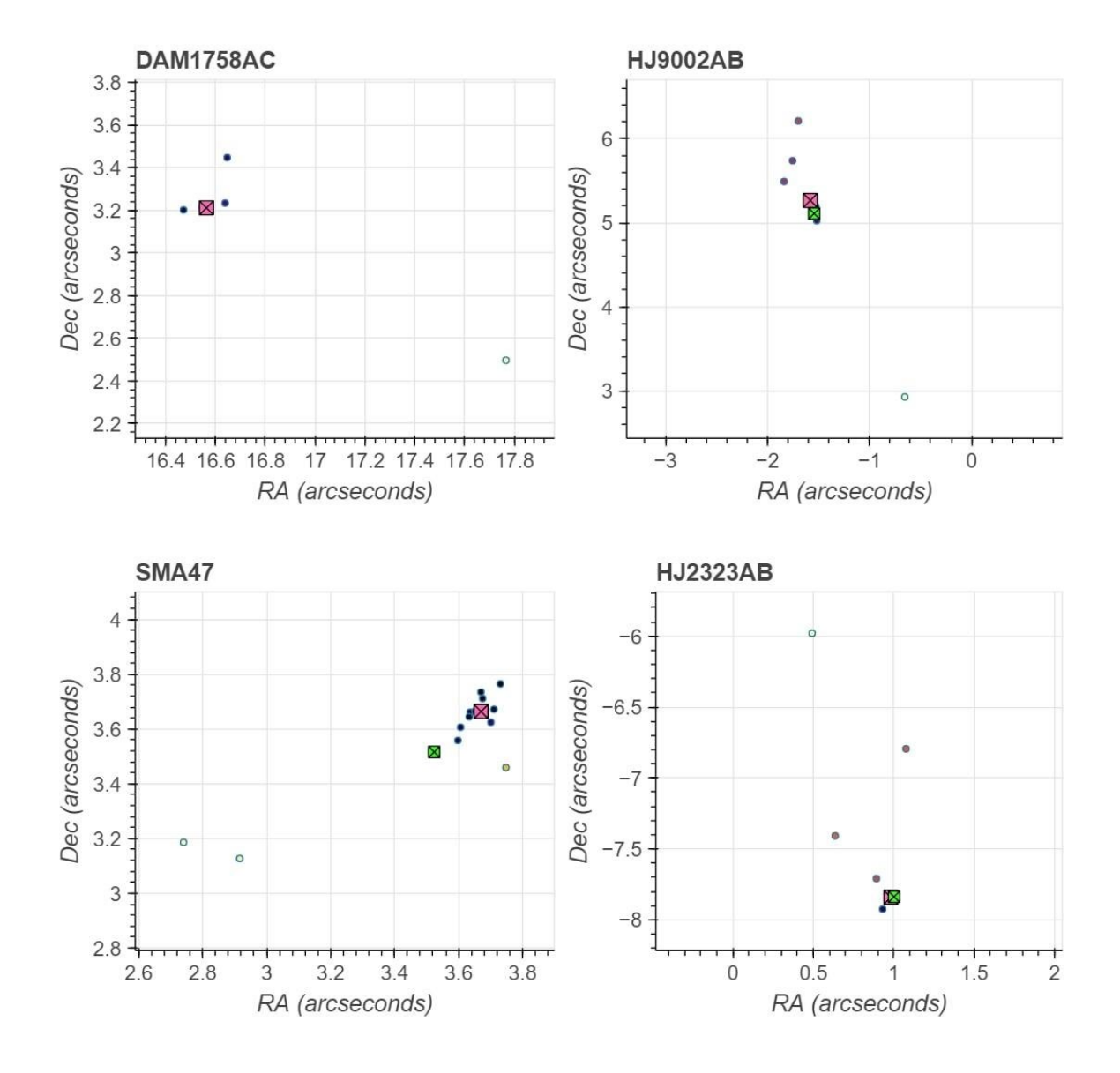


Figure 5: Historical data plots for DAM 1758, HJ 9002, SMA47, and HJ 2323. Gaia measurements are represented by green squares, and our measurements are represented by red squares. More recent measurements are darker.

8. Discussion

Vol 20 No 2 April 1, 2024

DAM1758 AC is a comoving physical double, with three-dimensional separation less than half a parsec in Table 8 and a relative PM vector almost 30 times smaller than its component PM vectors. We only have access to 4 previous observations of the system, so we do not have enough data to determine whether the relative motion is curving over time. However, our estimated relative velocity is around 35% greater than our estimated escape velocity for the system, suggesting that the stars, although physically related, are not gravitationally bound.

HJ9002 AB is also a physical double, while parallax shows that the C and D stars are optical. Historical data shows a trend, but we lack enough observations to confidently say whether the trend is linear. Our estimated relative velocity is greater than our estimated escape velocity, but only by around 5%. We can conclude that HJ9002 AB is physically related, but unlikely to be bound.

SMA47 AB is also a physical double, as indicated by the matching parallax and by the similarity of the PM vectors. However, the stars are almost certainly not bound, as the trend in the historical data is linear, and the estimated relative velocity is over 160 times the estimated escape velocity.

HJ2323 AB is very likely bound, as shown by matching parallax and by its almost-identical PM vectors. There is a clear trend in historical data, although curvature is not clearly visible. The stars have a relative 3d velocity of only 320 m/s, only a quarter of our estimated escape velocity. Therefore, the data we have suggests that HJ2323 AB is bound, and we can expect a curving trend to emerge over time.

9. Conclusion

This paper has examined four wide physical double star systems, and analyzed our own observations as well as available data to assess the strength of these systems' physical relationships.

We confirm DAM 1758 AB to be an optical double, and determine that DAM 1758 AC is physically related, but unlikely to be bound. The C and D stars in HJ 9002 are also optical doubles, and unrelated to HJ 9002 AB. We determine that the A and B stars of HJ 9002 are physically related but unlikely to be bound, given the combination of the historical data plot and escape velocity calculations. We find that SMA 47 AB is also physically related, but almost certainly not bound. Finally, we find that HJ 2323 AB is almost certainly a binary system. To better understand these stars, and our cosmos in general, more time and observations are needed.

Acknowledgments

This research was made possible by the Washington Double Star catalog maintained by the U.S. Naval Observatory, the Stelledoppie catalog maintained by Gianluca Sordiglioni, Astrometry.net, and AstroImageJ software which was written by Karen Collins and John Kielkopf.

This work has also made use of data from the European Space Agency (ESA) mission Gaia (https://www.cosmos.esa.int/gaia), processed by the Gaia Data Processing and Analysis Consortium (DPAC, https://www.cosmos.esa.int/web/gaia/dpac/consortium). Funding for the DPAC has been provided by national institutions, in particular the institutions participating in the Gaia Multilateral Agreement.

This work makes use of observations taken by the Planewave Delta Rho 350 + QHY600 CMOS camera systems of Las Cumbres Observatory Global Telescope Network located in Siding Spring, New South Wales, Australia.

The team would like to thank the JDSO reviewer for reading our study carefully and giving us helpful feedback.

References

- Andrews, J. Double Neutron Star Populations and Formation Channels. The Astrophysical Journal Letters. https://iopscience.iop.org/article/10.3847/2041-8213/ab2ed1
- Bessell, M. S (1990). Publications of the Astronomical Society of the Pacific, 102, 1181-1199. https://adsabs.harvard.edu/full/1990PASP..102.1181B
- Bonifacio, B., C. Marchetti, R. Caputo, and K. Tock. (2020). Measurements of Neglected Double Stars. Journal of Double Star Observations, 16(5), 411–423. http://www.jdso.org/volume16/number5/Bonifacio_411_423.pdf
- Brown, T. M. et al. (2013). Las Cumbres Observatory Global Telescope Network. Publications of the Astronomical Society of the Pacific, 125(931), 1031–1055. https://iopscience.iop.org/article/10.1086/673168/meta
- Fukugita, M. et al. (1996). The Sloan Digital Sky Survey Photometric System. Astronomical Journal, 111, 1748-1756. https://articles.adsabs.harvard.edu//full/1996AJ....111.1748F/0001756.000.html
- Gaia Collaboration, C. Babusiaux, C. Fabricius, S. Khanna, et al. (2023) Gaia Data Release 3. Catalogue validation. A&A 674, pp. A32. https://arxiv.org/abs/2206.05989
- Gaia Collaboration, T. Prusti, J.H.J. de Bruijne, et al. (2016b). The Gaia mission. A&A 595, A1. https://www.aanda.org/articles/aa/full_html/2016/11/aa29272-16/aa29272-16.html
- Gaia Collaboration, A. Vallenari, A. G. A. Brown, et al. (2023j) Gaia Data Release 3. Summary of the content and survey properties. A&A 674, pp. A1. https://arxiv.org/abs/2208.00211
- Herschel, J.F.W., 1847. Results of astronomical observations made during the years 1834, 5, 6, 7, 8, at the Cape of Good Hope. Smith, Elder and Co., 1847. https://doi.org/10.5479/sil.422148.39088007119118

- McDonald, I. (2012). Fundamental parameters and infrared excesses of Hipparcos stars. Monthly Notices of the Royal Astronomical Society. https://academic.oup.com/mnras/article/427/1/343/1029510?login=false
- Morgan, S. "Spectral type characteristics". https://sites.uni.edu/morgans/astro/course/Notes/section2/spectralmasses.html
- Oh, S. et al. (2017). Comoving Stars in Gaia DR1: An Abundance of Very Wide Separation Comoving Pairs. The Astronomical Journal. https://iopscience.iop.org/article/10.3847/1538-3881/aa6ffd
- Shatsky, N. et al. (1999). U B V absolute CCD photometry and differential astrometry of a sample of visual double stars with A-type primaries. https://aas.aanda.org/articles/aas/ps/1999/16/ds1676.ps.gz
- Williams, J. et al. (2010). Astrometric Observations of WDS Neglected Binary Stars. Journal of Double Star Observations, 6(1), 15–20. http://www.jdso.org/volume6/number1/Williams.pdf
- Zari, E. et al (2018). 3D mapping of young stars in the solar neighborhood with *Gaia* DR3. Astronomy and Astrophysics. https://doi.org/10.1051/0004-6361/201834150
- "Gaia Hertzsprung-Russell Diagram" https://sci.esa.int/web/gaia/-/60198-gaia-hertzsprung-russell-diagram

Desmos Graphical Analysis of Binary Stars

A Tutorial with HU 481 (WDS 16212+2259) Example

Russell Genet^{1,2}, Paul McCudden³, and Michael-James Ellis^{2,4}

- 1. Eastern Arizona College, Payson Campus
- 2. Fairborn Institute
- 3. Colorado Mountain College
- 4. Payson High School

Abstract This tutorial describes the basic concepts behind binary stars, Kepler's Three Laws of Planetary Motion (and binary star motion), and the vital role binary star orbits play in determining stellar mass. The primary source of past published binary star observations, the *Washington Double Star Catalog*, is illustrated with an example, HU 481 (WDS 1612+2259). An image of the apparent orbit of HU 481, published in the *Sixth Catalog of Orbits of Visual Binary Stars*, is described in detail, along with instructions on inserting it as a background into Desmos that, via rotation, scaling, and translation, precisely matches Desmos' Cartesian coordinates. Observations of HU 481 not included in these graphs were added via Desmos. An apparent orbit ellipse was created in Desmos that matched the published apparent ellipse, while a new ellipse was created that better matched recent observations of HU 480, as they appeared to be going off the published orbit's track.

1. Binary Stars

Binary stars are gravitationally bound pairs of stars that rotate around their common center of mass. *Astrometry* "... a branch of *astronomy* that involves precise measurements of the positions and movements of stars and other celestial bodies" (Wikipedia 2023a) is used to analyze the motions of the two stars over time. Johannes Kepler's Three Laws of Planetary Motion, which he developed to describe our solar system, also apply to binary stars. Kepler's First Law establishes that the shape of the orbit is an ellipse. His Second Law states that the speed of each star varies throughout its orbit, with equal areas being swept out in equal times. Kepler's third law—which relates the period of rotation, the semi-major axis of the ellipse, and the mass of the two stars—can then be used to determine the mass of the two stars, once the period and semi-major axis are established via observations and analysis.

$$(m_1 + m_2) = a^3 / P^2$$

where

 m_1 and m_2 are the masses of the primary and secondary stars, respectively, in solar masses a is the semi-major axis of the true ellipse in astronomical units P is the period in years

Binaries have been observed at high magnification with telescopes since 1781 (Herschel 1785). Each observation consists of measuring the angle the secondary (fainter) star makes with respect to the primary (brighter) star and celestial north (the position angle in degrees), and the separation between the two stars (in arc seconds, an angular measurement) as shown in Figure 1. The observed position angles and separations, gathered over decades or centuries, can then be used to determine the parameters of an apparent elliptical orbit via Kepler's First Law.

Kepler's Second Law can then be used to transform an apparent orbit into a true orbit, while Kepler's Third Law can be used to calculate the sum of the stellar masses $(m_1 + m_2)$. Kepler's three laws are summarized in Figure 2. Parsing this sum into individual masses is the last step in this long process, and is usually accomplished through the analysis of a radial velocity curve of the binary (a topic beyond the scope of this paper). The end result—the accurate knowledge of stellar masses made possible by the orbital analysis of binaries—is *the* key to understanding the life cycles of stars, i.e., how they evolve over time.

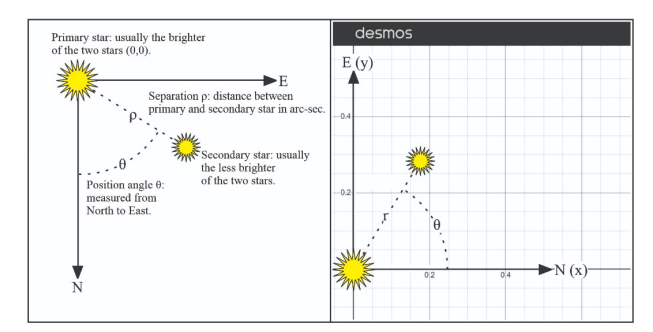


Figure 1: Position angle and separation for a binary star.

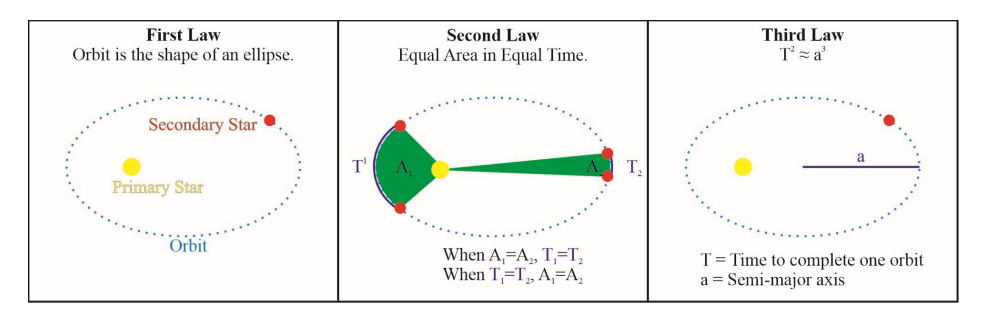


Figure 2: Illustrations of Kepler's Three Laws of Planetary Motion.

For many decades, the United States Naval Observatory (USNO) has served the international astronomical community by compiling all published observations of double stars into the Washington Double Star (WDS) Catalog (2023). Stars that at first appear to be single can, when viewed through a telescope at high magnification, be seen as two stars. Many of these double stars are far apart in space and only appear close together in the sky because of their chance alignment along the line of sight from Earth. These are referred to as *optical doubles* and are of limited scientific interest. However, as discovered by William Herschel (1803), some of these stars are not only close together, but they are rotating around a common center of gravity. Herschel named these gravitationally bound stellar pairs *binaries*.

Binaries fall into two major categories: *suspected* and *confirmed* binaries. Suspected binaries *may* be gravitationally bound, but no analytically derived equation for their elliptical orbit has yet been published for any of several reasons: there may be too few observations to compute an orbit, not much of an orbit has been observed yet, or the points are too scattered or confusing to make the orbital computation and publication worthwhile.

Confirmed (known) binaries, on the other hand, have published orbits. As another service to the international astronomical community, the USNO publishes the Sixth Catalog of Orbits of Visual Binary Stars (Matson et al. 2023). This catalog, often referred to as the 6th Orbit Catalog, provides a binary's *orbital elements*. These seven elements are the parameter values for the ellipse equation that shows the true orbit as it would be seen if it were viewed face-on from outer space, as well as parameters that describe how the orbit is tilted with respect to the line-of-sight from Earth. This catalog also provides a plot (graph) of the tilted ellipse (the apparent orbit) as seen from Earth. This plot allows one to tell, at a glance, how well the apparent ellipse fits the observations.

The Desmos graphing calculator routine described in this paper analyzes the apparent orbits, assumed to be elliptical per Kepler's First Law. The challenge in this analysis is creating an ellipse that matches the observations, i.e., matches the plotted points which are the changing position angles and separations between the two stars in the binary pair over time. This Desmos routine provides five sliders—one for each of the five parameters that describe a translated and rotated ellipse in the Desmos Cartesian plane.

These sliders can be iteratively adjusted until an apparent ellipse is found that is a good match to the observations.

To use Kepler's Third Law to determine stellar mass, we must know the orbital period and the semi-major axis of the true orbit. Fortunately, Kepler's Second Law—equal areas being swept out in equal times—can be used to transform an apparent orbit into a true orbit as it would be seen if it were viewed face-on from outer space. This transformation requires solving Kepler's Equation. This transcendental equation does not have a direct algebraic solution, so Kepler (1609) made laborious successive approximations to solve for the true orbit of Mars. Newton's subsequent invention of calculus produced a more efficient method, based on successive derivatives, that rapidly converge on a true orbit solution. Obtaining true orbits is beyond the scope of this paper. Please refer to Rowe et al. (2024) and Romero (2024) for two computerized iterative solution techniques. The focus of the paper is entirely on Desmos' analysis of apparent orbits. Since the USNO's plots of a known binary is the starting point for this graphical analysis, a detailed description of these plots is in order.

2. Binary Star Plots from the 6th Orbit Catalog

The apparent orbit plot from the Sixth Orbit Catalog for the binary WDS 16212+2259, used as the example for Desmos analysis in this paper, is shown in Figure 3. The number of the binary in the WDS Catalog (WDS 16212+2259) is provided in the upper left corner. When this binary, previously thought to be a single star, was first reported in a publication to be a double star, it was assigned its WDS number based on its Right Ascension (RA) of 16 hours and 21.2 minutes, and Declination (Dec) of 22 degrees and 59 minutes. The discoverer code, HU 481, was also assigned (HU 481 for William Hussey's 481st discovery). In the upper right corner is a reference to the paper where the latest orbit was published, Hrt2010a (a paper by William Hartkopf in 2010). The "a" indicates that this was the first published orbit for this binary. Later orbital solutions would have been assigned b, c, d, etc., but since this is the only one listed, it is also the latest published orbital solution.

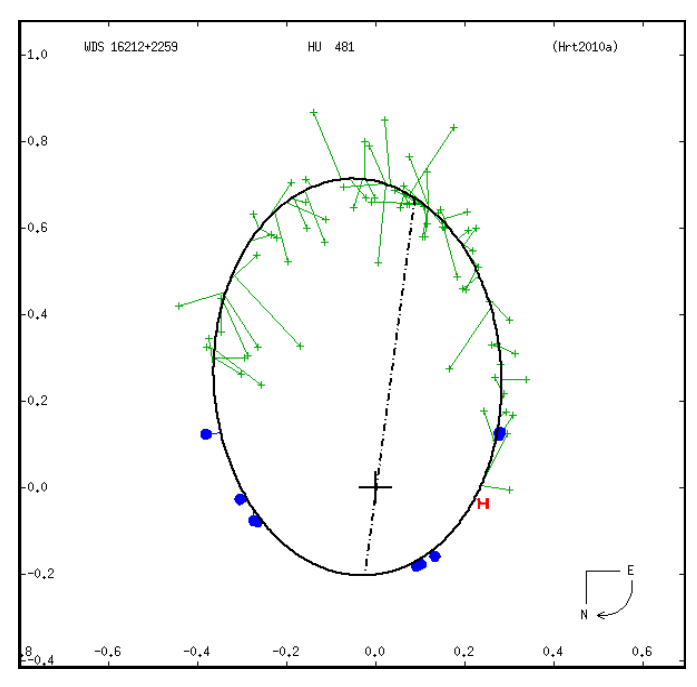


Figure 3: The apparent orbital plot of WDS 18044+0337 downloaded from the 6^{th} Orbit Catalog.

The tick marks around the border of the chart are in arcseconds or fractions of an arcsecond. The

horizontal and vertical zero points on the margins are aligned with the large + mark which is the location of the primary star. The measurements of the secondary (fainter star) are reported *relative* to the primary star, ignoring any actual motion in the sky of the primary star itself. This is done because it is much easier and more precise to measure relative positions between close stars rather than their absolute positions in RA and Dec.

The notation in the lower right corner of the plot provides the orientation of the plot with respect to celestial north; north being down and east to the right. The curved arrow shows the secondary star's direction of rotation relative to the "fixed" primary star, clockwise in this case.

The parameters that defined the true, face-on ellipse of the orbit were a best-fit calculation made by Hartkopf in 2010 based on the 84 published observations of this binary over 113 years from its discovery in 1902 to its (then) last reported observation in 2009. These parameter values, the *orbital elements*, are reported in the 6th Orbit Catalog. The black ellipse in the orbital plot is *not* the true face-on ellipse, but rather the reoriented (tilted) ellipse as it appears when viewed from Earth.

If Hartkopf's estimate of the orbital parameters was accurate, the observations of the secondary star over time would track the apparent ellipse around the primary star. While Hartkopf did the best he could in his 2010 paper to account for the then-published observations, subsequent observations (as we will see) deviated from his published ellipse. If several subsequent observations deviate from the ellipse in a coordinated manner, revising the orbital parameters to fit a new, better-fitting ellipse may be in order.

The black dashed line that passes through the primary star + is the *line of nodes* that shows where the plane of the true orbit intersects the plane of the apparent orbit. In other words, it is the hinge line that the true orbit is tilted about to obtain the apparent orbit.

Observations are color-coded. Each visual observation with filar a micrometer is shown as a **green +**, the **blue dots** are for speckle interferometry observations, while the **red H** is for a 1991 observation made by the European Space Agency's Hipparcos astrometric telescope.

Each observation is plotted as the angular distance of the secondary star from the primary star (their separation, r, in arcseconds) and the position angle of the secondary star (θ) with respect to the primary star and celestial north. Note the lines connecting the observational points to the black apparent orbit ellipse. These lines touch the ellipse at the point in time where the orbital equation predicts that the secondary star should have been.

As can be readily concluded from the plot, the **green +** visual observations were not very accurate in comparison to the **blue dot** speckle observations and **red H** astrometry space telescope observations. This disparity was primarily due to three factors.

First, visual observations (green +) were limited by the capabilities of the human eye as a detector. The eye's exposure time is fixed and can't be made longer to gather photons for observing fainter stars, or shorter to avoid atmospheric-induced motion smearing. Also, the quantum efficiency of the human eye is only about 10%, while that of a good electronic camera these days is about 90%.

Second, the refractor telescopes used in early observations generally had smaller apertures than the reflecting telescopes used in later observations, thus having lower resolution. This made it difficult for close binary stars to appear as two distinct stars in smaller-aperture telescopes.

Third, and of greatest importance, advances in technology allowed the adverse effects of poor *seeing* to be greatly reduced or eliminated. Seeing ... "is the degradation of the image of an astronomical object due to turbulence in the atmosphere of Earth that may become visible as blurring, twinkling, or variable distortion" (Wikipedia, 2023b). Seeing problems can be eliminated by placing telescopes above the

atmosphere, as has been done with the Hipparcos (red H) and (more recently) the European Space Agency's Gaia astrometric telescopes. Placing telescopes in space is expensive, however. Anton Labeyrie (1970) showed that a series of very short exposures (just tens of milliseconds) could eliminate atmospheric smearing in ground telescope images. While each image was filled with speckles due to the different paths that light could take through the many small air cells of different temperatures and refraction, hundreds or thousands of short-exposure images could be processed mathematically via a fast Fourier transform to produce an image much like one would have obtained if there were no atmosphere. This process is termed speckle interferometry (blue dots).

Given these three factors, it is not surprising that large reflecting telescopes (equipped with modern electronic cameras making speckle interferometric measurements) can provide much more accurate astrometric measurements than visual micrometer measurements.

3. Desmos Background 6th Orbit Plot

To initiate the Desmos analysis of binary stars, a new graph is started or, better yet, an existing graph can be downloaded and used as a template. Starting with a binary star analysis template has the advantage that all the needed equations and other expressions are already in place. The graph for this example, WDS 18044+0337 is available at https://www.desmos.com/calculator/aeem8b6oj4. It might be noted that graphs created in Desmos can be tagged with a URL and shared with others (a permalink).

Once the graph is opened and given a new name, the next step is to past in a 6th Orbit plot as a background. In Desmos this can be done by clicking the large + sign in the upper left and selecting Image.

On their plots, Astronomers have assigned north (0°) as straight down, and all angles are measured from north clockwise (NESW). In the Cartesian plane, angles are usually measured from the positive x-axis. As Desmos operates in the traditional Cartesian plane, the angle of the background plot is set to 90°, rotating north so it lies along the positive x-axis. Be sure to click on the Graph Settings wrench icon (upper right) and click Degrees, as the default is in Radians).

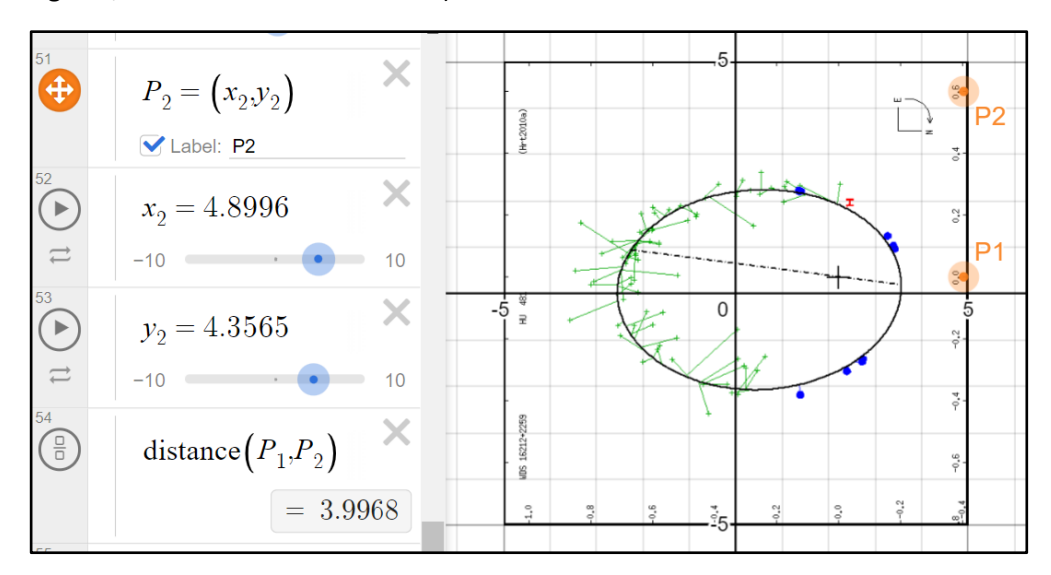


Figure 4: Using the movable pointers, P1 and P2, to measure the distance required for scaling.

The width and height of the background image plot is set by default as 10.0 Desmos units centered on the Desmos (0,0) origin as shown in Figure 4. The width and height both need to be equally reduced such that the Desmos scale (divisions) match those of the 6th Orbit plot. In the example, moveable points PI and P2

were moved to the 0.0 and 0.6 tick marks on the 6^{th} Orbit plot, and the distance between them was found to be 3.9968 Desmos units. The precise placements of P1 and P2 were made with the graph highly magnified. This provided the information needed as two equal ratios: 10 Desmos units (the initial size of the background plot) is to the P1-P2 measured distance, as the final height (and width) value is to the 6^{th} Orbit scale (tick marks). Thus, the final Desmos plot height (and width) = (10 Desmos units * 0.6 Orbit plot units)/3.9968 = 1.5012

Alternatively, clicking on the image will bring up the nine markers used to adjust the background. Any one of the four markers can be moved in or out to decrease or increase the size of the background image. The position of the primary star (the + on the orbital plot) can then be moved by dragging the center marker to position the + (primary star) on the plot to be precisely over the Desmos (0,0) coordinates. Again, magnification can aid precision. These two adjustments have to be done recursively as the movements interact with each other.

4. Washington Double Star Catalog Observations

The 6th Orbit plots often do not contain the most recent published observations. However, the *Washington Double Star Catalog,* maintained by the U.S. Naval Observatory, is a compilation of all published observations, including the first double star observations (Herschel 1785) as well as recent unplotted observations. Data on specific binaries can be requested from the Naval Observatory and supplied as a text file. In the analysis of binary stars, it is important to include recently published observations not yet appearing on 6th Orbit plots, as they are often the most helpful of all past observations in interpreting a just completed new observation.

The Washington Double Star Catalog (WDS) text files provided by the Naval Observatory consist of five sections: Measures, Orbital Elements, Orbital Ephemerides, Notes, and References. The Measures section can be copied into an Excel spreadsheet and (Data) Text-to-Columns applied. Unwanted information (both rows and columns) can then be deleted. For this example, just the WDS 16212+2259 Hipparcos and speckle interferometry observations were retained as shown in Table 1. A recent unpublished observation made on the 1.5-meter telescope at Mt. Wilson Observatory was added as the last row in the table. Also, an additional column (far left) was added with labels for the observer and year of observation. Bibliography codes in the References section can be pasted into a website (NASA ADS 2023) to download most of the references.

The most recent (June 2023) observation of WDS 16212+2259 is reported in this paper for the first time as the last row of Table 1. This observation, of course, was not included in the WDS Catalog text file received from the Naval Observatory. This binary was observed on the historic 1.5-meter telescope (once the world's largest) at Mt. Wilson Observatory. The instrumentation for the speckle interferometry observations and the initial data reduction technique using the Speckle Toolbox (Rowe & Genet 2915, Harshaw et al. 2017) have been documented by Faughn et al. (2023).

Table 1 column headers were added for clarification: Label identifies the observer and year, Date is the year and fraction of a year when the observation was made, Position Angle (θ °) is the angle of the secondary star (in degrees) relative to the primary star (+), Separation (Sep) is the distance between the two stars (r") in arcseconds, while Aperture (Ap in meters) is helpful in identifying the observational telescope. For instance, 2.5 meters is 100 inches, the famous 100-inch telescope Edwin Hubble used to discover the size and expansion of the universe, the Southern Astrophysical Research (SOAR) telescope in Chile is 4.1 meters, while the telescope used at Mt. Wilson Observatory is 1.5 meters. The # is the number of nights averaged together to form the reported r and θ . The Reference (Ref) is where the observation

was published, while Technique (T) is the type of measurement (ones starting with an "S" are speckle interferometry, while starting with H indicates a space telescope).

Table 1: Abbreviated extract from the WDS Catalog.

Label	Date	PA	Sep	Ар	#	Ref	Т
Bla1986	1986.455	113.7	0.3030	3.6	1	Bla1987	S
Bla1986	1986.455	114.7	0.3060	3.6	1	Bla1987	S
HIP1991	1991.250	81.0	0.2450	0.3	1	HIP1997a	Hh
Hrt1995	1995.438	39.7	0.2070	2.5	1	Hrt1997	Sc
Hrt1996	1996.323	29.5	0.2040	2.5	1	Hrt2000a	Sc
Hrt1996	1996.539	26.6	0.2030	2.5	1	Hrt2000a	Sc
Hrt2007	2007.313	286.5	0.2770	2.5	1	Hrt2009	Su
Gii2008	2008.390	285.7	0.2840	0.7	1	Gii2012	S
Tok2009	2009.262	275.1	0.3065	4.1	1	Tok2010	S
Gii2014	2014.524	253.1	0.3850	0.8	1	Gii2022	S
Tok2015	2015.337	252.1	0.4010	4.1	2	Tok2016a	St
Tok2018	2018.399	243.6	0.4446	4.1	2	Tok2019c	St
Tok2021	2021.319	237.2	0.4812	4.1	2	Tok2022f	St
MW02023	2023.489	233.2	0.5170	1.5	1	This Paper	S

WDS observations are given as the apparent separation between the primary and secondary stars in arcseconds (r), and the position of the secondary star with respect to celestial north in degrees (θ). Note that θ is reserved in Desmos for angles. The separation and position angle for each observation, r, and θ , are entered, as well as a label for the point, such as the three-letter observer designator and year of observation (e.g., Tok2018). Desmos does not directly plot points in polar coordinates, so the (x,y) position coordinates are calculated for the ith added (x_i, y_i) point as (r_i cos θ _i, r_i sin θ _i).

When labels for points are entered in Desmos, it automatically places them at (usually) a good location, although their location can be changed for added clarity. Points and their corresponding labels can also be color-coded and presented as a filled circle, open circle, or x marks the spot to help avoid confusion. Besides entering the coordinates and labels of new observations, it can also be useful to label some already included observations on the background, such as accurate speckle interferometry or space observations, as these labels can help clarify the analysis.

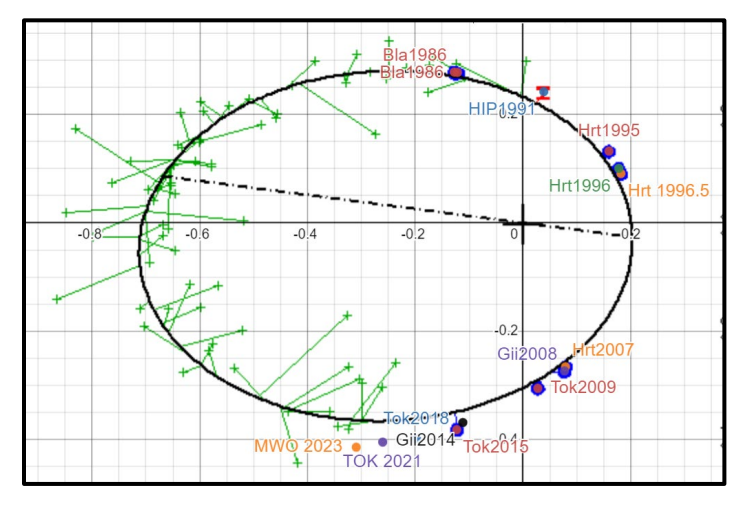


Figure 5: Three new and 12 past observations plotted and labeled.

Three new speckle observations (MWO 2023, Tok2021, and Tok2019), 12 past speckle observations, and one space observation have been added and labeled as shown in Figure 5. MWO2023 was a recent observation made by students and supporters on the 1.5-meter telescope at Mt. Wilson Observatory in June of 2023. If the 6th Orbit plot background image was precisely scaled and translated then, when the

coordinates are entered for previously plotted observations, the observations will show up as small dots in the center of the large blue dots on the plot.

5. General Ellipse Equations

The general equation for the x and y values of an ellipse centered on the origin with its major axis coincident with the x-axis is:

$$x^2/a^2 + v^2/b^2 = 1$$

where:

a is the semi-major axis

b is the semi-minor axis

For an ellipse not centered on the origin and not coincident with the x-axis, as is the binary star case, one can use the general parametric equations for an ellipse in the Cartesian plane:

$$x = (h + a \cos t)(\cos q) + (k + b \sin t)(-\sin q)$$

$$y = (h + a \cos t)(\sin q) + (k + b \sin t)(\cos q)$$

where:

a is the semi-major axis

b is the semi-minor axis

q is the angle from the x-axis to the ellipse major axis

h is the offset of the center of the ellipse from the primary star (the "+") along the ellipse's primary axis *after* the ellipse has been rotated

k is the y offset of the center of the ellipse from the primary star (the "+") perpendicular to the ellipse's primary axis *after* the ellipse has been rotated

(t is just the parametric variable that traces out the ellipse from 0° to 360°)

The (x,y) coordinates of the ellipse center are:

$$(h \cos q - k \sin q, h \sin q + k \cos q)$$

This is shown graphically in Figure 6 where the line segment from the Primary Star to the First Offset is from (0,0) to $(h \cos q, h \sin q)$ is of length h, and the segment from the First Offset to the Ellipse Center is $[(h \cos q, h \sin q), (h \cos q - k \sin q, h \sin q + k \cos q)]$ and is of length k. The line drawn through the center of the ellipse at angle q is the major axis of the ellipse. Note that it does *not* pass through the Primary Star at (0,0).

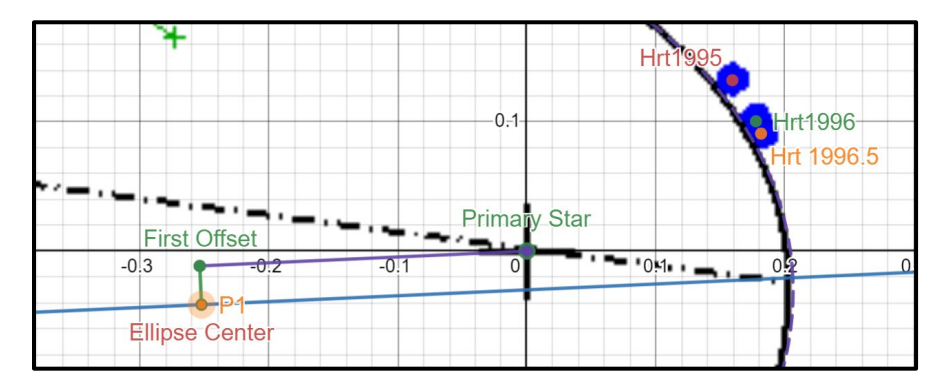


Figure 6: Ellipse center with respect to the h and k offsets at angle q.

6th Orbit Apparent Ellipse Equation

To obtain the five ellipse parameters for the 6th Orbit apparent ellipse, the five parameter sliders can be adjusted iteratively until an ellipse (small red dots) in Figure 7 overlays the black line of the 6th Orbit published ellipse.

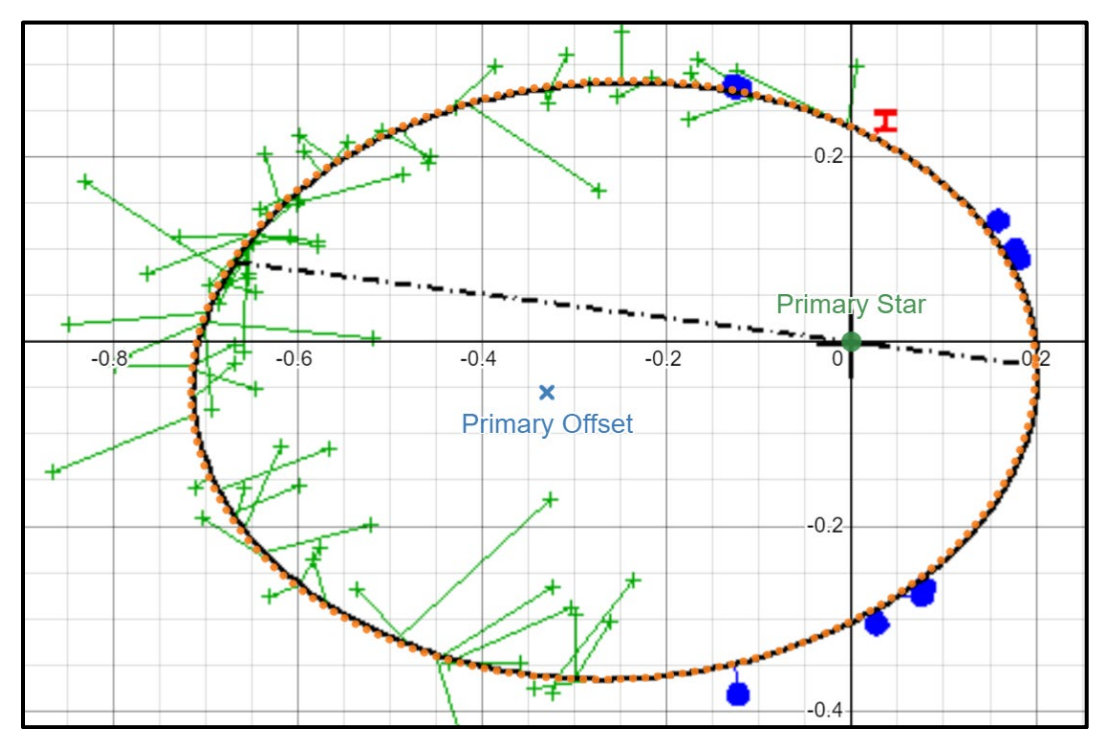


Figure 7: Ellipse (red dots) overlaid on the solid black line 6th Orbit ellipse.

An easier and more accurate way to obtain the apparent ellipse parameters is to analytically derive them from the true Orbital Elements published in the 6th Orbit Catalog (included in the WDS data supplied by the USNO on individual binaries). The new Orbits routine (Rowe & Genet 2024) in the Speckle Toolbox derives the apparent ellipse parameters from the true orbit parameters. The semi-major and semi-minor axes, as well as the rotation angle of the ellipse, can be entered directly from Orbits into Desmos, but the x,y offsets in Orbits have to be translated into the h,k Desmos offsets at the angle (q in Desmos) by:

 $h = x \cos q + y \sin q$ $k = y \cos q - x \sin q$

6. New Apparent Ellipse

The apparent orbit shown in Figure 7 (black ellipse overlaid with the red dot ellipse) was calculated by Hartkopf (2010) without the benefit of the five speckle observations made since his analysis. Given this new information, a new apparent ellipse was created in Desmos that fits the speckle interferometry points better than Hartkopf's 2010 orbit. Starting with the 6^{th} Orbit apparent ellipse, the five parameters were adjusted to fit an ellipse to the speckle and space observations. The visual observations (green +) were not considered while making this fit as their accuracy was low for this small-separation binary. The result is shown in Figure 8. As can be seen (and expected) the new ellipse provides a significantly better fit to the speckle observations.

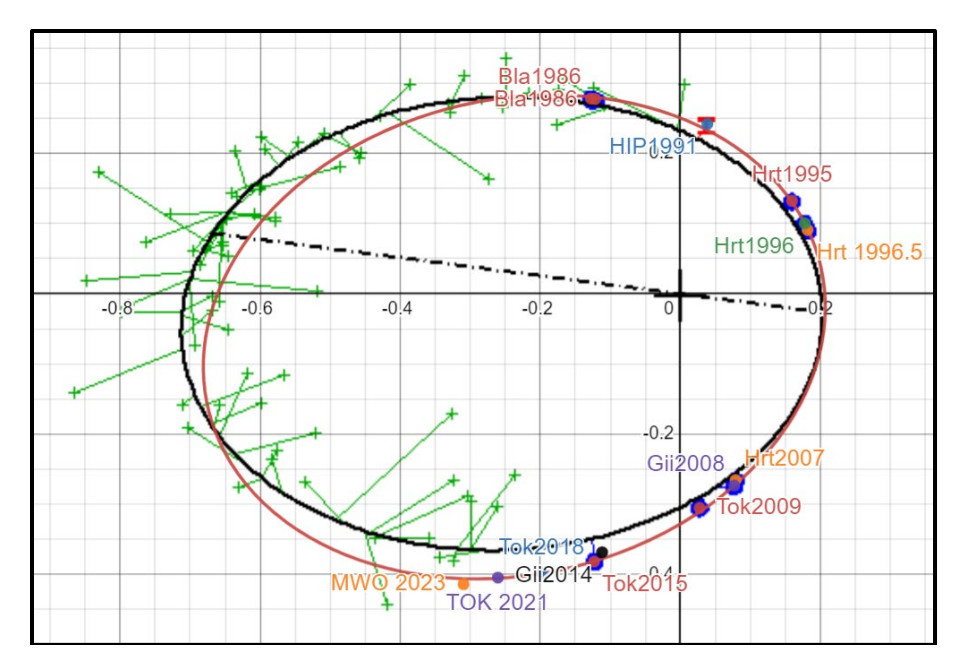


Figure 8: Apparent ellipse fitted to speckle interferometry and space observations.

Table 2 lists the values for the five ellipse parameters for both the original (black) apparent ellipse and the new (red) apparent ellipse.

Table 2: Ellipse parameter values for WDS 16212+2259 new orbit and 6th Orbit Catalog original ellipse.

Parameter	Name and Units	6th Orbit	New
а	semimajor axis "	0.458	0.456
b	semi-minor axis "	0.324	0.335
h	primary star x offset	-0.260	-0.250
k	primary star y offset	-0.028	-0.008
q	angle of major axis°	3.000	14.300

If the recent observations added in the Demos analysis do not suggest a systematic departure from the published orbit, then the Desmos apparent orbit analysis is completed. If, as is the case here, there is a significant, systematic departure from the published orbit, then a new orbit could be calculated, a procedure beyond the scope of this paper.

7. Conclusion

Desmos, combined with plots from the 6th Orbit Catalog and observational values from the Washington Double Star (WDS) Catalog can be used to analyze the apparent orbits of known binaries. Desmos combines mathematical precision with intuitive visual displays.

Acknowledgments

The United States Naval Observatory supplied past observations of WDS 16212+2259 from their Washington Double Star Catalog. The background plot was from the Sixth Catalog of Orbits of Visual Binary Stars. The Institute for Student Astronomical Research (InStAR) purchased time on the 1.5-meter telescope at Mt. Wilson Observatory where the new speckle interferometry of WDS 16212+2259 was made. Gravic Inc. provided travel funds for students to attend the run. Rachel Freed, Reed and Chris

Estrada, Nick Hardy, Leon Bewersdorff, Joseph Burch, Paul McCudden, Tom Smith and others helped organize the run and managed the observations. Thomas Meneghini, the Director of the Mt. Wilson Observatory, and his staff provided support during the run. We thank several external reviewers for their helpful comments.

References

Desmos. 2023. https://www.desmos.com/calculator

Faughn, Elias, John Major, & Paul McCudden. 2023. Speckle Astrometry of WDS 18181-0120. *Journal of Double Star Observations*, 19, 421.

Harshaw, Richard, David Rowe, & Russell Genet. 2017. The Speckle Toolbox: A Powerful Data Reduction Tool for CCD Astrometry. *Journal of Double Star Observations*, 13, 52.

Hensley, Hagan. 2018. The Double Star Orbit Initial Value Problem. *Journal of Double Star Observations*, 14, 363.

Herschel, W. 1785. Catalog of Double Stars. *Philosophical Transactions of the Royal Society of London,* 75, 24.

Herschel, W. 1803. Account of the changes that have happened, during the last twenty-five years, in the relative situation of double stars. *Philosophical Transactions of the Royal Society* **93**, 339.

Kepler, Johannes. 1609. *Astronomia Nova*. 2nd translated edition by William Donahue, Green Lion Press. Labeyrie, A. 1970. Attainment of diffraction limited resolution in large telescopes by Fourier analyzing speckle patterns in star images. *A&A*, 6, 85.

Matson, Rachel A., S. J. Williams, W. I. Hartkopf, & B. D. Mason. 2023. *Sixth Catalog of Orbits of Visual Binary Stars*, U.S. Naval Observatory, Washington, DC. http://www.astro.gsu.edu/wds/orb6.html

NASA ADS. 2023. https://ui.adsabs.harvard.edu/

Rowe, David, and Russell Genet. 2015. User's Guide to PS3 Speckle Interferometry Reduction Process. Journal of Double Star Observations, 11 (1s), 266.

Rowe, David, and Russell Genet. 2024. Speckle Toolbox Orbits Analysis: WDS 21001+0731 Example. Journal of Double Star Observations, in press.

Washington Double Star Catalog. 2023. United States Naval Observatory, http://www.astro.gsu.edu/wds/ Wikipedia 2023a, Definition of astrometry, https://en.wikipedia.org/wiki/Astrometry Wikipedia 2023b, Definition of seeing, https://en.wikipedia.org/wiki/Astronomical_seeing

Astrometric Measurements of Double Star Systems HEI 915, GRV 719, STI 2170, and RST 2531.

Nathan Bowman¹, Karthikeya Vattem^{1,2}, Sophia Bhatti^{1,3}, Kavi Bidlack^{1,4}, Kalée Tock¹

¹ Stanford Online High School, Redwood City, CA; nathanlbowman@gmail.com

² Independence High School, Frisco, TX

³ Unionville High School, Kennett Square, PA

⁴ Design Tech High School, Redwood City, CA

Abstract

The double star systems HEI 915, GRV 719, STU 2170, and RST 2531 were measured and analyzed in order to investigate the relationship of their component stars. Images were requested of each system from the Las Cumbres Observatory Global Telescope network and were measured for the position angle and separation. Historical data was also used to plot the position of the secondary star relative to the primary star for each system. Some of the systems appeared to have somewhat of a linear trend, though this was inconclusive. Finally, system escape velocity was calculated for all of the stars. Although all four systems are co-located and co-moving, indicating a physical relationship, all four have relative velocities that exceed the corresponding system escape velocity, suggesting that they are unlikely to be gravitationally bound. GRV 719's relative velocity only slightly exceeded its escape velocity, which may suggest that its stars could be gravitationally bound within the uncertainty in the calculations.

1. Introduction

WDS 05319+2220 HEI 915, WDS 06415+3045 GRV 719, WDS 06588+5532 STI 2170, and WDS 08094-3836 RST 2531 are double stars located in the constellations Taurus, Gemini, Lynx, and Puppis respectively. These stars have not been measured for several years, with HEI 915 last measured in 2014 (Zacharias et al., 2015), GRV 719 in 2016 (El-Badry, 2021), STI 2170 in 2015 (Zacharias et al., 2015), and RST 2531 in 1999 (Skrutsie, 2006), so the measurements of this paper offer an update. Furthermore, each system has interesting characteristics. The secondary of HEI 915 was once listed as a variable (Bronnikova, 1975), but it does not currently appear in the AAVSO Variable Star Index (Kloppenborg, 2023). The stars of RST 2531 are part of the "Gaia red clump," which are red giant stars of similar luminosities that can be used as standard candles (L. Ruiz-Dern et al., 2018). In addition, RST 2531 is a triple system, and the secondary B component of RST 2531 has a potentially binary companion in the system RST 2531 BC.

While variable in their locations and features, these targets were all selected from the Washington Double Star catalog based on similar criteria including their magnitude, separation, and classification as physical doubles. They all have a secondary star magnitude of less than 13 and a delta magnitude of less than 3 to ensure that both stars of the system will be visible and resolved in images with a consistent exposure time on the Las Cumbres Observatory Global Telescope (LCOGT) network instruments used. The separation was constrained to be above 5" so that the stars can be properly measured without overlap in the images,

and below 15" to increase the likelihood of a strong physical relationship. They are also identified on Stelle Doppie as physical doubles.

The Gaia G absolute magnitude, estimated spectral type, and estimated mass for each star was retrieved from the Gaia astrophysical parameters table. For stars where these parameters were not provided, Gaia Data Release 3 (DR3) parallax and apparent magnitude can be used with Eq. (1), along with the Gaia BP-RP color, to plot each star's position on the Gaia HR diagram (Gaia Collaboration, 2023; 2016b; 2023j).

$$M = m + 5 * (log p + I) \tag{1}$$

In Equation 1, M is the absolute G-filter magnitude, m is the apparent G-filter magnitude, and p is the parallax. Gaia BP-RP color on the x-axis of the Gaia HR diagram is a proxy for surface temperature, and Gaia G absolute magnitude on the y-axis is a proxy for luminosity. Figure 1 was used to estimate spectral type and temperature based on Gaia BP-RP color and Gaia G absolute magnitude, as shown in Table 1. Figure 2 was then used to estimate mass. However, Figure 2 estimated masses were only used for the primary of GRV 719 and the secondary of RST 2531, and the other star masses were taken from Gaia data. All four systems are on the Main Sequence near the turnoff point. In Table 1, the Gaia G absolute magnitude, Estimated spectral type, and Estimated mass columns were queried from the Gaia DR3 Astrophysical Parameters table as LUM_FLAME, SPECTRALTYPE_ESPHS, and MASS_FLAME, respectively.

Table 1. Spectral type and mass estimates from Gaia. Bold values were not provided by the Gaia data and are calculated or estimated based on Eq. (1), Fig. 1, and Fig. 2.

System	Primary or Secondary	Parallax (mas)	Gaia source ID	Gaia G apparent magnitude	Gaia G absolute magnitude	BP-RP color	Estimated spectral type	Estimated mass
HEI 915	Primary	3.45885 ± 0.0286	34040322 03677401 216	10.55	5.36	0.702	F	1.4
	Secondary	3.56317 ± 0.0178	34040321 99382932 096	11.53	1.66	0.967	F	0.9
GRV 719	Primary	2.6536 ± 0.0215	34350309 02501081 600	11.42	3.54	0.967	G	1.5
	Secondary	2.6303 ± 0.0174	34350309 06797222 400	11.78	2.21	0.838	G	1.1
STI 2170	Primary	2.09331 ± 0.0259	99996439 19150859 52	12.04	2.5	0.811	G	1.0
	Secondary	2.01821 ± 0.0274	99996431 88983334	12.10	2.58	0.822	G	1.1

			40					
RST 2531	Primary	4.7590 ± 0.0149	55409761 73741665 152	9.98	3.40	0.715	F	1.3
	Secondary	5.3248 ± 0.5422	55409761 73729454 336	11.25	4.50	0.945	F	1.5

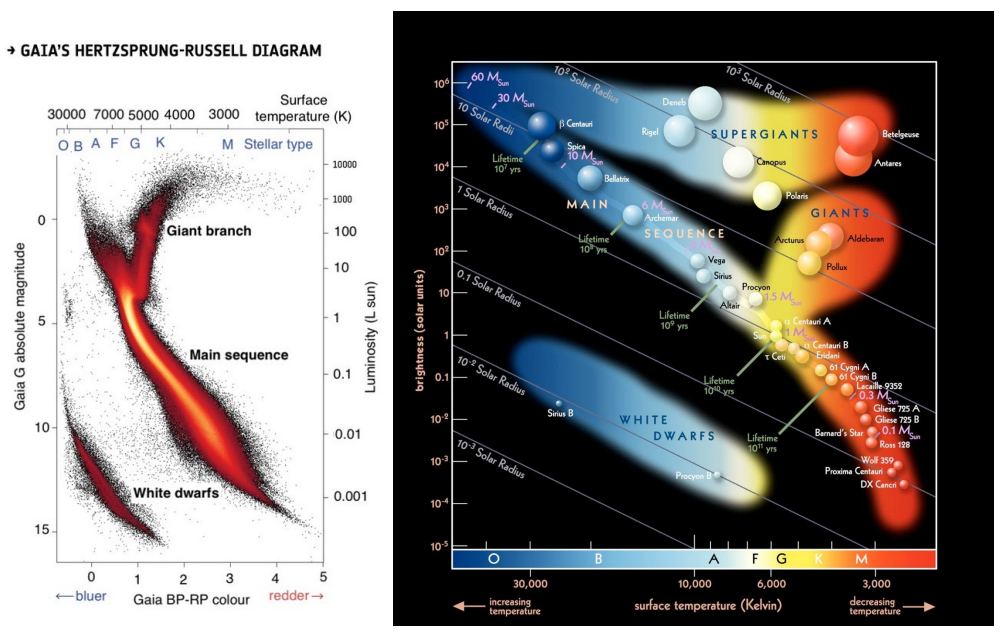


Figure 1 (left): Gaia HR Diagram (Gaia Collaboration et. al., 2023; Gaia Collaboration et. al.; 2016b; Gaia Collaboration et. al, 2023j). Figure 2 (right): HR diagram (ESO) with known masses labeled.

2. Instruments Used

Images of each system were requested through the online LCOGT network portal (Brown et al., 2013). Images of HEI 915 and GRV 719 were taken from the Teide Observatory in Tenerife, Spain. The images of STI 2170 were taken from the McDonald Observatory in Texas, USA, and the images of RST 2531 were taken from the Siding Spring Observatory in New South Wales, Australia.

All systems were imaged using the PlaneWave DeltaRho 350 + QHY600, which has a field of view of 30' x 30' in central mode, and a format of 2400 x 2400 pixels. Ten images were requested for each system. HEI 915, GRV 719, and RST 2531 were taken using the Bessell-V filter (Bessell, 1990) with exposure times of 9.5 seconds, 22.1 seconds, and 10 seconds respectively. These exposure times were calculated using the online LCOGT Exposure Time Calculator. For the system STI 2170, the V-filter exposure time was

computed to be 46 seconds, so in order to save telescope time, the exposure time was halved and the wider-bandpass PanSTARRS-w filter (Tonry et al., 2012) was used instead.

3. Data

The images were analyzed using AstroImageJ. Some images were re-requested because of technical problems with the original returned images, but all images were ultimately well-resolved. Fig. 3 contains screenshots of one sample measurement of each system. The image of HEI 915 shows an elongated primary star that may be related to an associated 20th magnitude star identified by Gaia. RST 2531's B component features a potentially binary companion that was not resolved in any of the images. Table 2 lists the summary measurements for each system after image reduction, including the size of the measurement aperture used and the decimal date of observation.

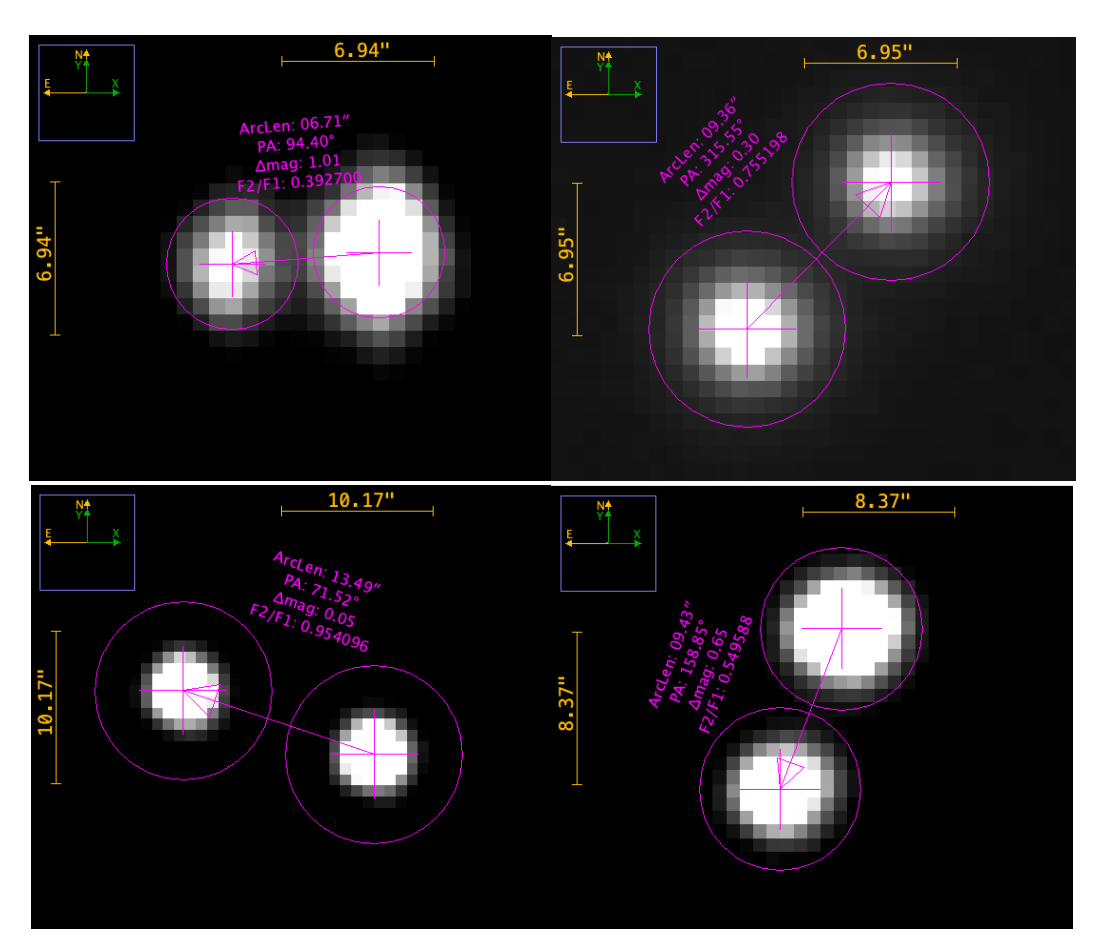


Figure 3: Sample measurements of each system using the AstroImageJ software. The separation is displayed as 'ArcLen' and the positional angle is displayed as 'PA.' Measurements are shown in the following order from top left to bottom right: HEI 915, GRV 719, STI 2170, RST 2531.

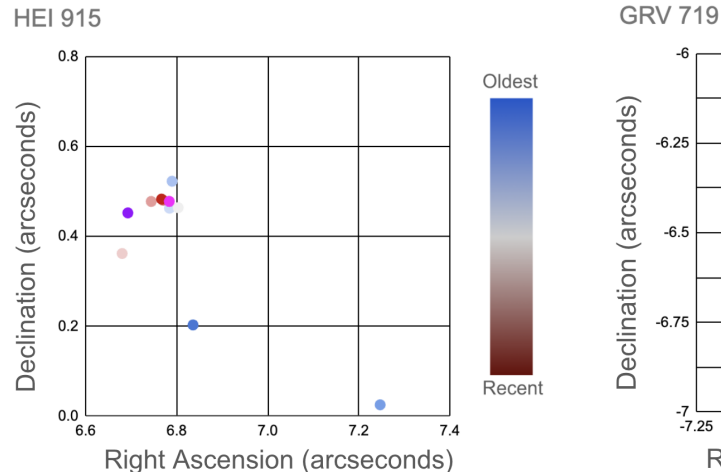
Table 2. Summary Measurements of Double Star Systems After Reduction.

System Aperture Date Number	Average Standard	Average	Standard	İ
-----------------------------	------------------	---------	----------	---

	Size (px)		of Images	Position Angle (°)	Error on Position Angle	Separation (")	Error on Separation
HEI 915	4	2024.0329	10	93.9	0.203	6.71	0.010
GRV 719	6	2024.0437	10	315.4	0.032	9.33	0.026
STI 2170	8	2024.0380	10	71.6	0.013	13.48	0.004
RST 2531	6	2024.0329	10	158.8	0.050	9.45	0.009

4. Plots

Plots of the historical measurements of each system are plotted below in Figs. 4 - 8. Gaia DR3 data measurements are shown in pink, and our measurements are shown in purple. The rest of the data points are colored chronologically, with blue data points being the oldest and red being the most recent. Note that one extreme outlier is not shown in the RST 2531 plot, due to being at a position angle of 165°, unlike most of the other historical data points which were around 156°. Also, for STI 2170, two plots are shown, the second of which has 3 outliers removed.



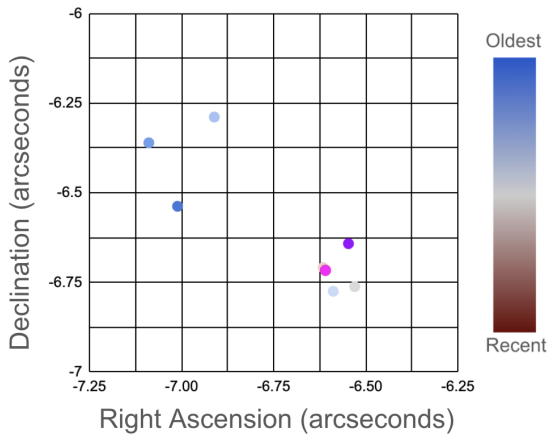


Figure 4. Measurements over time of HEI 915.

Figure 5. Measurements over time of GRV 719.

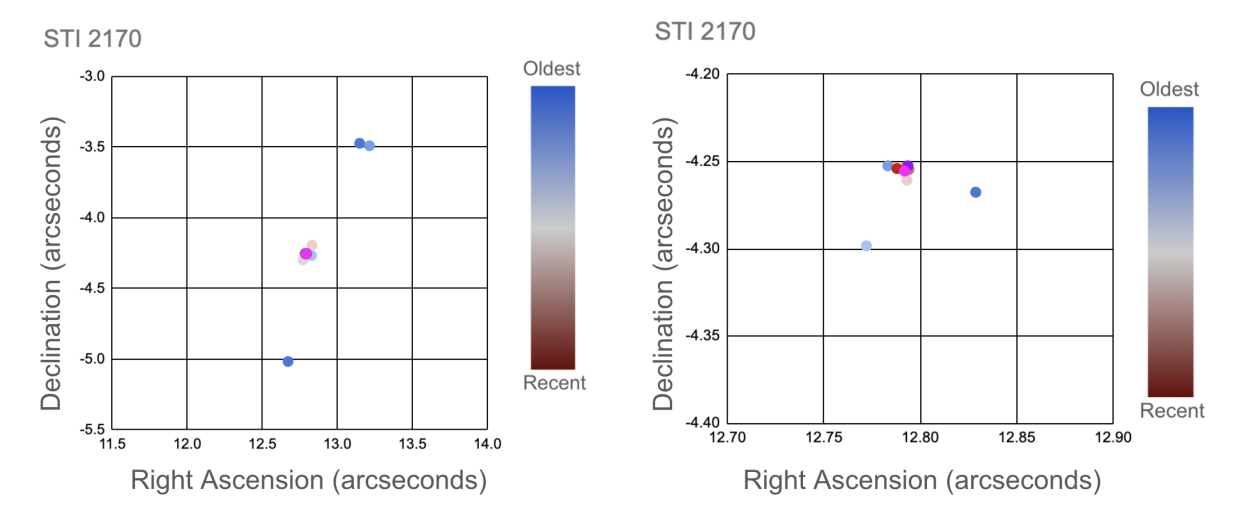


Figure 6. Measurements over time of STI 2170.

Figure 7. Measurements over time of STI 2170 with three outliers removed to see the other data points more clearly.

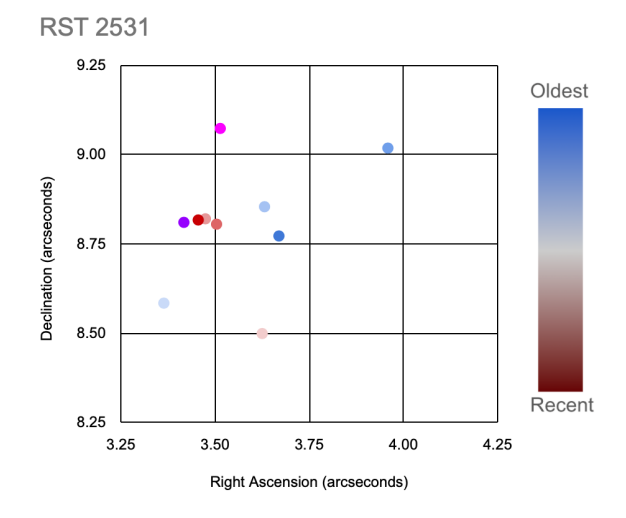


Figure 8. Measurements over time of RST 2531.

All of the plots show some roughly-linear movement of the secondary star relative to the primary, though none suggest the curvature that would be expected for a binary system. Some of the systems such as GRV 719 do not have enough measurements for curvature to be conclusive even if it were present.

5. Discussion

Data, shown below in Table 3, were queried from the Gaia Data Release 3 (DR3) to assess the physical relationship probability by analyzing each star's proper motion components. With these data, a relative proper motion (rPM) metric was calculated by subtracting the secondary stars' PM vector from the primary stars' PM vector and finding the magnitude of the resultant vector (Harshaw 2016). This metric compares

the relative transverse motion to the proper motion of the faster-moving one. A lower rPM value, therefore, correlates with a higher similarity of motions between the two stars in the system. As shown in Table 3, the rPM value for each system is low, indicating that the stars within each system are moving similarly and could be physically related.

System	Plx Primary (mas)	Plx Secondary (mas)	PM RA Primary (mas/yr)	PM RA Secondary (mas/yr)	PM Dec Primary (mas/yr)	PM Dec Secondary (mas/yr)	rPM
HEI 915	3.45885 ± 0.02864	3.56317 ± 0.01777	1.56350 ± 0.03639	-0.52490 ± 0.02269	-19.19521 ± 0.02439	-19.44186 ± 0.01510	0.108
GRV 719	$2.65366 \\ \pm 0.02152$	$2.63029 \\ \pm 0.01738$	$21.43298 \\ \pm 0.01793$	$21.72652 \\ \pm 0.01541$	-9.23882 ± 0.01610	-9.32412 ± 0.01541	0.013
STI 2170	$2.09331 \\ \pm 0.02591$	$2.01821 \\ \pm 0.02742$	-4.16140 ± 0.01967	-5.55450 ± 0.02060	-14.40618 ± 0.01865	-13.89846 ± 0.01881	0.099
RST 2531	4.75901 ± 0.01490	5.32480 ± 0.24222	-24.27940 ± 0.01448	-26.76894 ± 0.30093	2.92426 ± 0.01549	2.24515 ± 0.26812	0.096

Table 3. Gaia DR3 Parallaxes (Plx), Proper Motions (PM), and relative proper motion (rPM).

Additionally, the escape velocity for each system is calculated using the formula of Eq. (2), whose derivation is based on the fact that total mechanical energy of the system has to be zero for the stars to be orbiting each other (Bonifacio et al., 2020). In Eq. (2), since both stars are orbiting a common center of mass, M is the combined mass of the system (the sum of the component masses in Table 1 converted to units of kg), v refers to the system escape velocity, G is the gravitational constant, and r is the physical distance between the stars in meters.

$$v_{escape} = \sqrt{\frac{2GM}{r}} \tag{2}$$

The 3-dimensional separation r between the stars has 2 components: transverse and radial. The transverse angular separation is used to calculate a transverse physical separation in parsecs using the unit conversions shown in Eq. (3).

$$Sep_{pc} = \frac{Sep_{arcseconds} \cdot \frac{l^{\circ}}{3600''} \cdot \frac{2\pi \, rad}{360^{\circ}}}{parallax''}$$
 (3)

To find the 3-dimensional separation r, the transverse separation, computed via Equation 3 is combined with the stars' radial separation (equal to the difference of their inverted parallaxes) via the Pythagorean Theorem. For systems GRV 719 and RST 2531, where the stars' radial distances are within uncertainty of each other, the transverse separation of the systems is used as the distance between the stars without the radial component, since the overlapping uncertainties could mean that the stars are the same distance from the Earth.

The relative motion was found by using the Pythagorean theorem on the relative transverse motion and relative radial motion of the stars in the system. The relative radial motion was computed by subtracting the radial velocities of the two stars, multiplying it by 1000, and taking the absolute value. The relative transverse motion was found by first getting the relative PM vector from the difference in the two stars' proper motion in RA and Dec respectively using the Pythagorean theorem, and then dividing this by the parallax of the primary, and converting to m/s from mas/yr by the conversion factor of 4740 mas/yr to m/s.

Within each system, the stars' relative motion to each other is compared to the calculated escape velocity as a way of estimating whether the stars are likely to be gravitationally bound. If the escape velocity is substantially lower than the stars' relative motion, this is unlikely, and vice versa. These calculations will be shown for one of the systems, GRV 719, for clarity.

For GRV 719, the mass estimates from Gaia were 1.50 and 1.06 solar masses for the primary and secondary star respectively, meaning the combined mass was taken as 2.56 solar masses, and was then converted to kilograms. The transverse separation, calculated with Eq. (3), was used directly for this system because the parallaxes of the two stars overlap in uncertainty, as explained above, and equals about 0.02 parsecs. This was converted to meters using the conversion factor of 3.086E+16 meters per parsec. Substituting these values into Eq. (2) gives us an escape velocity of 1131 m/s.

With the same system, the relative motion was found through the process outlined above, with the final value being approximately 1199 meters per second.

The calculated escape velocities for the systems are shown in Table 4, and were calculated using Eq. (2), with the mass coming from the Gaia data in Table 1. As shown in Table 4, for three of the systems—HEI 915, STI 2170, and RST 2531—the system escape velocity is significantly lower than the stars' relative motion, so these systems are unlikely to be binary. For GRV 719, however, the estimated escape velocity is close to the system's relative motion. Therefore, within the uncertainty of the calculation, the stars of GRV 719 might be gravitationally bound to each other.

System	Calculated Escape Velocity (m/s)	Relative Motion (m/s)
HEI 915	49	2900
GRV 719	1131	1199
STI 2170	32	3457
RST 2531	1570	2019

Table 4. Calculated escape velocities and relative motions

6. Conclusion

A new measurement of PA and Sep for each system was found from our measurements. From the Gaia DR3 (parallax and proper motion), all of the systems are physically related. The calculated rPM constant is low, which supports this. The estimated escape velocities of each system are lower than the stars' relative

velocities, which suggests that they are not binary, though the fact that the escape and relative velocities of GRV 719's components were within 70 m/s of each other makes this system less conclusive. Corroborating this, the systems' historical data plots show vaguely linear trends over time in the position of the secondary star relative to the primary. Continued measurements of these systems would help confirm these trends and to refine the calculations.

7. Acknowledgements

This research was made possible by the Washington Double Star catalog maintained by the U.S. Naval Observatory, the Stelle Doppie catalog maintained by Gianluca Sordiglioni, Astrometry.net, and AstroImageJ software which was written by Karen Collins and John Kielkopf.

This work has made use of data from the European Space Agency (ESA) mission Gaia (https://www.cosmos.esa.int/gaia), processed by the Gaia Data Processing and Analysis Consortium (DPAC, https://www.cosmos.esa.int/web/gaia/dpac/consortium). Funding for the DPAC has been provided by national institutions, in particular the institutions participating in the Gaia Multilateral Agreement.

This work makes use of observations taken by the Planewave Delta Rho 350 + QHY600 CMOS camera systems of Las Cumbres Observatory Global Telescope Network located in Tenerife, Spain; Texas, USA; and New South Wales, Australia.

The Las Cumbres Observatory's education network telescopes were upgraded through generous support from the Gordon and Betty Moore Foundation.

This research has made use of the SIMBAD database, operated at CDS, Strasbourg, France (Wenger et al. 2000).

This publication makes use of data products from the Two Micron All Sky Survey, which is a joint project of the University of Massachusetts and the Infrared Processing and Analysis Center/California Institute of Technology, funded by the National Aeronautics and Space Administration and the National Science Foundation.

Thank you to our reviewer from JDSO for the insightful and helpful comments.

8. References

- Bonifacio, B., C. Marchetti, R. Caputo, and K. Tock. (2020). Measurements of Neglected Double Stars. Journal of Double Star Observations, 16(5), 411–423. http://www.jdso.org/volume16/number5/Bonifacio 411 423.pdf
- Bronnikova, N. M. (1975). Stars suspected of variability in the Taurus region. Peremennye Zvezdy Prilozhenie, 2(10), 225–236.
- Brown, T. M. et al. (2013). Las Cumbres Observatory Global Telescope Network. Publications of the Astronomical Society of the Pacific, 125(931), 1031–1055. https://iopscience.iop.org/article/10.1086/673168/meta
- El-Badry, K., Rix, H., Heintz, T. (2021). A million binaries from Gaia eDR3: sample selection and validation of Gaia parallax uncertainties. Monthly Notices of the Royal Astronomical Society, 506(2), 2269-2295.
- Gaia Collaboration, T. Prusti, J.H.J. de Bruijne, et al. (2016b). The Gaia mission. A&A 595, A1. https://www.aanda.org/articles/aa/full-html/2016/11/aa29272-16/aa29272-16.html
- Gaia Collaboration, A. Vallenari, A. G. A. Brown, et al. (2023j) Gaia Data Release 3. Summary of the content and survey properties. A&A 674, pp. A1. https://arxiv.org/abs/2208.00211
- Gaia Collaboration, C. Babusiaux, C. Fabricius, S. Khanna, et al. (2023) Gaia Data Release 3. Catalogue validation. A&A 674, pp. A32. https://arxiv.org/abs/2206.05989
- Harshaw, Richard (2016). CCD Measurements of 141 Proper Motion Stars: The Autumn 2015 Observing Program at the Brilliant Sky Observatory, Part 3. Journal of Double Star Observations, 12(4), 394–399. http://www.jdso.org/volume12/number4/Harshaw 394 399.pdf
- L. Ruiz-Dern, C. Babusiaux, et al. (2018). Empirical photometric calibration of the Gaia red clump: Colours, effective temperature, and absolute magnitude. A&A 609, A116. https://www.aanda.org/articles/aa/full html/2018/01/aa31572-17/aa31572-17.html
- Skrutsie, M. F. et al. (2006). The Two Micron All Sky Survey. The Astronomical Journal. 131(2), 1163-1183.
- Tonry, J. L, et al. (2012). The PanStarrs1 Photometric System. The Astrophysical Journal. https://iopscience.iop.org/article/10.1088/0004-637X/750/2/99/pdf
- Zacharias, N. et al. (2015). The First U.S. Naval Observatory Robotic Astrometric Telescope Catalog. The Astronomical Journal, 150(4), 101. https://ui.adsabs.harvard.edu/abs/2015AJ....150..101Z/abstract

Desmos Analysis of the Binary Star WDS 19471-1953

Michael-James L. Ellis^{1,2} and Russell M. Genet²

- 1. Payson High School, Payson, Arizona
- 2. Eastern Arizona College, Payson Campus

Abstract Speckle interferometry observation of the Binary Star WDS 19471-1953 on the 1.5-meter telescope at Mt. Wilson Observatory on 2023.484 provided a position angle of 83.3° and a separation of 0.552". The published orbit appeared to include three observations that were off by 180°. Desmos analysis—with the three values corrected and two new speckle interferometry observations—produced three new apparent orbits that were all equally good fits to these observations. We expect that just one of the apparent orbits will fit subsequent analysis that includes the times of observations and produces orbital elements.

Introduction

This paper analyzes a binary star, WDS 19471-1953, discovered in 1873 by S. W. Burnham. Some 26 visual observations were made of this binary prior to a 1991 observation by Hipparcos (the European Space Agency's astrometric space telescope). Since then, there have been seven published speckle interferometry observations (listed in the Washington Double Star Catalog by the U.S. Naval Observatory), and one other speckle interferometry observation made in June 2023 at Mt. Wilson Observatory and reported in this paper for the first time.

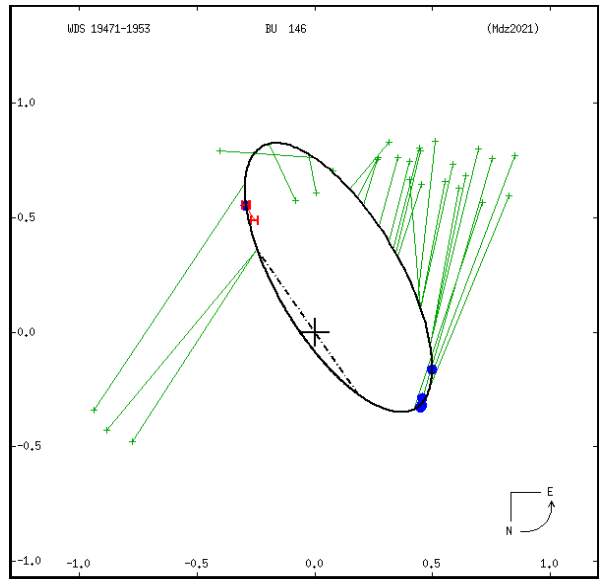


Figure 1: Orbital plot of WDS 19471-1953 from the Sixth Catalog of Orbits of Visual Binary Stars (hereafter the 6^{th} Orbit Catalog).

Desmos (https://www.desmos.com/), an easily learned online graphing calculator, is used in geometry, algebra, trigonometry, and calculus classes in many high schools and colleges. It is free, online, and easily accessed. Results are stored in the cloud at no cost. Familiarity with Desmos allows student teams to efficiently tackle the analysis of binary star orbits. A three-step Desmos apparent orbit analysis process (Genet 2023) was used to analyze WDS 19471-1953. Each step is outlined below.

The objectives of this paper were to report the new speckle interferometry observation made at Mt. Wilson Observatory, derive an improved apparent orbit if that seemed appropriate, and evaluate the three-step Desmos analysis process.

Please see the Demos online graph at https://www.desmos.com/calculator/eani846wcj that was used to analyze this binary and produce the graphical images in this paper.

Step 1: Paste in and Adjust the Background Orbital Plot

As shown in Figure 2, the plot of WDS 19471-1953 that was downloaded from the 6th Orbit Catalog was pasted in as background in Desmos, rotated 90 degrees, scaled so that the 6th Orbit scale (tick marks) matched the Desmo scale, and translated so that the 6th Orbit primary star (0,0 + mark) matched the Desmos 0.0 origin. Please see Genet (2023) for details on this and other Desmos analysis procedures.

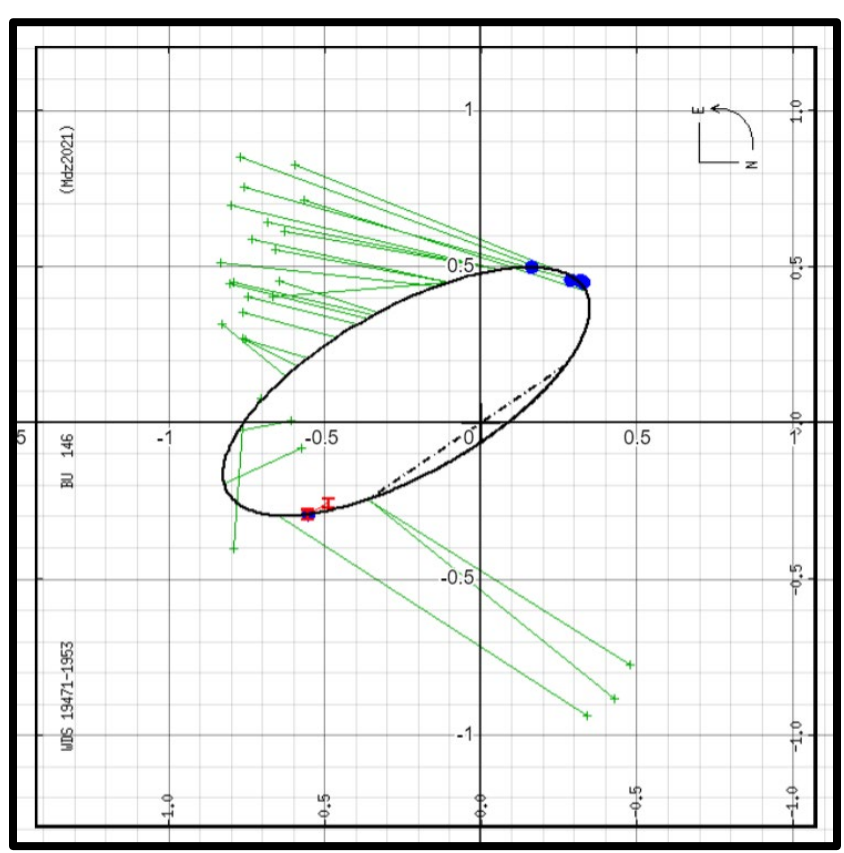


Figure 2: Background binary plot as it appeared in Desmos after appropriate rotation, scaling, and translation.

Step 2: Add New Observations and Label Previous Observations

The U.S. Naval Observatory's Washington Double Star Catalog is a database for all published observations of double stars (including binary stars). Information on the past published observations of any of the over 100,000 double stars in the catalog can be requested and will be supplied by return email as an attached text file. Space telescope and speckle interferometry observations received from the Naval Observatory for WDS 19471-1953 are shown in Table 1. The recent speckle interferometry observation made at Mt. Wilson Observatory (MWO) is also shown in the last row. Visual observations were not included as they were widely scattered (as can be seen from the plot) and the decision was made to only use the much more accurate space and speckle interferometry observations in the analysis.

Table 1: Key information on WDS 19471-1953. Column headings are the Label, Date (year and fraction of a year), position angle (PA) in degrees, the separation (Sep) in arcseconds, the aperture of the telescope (Ap) in meters, the Reference (code to the published observation), and the observational technique (Tech). The Tech codes are Hh Hipparcos, Ht Tyco, and the rest speckle interferometry (Sc CHARA 4m at CTIO, Su USNO, S ordinary speckle, and St Tokovinin HR Cam at SOAR).

Label	Date	PA	Sep	Ар	#	Referance	Tech
HIP1991	1991.250	27.7	0.6260	0.3	1	HIP1997a	Hh
Hrt1991	1991.720	28.1	0.6260	4.0	1	Hrt1996b	Sc
TYC1991	1991.750	27.6	0.5500	0.3	1	TYC2002	Ht
Tok2008	2008.539	53.8	0.5564	4.0	1	Tok2010	S
Tok2008	2008.765	54.2	0.5549	4.1	1	Tok2010	S
Tok2009	2009.262	55.1	0.5539	4.1	1	Tok2010	S
Mns2011	2010.591	57.8	0.5390	3.8	1	Msn2011d	Su
Tok2018	2018.251	72.0	0.5242	4.1	2	Tok2019c	St
Tok2019	2021.319	78.3	0.5130	4.1	2	Tok2022f	St
MWO2023	2023.484	83.3	0.5520	1.5	1	This paper	S

The observations in Table 1 were entered into Desmos, resulting in the graph shown in Figure 3. Note that the HIP1991, Hrt1991, and TYC1991 observational points on the right side of the plot were not associated with any points on the 6th Orbit background plot. The two red H symbols lying on their side (one over a blue dot for speckle interferometry) that appear in the lower left of the plot were not in agreement with the three 1991 observations listed in the Washington Double Star Catalog. Thomas Smith suggested that these points were in error by 180°, which was confirmed by plotting them as in Desmos with 180° added to their position angles. These points fell exactly on the lower left plot points, confirming the 180° error.

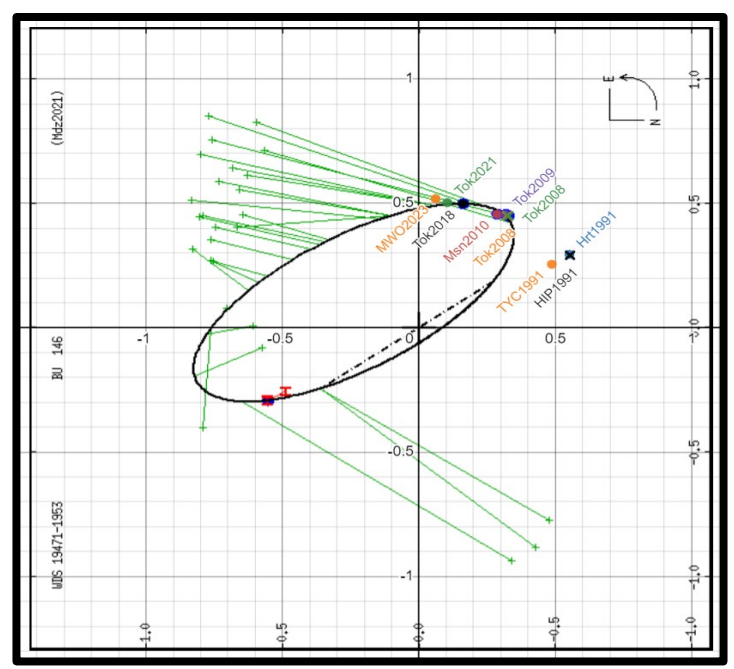


Figure 3: The Desmos graph for WDS 19471-1953 showing two new observations (MWO2023 and Tok2021, top middle) and eight previous space and speckle interferometry observations (now labeled).

Step 3: Create New Apparent Orbits

As can be seen from Figure 3, the published orbit of WDS 19471-1953 was not a good fit to the three corrected past observations (HIP 1991, Hrt1991, and Tyco1991, middle right). Desmos was used to generate a new apparent orbit to provide a better fit to the Hipparcos space telescope observation (the Tycho observation with its lower astrometric precision was not included in further analysis) and the speckle interferometry observations.

For an ellipse not centered on the origin and not coincident with the x-axis, the general parametric equations for an ellipse in the Cartesian plane are:

```
x = (h + a \cos t)(\cos q) + (k + b \sin t)(-\sin q)

y = (h + a \cos t)(\sin q) + (k + b \sin t)(\cos q)
```

where:

a is the semi-major axis

b is the semi-minor axis

h is the x offset of the center of the ellipse from the primary star (the "+")

k is the y offset of the center of the ellipse from the primary star (the "+")

q is the angle from the x axis to the ellipse major axis

(t is just the parametric variable that traces out the ellipse from 0 to 360°)

The values of the five parameters for a general ellipse were adjusted via Desmos sliders to obtain the fit shown in Figure 4. Two points, Tok 2021 and Msn 2010 were off slightly (around 10 mas). The ellipse parameters are shown to the left of the Desmos plot.

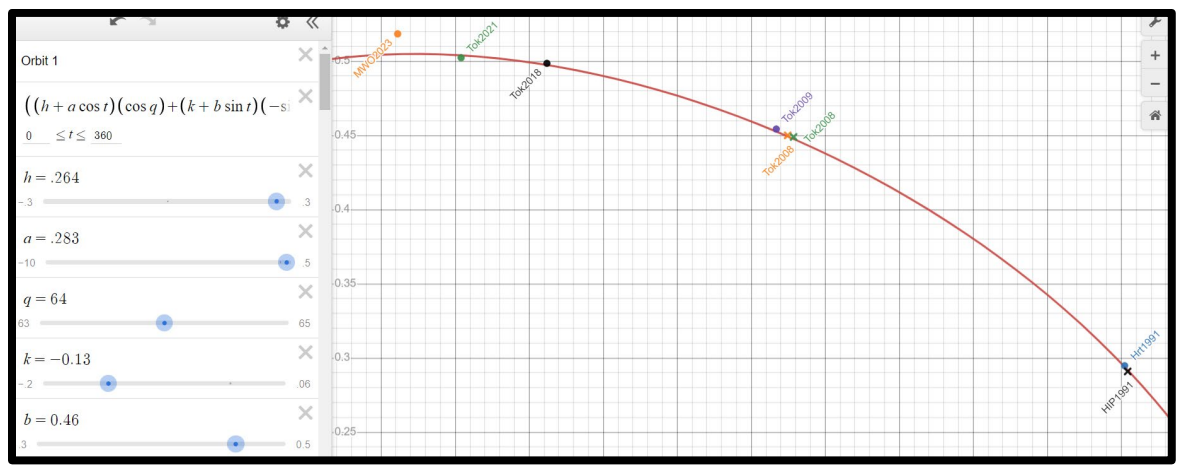


Figure 4: Desmos fit of an ellipse to eight high-quality observations.

As can be seen in Figure 5, the first new orbit is wildly different than the Mdz2001 published orbit. Assuming the three Mdz2002 points in the lower left (HIP 1991, Hrt1991, and Tyco1991) were in error by 180°, the new orbit appears to be a much better fit for the space telescope and speckle interferometry observations.

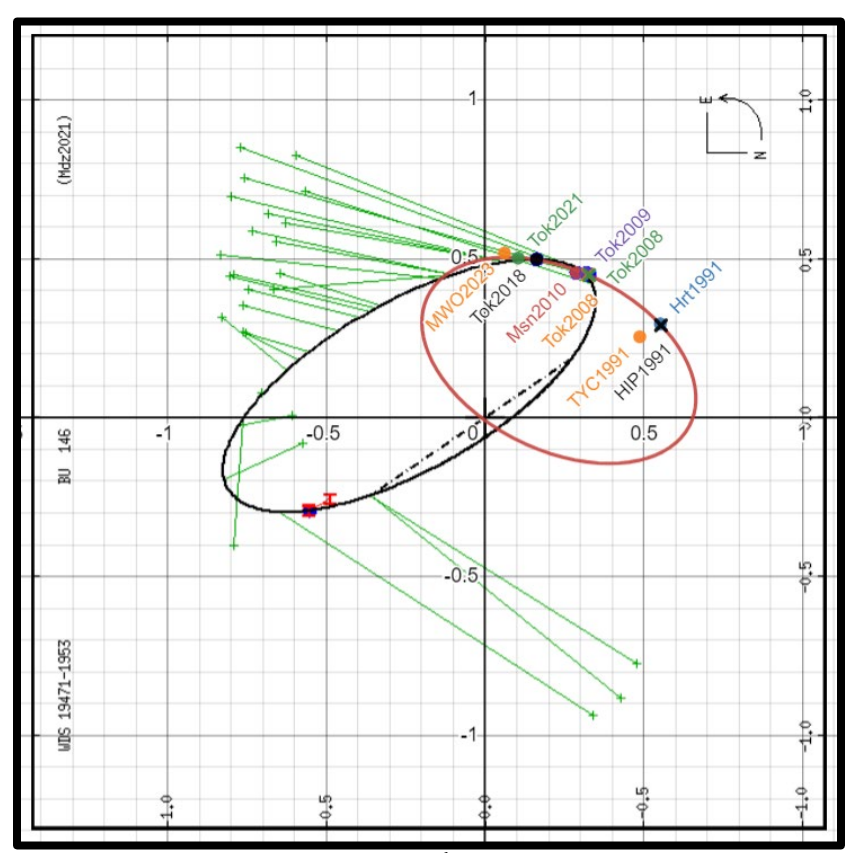


Figure 5: A comparison of the original orbit in the 6th Orbit Catalog (black) and the revised orbit (red).

Normally, only one new apparent orbit would provide a better fit to the observations than the original orbit. However, when the high-accuracy space and speckle interferometry observations only cover a small portion of the orbit, as is the case with WDS 19471-1953, more than one ellipse may make a reasonable fit to the observations. In the case of WDS 19471-1953, two additional apparent orbits were found that were also a good match to the space telescope and speckle interferometry observations as shown in Figures 6 and 7. The two observations, MWO2023 and Msn2010, still departed somewhat from the other observations.

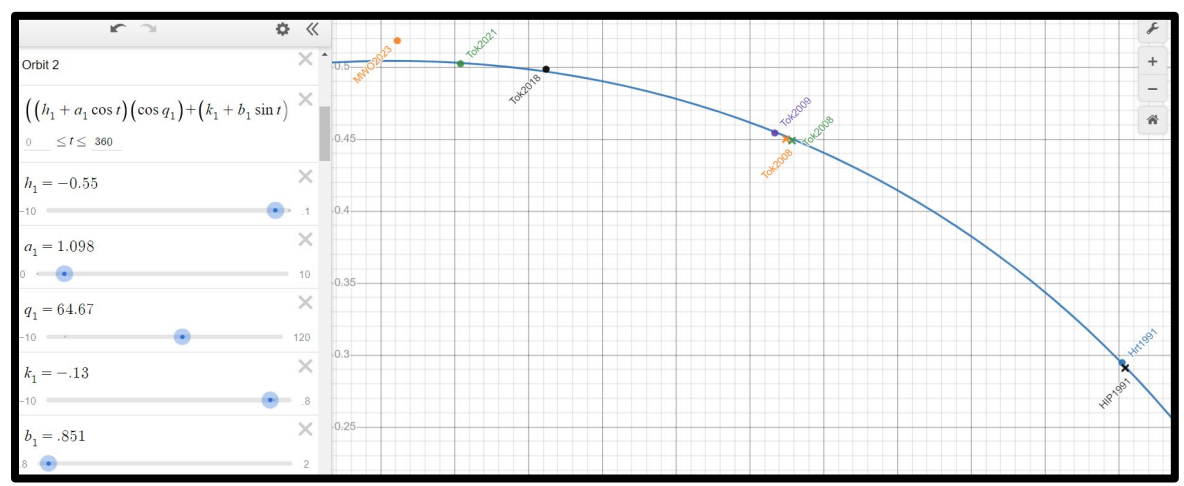


Figure 6: Desmos fit of an ellipse to nine high-quality observations.

Finally, a third new orbit was found that was also a good fit as shown in Figure 7

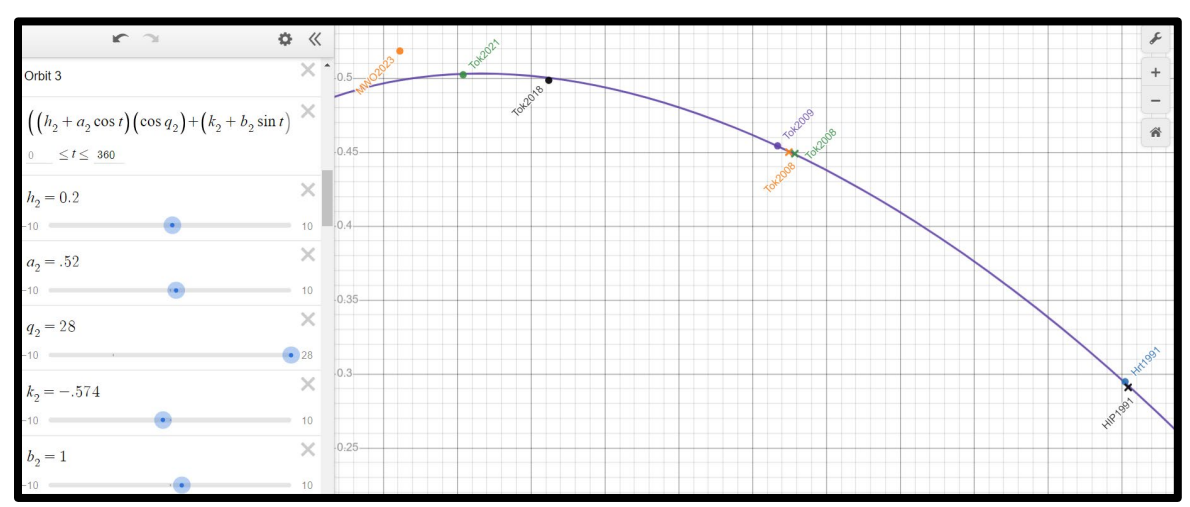


Figure 7: Desmos fit of an ellipse to nine high-quality observations.

The original 6th Orbit apparent background orbit (black), and all three of the new Desmos-derived apparent orbits are shown in Figure 8.

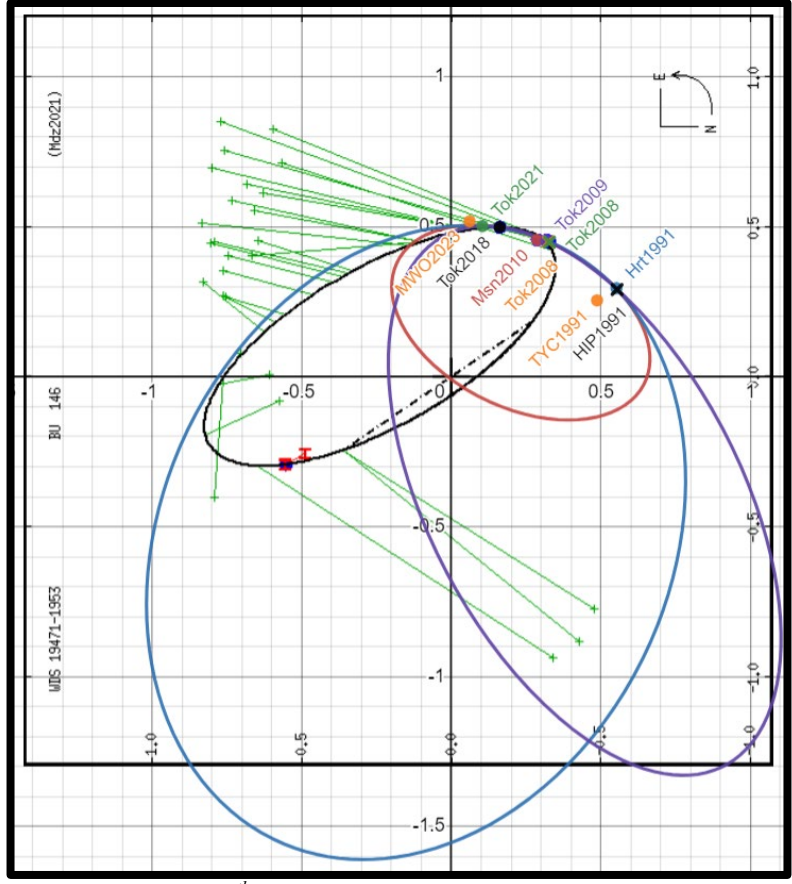


Figure 8: The original orbit in the 6th Orbit Catalog (black) and the three new orbits (red, blue, and purple).

The three new Desmos apparent plots shown above in Figure 8 are magnified to cover the portion of the orbit with the Hipparcos space telescope and speckle interferometry observations. As can be seen in Figure 9, all three match these observations closely except, as before MWO2023 and MSN2010. We expect that by including the date/time of each observation one of the three apparent orbits will be superior. These results will be included in a follow-up paper.

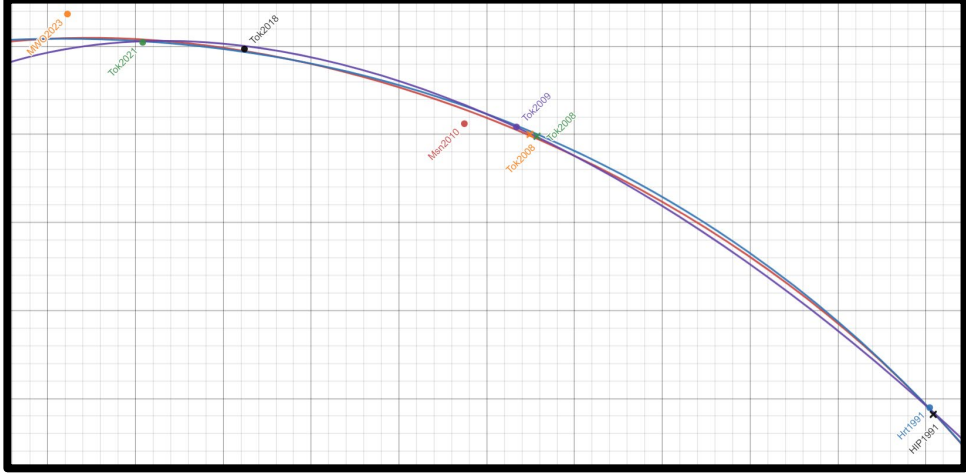


Figure 9: Desmos fit of the three new orbits (red, blue, and purple) to nine high-quality observations.

Conclusions

The new speckle interferometry observation of WDS 19471-1953 made at Mt. Wilson Observatory was reported for the first time in this paper. Three unexpected errors in the 6th Orbit plot of this binary were corrected.

While the published 6th Orbit plot was not a good fit for the corrected observations, using Desmos a much better fitting apparent orbit was found, although it was not unique as two additional equally good-fitting orbits were found. It is expected that further analysis that includes the date/time of the observations will determine which of these three orbits is the best fit.

The three-step Desmos analysis process worked well after adding several refinements. Desmos appears to be a useful tool for the analysis of binaries with apparent orbits plotted in the 6th Orbit Catalog.

Acknowledgments

Thanks to the United States Naval Observatory for the use of a plot from their Sixth Catalog of Orbits of Visual Binary Stars, and for supplying past observations from their Washington Double Star Catalog. Thanks also to Thomas Smith for his suggestion that the three points on the 6th Orbit plot that disagreed with the WDS values were all in error by exactly 180°. Gravic Inc. kindly provided travel funds for students to attend the run at Mt. Wilson Observatory. Rachel Freed, Reed and Chris Estrada, Nick Hardy, Leon Bewersdorff, Joseph Burch, Paul McCudden, Mark Harris and others either generated the target lists or managing the observations. We thank Thomas Meneghini, the Director of the Mt. Wilson Observatory, and his staff for their support during our observation run. Finally, we thank several external reviewers for their helpful comments.

References

Genet, Russell. 2023. Desmos Graphical Analysis of Known Binaries, *Journal of Double Star Observations*, in press.

Matson, Rachel A., Stephen J. Williams, William I. Hartkopf & Brian D. Mason. 2023. *Sixth Catalog of Orbits of Visual Binary Stars*, U.S. Naval Observatory, Washington, DC. http://www.astro.gsu.edu/wds/orb6.html

Washington Double Star Catalog. 2023. United States Naval Observatory, http://www.astro.gsu.edu/wds/

Astrometric Measurements of Three Double Star Systems Near 5h of Right Ascension

Leonid Vishnevskiy¹, Denis Levine¹, Nicholas Dunn^{1,2}, Khensa Musaddequr Rahman¹, Kalée Tock1

¹ Stanford Online High School, Redwood City, California; <u>leonid59@ohs.stanford.edu</u>

² Wellington College, Berkshire, UK

Abstract

We investigate three double star systems with a right ascension between 5h and 6h, imaging them using the Las Cumbres Observatory Global Telescope network. We perform astrometric measurements using AstroImageJ, obtaining position angles and separations for all of the systems that are similar to each system's most recent measurements. Historic measurements from the US Naval Observatory are plotted, and linear and quadratic regressions are performed, with the result that a quadratic regression fits slightly, but not conclusively, better for most of the systems. Based on our measurements, historic data plots, and calculations performed using data from Gaia Data Release 3, we conclude that all of the target star systems are physically related. In addition, WDS 05553+0729 DOO 95 is likely to be binary, while WDS 05033+5821 STI 2082 and WDS 05207+2442 POU 674 are unlikely to be binary.

1. Introduction

Double star systems have the potential to be binary systems, in which the stars are mutually bound by gravitational forces. However, they are also interesting if they are physically related in any other way, such as sharing an origin. Studying the nature and evolution of this relationship gives us insight into the history and dynamics of the galaxy.

The focus of our investigation was limited to double stars listed in the Washington Double Star (WDS) Catalog, adhering to a few specific constraints:

- 1. Magnitude (m) secondary < 13: Both stars in each pair were constrained to be brighter than magnitude 13 so that they could be distinguished using the instruments described in Sec. 2.
- 2. 5" ≤ separation ≤ 15": The lower bound was chosen to ensure that our instruments can resolve two separate stars. The upper bound was chosen in hopes that the measurement we obtain would be more likely to be different from previous observations, since stars that are closer together are more likely to orbit faster. While this does not account for radial separation, the correlation still holds in general.
- 3. $\Delta m < 3$: The stars in the pair were constrained to be close together in magnitude, so that both could be exposed properly in a single image with a single exposure time.
- 4. Physical: The system was constrained to be listed as "physical" according to Stelle Doppie, which means that the two component stars have similar parallaxes and proper motions.
- 5. 05h < Right Ascension < 13h: The right ascension of the system was constrained to be between 05h and 13h, to ensure that it is positioned near zenith during the night at the time the study was conducted; this makes the observing position optimal. Declination was not taken into account because the telescope network we used has sites available across the globe.

The targets selected for this study according to the constraints above are all near 5 hours of right ascension. Although their magnitudes make the systems too dim to be seen with the naked eye, their approximate locations can be found by star-hopping from nearby bright stars and asterisms. For example, STI 2082 is close to Capella in the Camelopardalis constellation, and POU 674 is located in Taurus. DOO 95 is in Orion, very close to Betelgeuse. The positions of all three targets shown in Fig. 1.

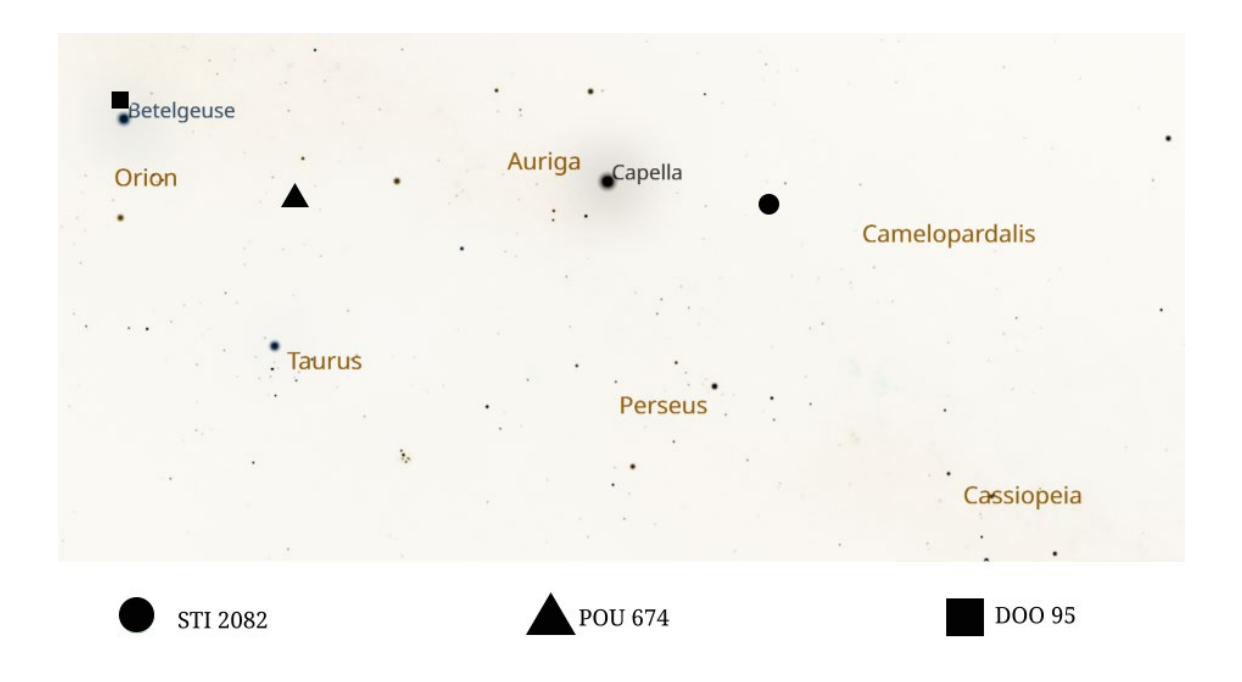


Figure 1: Approximate location of each system, relative to the surrounding constellations and bright stars

Many of these stars are Sun-like, and some are hotter than the Sun. Our measurements for each star were made eight to nine years after the last recorded data, which ranged from 2015 to 2016.

We calculated the absolute magnitude of each star using the Gaia Data Release 3 (DR3) apparent G-filter magnitude and parallax according to Eq. 1 from Morgan, 2019. We invert the distance in parsecs to get parallax, and convert the parallax from " to milliarcseconds:

$$mag_{abs} = mag_{vis} + 5 \times (log_{10} (plx \times \frac{1}{1000 mas}) + 1)$$
 Eq. 1

Where *plx* is the parallax of the star in milliarcseconds. Then we approximated each star's spectral class and mass using our calculations from Eq. 1 of each star's absolute magnitude, and matched this to a mass using a list relating mass to absolute magnitude (Morgan, 2023). The masses and spectral types resulting from this analysis, along with temperature values from the literature for DOO 95, are shown in Table 1.

Star System	Parallax: Primary (mas); Parallax: Secondary (mas)	Gaia DR3 Gmag (Primary; Secondary)	Gaia DR3 BP - RP (Primary; Secondary)	Spectral Type: Primary; Spectral Type: Secondary	Effective Temperature Primary; Secondary (K)	Mass: Secondary (M⊙); Mass: Secondary (M⊙)
WDS 05033+5821 STI 2082	1.64; 1.68	11.36; 11.57	0.46; 0.79	A5; A7	N/A	1.73; 1.61
WDS 05207+2442 POU 674	1.71; 1.73	11.76; 13.16	1.18; 1.35	A7; G0	N/A	1.61; 1.07
WDS 05553+0729 DOO 95	1.62; 1.60	12.23; 12.95	0.73; 0.83	F0; F6	6606.4; 6296.41	1.44; 1.20

Table 1. Masses, spectral types, and colors for each double star system.

2. Equipment and Methods

We used the Las Cumbres Observatory Global Telescope (LCOGT) network to take images of all of our chosen star systems in the Bessell-V filter (Bessell, 1990). The exposure times and observatory locations used for our measurements are summarized in Table 2.

Table 2. The number of images and their exposure times for each system. All images for each system had constant exposure times.

System	Images Taken	Observatory (Location)	Exposure Time (s)
WDS 05033+5821 STI 2082	16	Teide Observatory (Tenerife, Spain)	21
WDS 05207+2442 POU 674	10	McDonald Observatory (Texas, USA)	19
WDS 05553+0729 DOO 95	10	Siding Spring Observatory (NSW, Australia)	19

All of the telescopes involved in this study used a Planewave Delta Rho 350 + QHY600 CMOS camera system, which has a field of view of $1.9^{\circ} \times 1.2^{\circ}$. However, we used the central $30' \times 30'$ mode, which produced images each with a size of 2400 pixels \times 2400 pixels and covering the camera's central $30' \times 30'$ field of view. The pixel size of the camera is 0.73'' per pixel, in 1×1 binning mode. The images were directly analyzed using the AstroImageJ software.

¹Temperature values for DOO 95 from Wenger, 2020.

3. Measurements

3.1. Images

All LCOGT images were processed directly in AstroImageJ using its multi-aperture measurement tool, which allows the user to find the centroid of a star within an aperture, and then calculate the position angle and separation between the two centroids. Sample measurements of each system are shown in Figure 2, along with the measurement aperture radius used. Individual measurements are tabulated in Table 7 of the Appendix.

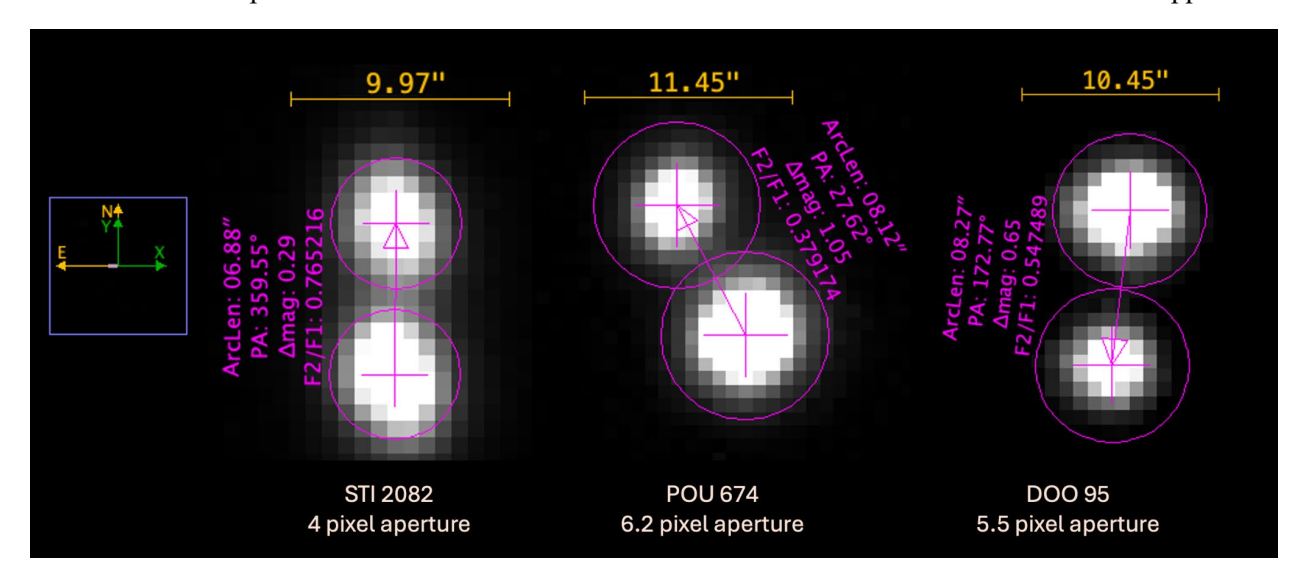


Figure 2: Measurements of STI 2082, POU 674, and DOO95 in AstroImageJ.

A summary of the measurements of the three systems is shown in Table 3, where "Number of Images Used" excludes some images that were lower in quality than those shown above.

Table 3. Summary of obtained astrometric data for all three systems.

System	Decimal Date (Epoch)	Number of Images Used	Average Position Angle (°)	Standard error on Position Angle	Average Separation (")	Standard Error on Separation
WDS 05033+5821 STI 2082	2024.0301	14	359.5	0.05	6.93	0.019
WDS 05207+2442 POU 674	2024.0444	10	27.5	0.04	8.13	0.007
WDS 05553+0729 DOO 95	2024.0329	10	172.8	0.08	8.21	0.015

3.2 Historic Data plots

Below are historical data plots made using data from the USNO. We fit quadratic and linear fits on each system, excluding outlying points where noted, in order to assess the trends of the graphs and the plausibility of curvature. The origin represents the position of the primary star.

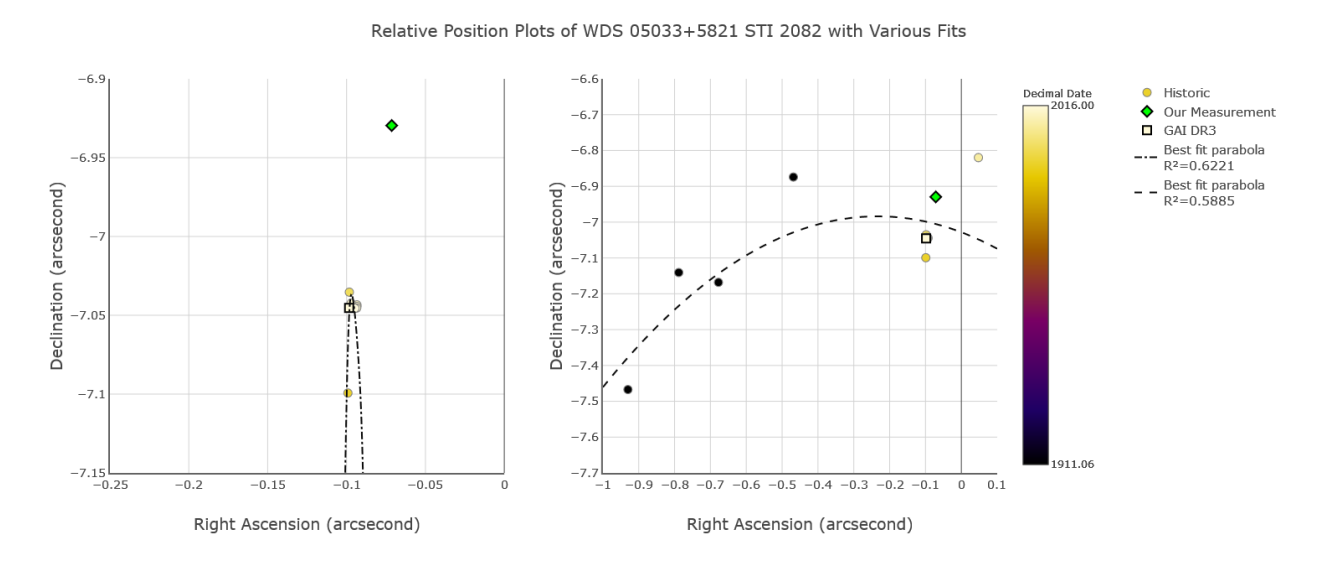


Figure 3: Relative position plots of STI 2082 with a parabolic fit. The right graph contains all points, and the left graph excludes all 1911 points and the 2010 data point

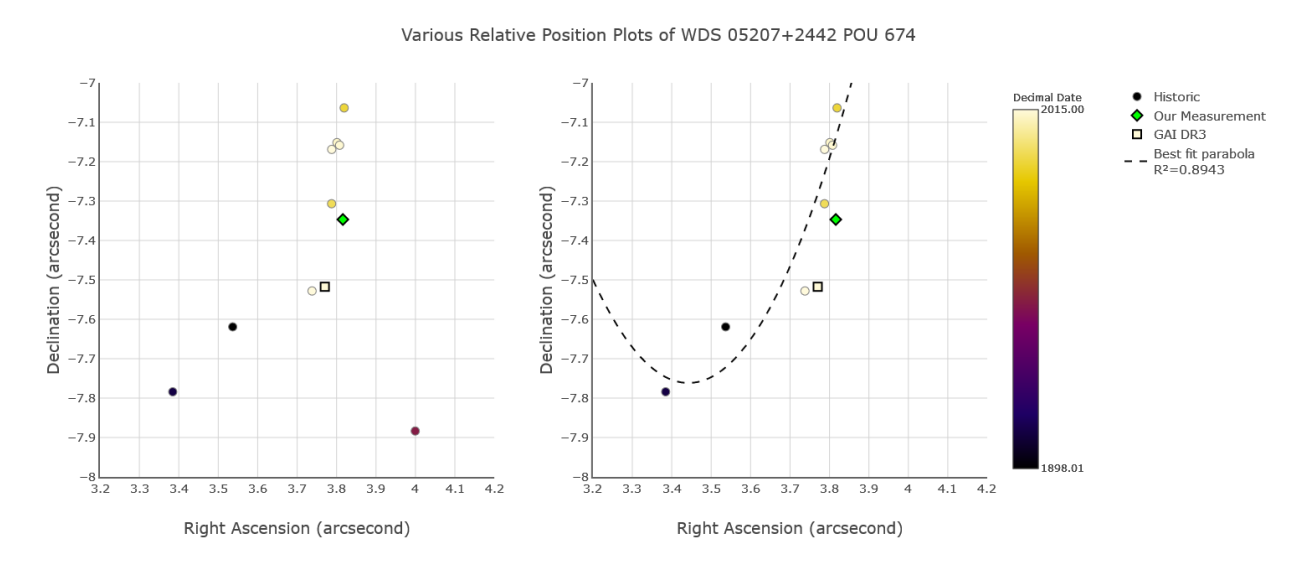


Figure 4: Relative position plot of POU 674. The left graph has all points, and the right graph excludes an outlying data point and has a parabolic fit

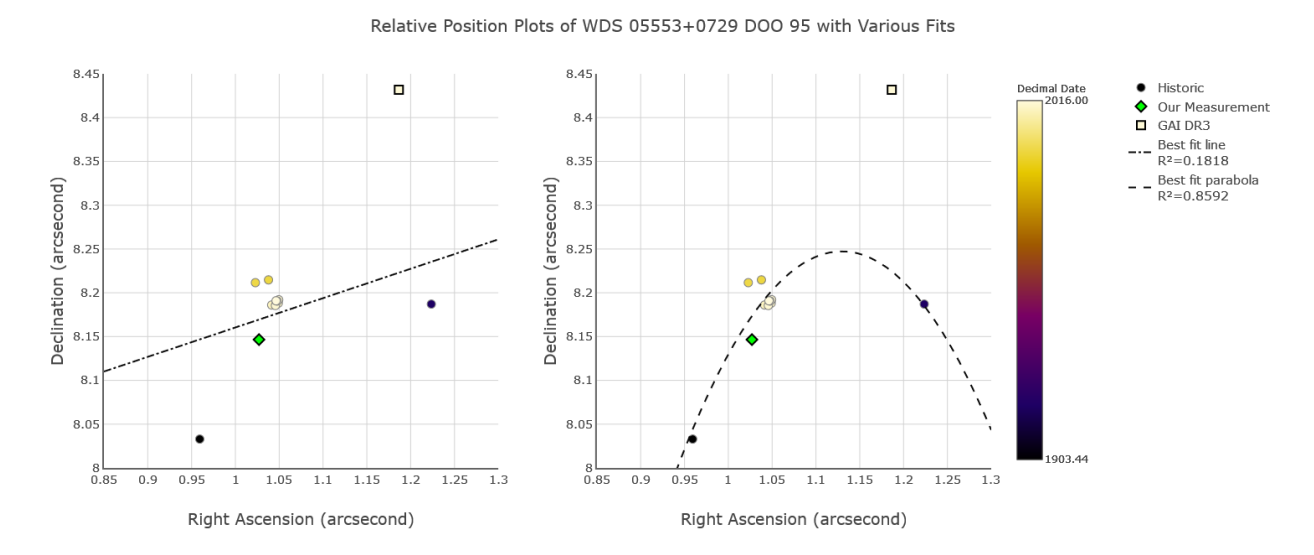


Figure 5: Relative position plots of DOO 95, excluding an outlier from Fay, 2021. The left graph has a linear fit, while the right graph has a parabolic fit.

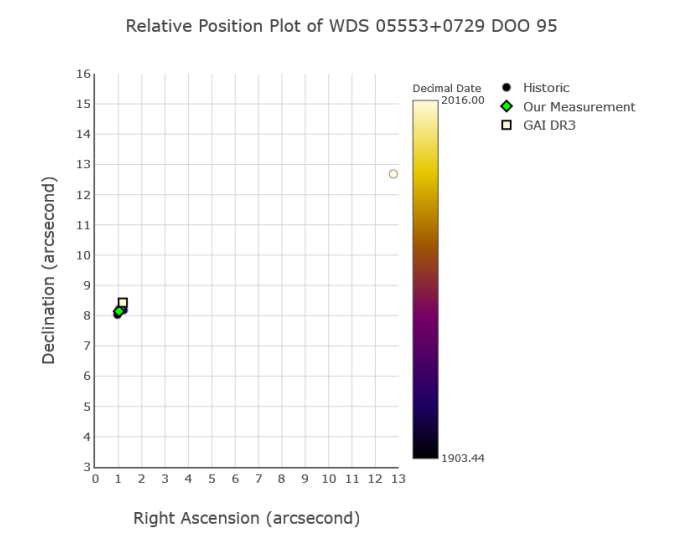


Figure 6: Relative position plot of DOO 95, with outlier included

4. Analysis of the Stars' Motions

To assess the physical relationship between the stars, we obtained proper motion and parallax data from Gaia DR3 which are shown in Table 4.

System	PM RA Primary (mas/yr)	PM RA Secondary (mas/yr)	PM Dec. Primary (mas/yr)	PM Dec. Secondary (mas/yr)	Parallax of Primary (mas)	Parallax of Secondary (mas)
WDS 05033+5821 STI 2082	-0.99934 ± 0.01917	-0.96604 ± 0.01553	2.40102 ± 0.01863	2.13951 ± 0.01472	1.63893 ± 0.02424	1.68483 ± 0.01992
WDS 05207+2442 POU 674	-1.37158 ± 0.02480	-1.25725 ± 0.01866	-2.12339 ± 0.01723	-1.84413 ± 0.01285	1.71328 ± 0.02068	1.72545 ± 0.01530
WDS 05553+0729 DOO 95	4.71638 ± 0.01642	4.69297 ± 0.02168	-14.45043 ± 0.01325	-14.48876 ± 0.01826	1.61591 ± 0.01548	1.59932 ± 0.02143

Table 4. Proper Motions and Parallaxes

We first calculate the rPM values of all the systems, which is a measure of how similar the proper motions of double star systems are and thus how likely they are to be physically related (Harshaw, 2016). A lower rPM value implies that the stars are moving together and therefore may share an origin. Next, we calculated the relative velocities of the secondary stars to the primary stars of each system as well as the escape velocity of each system; this allows us to assess the likelihood of the stars being binary.

4.1 Derivation and Calculation of rPM Values

To derive the rPM from the data, we divide the magnitude of the stars' relative motion by the magnitude of the larger proper motion vector (Harshaw, 2016). In the following equations, PM represents proper motion of the right ascension or declination, and the number suffix represents primary star (for 1) or secondary star (for 2). Pythagoras' theorem is used to combine the x and y components of the total vector. The total relative motion vector is shown in Eq. 2 below:

$$|m_r| = \sqrt{(PM RA 1 - PM RA 2)^2 + (PM Dec 1 - PM Dec 2)^2}$$
 Eq. 2

The magnitude for the proper motion vector of a singular star is computed using Eq. 3:

$$|m_{singular}| = \sqrt{(PM RA 1)^2 + (PM Dec 1)^2}$$
 Eq. 3

We then divide the total value in Eq. 1 by the larger proper motion magnitude (out of the primary and second stars) in Eq. 2 to get the rPM for each system. This is represented in Eq. 4:

$$rPM = \frac{|m_r|}{|m_{larger}|}$$
 Eq. 4

The results of our rPM calculations are presented in Table 5 below. According to the classification scheme defined by Harshaw (2016), all of our star systems exhibit common proper motion (CPM), meaning they share proper motion to a high degree and likely have a common origin in space.

System	Relative PM Magnitude (mas/yr.)	Larger PM Magnitude (mas/yr)	rPM Value	Interpretation
WDS 05033+5821 STI 2082	0.2636	2.6007	0.1014	СРМ
WDS 05207+2442 POU 674	0.3018	2.5279	0.1194	СРМ
WDS 05553+0729 DOO 95	0.0449	15.2298	0.0030	СРМ

Table 5: Results of our rPM calculations.

4.2 Derivation and Calculation of Relative and Escape Velocities

To convert the relative PM vectors from angular units (mas) to physical units (meters per second), we multiply by the distance to the system, which entails dividing by the parallax of the primary star. (Since the primary and secondary of each system have similar parallax, the choice of which star's parallax to use is arbitrary.) We then multiply by several conversion factors to obtain the transverse velocity of the system:

$$V_{transverse} = PM_{Relative} \times \frac{1}{plx \times \frac{1}{1000 \, mas}} \times \frac{1}{1000 \, mas} \times \frac{1^{\circ}}{3600} \times \frac{\pi \, rad}{180^{\circ}} \times \frac{3.086 \times 10^{16} \, m}{pc} \times \frac{1 \, yr}{3.1536 \times 10^{7} \, s} \quad \text{Eq. 5}$$

Next, we need the relative radial motion through space, which is found using Eq. 6:

$$V_{radial} = 1000 \frac{m}{km} \left(V_{1 \, rad} \, \frac{km}{s} - V_{2 \, rad} \, \frac{km}{s} \right)$$
 Eq. 6

To obtain a relative 3D space velocity, we combine $V_{transverse}$ and V_{radial} using Pythagorean's Theorem.

As for the velocities, the 3D separation r has two components: transverse and radial. The 3D radial separation is computed from Eq. 7 using the Gaia DR3 parallaxes in Table 4. The 2D transverse separation is computed from the Washington Double Star Catalog separation using Eq. 8.

$$Sep_{radial\ 3D} = \frac{1}{\frac{plx_1 mas}{1000 \frac{mas}{arcsec}}} - \frac{1}{\frac{plx_2 mas}{1000 \frac{mas}{arcsec}}} = 1000 \frac{mas}{arcsec} \left(\frac{1}{plx_1} - \frac{1}{plx_2}\right)$$
Eq. 7

$$Sep_{transverse\ 2D} = Sep_{"} \times \frac{\circ}{"} \times \frac{\pi}{180} \frac{rad}{deg} \times \frac{1}{parallax\ "}$$
 Eq. 8

The escape velocity can be computed according to Eq. 9, which requires the masses of the stars $(m_1 \text{ and } m_2)$ from Table 1 as well as their 3D separation in space (r), and the gravitational constant G. (Bonifacio et al., 2020).

$$V_{escape} = \sqrt{\frac{2 \times G \times (m_1 + m_2)}{r}}$$
 Eq. 9

As an example, the quantities for Table 6 are calculated for STI 2082 like so. The parallaxes for the primary and secondary stares are used from Table 4, and are about 1.64 mas and 1.68 mas, respectively.

$$V_{transverse} = 0.2636 \frac{mas}{yr} \times \frac{1}{1.63893 \times \frac{1}{1000 \, mas}} \times \frac{1}{1000 \, mas} \times \frac{1^{\circ}}{3600^{\circ}} \times \frac{\pi \, rad}{180^{\circ}} \times \frac{3.086 \times 10^{16} \, m}{pc} \times \frac{1 \, yr}{3.1536 \times 10^{7} \, s}$$

$$V_{transverse} = 763 \, \frac{m}{s}$$

$$V_{radial} = 1000 \, \frac{m}{km} \left(-33.63518 \, \frac{km}{s} + 21.25268 \, \frac{km}{s} \right) = -12382.5 \, \frac{m}{s}$$

$$Sep_{radial} = 1000 \; \frac{mas}{arcsec} (\frac{1}{1.63893mas} - \frac{1}{1.68483mas}) = 16.6225 \; pc$$

$$Sep_{transverse} = 7.046 \times \frac{\circ}{3600''} \times \frac{\pi}{180} \frac{rad}{deg} \times \frac{1}{1.63893''} = 0.0208 \text{pc}$$

$$V_{escape\;radial} = \sqrt{\frac{2*6.67*10^{-11}\;\frac{N*m^2}{kg}*1.99*10^{30}\;\frac{kg}{M\odot}(1.73\;M\odot + 1.61\;M\odot)}{16.6225\;pc*3.09*10^{16}\;\frac{m}{pc}}} = 42\;\frac{m}{s}$$

$$V_{escape\ transverse} = \sqrt{\frac{2*6.67*10^{-11}\ \frac{N*m^2}{kg}*1.99*10^{30}\ \frac{kg}{M\odot}(1.73\ M\odot + 1.61\ M\odot)}{16.6225\ pc\ *\ 3.09\ *\ 10^{16}\ \frac{m}{pc}}} = 1174\ \frac{m}{s}$$

For POU 674 and DOO 95, the parallaxes of the two component stars overlap within their respective uncertainties. Therefore, the radial separation may be taken to be 0, so that the 3D separation is equivalent to the 2D (transverse) separation. In Table 6, we show escape velocities for both cases, with the 2D separation escape velocity bolded for POU 674 and DOO 95 to indicate that, and the 3D separation escape velocity bolded for STI 2082.

Table 6. Escape velocity calculations, with the relevant escape velocity for each system bolded. Relative radial motion is listed as N/A for DOO 95 because its components' radial velocities were not listed in Gaia.

System	Relative Transverse Motion (m/s)	Relative Radial Motion (m/s)	Relative 3D Velocity (m/s)	3D Separation (pc); 2D Separation (pc)	3D Escape Velocity (m/s); 2D Escape Velocity (m/s)
WDS 05033+58 21 STI 2082	763	12383	12406	16.6225; 0.0208	42 ; 1174
WDS 05207+24 42 POU 674	835	4493	4570	4.1169; 0.0238	75; 985
WDS 05553+07 29 DOO 95	132	N/A	132	6.4194; 0.0243	59; 967

For STI 2082 and POU 674 the escape velocities are much lower than the relative velocities even if the larger 3D separation is used in the calculation. Therefore, we conclude that the systems are unlikely to be gravitationally bound. However, their common proper motion implies that they are both physical systems.

For DOO 95, the case where the stars' parallax uncertainties overlap applies, so we can take the two stars to be the same distance from Earth. When considering the escape velocity of the system like this, the radial 3D velocity is much lower than the escape velocity and implies that there is a high likelihood of the system being gravitationally bound. However, in the case we take the parallaxes as directly reported by Gaia, assuming they do not overlap, the relative 3D velocity of the system is about twice that of the escape velocity, implying a low likelihood of a gravitational relationship in that case. Additionally, Gaia data does not list radial velocities for the stars in DOO 95, meaning that the relative 3D velocity of the system is likely higher than reported here. Regardless, from the data currently available, we conclude that there is a significant chance of the system being binary.

5. Discussion

5.1 STI 2082

STI 2082 and DOO 95 have a chance alignment coefficient \mathcal{R} calculated by El Badry et al. (2021), which is related to the chance of a star system being an optical double and not gravitationally bound. The paper notes that this value is not directly a probability–for example, it can be higher than 1. The lower the value is, the higher chance of the system being a binary double. STI 2082 had \mathcal{R} at 2.5×10^{-4} . Since the paper defines a high chance of being a binary double as a \mathcal{R} value of less than 0.1, this corresponds to a 90% chance of being gravitationally bound. However, our escape velocity calculation suggests otherwise, as shown in Table 6.

STI 2082's historical data plots in Fig. 3 show weak curves that point away from the primary star, which would not indicate an orbit around the primary even if the trend were stronger. If we remove all of the points from 1911, the remaining data, with the exception of the data point from 2010, is clumped on the graph. Removing the 1911 and 2010 points results in only a few measurements. Our current measurement deviates from these, though not as strongly as the 2010 data. One hypothesis for this unexpected behavior is that the stars may have been in a position that caused their acceleration due to a mutual gravitational influence temporarily increased, but this is difficult to support with the evidence of only a few data points. In any case, this plot is inconclusive evidence of an orbital relationship between STI 2082's component stars.

5.2 Discussion of POU 674

The escape velocity versus relative velocity calculations do not support an orbital relationship for the components of POU 674, regardless of whether the 2D or 3D separation is taken as the separation between the component stars. The historical measurements also do not show evidence of a clear trend over time. The polynomial regression (excluding the potentially erroneous measurement off to the bottom left of the plot taken in 1950) does fit a curve that revolves around the origin, as would be expected for a binary system, but the trend is not sufficiently strong as to be conclusive, and a linear relationship is also possible. Based on the common proper motion of the stars, their relationship appears to be physical but not gravitational.

5.3 Discussion of DOO 95

DOO 95 has an \mathcal{R} of approximately 10^{-4} , implying that it is also binary according to El Badry's criterion cited above. Even if we have overestimated the stars' masses, it is still possible that they are bound, because their relative velocity is significantly lower than the escape velocity. If the stars are not bound, we can instead say that the pair likely shares a common origin, because of the very low rPM value. Additionally, the two stars

in DOO 95 have a transverse separation of only 0.02 parsecs. Therefore, based on the available evidence, there appears to be a significant likelihood of the stars in DOO 95 being gravitationally bound to each other.

One historical measurement of DOO 95 (Fay, 2021), shown in Fig. 6, appears to be an outlier from the broader data. Using a CCD sensor on a 28.3 cm diameter camera, Fay (2021) reported a separation of 18 arcseconds and a position angle of about 135 degrees, which is substantially different than any other measurement recorded. Current models of stellar motion do not allow for such behavior, which is why we have presented an analysis of DOO 95 with and without this peculiar data point.

6. Conclusions

Both STI 2082 and POU 674 are physical doubles due to their low rPM values, but are unlikely to be gravitationally bound systems. STI 2082 has been previously listed as having a high likelihood of being binary according to El Badry's chance alignment probability coefficient value \mathcal{R} , but our velocity calculations imply the stars are moving too fast relative to each other to sustain a binary relationship, and the historical data plots do not imply an orbit. However, the physical similarity of the two stars and their shared motion through space imply that increased uncertainty of their positions or proper motions may lead to a different conclusion. Therefore, further measurements are recommended.

The component stars of DOO 95 are certainly physically related and have a considerable chance of the system being binary, based on our escape and relative system velocity calculations, as well as the \mathcal{R} criterion of El-Badry et al. (2021). Additionally, from the historic data file from the USNO, we observed a significant increase in measurement of this system starting around 2013, which seems to stem from Gaia data. We therefore recommend further measurement of this system when considering double star system observations from telescopes or catalog data.

Acknowledgements

This research was made possible by the Washington Double Star catalog maintained by the U.S. Naval Observatory, the Stelle Doppie catalog maintained by Gianluca Sordiglioni, Astrometry.net, and AstroImageJ software which was written by Karen Collins and John Kielkopf.

This work has made use of data from the European Space Agency (ESA) mission Gaia (https://www.cosmos.esa.int/gaia), processed by the Gaia Data Processing and Analysis Consortium (DPAC, https://www.cosmos.esa.int/web/gaia/dpac/consortium). Funding for the DPAC has been provided by national institutions, in particular the institutions participating in the Gaia Multilateral Agreement.

This work makes use of observations taken by the Planewave Delta Rho 350 + QHY600 CMOS camera systems of Las Cumbres Observatory Global Telescope Network at the Siding Spring Observatory in New South Wales, Australia; Teide Observatory at Mount Teide, Spain; and the McDonald observatory in Fort Davis, Texas. The Las Cumbres Observatory's education network telescopes were upgraded through generous support from the Gordon and Betty Moore Foundation.

This research has made use of the SIMBAD database, operated at CDS, Strasbourg, France (Wenger et al. 2000).

We thank the JDSO reviewer for reading this study thoroughly and thoughtfully, and for giving us many helpful and actionable comments to improve our work.

References

- Bonifacio, B., C. Marchetti, R. Caputo, and K. Tock. (2020). Measurements of Neglected Double Stars. Journal of Double Star Observations, 16(5), 411–423. http://www.jdso.org/volume16/number5/Bonifacio 411 423.pdf
- Doolittle, E., 1903. Mean Results of the Measures of 227 Double Stars, The Astronomical Journal, 23, 547. https://adsabs.harvard.edu/pdf/1903AJ....23..175D
- Gaia Collaboration, A. Vallenari, A. G. A. Brown, et al. (2023j) Gaia Data Release 3. Summary of the content and survey properties. A&A, 674, A1. https://arxiv.org/abs/2208.00211
- Gaia Collaboration, C. Babusiaux, C. Fabricius, S. Khanna, et al. (2023) Gaia Data Release 3. Catalogue validation. A&A 674, pp. A32. https://arxiv.org/abs/2206.05989
- Gaia Collaboration, T. Prusti, J.H.J. de Bruijne, et al. (2016b). The Gaia mission. A&A 595, A1. https://www.aanda.org/articles/aa/full-html/2016/11/aa29272-16/aa29272-16.html
- El-Badry, K. et al. (2021) A million binaries from *Gaia* eDR3: sample selection and validation of *Gaia* parallax uncertainties. Monthly Notices of the Royal Astronomical Society, 506(2), 2269–2295. https://doi.org/10.1093/mnras/stab323
- Fay, M. (2021) . El Observador de Estrellas Dobles, Issue #16, 94–96, http://www.infoastro.com/dobles/oed16.pdf
- Bessell, M. S (1990). Publications of the Astronomical Society of the Pacific, 102, 1181-1199. https://adsabs.harvard.edu/full/1990PASP..102.1181B
- Harshaw, Richard (2016). CCD Measurements of 141 Proper Motion Stars: The Autumn 2015 Observing Program at the Brilliant Sky Observatory, Part 3. Journal of Double Star Observations, 12(4), 394–399. http://www.jdso.org/volume12/number4/Harshaw 394 399.pdf
- Morgan, S. (2023). Spectral Type Characteristics. https://sites.uni.edu/morgans/astro/course/Notes/section2/spectralmasses.html
- Morgan, S. (2019). Formula Milky Way. https://sites.uni.edu/morgans/astro/course/Notes/section3/math11.html
- Bonifacio, B., C. Marchetti, R. Caputo, and K. Tock. (2020). Measurements of Neglected Double Stars. Journal of Double Star Observations, 16(5), 411–423. http://www.jdso.org/volume16/number5/Bonifacio 411 423.pdf
- Wenger, M. et al. (2000). "The SIMBAD astronomical database. The CDS reference database for astronomical objects". In: Astronomy and Astrophysics Supplement 143, pp. 9–22. DOI: 10.1051/aas: 2000332. arXiv: astro-ph/0002110 [astro-ph].

Appendix A

Table 7 contains individual astrometric measurements for each star system.

Table 7. Individual Measurements

	of STI 2082 .0302)	10 images of POU 674 (2024.0444)		10 images (2024.	
Position Angle (degrees)	Separation (arcseconds)	Position Angle (degrees)	Separation (arcseconds)	Position Angle (degrees)	Separation (arcseconds)
359.55	6.88	27.62	8.12	172.77	8.27
359.64	6.91	27.61	8.09	172.94	8.26
359.34	6.88	27.38	8.13	172.71	8.19
359.39	6.94	27.65	8.13	172.78	8.22
359.35	7.05	27.51	8.11	172.75	8.28
359.33	6.95	27.44	8.10	172.42	8.15
359.37	6.94	27.79	8.13	173.01	8.18
359.56	6.88	27.37	8.16	172.68	8.22
359.60	6.85	27.51	8.14	172.75	8.16
359.83	6.92	27.51	8.14	173.34	8.18
359.26	7.08				
359.76	6.83				
359.43	7.06				
359.41	6.93				

Astrometry of Double Star WDS 18026-5234

Nora Furlong, Sofia Robinson, Beatrix Picotte, Ryan Fantasia, Romy Gaudet, Laurel Halfman, Mark H.

Brooks Hedstrom

Winsor School, Boston, MA

Abstract

Using the Las Cumbres Observatory global telescope network, we investigated potential double star WDS 18026-5234. We focused on taking new position angle and separation measurements and then examined our measurements alongside historical data. On October 21, 2023, we measured the separation at 7.685 arcseconds and the position angle at 226.659 degrees, with standard deviations of 0.2085 and 1.44584, respectively. We then calculated the separation between the two stars in the system to be approximately 4920 astronomical units, making it unlikely that the two stars are gravitationally bound.

1. Introduction

When choosing a star system to study, we used the Stelle Doppie database. Our parameters included double stars that had not been observed since 2015, had a right ascension that put them over the skies of Chile during our observation time, and had a separation between 5 and 10 arcseconds. The magnitude of the primary star was set to be between 9 and 11, and the delta magnitude between the primary and secondary star was set to less than 4. Additionally, we looked for star systems whose natures were either physical or uncertain.

From the double stars that fulfilled these parameters, we chose the double star WDS 18026-5234. This system is located in the constellation Ara. The primary star's right ascension and declination are 18h 02m 36.26s and -52° 33' 50.3". The magnitude of the primary star is 9.13, and the magnitude of the secondary star is 12.00. This star system's entry in Stelle Doppie has a first observation in 1974 and a most recent observation in 1998. Those are the only previously existing observations of this star system in Stelle Doppie.

2. Instruments

We used Las Cumbres Observatory (LCO) Global Telescope network's 0.4 meter diameter telescopes to capture our images. Our data was captured from the Cerro Tololo Inter-American Observatory in the Coquimbo region of Northern Chile. The images were taken on SBIG STL6303 cameras, which have a 29.2" x 19.5" field of view and a pixel size of 0.571"/pixel.

3. Procedure

We focused on the likely double star WDS 18026-5234 and measured the current position angle and separation of the two stars using 10 images obtained from the LCO Global Telescope Network with a 3 second exposure time. The images were captured on October 21, 2023 from 23:51:39 to 23:55:04 UTC. We used Afterglow Access (Reichart et al., 2023) to take these measurements (shown in Fig. 1).

3.

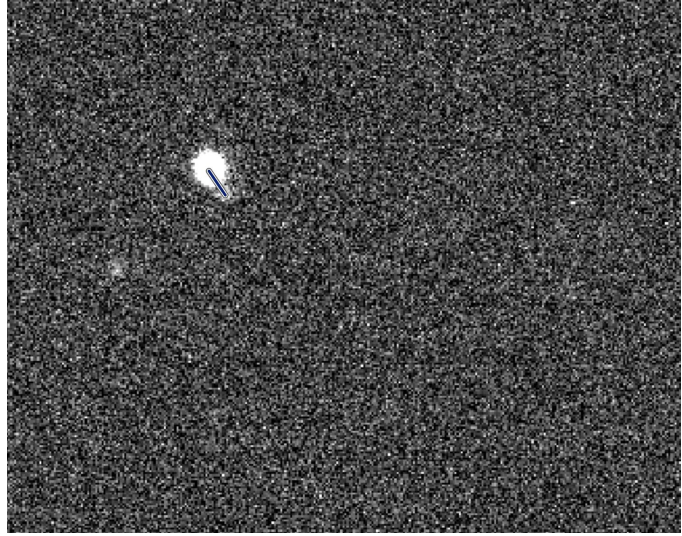


Figure 1: This image shows the star system, WDS

4. Results

The individual measurements are shown in Table 1 b average position angle was 226.569°.

A	7.685	226.659
Average		
Standard deviation	0.2085	1.44584
Standard error of the mean	0.06594	0.457214

We then compared our data with historical data obtained from the U.S. Naval Observatory, shown in Table 2.

Table 2: Historical and new measurements of WDS 18026-5234.

Year Observed	Position Angle	Separation
	(degrees)	(arcseconds)
1974	231	7.6
1998.591	227.8	7.467
2023.8	226.659	7.685

The bold values are our measurements; the top two are from the USNO.

We graphed the system's position angle over time (Figure 2) and separation over time (Figure 3) using the historical data. We then converted the position angle and separation measurements into Cartesian coordinates and graphed the position of the secondary relative to the primary (Figure. 4).

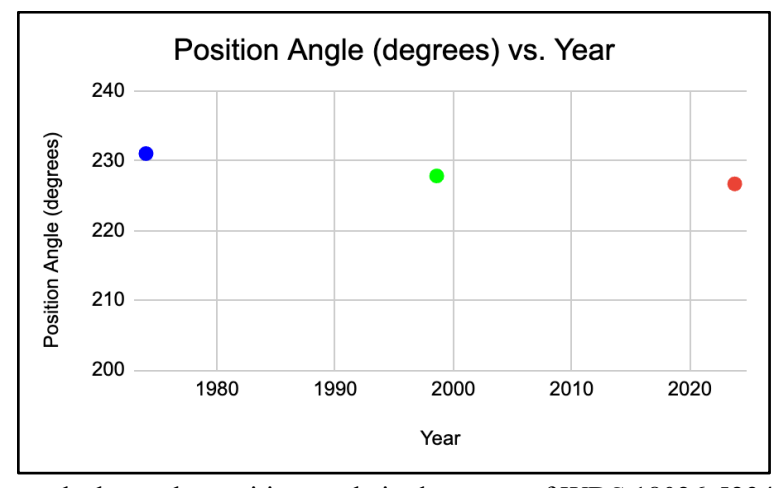


Figure 2: This graph shows the position angle in degrees e of WDS 18026-5234, with the 1974 measurement in blue, the 1998 measurement in green, and our measured value in red.

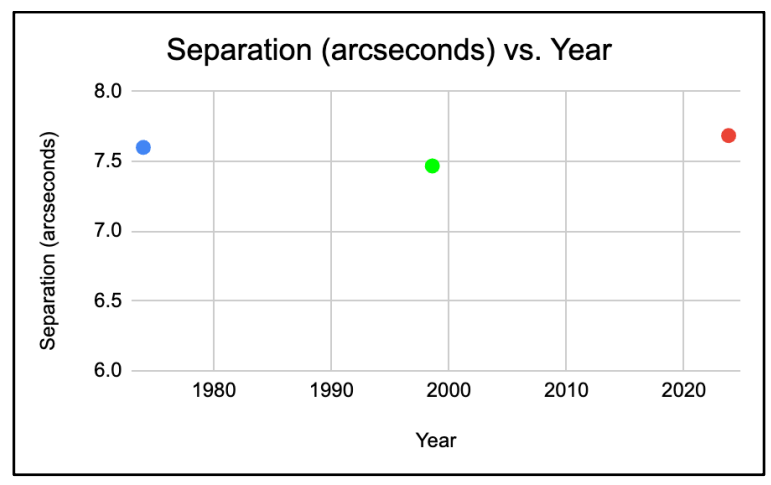


Figure 3: This graph shows the separation in arcseconds over time of WDS 18026-5234 with the 1974 measurement in blue, the 1998 measurement in green, and our measured value in red.

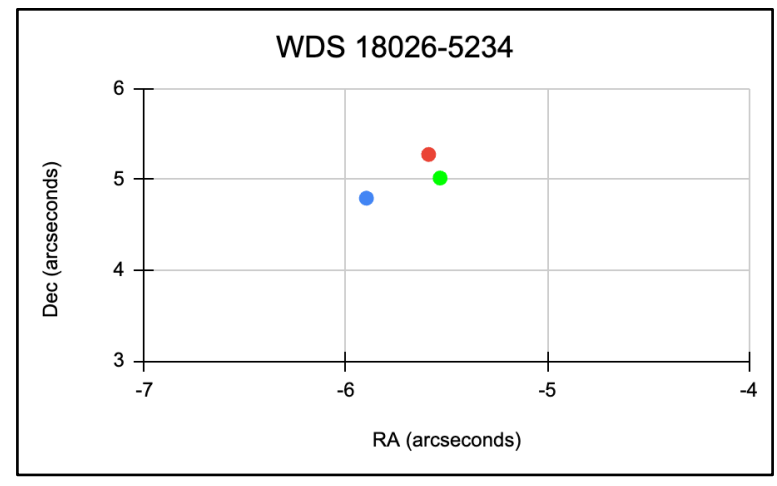


Figure 4: This graph shows the position of the secondary star relative to the primary, with the primary star being at the origin. The 1974 measurement is in blue, the 1998 measurement in green, and our measured value in red.

5. Discussion

By using Afterglow Access to analyze the ten images collected by the LCO telescopes, and then taking the average of these measurements, we found that the current position angle of the double star, WDS 18026-5234 is 226.659 degrees, and the separation of the two stars is 7.685 arcseconds. It is difficult to make a confident conclusion about trends because we only have three data points. According to Gaia Data Release 2, the primary star in our system has a parallax of 1.5622 milliarcseconds, giving it a distance of 640 parsecs, or 132 million astronomical units. If we assume both the primary and the secondary are at this distance, then the small angle formula, using the separation angle of 7.685 arcseconds, yields a separation of 4920 astronomical units. As Harshaw notes that "very few known binaries have separations that exceed 3,000 AU, and most are closer than 1,000 AU," it is unlikely that WDS 18026-5234 is a binary system (Harshaw, 736). Rather, it is likely an optical double.

Acknowledgments

This research was made possible by the Washington Double Star catalog maintained by the U.S. Naval Observatory, the Stelle Doppie catalog, and Afterglow Access software. This work has also made use of data from the European Space Agency's Gaia space observatory (www.cosmos.esa.int/gaia), processed by the Gaia Data Processing and Analysis Consortium

(https://www.cosmos.esa.int/web/gaia/dpac/consortium). Funding for the DPAC has been provided by national institutions, particularly those participating in the Gaia Multilateral Agreement. This work incorporated observations taken by the 0.4m telescopes of Las Cumbres Observatory Global Telescope Network located in the Coquimbo region of Northern Chile. Particular thanks goes to Dr. Rachel Freed for making this opportunity available to us and for her generous assistance in helping us complete this project.

References

18026-5234 RSS 467. (n.d.). Stelle Doppie. Retrieved November 7, 2023, from https://www.stelledoppie.it/index2.php?iddoppia=72656

Genet, R. M., Johnson, J., Buchheim, R., Harshaw, R., & Freed, R. (Eds.). (2018). Small Telescope and Astronomical Research Handbook. Institute for Student Astronomical Research.

Harshaw, R. (2018). Gaia DR2 and the Washington Double Star Catalog: A Tale of Two Databases. *Journal of Double Star Observations*, 14(4), 734-740.

- Reichart, D. E., Haislip, J., Kouprianov, V., Fu, R., Selph, L., Xu, S., ... & Converse, S. (2023). Next-Level, Robotic Telescope-Based Observing Experiences to Boost STEM Enrollments and Majors on a National Scale: Year 1 Report. arXiv preprint arXiv:2304.02545.
- The Washington Double Star Catalog. (n.d.). The United States Naval Observatory. Retrieved November 7, 2023, from https://crf.usno.navy.mil/wdstext

Observation and Investigation of 5 Physical Doubles in the Washington Double Star Catalog

Liam Oscaris, Mel Neffe, Samuel Lafiaji, Dali Mlilo, Carter Zimmerman, Kayla Oltman University of Saskatchewan, Saskatoon, Saskatchewan; liamoscaris@gmail.com

Abstract

This paper examines five physical double stars selected from the Washington Double Star Catalog and observed using telescopes from the Skynet Robotic Telescope Network. To determine whether the systems are gravitationally bound, our approach involved utilizing Skynet's Afterglow tool to measure each system's position angle and separation, which was used with data from Gaia Data Release 3 (DR3) to calculate its relative proper motion (rPM), system escape velocity, and relative space velocity. To discern formations of orbits that indicate binary star systems, we requested data from the United States Naval Observatory to create orbital plots. Our findings show that all five systems lack the gravitational relationships necessary to be classified as binary systems due to their relative space velocities exceeding their system escape velocities and the absence of orbiting trends in their plots.

1. Introduction

Physical double stars are stars that could have formed from the same gas cloud, at the same distance, and have the same proper motion through the celestial sphere. The study of these stars, even if they may not be binary, is valuable because historical records and measurements can be analyzed to extrapolate a common origin point in the Milky Way Galaxy when the two stars are close together in space, allowing estimates of their ages to be made. If a double star system is part of a larger star cluster, the age of the system also reveals information about the cluster's age, which in turn deepens our understanding of the history of the Milky Way.

The stars we have chosen in our study have been carefully selected using several constraints. Each pair needed to have a secondary magnitude less than 18, a primary magnitude greater than 9, and a delta magnitude less than 5. They also needed to be visible, physical pairs that had similar parallax and proper motions in right ascension and declination or had orbits that were previously solved. During the months in which the stars were observed, stars with a right ascension between 4 and 13 hours and a separation between 5" and 20". These constraints allowed us to find double star systems where both primary and secondary stars can be captured in the same images.

2. Instruments Used

Instruments used in our observation projects include the telescopes PROMPT-MO-1 and Prompt5 from the Skynet Robotic Telescope Network. A 16-bit CCD with a flux of 0 - 65353 flux and a Hithru filter was used to take images among all the telescopes. 10 images were taken, each with 3x3 dithering and 10-arcsecond spacing. PROMPT-MO-1, located at Meckering Observatory in Australia, has a focal length of 4477.0mm, a field ratio of 11.0, and a field of view of 10.2 x 10.2 arcmin. Prompt5, located at Cerro Tololo Inter-American Observatory in Chile, has a focal length of 4576.0mm, a field ratio of 11.3, and a field of view of 10.0 x 10.0 arcmin.

3. Measurements

Skynet's image processing suite, Afterglow, was used to measure the positional angle and separation between stars. The images were aligned, stacked, and saturated for clarity, and then Afterglow's plotter tool was used to measure the position angle and separation, as shown in Figure 1. These measurements were then used with data obtained from Gaia Data Release 3 (DR3) to obtain the values shown in Table 2 in the following section (A. Vallenari, A. G. A. Brown, et al, 2022).

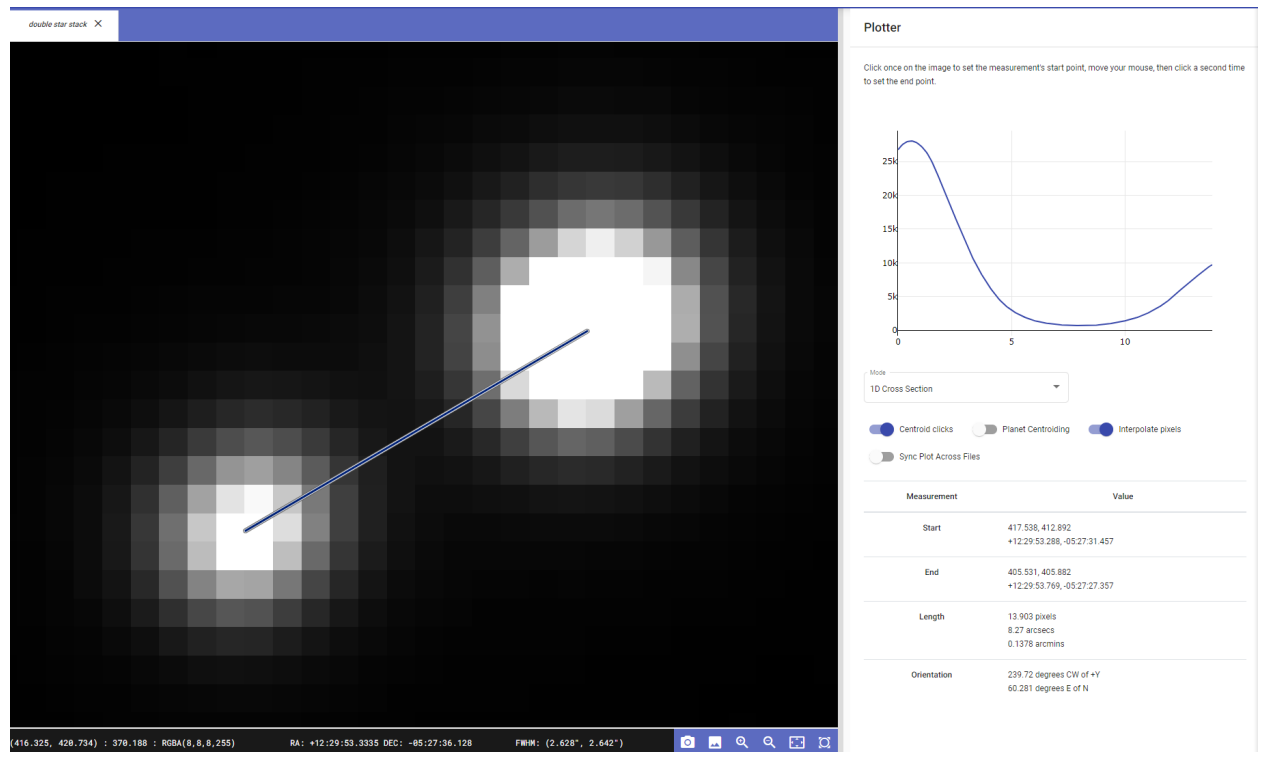


Figure 1: Position Angle and Separation measurements for B 2737.

4. Results

Table 1 contains the measurements made using Afterglow for each system selected in our study. The values for the columns titled, "Standard Error on Position Angle" and "Standard Error on Separation" were obtained by comparing the Afterglow measurements for each of the 10 images in our observations.

Table 2 contains the data obtained from Gaia DR3, in addition to the last column, titled "rPM," which represents the proper motion ratio of a double star system moving across the celestial sphere. It is calculated using the following equations. Equation 1 calculates the magnitude of the stars' relative motion by taking the magnitude of the difference vector between the primary and secondary proper motion vectors (Bonifacio, 2020).

$$pm_{Mag} = \sqrt{(pm_{RA1} - pm_{RA2})^2 + (pm_{Dec1} - pm_{Dec2})^2}$$

Equation 1: Proper motion of stars

Equation 2 calculates the rPM of a double star system by dividing the magnitude of the proper motion by the magnitude of the larger proper motion (Bonifacio, 2020). The rPM value is used to determine the classification of our systems based on their proper motions. There are three classifications: if the rPM range is less than 0.2, the system exhibits Common Proper Motion (CPM), which is the classification of the majority of our selections, and indicates that the stars are moving together through space; if the rPM range is between 0.2 and 0.6, the system exhibits Similar Proper Motion (SPM), which is the classification of the system BAL 1692, and indicates that the stars are moving in a similar way; and if the rPM range is greater than 0.6, the system exhibits Different Proper Motion (DPM), which indicates that the stars are not moving together through space (Harshaw, 2016).

$$rpm = \frac{pm_{Mag}}{\sqrt{pm^2_{RA1} + pm^2_{Dec1}}}$$

Equation 2: Relative proper motion of stars

Table 3 contains our estimates of the system escape velocity and relative space velocity for each system. These values are calculated using the equations presented in B. Bonifacio et al, 2020, and are what we compared to determine whether our double star systems could be binary systems.

System	Date	Number of Images	Positio n Angle (°)	Standard Error on Position Angle	Separation (")	Standard Error on Separation
B 2737 (WDS 12298-0427)	Feb 6, 2024	10	61	0.119	8.2	0.004
HJ 4545 (WDS 12459-7511)	Feb 6, 2024	10	193	0.053	9.2	0.009
BAL 1692 (WDS 06233+0245)	Feb 4, 2024	10	276	0.037	8.9	0.012
GRV 729 (WDS 07103+2540)	Feb 4, 2024	10	74	0.071	9.6	0.009
B 2657 (WDS 08272-2845)	Feb 7 2024	10	90	0.121	6.8	0.018

Table 1: Summary of Measurements.

Table 2: Skeleton Table for Gaia Data.

System	Parallax of Primary (mas)	Parallax of Secondary (mas)	Proper Motion of Primary (mas/yr)	Proper Motion of Secondary (mas/yr)	rPM
B 2737 (WDS 12298-0427)	46.986647 ± 0.04307	47.08963 ± 0.06245	-570.1723 (R.A) - 304.26559 (DEC)	-560.82031(R.A) - 293.6948(DEC)	0.022 (CPM)
HJ 4545 (WDS 12459-7511)	4.273027 ± 0.01272	4.28004 ± 0.01268	-28.224 (R.A) 2.43691 (DEC)	-28.54036(R.A) 2.29978(DEC)	0.012 (CPM)
BAL 1692 (WDS 06233+0245)	5.7027 ± 0.0257	5.603 ± 0.254	-3.426 (R.A) -4.162 (DEC)	-2.203(R.A) - 4.091(DE C)	0.227 (SPM)
GRV 729 (WDS 07103+2540)	2.96048 ± 0.01491	2.92625± 0.01232	-10.05923(R.A) - 35.566(DEC)	-10.2826(R.A) - 35.5405(DEC)	0.006 (CPM)
B 2657 (WDS 08272-2845)	2.45544 ± 0.03855	2.37059± 0.01986	0.97789(R.A) 5.24517(DEC)	0.80577(R.A) 5.3873(DEC)	0.041 (CPM)

Table 3: Estimates of System Escape Velocity and Relative Space Velocity.

System	System Escape Velocity (m/s)	Relative 3D Space Velocity (m/s)
B 2737 (WDS 12298-0427)	397	1428
HJ 4545 (WDS 12459-7511)	370	383
BAL 1692 (WDS 06233+0245)	87	1019
GRV 729 (WDS 07103+2540)	81	360
B 2657 (WDS 08272-2845)	50	429

5. Plots

For each system our group studied, we requested historical data from the United States Naval Observatory. Using the position angles and separations measured over the past, we created plots to determine if they had any trends or orbits. If a curve resembling an orbit was found, it would suggest the possibility of a double star system being a binary pair. Our plots, as shown in Figure 2, are labeled according to their WDS numbers and discoverer codes.

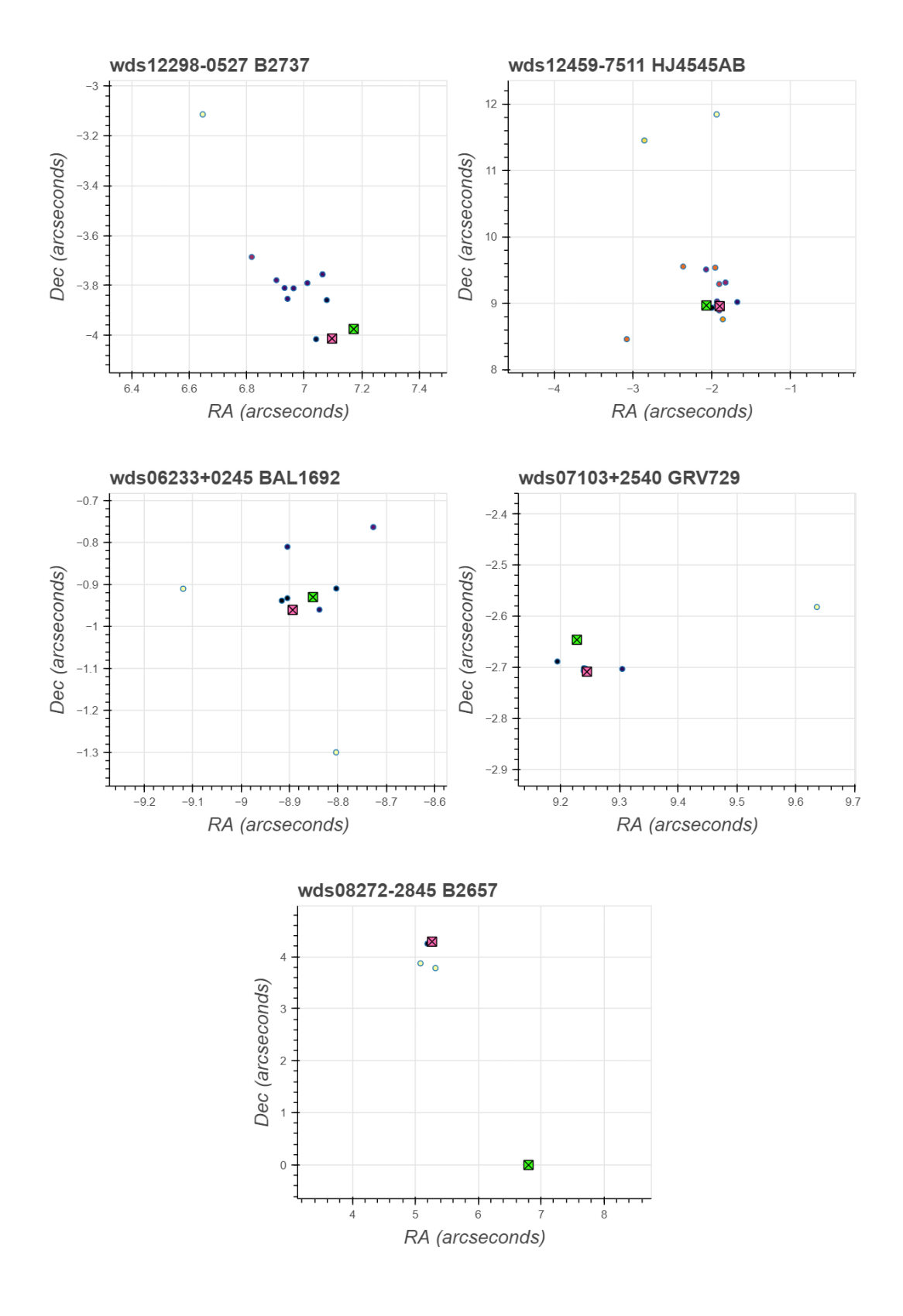


Figure 2: Historical data plots, where darker points are more recent, green boxes marked with an X are our measurements, and hot pink boxes marked with an X are measurements from Gaia.

6. Conclusion

The values in Table 3 show that in each system, because the system escape velocity is exceeded by the relative 3D space velocity, the double star system is not gravitationally bound and is therefore not binary. The data plots in Figure 2 support these assessments, as all plots except for system B 2737, have scattered data points and thus do not show any signs of orbit. However, these deductions are not definitive; each system requires further observations and analyses from astronomers in the future.

Acknowledgements:

This research was made possible by the Washington Double Star catalog maintained by the U.S. Naval Observatory, the Stelledoppie catalog maintained by Gianluca Sordiglioni, Astrometry.net, and Skynet's Afterglow Access software which was written by Joshua Haislip, Vladimir Kouprianov, and Daniel Reichart.

This work has also made use of data from the European Space Agency (ESA) mission Gaia (https://www.cosmos.esa.int/gaia), processed by the Gaia Data Processing and Analysis Consortium (DPAC, https://www.cosmos.esa.int/web/gaia/dpac/consortium). Funding for the DPAC has been provided by national institutions, in particular the institutions participating in the Gaia Multilateral Agreement.

This work makes use of observations taken by the 0.4m PROMPT MO-1 and Prompt5 telescopes of the Skynet Robotic Telescope Network located in Meckering, Australia and Cerro Tololo Inter-American Observatory, Chile.

References:

- Bonifacio, B., C. Marchetti, R. Caputo, and K. Tock. (2020). Measurements of Neglected Double Stars. Journal of Double Star Observations, 16(5), 411–423. http://www.jdso.org/volume16/number5/Bonifacio 411 423.pdf
- Brown, T. M. et al. (2013). Las Cumbres Observatory Global Telescope Network. Publications of the Astronomical Society of the Pacific, 125(931), 1031–1055. https://iopscience.jop.org/article/10.1086/673168/meta
- Cruzalèbes, P. et al. (2019). A catalogue of stellar diameters and fluxes for mid-infrared interferometry. Monthly Notices of the Royal Astronomical Society, 490(3), 3158–3176. https://doi.org/10.1093/mnras/stz2803
- Gaia Collaboration, C. Babusiaux, F. Van Leeuwen, et al. (2018). Gaia Data Release 2: Observational Hertzsprung-Russell diagrams. A&A 616, A10. https://www.aanda.org/articles/aa/full html/2018/08/aa32843-18/aa32843-18.html
- Gaia Collaboration, T. Prusti, J.H.J. de Bruijne, et al. (2016b). The Gaia mission. A&A 595, A1. https://www.aanda.org/articles/aa/full html/2016/11/aa29272-16/aa29272-16.html
- Gaia Collaboration, A. Vallenari, A. G. A. Brown, et al. (2022k). Gaia Data Release 3: Summary of the content and survey properties. arXiv e-prints, https://arxiv.org/abs/2208.00211
- Harshaw, Richard (2016). CCD Measurements of 141 Proper Motion Stars: The Autumn 2015 Observing Program at the Brilliant Sky Observatory, Part 3. Journal of Double Star Observations, 12(4), 394–399. http://www.jdso.org/volume12/number4/Harshaw 394 399.pdf
- Jiménez-Esteban, F. M., E. Solano, and C. Rodrigo. (2019). A Catalog of Wide Binary and Multiple Systems of Bright Stars from Gaia-DR2 and the Virtual Observatory. The Astronomical Journal. 157(2):78, 1–10.https://iopscience.iop.org/article/10.3847/1538-3881/aafacc/pdf